THE UNIVERSITY OF QUEENSLAND

AUSTRALIA

Conserved and divergent mechanisms of cortical development across mammalian brain evolution

Dr Annalisa Paolino

MBBS

A thesis submitted for the degree of Doctor of Philosophy at

The University of Queensland in 2019

Queensland Brain Institute

Abstract

During vertebrate evolution, the mammalian brain underwent significant changes, such as the emergence of a six-layered neocortex and an expansion and diversification of interhemispheric connectivity. The subsequent emergence of the corpus callosum exclusively in eutherian mammals, after they diverged from marsupials and monotremes, was another notable evolutionary innovation that allowed the expansion of neocortical connectivity in large-brained species, such as humans. The correct development of the neocortex and its circuits is essential for sensory-motor and cognitive functions, and requires a precise orchestration of myriad events including the generation, migration and differentiation of neurons, as well as elongation and guidance of axons to their appropriate targets. Impairments of any of these processes can result in neurodevelopmental disorders in humans, hence the importance of understanding the basic mechanisms regulating these developmental steps to ensure healthy brain formation. Due to the absence in fossil records of soft tissue anatomical detail, such as the nervous system, many questions regarding the evolution and development of the brain remain unanswered. One way to investigate how the mammalian neocortex originated, expanded and evolved, is to adopt a comparative approach in extant species. This allows the identification of features that have been conserved or that have diverged across lineages.

This thesis focuses on identifying key mechanisms regulating the development and evolution of the neocortex and its connections, combining experimental insights from mice, as a well-established model of eutherian brain development, and a similarly-sized marsupial, the Australian fat-tailed dunnart (*Sminthopsis crassicaudata*, Dasyuridae). By comparing the development of the neocortex and its circuits between therian mammals (marsupials and eutherians), this thesis also explores the molecular processes involved in the evolution of new brain structures, such as the corpus callosum. In order to address these questions, several methods from molecular, developmental and comparative neurobiology were employed, including gene transfection of specific neuronal populations via in pouch and *in utero* electroporation, as well as stereotaxic brain injections, assays of neurogenesis, immunofluorescence and advanced microscopy analyses.

The first part of this thesis describes the characterisation of the fat-tailed dunnart as an innovative model system to study brain development and evolution. A developmental staging

system, with a detailed characterisation of maturation features of dunnart brain and body, is presented in relation to mouse and human development. Then, cortical neurogenesis is investigated in dunnarts and compared to mice, concluding that, despite the postnatal and protracted development of the neocortex in marsupials, the main steps and patterns of neocortical formation are broadly conserved across therian mammals. Following this, the establishment of corticocortical connectivity in dunnarts is explored, including axonal elongation and targeting of long-range projection neurons. Finally, an analysis of the expression of major transcription factors known to direct projection fate in eutherians (i.e. SATB2 and CTIP2), as well as manipulatory experiments that altered their expression in dunnarts and mouse, reveals the existence of a broadly conserved and ancient program of molecular specification of commissural and subcerebral axonal fates during neocortical development of therian mammals.

In summary, this thesis not only introduces the fat-tailed dunnart as an innovative model to investigate brain evolution and development, but also provides mechanistic insights into the main principles guiding mammalian brain formation and evolution. By comparing developmental processes in marsupial and eutherian species, this thesis concludes that key aspects of neocortical neurogenesis, neuronal projection fate determination, and targeting, many of which were previously assumed to be novel traits of eutherians related to the evolution of the corpus callosum, show remarkable conservation between mammalian lineages with different commissural routes. This evidence suggests that these conserved mechanisms play a critical role in the formation of functional and healthy cortical circuits in therian mammals, regardless of commissural route.

Declaration by author

This thesis is composed of my original work, and contains no material previously published or written by another person except where due reference has been made in the text. I have clearly stated the contribution by others to jointly-authored works that I have included in my thesis.

I have clearly stated the contribution of others to my thesis as a whole, including statistical assistance, survey design, data analysis, significant technical procedures, professional editorial advice, financial support and any other original research work used or reported in my thesis. The content of my thesis is the result of work I have carried out since the commencement of my higher degree by research candidature and does not include a substantial part of work that has been submitted to qualify for the award of any other degree or diploma in any university or other tertiary institution. I have clearly stated which parts of my thesis, if any, have been submitted to qualify for another award.

I acknowledge that an electronic copy of my thesis must be lodged with the University Library and, subject to the policy and procedures of The University of Queensland, the thesis be made available for research and study in accordance with the Copyright Act 1968 unless a period of embargo has been approved by the Dean of the Graduate School.

I acknowledge that copyright of all material contained in my thesis resides with the copyright holder(s) of that material. Where appropriate I have obtained copyright permission from the copyright holder to reproduce material in this thesis and have sought permission from co-authors for any jointly authored works included in the thesis.

Publications included in this thesis

Suárez R, **Paolino A**, Fenlon LR, Morcom LR, Kozulin P, Kurniawan ND, and Richards LJ (2018). A pan-mammalian map of interhemispheric connections predates the evolution of the corpus callosum. Proc Natl Acad Sci U S A. 115(38): 9622-9627 doi: https://doi.org/10.1073/pnas.1808262115

Paolino A, Fenlon LR, Suárez R, Richards LJ (2018). Transcriptional control of long-range cortical projections. Curr Opin Neurobiol. 53:57-65. doi: https://doi.org/10.1016/j.conb.2018.05.005

Paolino A, Fenlon LR, Kozulin P, Richards LJ, Suárez R (2018). Multiple events of gene manipulation via in pouch electroporation in a marsupial model of mammalian forebrain development. J Neurosci Methods. 293:45-52. doi: https://doi.org/10.1016/j.jneumeth.2017.09.004

Suárez R, **Paolino A** (co-first author), Kozulin P, Fenlon LR, Morcom LR, Englebright R, O'Hara PJ, Murray PJ, Richards LJ (2017). Development of body, head and brain features in the Australian fat-tailed dunnart (Sminthopsis crassicaudata; Marsupialia: Dasyuridae); A postnatal model of forebrain formation. PLoS ONE. 12(9): e0184450. doi: https://doi.org/10.1371/journal.pone.0184450

Submitted manuscripts included in this thesis

No manuscripts currently submitted for publication.

Other publications during candidature

Peer-reviewed papers:

Gobius I, Suárez R, Morcom L, **Paolino A**, Edwards TJ, Kozulin P, Richards LJ (2017). Astroglial-mediated remodeling of the interhemispheric midline during telencephalic development is exclusive to eutherian mammals. Neural Development. **12**:9. https://doi.org/10.1186/s13064-017-0086-1

Marsh, APL, Heron D, Edwards TJ, Quartier A, Galea C, Nava C, Rastetter A, Moutard ML, Anderson V, Bitoun P, Bunt J, Faudet A, Garel C, Gillies G, Gobius I, Guegan J, Heide S, Keren B, Lesne F, Lukic V, Mandelstam SA, McGillivray G, McIlroy A, Méneret A, Mignot C, Morcom LR, Odent S, **Paolino A**, Pope K, Riant F, Robinson GA, Spencer-Smith M, Srour M, Stephenson SEM, Tankard R, Trouillard O, Welniarz Q, Wood A, Brice A, Rouleau G, Attié-Bitach A, Delatycki1 MB, Mandel JL, Amor DJ, Roze E, Piton A, Bahlo M, Billette de Villemeur T, Sherr EH, Leventer RJ, Richards LJ, Lockhart PJ, Depienne C (2017). Mutations in DCC cause isolated agenesis of the corpus callosum with incomplete penetrance. Nature Genetics. doi: https://doi.org/10.1038/ng.3794

Conference abstracts:

Paolino A, Fenlon LR, Kozulin P, Richards LJ, Suárez R (2018). Conserved and divergent mechanisms of cortical development across mammalian brain evolution. QBI Student Symposium. Stradbroke Island, Australia. PhD Exit Talk.

Paolino A, Fenlon LR, Kozulin P, Richards LJ, Suárez R (2018). The molecular specification of commissural and subcerebral projection neurons in the neocortex is conserved in therian mammals. Australasian Neuroscience Society Meeting. Brisbane, Australia. Oral.

Paolino A, Fenlon LR, Kozulin P, Richards LJ, Suárez R (2018). The molecular specification of commissural and subcerebral projection neurons in the neocortex is conserved in therian mammals. Cell and Developmental Biology Meeting. Brisbane, Australia. Poster.

Paolino A, Suárez R, Kozulin P, Fenlon L, Richards LJ (2017). Investigating cortical connectivity in the developing Australian marsupial fat-tailed dunnart (Sminthopsis crassicaudata, Dasyuridae). System and Computational Neuroscience Down Under. Brisbane, Australia. Poster.

Paolino A, Suárez R, Kozulin P, Fenlon L, Richards LJ (2017). The fat-tailed dunnart (Sminthopsis crassicaudata, Dasyuridae) as an animal model to investigate the pattern of connectivity between and within the hemispheres in mammals. Cortical Development Conference. Chania, Greece. Poster.

Paolino A, Suárez R, Kozulin P, Morcom L, Fenlon L, Richards LJ (2016). SATB2 and CTIP2 expression in the marsupial neocortex reveals a regulatory network that predates the evolution of the corpus callosum. Australasian Neuroscience Society Meeting. Hobart, Australia. Poster.

Paolino A, Suárez R, Kozulin P, Morcom L, Fenlon L, Richards LJ (2016). The genetic program for commissural fate determination is conserved across mammals. QBI Postgraduate Student Symposium. Brisbane, Australia. Oral.

Paolino A, Suárez R, Kozulin P, Morcom L, Fenlon L, Richards LJ (2016). SATB2 expression is involved in commissural projection fate in the acallosal marsupial fat-tailed dunnart (*Sminthopsis crassicaudata; Dasyuridae)*. Axon guidance, synapses formation and regeneration meeting. Cold Spring Harbor, New York, USA. Poster.

Contributions by others to the thesis

Chapter 1: As stated in paper contribution section at the beginning of the corresponding chapter

Chapter 3: As stated in paper contribution section at the beginning of the corresponding chapter

Chapter 4: As stated in paper contribution section at the beginning of the corresponding chapter

Chapter 5: Peter Kozulin and Rodrigo Suárez performed the stereotaxic brain injections, assisted by Annalisa Paolino. Linda J Richards, Rodrigo Suárez and Laura R Fenlon assisted in the conception, design and interpretation of the results of most of the experiments.

Chapter 6: Peter Kozulin designed and cloned the dunnart-specific overexpression constructs for SATB2, CTIP2, and SKI. The mouse-specific overexpression constructs for SATB2, CTIP2 and SKI were a gift from the lab of Prof Victor Tarabykin, Prof Nenad Sestan and Prof Suzana Atanasoski. Linda J Richards, Rodrigo Suárez and Laura R Fenlon assisted in the conception, design and interpretation of the results of most of the experiments.

Statement of parts of the thesis submitted to qualify for the award of another degree

No works submitted towards another degree have been included in this thesis.

Research Involving Human or Animal Subjects

All animal procedures, including laboratory breeding, were approved by The University of Queensland Animal Ethics Committee (AEC approval numbers: QBI/044/18, previous and QBI/045/15/NHMRC) and the Queensland Government Department of Environment and Science (permit number: WA0008250), and were performed according to the current Australian Code for the Care and Use of Animals for Scientific Purposes (NHMRC, 8th edition, 2013), as well as international guidelines on animal welfare.

Acknowledgements

To every single member of the Richards lab. You truly create an amazing work environment, thank you for your help and support during these four years.

To Rodrigo, your passion for Science is contagious. Thank you for your guidance, for believing in me, for being a great mentor, an encouraging supervisor and an awesome friend.

To Linda, your advice has guided me through this journey. Thank you for giving me the chance of joining your lab, which introduced me to the fascinating world of Science. You took a chance on me and allowed me to become a scientist, I will always be grateful for it.

To Laurita, words cannot describe all the roles you have covered in my life since the first day we met. You are my colleague, my supervisor, my mentor, my Aussie best friend, my Aussie sister. I am so grateful for everything you have taught me, for all the great memories we have shared together, for being my anchor here in Australia.

To Peter. I have started this adventure with you, meeting you at the HR office, in 2014. Somehow I knew from that moment that you would have become a crucial part of my life. Thank you for being such a great person, thank you for your invaluable support and infinite patience.

To Morcky, my Aussie twin, Toby and Lizzy, the rest of the awesome marsupial group, thanks for sharing this PhD journey with me, thanks for all the laughs, the chats, for all the time we have spent together.

To my milestone committee members: Pato, Jenny, Helen and Steven, for evaluating my progress during my PhD, for guiding me with their precious advices.

To all the supporting staff from QBI, Hidden Vale and SCMB. Without your daily help, this project would have not been possible.

To my parents, who have always done everything that was in their power to make my dreams come true, who have always supported any decision I have ever taken in my life, even when I chose to move to Australia five years ago. Despite the almost 17000 km that physically divide us, you make me feel loved every day. You are my strength, and having you as parents is the best thing that has ever happened to me.

To the rest of my family. Especially my amazing brothers, with you in my life I will never be lonely. To my granny, who, despite disapproving my choice of living far away, is always

there to listen to me and support me. To my uncles and aunties. To my cousins, especially Francesca, who is like a sister to me. You are my example, a perfect mixture of kindness, sweetness, strength and determination.

To my lifetime friends:
Marty, Mary, Ely, and Micky, the best friends a person could possibly imagine. We have shared so much, since the first day of high school. I feel blessed every day for having the chance of sharing my journey with you. Thanks for that kind of friendship that will never be spoiled by distance.

To Coqui, who is always with me, especially in the crucial moments of my life.

To Cicci and Semmi, who have always believed in me since the first anatomy class at Med School. We shared important periods of our life, supporting each other as well as reading the horoscope and the soccer news during the long commute to University.

To Ila, Cate, Alessandro, Alessandra, Owen and my beloved baby Oscarino, my irreplaceable Aussie Family. It always feels like home whenever I am with you.

To all the rest of my friends back in Italy and around the World, I would need 200 pages to acknowledge you all. I am so lucky to have you all in my life.

This journey was long, but exciting and successful. I grew a lot, I learnt a lot and now I am ready to explore what the future holds for me... Dai dai dai!!!

Financial support

This research was supported by a UQ International tuition fee scholarship, as well as a QBI living allowance scholarship and a QBI top-up scholarship and grants from the Australian Research Council (ARC; DP160103958 and DE160101394)

Keywords

Mammalian brain evolution, cortical development, cortical evolution, brain wiring, transcription factors, pyramidal neurons, corticospinal, corticothalamic, corpus callosum, anterior commissure.

Australian and New Zealand Standard Research Classifications (ANZSRC)

ANZSRC code: 110903, Central Nervous System, 60%

ANZSRC code: 060305, Evolution and developmental system, 40%

Fields of Research (FoR) Classification

FoR code: 1109, Neuroscience, 80%

FoR code: 0603, Evolutionary biology, 20%

Table of contents

List of figures

List of tables

List of abbreviations

5HT3aR	5-hydroxytryptamine 3a receptor
A	Anterior
A1/TeA	Auditory cortex/temporal association area
ac	Anterior commissure
ACAd	Anterior cingular area dorsal
aM	Anterior motor cortex
AON	Anterior olfactory nucleus
Aud	Auditory cortex
Av	Ventral arcopallium
Bcl6	B Cell CLL/Lymphoma 6
BG	Basal ganglia
Bhlhe22	Basic Helix-Loop-Helix Family Member E22
BS	Brainstem
CA	Cornu ammonis hippocampi
CAG	Chicken ß actin promoter
Cb	Cerebellum
cc	Corpus callosum
Cd	Caudate
cDNA	Complementary DNA
Cg	Cingulate cortex
Cited2	Cbp/P300 interacting transactivator with Glu/Asp rich carboxy-terminal domain 2
Cla	Claustrum
cM	Central motor cortex
Co	Cornea
CO-Ip	Co-immunoprecipitation
contra	Contralateral
CP	Cortical plate
CPN	Callosal projection neuron
CR	Cajal-Retzius
CrP	Cribiform plate
CTB	Cholera toxin subunit B
CThPN	Corticothalamic projection neuron
Ctip2	Chicken ovalbumin upstream promoter transcription factor (COUP-TF)-interacting protein (also known as Bcl11b: B cell leukemia/lymphoma 11B)
Cux	Cut-like homeobox
Cxxc5	CXXC-type zinc finger protein 5
D	Dorsal
DAPI	4',6-Diamidine-2'-phenylindole dihydrochloride
DG	Dentate gyrus
Di	Diencephalon
DiD	1,1'-Dioctadecyl-3,3,3',3'-Tetramethylindocarbocyanine 4-Chlorobenzensulfonate
DiI	1,1'-Dioctadecyl-3,3,3',3'-Tetramethylindodicarbocyanine Perchlorate
DL	Deeper layers
DNA	Deoxyribonucleic acid

E	Embryonic day
ec	External capsule
EdU	Ethynyl deoxyiuridine
Efn	Ephrin
En	Endopiriform nucleus
Ent	Entorhinal cortex
EP	Electroporation
Eph	Ephrin receptor
Et	Ethmoid bone
Ey	Eyes
eYFP	Enhanced yellow fluorescent protein
F	Follicle
f	Fornix
Fezf	Forebrain Embryonic Zinc Finger-Like Protein 2
Foxg1	Forkhead Box G1
Foxp2	Forkhead box protein P2
Fr	Frontal cortex
Ga	Ganglion layer
GABA	Gamma-aminobutyric acid
GE	Ganglionic eminence
GFAP	Glial fibrillary acidic protein
Gse1	Genetic Suppressor Element 1
HARDI	High angular resolution diffusion imaging
hc	Hippocampal commissure
HI	Hyperpallium intercalatum
Hp	Hippocampus
ic	Internal capsule
IC	Inferior colliculus
IG	Indusium griseum
IHC	Immunohistochemistry
Ins	Insular cortex
ipsi	Ipsilateral
IsoCx-S1	Primary somatosensory cortex
IsoCx-M	Motor cortex
IZ	Intermediate zone
L	Layer
LE	Lens epithelium
LF	Lens fibres
Lhx2	LIM Homeobox Protein 2
Li	Eyelid
Lmo4	LIM Domain Only 4
lot	Lateral olfactory tract
LV	Lateral ventricle
LVe	Lens vesicle
M	Mesopallium

Mb	Mandible
Mo	Mouth
Moxd1	Monooxygenase DBH Like 1
MRI	Magnetic resonance imaging
mRNA	Messenger ribonucleic acid
MS	Mouse
Mx	Maxillary
mya	Million years ago
MZ	Marginal zone
N	Nidopallium
NaCl	Sodium Chloride/saline
Nb	Neuroblastic layer
NC	Nasal cavities
NCx	Neocortex
Neto	Neuropilin And Tolloid Like
NeuroD	Neurogenic differentiation
Nfe2l3	Nuclear Factor, Erythroid 2 Like 3
Ngn2	Neurogenin 2
Nse	nasal septum
Ntng2	Netrin G2
Nurr1	Nuclear receptor related 1 protein
OB	Olfactory bulb
Occip	Occipital cortex
OE	Olfactory neuroepithelium
Olf	Olfactory branch
ON	Optic nerve
onl	Olfactory nerve layer
Orb	Orbital bone
OS	Optic stalk
OT	Olfactory tubercle
P	Postnatal day
Pal	Palate
Pax6	Paired box 6
PBS	Phosphate-buffered saline
PCR	Polymerase chain reaction
PFA	Paraformaldehyde
PFC	Prefrontal cortex
Pi	Pigment epithelium
Pir	Piriform
Plxn	Plexin
pM	Posterior motor cortex
PoA	Preoptic area
Pou3f2	POU domain, class 3, transcription factor 2 (also known as Brn2: Brain-specific homeobox/POU domain protein 2)

Pou3f3	POU domain, class 3, transcription factor 3 (also known as Brn1: Brain-specific homeobox/POU domain protein 1)
Pp	Preplate
PRh	Perirhinal
PSp	Presphenoid bone
Pu	Putamen
R	Rostral
Re	Retina
rf	Rhinal fissure
RNAseq	Ribonucleic acid sequencing
Robo	Roundabout guidance receptor
ROI	Region of interest
RSPv	Retrosplenial cortex ventral
S	Stage
S1	Primary somatosensory cortex
S2	Secondary somatosensory cortex
Satb2	Special AT-rich sequence binding protein 2
SC	Superior colliculus
SCPN	Subcerebral projection neuron
SDS	Sodium dodecyl sulphate
Se	Septum
SEM	Standard error of the mean
Sema	Semaphorin
Ski	SKI Proto-Oncogene
Slit	Slit homolog
Sox5	SRY (Sex Determining Region Y)-Box 5
Sp	Subplate
St	striatum
Sub	Subiculum
SVZ	Subventricular zone
T	Tongue
Tbr1	T-Box, Brain 1
Tbr2	T-Box, Brain 2
Th	Thalamus
Tle3	Transducin Like Enhancer Of Split 3
Tle4	Transducin Like Enhancer Of Split 4
UL	Upper layers
Unc5	Unc-5 Netrin Receptor
V1	Primary visual cortex
V2L	Lateral field of the secondary visual cortex
VC	Vomeronasal capsule
VE	Vomeronasal neuroepithelium
VF	Vibrissal follicles
VLu	Vomeronasal lumen
VO	Vomeronasal organ

VZ	Ventricular zone
WM	White matter
Zfp703	Zinc finger protein 703
Zfpm2	Zinc Finger Protein, FOG Family Member 2

Chapter 1. General introduction

Section 1.5 of this chapter includes material (e.g., Table 1.1 and Figure 1.3) that were published in the following review:

Paolino A, Fenlon LR, Suárez R, Richards LJ (2018). Transcriptional control of long-range cortical projections. Curr Opin Neurobiol. 53:57-65. doi: https://doi.org/10.1016/j.conb.2018.05.005

Contributor	**Statement of contribution**
Annalisa Paolino (candidate)	Conceptual advance 30% Researched article 50% Wrote and edited article 40%
Laura R Fenlon	Conceptual advance 25% Researched article 30% Wrote and edited article 20%
Rodrigo Suárez	Conceptual advance 20% Researched article 10% Wrote and edited article 25%
Linda J Richards	Conceptual advance 25% Researched article 10% Wrote and edited article 15%

OVERVIEW

The expansion and diversification of interhemispheric connectivity was a key event in the evolution of the mammalian brain, and the correct establishment of interhemispheric circuits during development is crucial for correct brain function (Suárez *et al.* 2014b). Abnormal development of interhemispheric connectivity has been associated with numerous neurodevelopmental disorders in humans, such as attention deficit hyperactivity disorder (Gilliam *et al.* 2011, Cocchi *et al.* 2012), schizophrenia (Swayze *et al.* 1990, Lungu *et al.* 2012), autism (Wass 2011, Paul *et al.* 2014), bipolar disorders (Trehout *et al.* 2017), intellectual disabilities (Paul *et al.* 2014, Margari *et al.* 2016) and behavioural problems (Sarkar *et al.* 2013, Zhang *et al.* 2014, Labadi *et al.* 2017, Menks *et al.* 2017a, Menks *et al.* 2017b). One tract that is commonly affected in these disorders is the corpus callosum (Funnell *et al.* 2000, Mihrshahi 2006, Hinkley *et al.* 2012, Fenlon *et al.* 2015), which is an evolutionary novelty that emerged exclusively in eutherian mammals after they diverged from the common ancestors with modern marsupials. Despite the high incidence of impaired formation of interhemispheric connectivity in humans [1:4000 newborns have malformations of the corpus callosum (Paul *et al.* 2007, Glass *et al.* 2008)], the developmental events that underlie the correct formation of the neocortex and its connections remain unclear. Understanding the evolutionary history of the neocortex and its expanded and diversified interhemispheric connection can help to shed light on the development of these brain structures.

Interestingly, it has been previously shown that in some cases of callosal agenesis, the neocortical axons that would normally cross the midline via the corpus callosum can instead reroute through the anterior commissure to successfully reach the contralateral hemisphere (Barr *et al.* 2002, Barr *et al.* 2003, Tovar-Moll *et al.* 2014), thus resembling the brain of non-eutherian mammals. Therefore, elucidating the mechanisms of neocortical evolution and development has the potential to lead to a better understanding about the healthy and pathological formation, as well as the plasticity, of cortical circuits in humans (Swayze *et al.* 1990, Funnell *et al.* 2000, Mihrshahi 2006, Leventer *et al.* 2008, Gilliam *et al.* 2011, Hinkley *et al.* 2012, Lungu and Stip 2012, Paul *et al.* 2014, Fenlon and Richards 2015, Moffat *et al.* 2015).

Due to the absence of information about brain microanatomy from the fossil record, the best way to increase our understanding of the evolution, expansion, connectivity and function of the mammalian neocortex is by adopting a comparative approach. This thesis introduces an Australian marsupial species, the fat-tailed dunnart (*Sminthopsis crassicaudata*, Dasyuridae), as an experimental model *in vivo* to compare with better known eutherian species (such as mice and humans). The postnatal and protracted neocortical development of this marsupial species allows

continuous and non-invasive access at early stages of brain development, equivalent to embryonic rodents and humans, providing unprecedented opportunities for experimental manipulations to study developmental processes (Suárez *et al.* 2017, Paolino *et al.* 2018). This thesis investigates evolutionary questions at a basic biology level, with a focus on the developmental, molecular and anatomical features that have been conserved or that have diverged throughout mammalian evolution.

1.1. Evolution of the mammalian telencephalon

During evolution, the mammalian brain underwent significant changes in organisation, which led to the emergence of a six-layered neuronal configuration of the dorsal telencephalon, in contrast to the nuclear arrangement of neurons found in other amniotes, such as birds and reptiles (Jarvis *et al.* 2005, Cheung *et al.* 2010, Wang *et al.* 2010, Briscoe *et al.* 2018) (Figure 1.1). Another major change in terms of telencephalic development between sauropsids and mammals was in the pattern of sequential neurogenesis and radial migration of cortical neurons, whereby the brains of birds and reptiles are generated according to an outside-in pattern, with the oldest neurons situated farthest away from the lateral ventricle (Goffinet *et al.* 1986, Striedter *et al.* 2000, Jarvis 2009), while the six-layered mammalian neocortex is generated in an inside-out fashion, with later-born neurons migrating past the earlier-born cells (Angevine *et al.* 1961, Smart *et al.* 1982, Rakic 1995, Puzzolo *et al.* 2010).

Despite the different neuronal arrangement of the dorsal telencephalon, mammals and sauropsids share broad features of brain organisation, including patterns of neural connectivity and gene expression profiles (Jarvis 2009, Wada *et al.* 2017, Briscoe and Ragsdale 2018). According to the nuclear-to-layered hypothesis of brain evolution, during the specification of laminar versus nuclear organisation of the dorsal telencephalon, connectivity features of the ancestral amniote network were maintained, such that specific nuclei in the telencephalon of birds have homologous patterns of connections to that of the specific mammalian neocortical layers that subserve equivalent functions (Karten 1991, Karten 1997, Dugas-Ford *et al.* 2012, Faunes *et al.* 2015). In addition to this, gene expression analysis of several cell types in mammals and non-mammalian species has shown that some nuclei and layers that present the same pattern of connectivity also express similar gene networks (Karten 1997, Dugas-Ford *et al.* 2012, Briscoe and Ragsdale 2018). As a result, this evidence supports the hypothesis that projection neurons might be conserved in amniotes and have organised into lineage-specific morphological structures across evolution (Briscoe and Ragsdale 2018). Nevertheless, the precise correlation between sauropsid brain structures and homologous areas in the mammalian brain is still being debated, the major difficulty being that non-homologous anatomical structures can share homologous characteristics (Briscoe and Ragsdale 2018). Ideally, the definition of homology would require the addition of phylogenetic studies of the common ancestors, however these are predominantly extinct (Montiel *et al.* 2018). For this reason, the best approach to explore homology between structures is by combining molecular and developmental approaches, as well as analysis of embryological origin, cellular type,

and/or topology of connections (Striedter 1997, Striedter *et al.* 1997, Fernandez *et al.* 1998, Medina *et al.* , Puelles *et al.* 2000, Faunes *et al.* 2015).

In addition to an expansion in telencephalic size and the structural reorganisation of the dorsal telencephalon into a six-layered neocortex in early mammals, other features evolved exclusively in this group, including a diversification of telencephalic connectivity in mammals, which is particularly evident in eutherians, with the evolution of an additional tract connecting the two hemispheres of the brain: the corpus callosum (Owen 1837, Flower 1865, Rakic 1995, Molnár *et al.* 2006, Suárez *et al.* 2014b) (Figure 1.1). The mechanisms underlying the evolution of this new commissural tract still remain largely unknown.

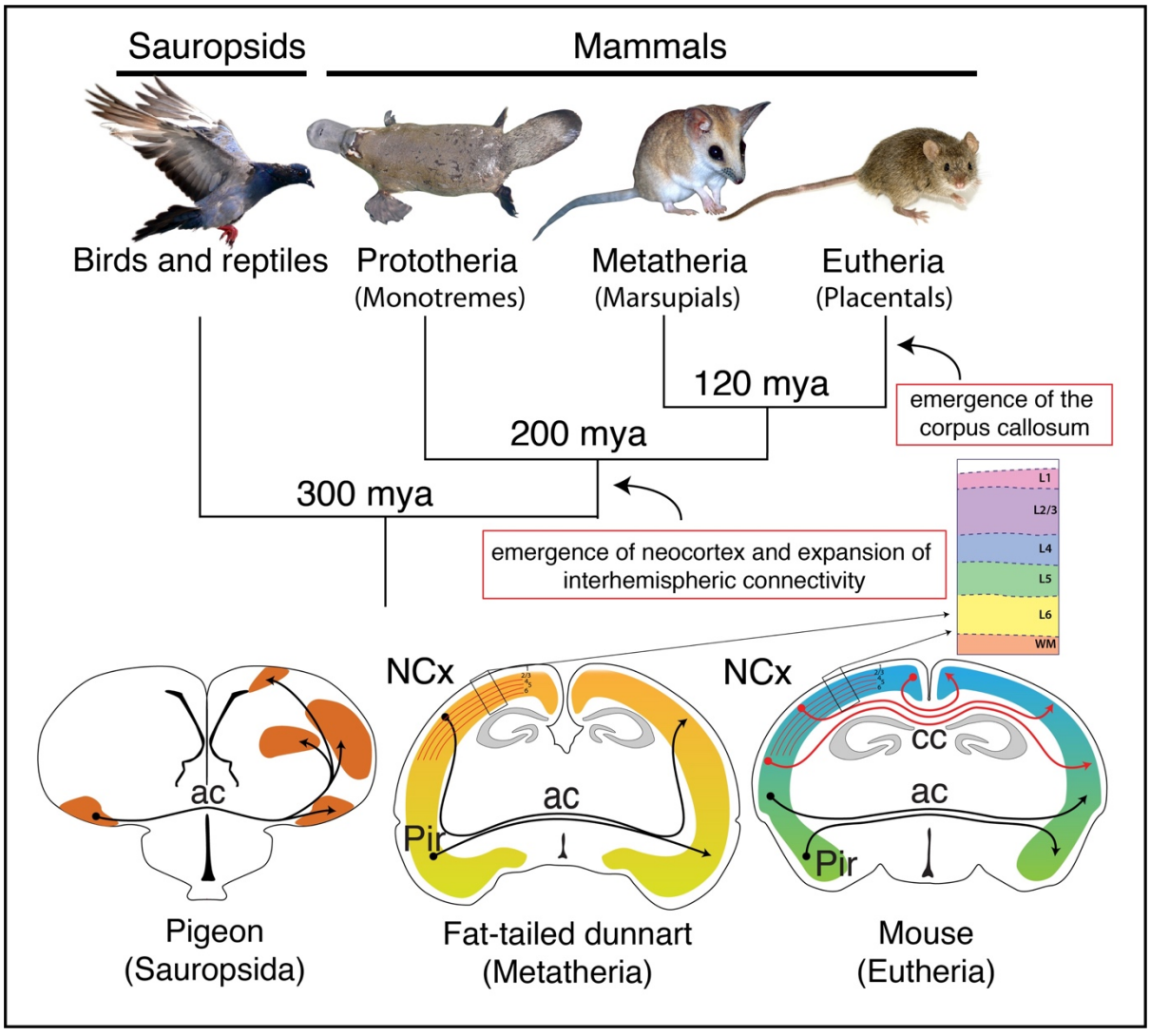

Figure 1.1: Evolution of the neocortex and cortical commissures.

During amniote evolution, early mammals evolved a neocortex (NCx), which differs substantially from the nuclear arrangement found in the telencephalon of birds and reptiles. The expansion of the

neocortex is also associated with an increase of interhemispheric connectivity derived from the dorsal pallium. Ac = anterior commissure, cc = corpus callosum, mya = million years ago, NCx = neocortex, Pir = piriform cortex. Adapted from Suárez *et al.* 2018.

1.2. Evolution of telencephalic connections

Previous studies have suggested that, despite the different morphological arrangement of the dorsal telencephalon of mammals, birds and reptiles, all vertebrates share similar populations of long-range projection neurons that express broadly conserved molecular markers (Briscoe and Ragsdale 2018, Tosches *et al.* 2018). These neuronal populations are involved in the formation of specific long-range circuits that are essential for the correct function of the telencephalon, and can be broadly categorised into those with targets outside of the cortex (subcortical) and those projecting within the cortex (corticocortical).

1.2.1. Evolution of subcortical projections

In all vertebrates, the telencephalon integrates sensory input coming from specific nuclei of the thalamus (Jones 1985), and produces outputs that project back to the thalamus, thus creating a topographically arranged feedback loop from the telencephalon, which is crucial for the integration and processing of complex information controlling animal behaviour (Jones 2002, Alitto *et al.* 2003, Csillag *et al.* 2005). In mammals, projections to the thalamus are known as corticothalamic projections and arise mostly from deep layer neurons located in layer (L) 6 of the neocortex (Thomson 2010).

Descending telencephalic pathways also control motor responses and connect other regions of the central nervous system across vertebrates, such as the striatum, the brainstem, and the spinal cord in mammals, and their complexity is associated with species-specific locomotor patterns (Ten Donkelaar 1988, Webster *et al.* 1990). For example, in non-mammalian tetrapods, motor responses are broadly controlled by telencephalic projections to the brainstem (Jarvis *et al.* 2005) and the rubrospinal pathway, which originates from the red nucleus of the midbrain (Ten Donkelaar 1982, Webster *et al.* 1990). On the other hand, in mammals, voluntary movements are under the control of an additional descending projection: the corticospinal tract, which connects the motor cortex directly to motoneurons in the spinal cord (Ten Donkelaar 1982, Webster *et al.* 1990, Welniarz *et al.* 2016). This tract arises from neurons located mostly in L5, and its size, length and spatial extent is highly variable, depending on the dexterity possessed by each mammalian species (Martin *et al.* 1970, Watson *et al.* 1977). The vast majority of the axons that form this descending tract project through the internal capsule and cerebral peduncle, to then cross the midline at the level of the pyramidal decussation, which is crucial for the lateralisation of motor control (Armand 1982, Marsh *et al.* 2017). Understanding the evolution and development of the corticospinal projection can help

us understand the causes and develop possible treatment for several developmental disorders characterised by altered motor functions (Welniarz *et al.* 2016, Marsh *et al.* 2017).

1.2.2. Evolution of interhemispheric connections

Corticocortical projection neurons extend their axons to the contralateral hemisphere and/or to other cortical regions within the same hemisphere (Economo *et al.* 2016, Fenlon *et al.* 2017, Swanson *et al.* 2017, Suárez *et al.* 2018). Relatively little is known about the evolution, development and function of neurons that project exclusively within the same hemisphere, so the evolution of interhemispheric connections will be the main focus of this section.

Commissural systems connecting the two cortical hemispheres can be found in both vertebrates and invertebrates, and are essential for the correct integration of lateralised sensory, motor and associative functions (Arendt *et al.* 2008, Semmler *et al.* 2010, Suárez *et al.* 2014b). During evolution, amphibians, birds, reptiles and mammals (all included in the Tetrapoda superclass of vertebrate) colonised different niches and evolved behavioural and locomotor adaptations, resulting in an increase in the connections between pallial regions compared to other vertebrates (Suárez *et al.* 2014b). Despite differences in commissural circuits between vertebrate species, a general plan of cellular and molecular organisation of the midline has been suggested to be conserved during evolution, with similar expression of morphogens guiding forebrain midline development and similar populations of guidepost neurons and glia affecting axonal crossing in vertebrates (Suárez *et al.* 2014b, Suárez 2017). However, the intricacies of the conserved and changed mechanisms underlying formation of these commissures throughout evolution remains to be elucidated.

Non-mammalian and mammalian vertebrates share the presence of two main telencephalic commissures, which also present similar features across tetrapods: the hippocampal and the anterior commissures (Suárez 2017). The axons crossing the midline via the hippocampal commissure of birds, for example, have been shown to be topographically arranged within the tract and connect broadly homotopic regions of the medial portion of the telencephalon, as well as heterotopic portions including the septum, the entorhinal cortex and the hypothalamus, similar to that of mammals (Atoji *et al.* 2002, Shinohara *et al.* 2012, Cui *et al.* 2013, Cappaert *et al.* 2015, Suárez 2017). This conserved organisation of the hippocampal commissure may be relevant to its function, or instead it could be a common by-product of its development across evolution without significant functional relevance.

The second shared interhemispheric telencephalic tract is the anterior commissure, which in mammals connects telencephalic regions in a bidirectional way, while in birds carries axons that are mostly unidirectional and broadly heterotopic, as they extend from neurons in the arcopallium and the posterior amygdala to reach the contralateral dorsal ventricular ridge and the striatum (Letzner *et al.* 2016, Paterson *et al.* 2017). It is still unclear whether this major difference in the axonal arrangement of the anterior commissure of birds and mammals is a result of an evolutionary specialisation of birds, or whether it represents the ancestral state before a reorganisation of the anterior commissure in other vertebrates (Suárez 2017).

In monotremes and marsupials, the anterior commissure is the main interhemispheric connection (Heath *et al.* 1971, Robinson 1982), which transfers information from both olfactory allocortical and neocortical parts of the pallium (Putnam *et al.* 1968, Heath and Jones 1971, Robinson 1982). In addition to this, in diprotodont marsupials, the anterior commissure also receives neocortical axons from the internal capsule via an additional tract, the fasciculus aberrans, which functions as a shortcut for axons arising from the neocortex (Smith 1902, Ashwell 2010). Eutherians also have an anterior commissure, but in these species it connects mainly olfactory structures (Pires-Neto *et al.* 1993, Cummings *et al.* 1996, Pires-Neto *et al.* 1998). In eutherians, neocortical axons instead project to the contralateral hemisphere via the corpus callosum, which allows for an increased number of interhemispheric connections in large brained species (Ashwell 2016) and has been speculated to afford faster integration of information between the two neocortices via a shorter cortical route, compared to the evolutionary more ancient anterior commissure (Mihrshahi 2006). However, evidence for this remains inconclusive, and it thus remains unclear whether the corpus callosum is functionally advantageous for eutherian mammals.

A major difference in terms of commissure development between marsupials and eutherians is the developmental context in which the forebrain connections appear. In marsupials, the development of forebrain interhemispheric tracts begins after birth (Molnár *et al.* 1998, Suárez *et al.* 2017), while in eutherian mammals it begins exclusively prenatally (Silver *et al.* 1982, Pires-Neto and Lent 1993, Ashwell *et al.* 1996, Lindwall *et al.* 2007). It is unclear whether these different commissural strategies may result from developmental constraints, due to the different gestational length between marsupials and eutherians. In addition to this, a different order in the appearance of cortical commissures has also been shown, whereby the development of the hippocampal commissure relative to the neocortical commissure appears to be delayed in marsupials, while in eutherian mammals neocortical axons cross the midline only once the hippocampal commissure has been formed (Ashwell *et al.* 1996, Ashwell *et al.* 1996). This could be due to the prenatal fusion of the two septal hemispheres in developing eutherian mammals that facilitates the early growth of the

dorsal hippocampal commissure and is essential for the formation of the corpus callosum in eutherian mammals, which does not occur in marsupials (Gobius *et al.* 2016, Gobius *et al.* 2017).

Despite these differences, it has been shown that marsupial and eutherian mammals share a common basic configuration of commissural systems in terms of initiation of commissure formation by pioneer axons through the formation of axon scaffolds (Pires-Neto and Lent 1993, Koester *et al.* 1994, Ware *et al.* 2015), and the production of attractive/repellent cues from glial cells located at the midline (Cummings *et al.* 1996, Pires-Neto *et al.* 1998, Shu *et al.* 2001). It has remained unclear whether other characteristics that have been described for the corpus callosum, such as the coexistence of homotopic and heterotopic connections, as well as a spatially segregated arrangement of axons within the tract (de Lacoste *et al.* 1985, Zhou *et al.* 2013), are typical of this eutherian novelty or are instead features of interhemispheric connectivity shared across mammals. These questions will be investigated in chapter 4.

1.3. Development and composition of the mammalian neocortex

The correct development of the six-layered mammalian neocortex and its connections requires a precise orchestration of events, which are often temporally overlapping, such as the generation, migration and differentiation of heterogeneous populations of neocortical neurons, as well as elongation and guidance of axons to their appropriate targets (Angevine and Sidman 1961, Takahashi *et al.* 1999, Rakic 2009). Both cell-autonomous and non-cell-autonomous developmental mechanisms are involved in regulating and balancing these processes, resulting in the molecular, cellular and anatomical heterogeneity of the neocortical projection neurons (Figure 1.2), which is fundamental for its correct function, including sensory integration, motor planning, social interaction, attention and learning (Gillies *et al.* 1993, McConnell 1995, Reillo *et al.* 2017). As most of the current knowledge about neocortical development comes from studies of eutherians, such as rodents, the following section explores the developmental events in neocortical formation in these mammalian species, with references to these mechanisms in other mammals, such as monotremes and/or marsupials, where they are known.

1.3.1. Subplate cells and marginal zone cells

The different layers of the mammalian neocortex are composed of heterogeneous classes of neurons, which are born in a controlled order (Rakic 1995, Molyneaux *et al.* 2009, Fame *et al.* 2011), with temporal control likely being an evolutionary conserved mechanism for neuronal

diversity generation throughout vertebrates (Pearson *et al.* 2004, Nomura *et al.* 2008, Cepko 2014, Lodato *et al.* 2015). One of the first events in the formation of the six-layered neocortex is the splitting of the first layer of neuroepithelium of the developing neocortex, the preplate, into the upper marginal zone (MZ) and the lower subplate (Gilmore *et al.* 1997). Later-born migrating neurons will localise between these two layers, forming the cortical plate and subsequent cortical layers (Allendoerfer 1994).

The cells of the subplate play several fundamental roles in cortical development; they are the earliest-generated neurons of the cortex, the earliest to mature and differentiate and the earliest to form cortical connections and complex neural circuits (Molliver 1973, Kostovic *et al.* 1980, König *et al.* 1981, Blue *et al.* 1983, Friauf *et al.* 1990, Allendoerfer 1994, Kanold 2003, Kanold *et al.* 2010, Hoerder-Suabedissen *et al.* 2015). The axons of the subplate cells pioneer the descending projections from early born deeper layer neurons of the cortical plate (Ghosh *et al.* 1993, McConnell *et al.* 1994). Moreover, subplate cells receive thalamic input before the thalamic axons reach the cortical plate and relay this input to newborn layer 4 neurons, via feed-forward glutamatergic excitation (Friauf *et al.* 1991, Allendoerfer *et al.* 1994, Molnár *et al.* 2003), and contribute to the guidance of thalamocortical axons towards the correct cortical layers (Ghosh *et al.* 1990, Ghosh and Shatz 1993, Allendoerfer 1994). Subplate cells are also crucial to the organisation of the cerebral cortex itself, such that their removal during the development of the cortex affects the correct formation of its overall functional architecture (Kanold 2003). In addition to this, it has been recently suggested that subplate cells might also regulate the speed of neuronal migration during cortical development by controlling neuronal shape from multipolar to bipolar (Ohtaka-Maruyama *et al.* 2018).

Across evolution, species phylogenetically closer to humans display a larger subplate area relative to the cortical plate, with higher cell density, suggesting that a more complex brain architecture evolved in concert with an increased ratio of subplate cells (Kostovic *et al.* 1990). Interestingly, the existence of a subplate region in marsupial species has been questioned in the past (Harman *et al.* 1995, Marotte *et al.* 2000, Reep 2000), as its identification is challenged by the absence of a waiting period of thalamocortical axons at the subplate (Pearce *et al.* 2003), as well as differences in the timing of neuronal maturation and structural organisation in marsupials compared to eutherian mammals (Harman *et al.* 1995, Marotte and Sheng 2000, Reep 2000). Indeed, in marsupials, deeper layer neurons mature relatively earlier compared to eutherians, and then migrate to form rapidly expanding layers of loosely packed cells, such that the boundary between the cortical plate and the subplate is less distinct (Reynolds 1985, Marotte *et al.* 1997, Molnár *et al.* 1998). Despite these challenges, further studies in the opossum aiming to analyse the expression of

subplate markers, such as Nurr1 and Moxd1 (Wang *et al.* 2011), together with topographical and functional studies in the opossum and in the wallaby (Pearce and Marotte 2003, Wang *et al.* 2011), have demonstrated the presence of putative subplate cells in marsupials, although they are more dispersed, with less defined layer boundaries than the equivalent structure in eutherians (Pearce and Marotte 2003).

Another group of early-generated cells in the cortical plate includes the Cajal-Retzius (CR) cells of the marginal zone. This neuronal population, which originates from different brain regions and then migrate tangentially to form L1 of the cortical surface (Takiguchi-Hayashi *et al.* 2004, Bielle *et al.* 2005, Nomura *et al.* 2008, de Frutos *et al.* 2016), has a complex cytochemistry, expressing different molecules at different times, which suggests that they regulate different functions throughout cortical development (Marín-Padilla 1998). It has indeed been shown that CR cell appearance in the cortex predates the splitting of the preplate (Mallamaci *et al.* 2000) and that they regulate the migration, the inside-out stratification pattern and differentiation of the later born neurons of the cortical plate through a combination of cell-cell interaction mechanisms (D'Arcangelo *et al.* 1995, Ogawa *et al.* 1995, Frotscher 1997, Marín-Padilla 1998, de Frutos *et al.* 2016), as well as the secretion of the guidance molecule Reelin (Gil-Sanz *et al.* 2013). Interestingly, despite this body of evidence, a paper by Yoshida *et al.* showed that, when the cortical hem is genetically ablated, causing an absence of CR cells in the MZ, neocortical layers maintain a correct order of anatomical organisation. The authors suggest that the small amount of Reelin produced by the few CR cells still present in mice with an ablated hem is likely sufficient for correct neocortical layering (Yoshida *et al*. 2006).

The expression of CR markers, such as Calretinin, and especially Reelin, have also been identified in the marsupial developing cortex, specifically in CR cell birthplaces that have already been described in eutherian mammals, such as the ventral pallium and the septum (Takiguchi-Hayashi *et al.* 2004, Bielle *et al.* 2005, Puzzolo and Mallamaci 2010), confirming the conservation of this cell population across evolution (Meyer 2010).The only known difference between mammalian lineages in this population is in the timing of CR cell development in marsupials, which occurs after preplate splitting, suggesting that CR cells may not be necessary for this process, but might still be required for proper inside-out organisation of the six-layered neocortex (Puzzolo and Mallamaci 2010).

1.3.2. Radial glia and intermediate progenitors

Subplate and CR cells play crucial roles in establishing the organisation of the cortical plate, which is composed of heterogeneous neuronal populations originating from multipotent radial glial

cells located in the ventricular zone, where they proliferate (Angevine and Sidman 1961, Sauerland *et al.* 2016) and from where they extend long processes that guide newborn cells during their migration within the cortical plate (Campbell *et al.* 2002). The way in which few multipotent progenitor cells give rise to the immense heterogeneity of neurons, as well as glial cells, in the mammalian neocortex is still debated and many hypotheses have arisen over the years (Rossi *et al.* 2016). According to the "sequential hypothesis", different neuronal populations located in deeper and upper layers of the neocortex arise from the same multipotent precursors in a sequential way (McConnell 1988, Frantz *et al.* 1996, Desai *et al.* 2000, Lai *et al.* 2008, Gao *et al.* 2014, Okamoto *et al.* 2016, Kaplan *et al.* 2017, Guo *et al.* 2013, Eckler *et al.* 2015). In contrast with this view, it has been suggested that different subtypes of radial glial cells might be fate-restricted and committed from the beginning to produce a selected lineage of cells or population of neurons (Franco *et al.* 2012, Gil-Sanz *et al.* 2015). Other studies put forward the possibility of merging these two views, suggesting that, in the mammalian neocortex, there might be a spatial and temporal coexistence of radial glial cells that sequentially produce different neurons and radial glial cells that produce only a specific neuronal population (García-Moreno *et al.* 2015). According to this last scenario, the fate-restricted radial glial cells are initially non-neurogenic and divide symmetrically within the ventricular zone, thus producing two identical multipotent cells and increasing the pool of progenitor cells (Molnár *et al.* 2014, García-Moreno and Molnár 2015). As cortical development proceeds, fate-restricted radial glial cells then start to divide asymmetrically, producing a specific neuronal lineage. The asymmetric division of radial glial cells can give rise to either neurogenic committed cells or to transient amplifying intermediate progenitor cells, which amplify the neuronal production in the subventricular zone, thus contributing to the expansion of the neocortex during evolution (Noctor *et al.* 2004, Kriegstein *et al.* 2006, Martínez-Cerdeño *et al.* 2006, Molnár 2011, Molnár *et al.* 2014, García-Moreno and Molnár 2015). Indeed, larger and more diverse intermediate progenitor populations correlate with brain size, as well as with neuronal diversity and density, across species (Molnár 2011, Molnár *et al.* 2016). Interestingly, in line with this hypothesis, it has been shown that in marsupials, which have a neocortex characterised by lower neuronal density compared with eutherians (Seelke *et al.* 2013, Seelke *et al.* 2014), the band of dividing cells within the subventricular zone emerges relatively later in development than in mouse (Cheung *et al.* 2010).

The transition from a proliferative to neurogenic state, specifically from radial glial cells to intermediate progenitor cells and from intermediate progenitor cells to differentiated neurons, is under strict molecular regulation, such that these cellular populations at different stages of differentiation are specified by the expression of transcription factors that can regulate neuronal differentiation (Götz *et al.* 1998, Hevner *et al.* 2001, Englund *et al.* 2005, Okamoto *et al.* 2016). For

example, radial glial cells, which produce both neurons and glia and divide at the ventricular zone, are characterised by the expression of PAX6; PAX6 is then downregulated in favour of TBR2 expression in intermediate progenitor cells, which are generated from radial glia, and which proliferate in the subventricular zone and give rise to exclusively neuronal populations. Postmitotic neurons downregulate TBR2 and instead express TBR1, and/or other transcription factors that specifically define their projection fate (Götz *et al.* 1998, Hevner *et al.* 2001, Englund *et al.* 2005, Sessa *et al.* 2008), as further described in detail in section 1.5 below. Comparable mRNA and protein expression patterns of important developing transcription factors specifying radial glial cells (PAX6), intermediate progenitor cells (TBR2) and postmitotic neurons (TBR1, TLE4, CUX1, CUX2, NEUROD6) have been described in marsupials as well, suggesting that some aspects of the transcriptional regulation of neuronal differentiation might be conserved across therian mammals (Cheung *et al.* 2010, Puzzolo and Mallamaci 2010, Sauerland *et al.* 2016). The majority of the transcription factors so far identified in marsupials belong to a general and early molecular network of neuronal differentiation, while the molecular specification of later stages of cortical development are yet to be fully elucidated in non-eutherian mammalian species.

1.3.3. Interneurons and pyramidal neurons

In eutherians and marsupials, the neurons that populate the six-layered neocortex can be broadly divided into two major populations that differ in their origins and migration into the neocortex, as well as in their morphological and functional features: interneurons and pyramidal neurons (Parnavelas 1991, Luskin 1993, Mione *et al.* 1994, Puzzolo and Mallamaci 2010). Interneurons arise from neuroepithelial compartments in the subpallium (e.g., ganglionic eminences) and migrate tangentially, occupying all the layers of the neocortex. They have a multipolar morphology and their axons arborize locally, creating inhibitory circuits due to the action of GABA as their main neurotransmitter (Anderson *et al.* 1997, Lavdas 1999, Molnár *et al.* 2006, Puzzolo and Mallamaci 2010). Several subtypes of interneurons exist in the mammalian brain (Rudy *et al.* 2011, Kepecs *et al.* 2014, Tremblay *et al.* 2016) and their heterogeneity is defined by their specific birthplace within the ventral subpallium, and by their specific post-mitotic transcriptional program, which determines cellular location, morphology, connectivity and physiological properties (Mi *et al.* 2018). For example, interneurons originating from the lateral ganglionic eminence mostly migrate ventrally and anteriorly to the striatum, nucleus accumbens, olfactory tubercle and olfactory bulb. On the other hand, interneurons that are born in the medial ganglionic eminence migrate dorsally and invade developing neocortex (Lavdas 1999, Corbin *et al.* 2001, Wichterle 2001, Nery *et al.* 2002, Métin *et al.* 2006). The different origin of each population

of interneurons is also reflected in the different markers that they express: for example, interneurons expressing parvalbumin are mainly generated in the ventro-medial ganglionic eminence, those expressing the neuropeptide somatostatin come from the dorso-medial ganglionic eminence and those producing the ionotropic serotonin receptor 5HT3aR are predominantly born in the caudal ganglionic eminence (Rudy *et al.* 2011, Tremblay *et al.* 2016).

Pyramidal neurons of the mammalian neocortex arise locally from radial glial progenitors at the ventricular zone of the pallium, in both eutherians and marsupials. They then migrate radially towards the pial surface along radial glial processes to localise in specific layers in an inside-out fashion, whereby early-born neurons remain in deeper layers and later neurons migrate across these to populate the upper layers (Angevine and Sidman 1961, Campbell and Götz 2002, Li *et al.* 2018). They have a pyramidal shape with basal and apical dendrites and long axons that extend within the cortex or to subcortical targets, forming the major tracts in the brain. Additionally, pyramidal neurons employ glutamate to exert excitatory transmission onto target cells (Rakic 1995, Molnár *et al.* 2006). Circuit mapping experiments using retrograde tracers in eutherians have demonstrated three major types of excitatory long-range projection neurons in the neocortex: 1) corticothalamic projection neurons, located in L6, which send connections to reciprocal regions of the sensory thalamus (McKenna *et al.* 2011, Kim *et al.* 2014); 2) subcerebral projection neurons, which occupy L5 and project to subcerebral targets, such as the midbrain, hindbrain and spinal cord (Arlotta *et al.* 2005, Chen *et al.* 2008); and 3) corticocortical projection neurons, which are located primarily in L2/3 and 5 of the cortex, and extend their axons to the contralateral hemisphere through the corpus callosum, as well as to other areas of the same hemisphere (Economo *et al.* 2016, Fenlon *et al.* 2017, Swanson *et al.* 2017). These neuronal populations differentiate at different stages of cortical development and express different combinations of transcription factors that trigger specific developmental programs of neuronal fate, axon guidance and long-range targeting, as described in section 1.5 and further investigated in chapter 6.

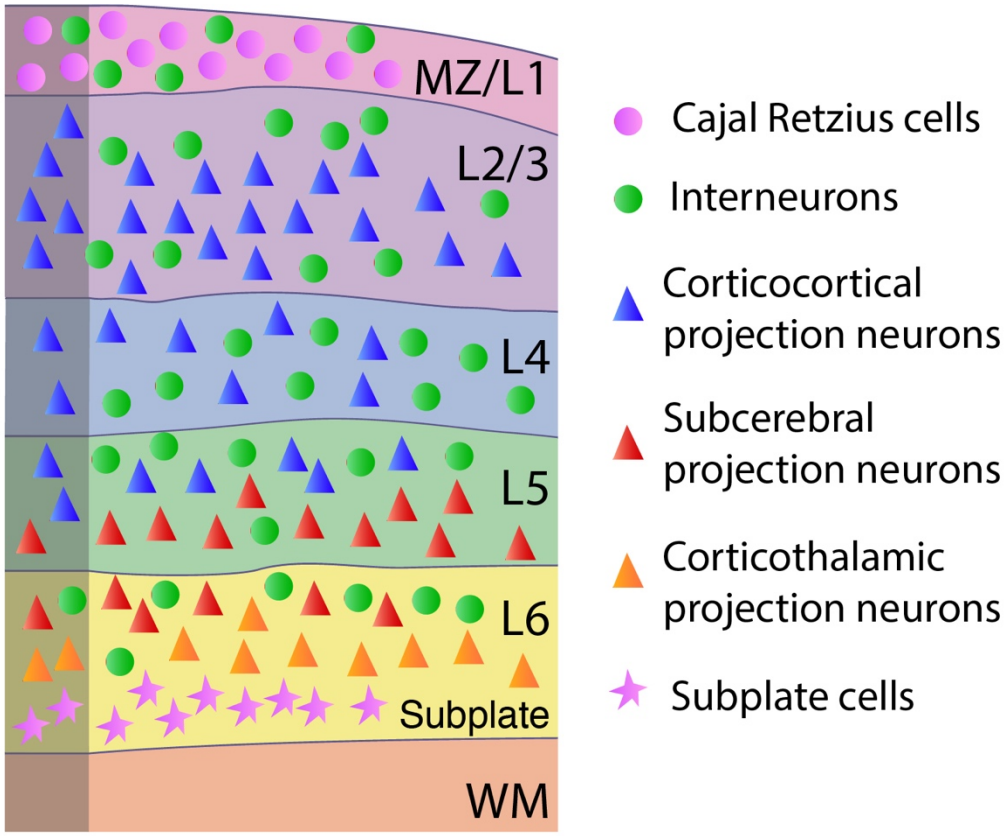

Figure 1.2: Schematic depicting the heterogeneity of neocortical cell populations.

Corticocortical projection neurons (blue) are mainly localised in layers (L) 2/3 and 5 of the neocortex, but also in L4. Subcerebral projection neurons (red) can be found mainly in L5, but also in L6, where most corticothalamic projection neurons (orange) reside. Interneurons (green) arrive to the neocortex after tangential migration from the subpallium and occupy all layers. Cajal-Retzius cells (pink circles) are located in the marginal zone (MZ), which becomes L1, and subplate cells (pink stars) in deep L6, above the white matter (WM); the majority of neurons from both of these latter two populations die postnatally after playing organisational roles during cortical layers development.

1.4. Development of telencephalic connections

Eutherian mammals, such as rodents and primates, have been widely employed as animal models to study brain development and, as a result, much more has been discovered about the formation of the telencephalon and its connections in this group than in non-eutherian mammals. The following section explores the formation of cortical projections in eutherians, as well as in monotremes and/or marsupials, when known.

1.4.1. Development of subcortical projections

In all mammals, descending cortical projections extend from the deeper layers of the neocortex and reach targets such as the midbrain, the hindbrain, the spinal cord (subcerebal projections), as well as the thalamus (corticothalamic projections) (Arlotta *et al.* 2005, Chen *et al.* 2008, McKenna *et al.* 2011, Kim *et al.* 2014). In rodents, it has been shown that, despite the coexistence of commissural and subcerebral projection neurons in the deeper layers of the neocortex, descending axons via the internal capsule arise before the axons forming the corpus callosum, as lateral projections reaching subcortical targets are extended before medial projections (Richards *et al.* 1997). During eutherian cortical development, several transcription factors have been shown to be involved in the regulation of this initial lateral axonal elongation (Lickiss *et al.* 2012) and in the further differentiation into corticothalamic and subcerebral projection fates, as further described in section 1.5. For example, L6 corticothalamic neurons express the transcription factor TBR1 and project through the internal capsule to reach the nearby thalamus in the dorsal diencephalon, while L5 corticospinal neurons express FEZF2 and its downstream effector CTIP2 and their axons descend through the cerebral peduncle to target further regions of the superior colliculus, ventral hindbrain and spinal cord (Bedogni *et al.* 2010, Han *et al.* 2011, McKenna *et al.* 2011). Most of the transcription factors involved in specifying subcerebral neuronal fate have also been found in homologous neurons in marsupials (Cheung *et al.* 2010, Puzzolo and Mallamaci 2010), and their patterns of terminations are broadly conserved with that of eutherians, except for the shorter corticospinal tract (Ashwell 2010).

1.4.2. Development of neocortical commissures

The main feature of the brain of eutherians that differs from all non-eutherian mammals is the evolution of the corpus callosum as an additional interhemispheric tract in the dorsal midline. This evolutionary innovation involved a medio-dorsal projection of the axons extending from

commissural neurons, whereas in non-eutherians these axons turn latero-ventral to cross the midline at the anterior commissure. While in eutherians the anterior commissure connects the anterior olfactory nucleus and the anterior piriform cortex (anterior limb, pars olfactoria), the perirhinal and rostral cortex (posterior limb, pars interhemispherica) and regions of the amygdala (stria terminalis) (Pires-Neto and Lent 1993, Cummings *et al.* 1996, Pires-Neto *et al.* 1998), in marsupials the anterior commissure is the major commissure connecting all those targets, plus most neocortical areas and cingulate cortices (Putnam *et al.* 1968, Heath and Jones 1971, Robinson 1982). Studies in hamsters and rats have shown that, in these species, the pioneering fibres of the anterior commissure, which extend from neurons located in the olfactory (piriform) cortex, cross the midline from embryonic day (E) 14 and E16, respectively (Santacana *et al.* 1992, Pires-Neto and Lent 1993, Silver 1993, Pires-Neto *et al.* 1998), using chemical and physical cues from surrounding guidepost glial cells (Silver *et al.* 1982, Silver 1993, Cummings *et al.* 1996, Pires-Neto *et al.* 1998). Similarly, in marsupials, such as American opossums and Australian wallabies, axons forming the developing anterior commissure cross the midline under the guidance of GFAP-immunoreactive glia through a region of wide extracellular space, and this process occurs postnatally (Cabana *et al.* 1985, Ashwell *et al.* 1996, Cummings *et al.* 1996, Molnár *et al.* 1998). After the second postnatal week, the anterior commissure is thick and histologically visible in these species (Ashwell *et al.* 1996, Ashwell *et al.* 1996, Shang *et al.* 1997), and when it reaches its morphological maturity, neither the extracellular space nor the glial cells are visible (Cummings *et al.* 1996).

The emergence of the corpus callosum in eutherians, which is the largest fibre tract within their central nervous systems (Funnell *et al.* 2000, Houzel *et al.* 2002), allowed a further expansion of interhemispheric connectivity (Suárez *et al.* 2014b, Ashwell 2016), as well as a possible faster transmission of information compared to the anterior commissure, due to the shorter route taken by neocortical axons (Mihrshahi 2006). The formation of the corpus callosum is regulated by a complex interplay of cell-autonomous mechanisms, with the expression of specific transcription factors regulating projection fate and the initial axonal extension (see section 1.5 and Table 1.1), as well as non-cell-autonomous mechanisms, such as contact and secreted cues produced by neighbouring cells (Lindwall *et al.* 2007). The formation of the corpus callosum thus involves finely timed developmental steps, including initial axon elongation, midline crossing and contralateral targeting.

In mice, the callosal tract is pioneered by axons extending from cingulate neurons, which project across the midline and enter the contralateral hemisphere by E15.5 (Koester and O'Leary 1994, Rash *et al.* 2001). By E16, neocortical commissural neurons project their axons dorso-medially towards the midline, while they are still migrating into their specific neocortical layers

(Shoukimas *et al.* 1978, Schwartz *et al.* 1991, Noctor *et al.* 2004), with particular initiation of axonal growth within the intermediate zone (Lickiss *et al.* 2012, Hatanaka *et al.* 2016). Previous studies in mice have shown that this process of initial axonal elongation coincides with the onset of expression of specific transcription factors, such as SATB2 and NGN2, suggesting that these proteins might be involved in the initial phase of the dorso-medial axonal elongation (Hand *et al.* 2011, Lickiss *et al.* 2012, Hatanaka *et al.* 2016). As previously stated, in marsupials, mature commissural neurons project their axons laterally to cross the midline via the anterior commissure. However, it is still unclear whether this might be due to a specific initial axonal elongation exclusively directed laterally, or whether it is the consequence of a process of branching, in both medial and lateral directions, followed by pruning of axons that did not reach the contralateral hemisphere. Similarities and differences between mouse and dunnarts in terms of development of cortical projections and transcriptional regulation of these events will be explored in chapters 5 and 6, to better understand the medial-lateral initial axonal extension in these two mammalian lineages.

Transcriptional regulators can affect the initial axonal elongation of long-range projection neurons cell-autonomously, by regulating the expression of axon guidance genes in a neuron-specific manner (Lickiss *et al.* 2012, Molyneaux *et al.* 2015), as further described in section 1.5, but also in a non-cell-autonomous way. Examples of the latter include controlling the development and positioning of guidepost cells, which guide axons to their appropriate targets by releasing cues in strategic positions (Benadiba *et al.* 2012, Lavado *et al.* 2014), as well as guiding correct fasciculation within the tract (Zhou *et al.* 2013), and the correct formation of tissue substrates for axonal growth (Gobius *et al.* 2016). For example, different glial populations located at the midline play an essential role in the formation of interhemispheric commissures in mammals, actively creating a scaffold that permits axonal growth and midline crossing (Gobius *et al.* 2016) and/or secreting guidance cues that act as repellent or attractive cues for axons, thus influencing axonal directionality (Silver *et al.* 1982, Norris *et al.* 1991, Lindwall *et al.* 2007). The correct development, position, orientation and morphology of glial cells at the midline is thus required for the formation of the corpus callosum in eutherians (Shu and Richards 2001, Tole *et al.* 2005, Smith *et al.* 2006, Gobius *et al.* 2016). Among these glial populations, particularly crucial are the cells forming the glial wedge (Shu and Richards 2001, Shu 2003, Lent *et al.* 2005, Andrews *et al.* 2006, Darki *et al.* 2016, Calloni *et al.* 2017), as well as the indusium griseum (Shu and Richards 2001, Shu 2003), which express several chemorepellent molecules that act to channel callosal axons through a specific corridor through the midline territory (Shu and Richards 2001, Shu 2003, Lent *et al.* 2005, Andrews *et al.* 2006, Darki *et al.* 2016, Calloni *et al.* 2017). The midline zipper glia also play a critical role in callosal development by secreting cues that provide turning signals to the crossing

axons (Silver 1993, Shu and Richards 2001, Shu 2003, Shu *et al.* 2003, Gobius *et al.* 2016), as well as actively remodelling the interhemispheric fissure in eutherians, thus creating a permissive substrate for callosal axons to cross the midline and reach the contralateral hemisphere (Gobius *et al.* 2016). Similar to eutherians, in marsupials, glial cells are located at the midline and have been shown to be involved in the formation of the anterior commissure (Cummings *et al.* 1996, Pires-Neto *et al.* 1998). However, in marsupial adult brains, the interhemispheric fissure is fully retained, as the midline glia do not intercalate during brain development and do not remodel the interhemispheric fissure (Gobius *et al.* 2017). This suggests that, despite the conserved presence of midline glia in developing marsupials (Cummings *et al.* 1996, Gobius *et al.* 2017), their role in remodelling the interhemispheric fissure appeared with the emergence of the corpus callosum in eutherian mammals (Gobius *et al.* 2017).

Once the neocortical commissural axons have reached and crossed the midline, they are repelled from this region and continue their elongation towards their appropriate targets in the contralateral hemisphere to finalise their development. Contralateral targeting of commissural neurons is a relatively understudied process (Fenlon and Richards 2015, Fenlon *et al.* 2017), dependent on the coordinated expression of multiple guidance factors, which are integrated at the level of the growth cone, ultimately determining its trajectory (Bagnard *et al.* 1998). In mice, axons extending from commissural neurons located in the upper layers, which contains the majority of callosal neurons in the neocortex, cross the midline at P3 (Wang *et al.* 2007). By P5 they reach the contralateral white matter, contacting the deeper layers of the contralateral hemisphere by P6 and the superficial layers by P7 (Wang *et al.* 2007, Fenlon *et al.* 2017). During the second postnatal week, the region- and layer-specific contralateral innervation and arborisation of callosal neurons takes place and the electrical activity of these neurons during the early postnatal period is crucial for establishing correct contralateral targeting, suggesting the importance of environmental influence on this process (Wang *et al.* 2007, Zhou *et al.* 2013, Mizuno *et al.* 2014, Suárez *et al.* 2014a, Fenlon *et al.* 2017). Once callosal axons have reached the contralateral hemisphere, they project to predominantly homotopic regions (Yorke *et al.* 1975, Krubitzer *et al.* 1998, Rash and Richards 2001, Hofer *et al.* 2006, Fenlon *et al.* 2017), and the order in which the axons are arranged within the corpus callosum correlates with their contralateral projections, with axons located dorsally projecting more medially and axons located ventrally projecting more laterally (Zhou *et al.* 2013). In addition to the homotopic projections (Gazzaniga *et al.* 1962, Witelson 1985, Gazzaniga 2000), callosal axons also project to heterotopic cortical areas, such as dorso-medial regions of the cortex (Boyd *et al.* 1971, Sloniewski *et al.* 1986, Kretz *et al.* 1990, Alboitiz *et al.* 2003, Smith *et al.* 2014, Wang *et al.* 2016, Fenlon *et al.* 2017, Suárez *et al.* 2018). Similar to the corpus callosum in

eutherians, the anterior commissure connects neocortical portions of the telencephalon in monotremes and marsupials, but it has remained unclear whether this commissure shares the same pattern of organisation as the corpus callosum, with a topographical rearrangement of the axons within this interhemispheric tract and bilateral connection of homotopic as well as heterotopic neocortical regions (de Lacoste *et al.* 1985, Tovar-Moll *et al.* 2007, Zhou *et al.* 2013). These aspects are investigated in chapter 4 of this thesis.

The fact that commissural neurons that are broadly located within the same cortical regions project to either homotopic or heterotopic areas of the contralateral hemisphere (Fenlon *et al.* 2017, Suárez *et al.* 2018), similar to the presence of both subcerebral and corticocortical neurons within L5, suggest that the differential expression of transcription factors in neuronal populations might also be involved in regulating axonal projection fate (Fenlon and Richards 2015, Fenlon *et al.* 2017), as further examined in the following section.

1.5. Transcriptional regulation of axon guidance in long-range neocortical neurons

Corticothalamic, subcerebral and corticocortical projection neurons are born at different stages of cortical development (Angevine and Sidman 1961, Li *et al.* 2018) and express different combinations of regulatory genes that trigger specific developmental programs of neuronal fate (Alcamo *et al.* 2008, Britanova *et al.* 2008, Chen *et al.* 2008, Han *et al.* 2011, Guo *et al.* 2013, Greig *et al.* 2016, Woodworth *et al.* 2016, Nomura *et al.* 2018). Although the precise mechanisms of action of these transcriptional networks remain unknown, it has been suggested that amongst their functions is the regulation of differential expression of axon guidance genes (Alcamo *et al.* 2008, Molyneaux *et al.* 2009, Paolino *et al.* 2018).

Corticothalamic projection neurons are born at E12 in mice, they are located in L6 and are characterised by the expression of TBR1 and its downstream effector TLE4, with knockout mice for these genes lacking both the corticothalamic and reciprocal thalamocortical projections (Bedogni *et al.* 2010, McKenna *et al.* 2011, Galazo *et al.* 2016). It has been previously shown that the axon guidance gene *Epha7*, which plays a critical role in the guidance of corticothalamic axons (Torii *et al.* 2013, Son *et al.* 2016), is highly enriched in TLE4-positive neurons (Molyneaux *et al.* 2015), suggesting that TLE4 might be responsible for EPHA7 expression. Corticothalamic projection neurons also express FOXP2 (Hisaoka *et al.* 2010, Galazo *et al.* 2016), and ZFPM2 (FOG2), which controls corticothalamic neuronal identity and axonal targeting by downregulating the expression of CTIP2 (Galazo *et al.* 2016) (Table 1.1, Figure 1.3).

Subcerebral projection neurons migrate past the layer of corticothalamic neurons (L6) to located in L5, and extend their axons forming the main descending tracts of the neocortex, including corticotectal, corticobulbar and corticospinal projections. In mice, these neurons are characterised by the expression of the transcription factors BCL6, CTIP2 (BCL11B), FEZF2 (FEZL), and SOX5 (Arlotta *et al.* 2005, Chen *et al.* 2005, Chen *et al.* 2008, Lai *et al.* 2008, Leamey *et al.* 2008, Srinivasan *et al.* 2012). These transcription factors are essential for corticofugal projection formation, such that knockout mice for these genes fail to form the corticospinal tract (Arlotta *et al.* 2005, Chen *et al.* 2005, Chen *et al.* 2008, Lai *et al.* 2008, Leamey *et al.* 2008, Srinivasan *et al.* 2012). CTIP2 has been suggested to regulate the initial axonal extension of subcortical projection neurons laterally, as they migrate through the intermediate zone (Lickiss *et al.* 2012, Hatanaka *et al.* 2016) (Figure 1.4). Moreover, axon guidance genes regulating the formation of the corticospinal tract, such as *Ephb1* (Lodato *et al.* 2014), were found to be highly enriched in CTIP2-positive neurons (Molyneaux *et al.* 2015), suggesting that this transcription factor might regulate subcerebral projection fate directly or indirectly regulating the expression of axon guidance genes. Subcerebral projection neurons are also characterised by the expression of the transcription factor BHLHE22 (BHLHB5), which is a postmitotic regulator of area identity; *Bhlhe22*-knockout mice show disorganisation of the barrels in the somatosensory cortex, as well as altered differentiation of corticospinal neurons in the motor cortex (Joshi *et al.* 2008) (Table 1.1).

The majority of migrating corticocortical projection neurons reach L2/3 and L5 by E19-20 (Shoukimas and Hinds 1978, Smart and Smart 1982), and extend their axons to the contralateral hemisphere through the corpus callosum in eutherian mammals, through the anterior commissure in non-eutherian mammals, and/or to other cortical regions within the same hemisphere (Economo *et al.* 2016, Fenlon *et al.* 2017, Swanson *et al.* 2017). In eutherians, callosal neurons located in both L2/3 and L5 are largely characterised by the expression of the transcription factor SATB2 (Alcamo *et al.* 2008, Britanova *et al.* 2008, Molyneaux *et al.* 2009, Srinivasan *et al.* 2012), which in the brain is exclusively expressed in cortical neurons (Zhang *et al.* 2012). Previous studies in mice have suggested that SATB2, as well as NGN2, might regulate the initial axonal elongation of callosal neurons medially, as they migrate through the intermediate zone, thus determining the projection fate of neocortical neurons in a cell-autonomous way (Hand and Polleux 2011, Lickiss *et al.* 2012, Hatanaka *et al.* 2016) (Figure 1.4). Indeed, it has been shown that when *Satb2* or *Ngn2* genes are knocked out in mice, commissural axons fail to project medially towards the corpus callosum and instead project laterally (Alcamo *et al.* 2008, Britanova *et al.* 2008, Hand and Polleux 2011), reaching subcortical targets via the internal capsule, and the contralateral hemisphere through the anterior commissure (Alcamo *et al.* 2008, Britanova *et al.* 2008). It has been previously shown that

SATB2-positive callosal neurons express high levels of axon guidance genes such as *Unc5c*, *Plxna4*, and *Epha4* (Molyneaux *et al.* 2015), which in additional studies were shown to be downregulated in *Satb2*-knockout animals, further suggesting that they are directly or indirectly regulated by SATB2 (Alcamo *et al.* 2008) (Figure 1.3). In addition to this, *Unc5c* and *Epha4* have also been shown to be necessary for callosal development, and restoring their expression in *Satb2* mutants partially rescues the formation of the corpus callosum (Srinivasan *et al.* 2012, Srivatsa *et al.* 2014). From early stages of development, L2/3 and L5 callosal neurons also express the transcription factor LMO4, which is crucial for neuronal differentiation (Asprer *et al.* 2011), as well as CITED2, which acts in progenitor cells to establish callosal identity (Molyneaux *et al.* 2009, Fame *et al.* 2016). In addition to this, L2/3 and L5 callosal neurons are characterised by the expression of LHX2, which specifies a callosal fate, especially during deeper layer neurogenesis (Muralidharan *et al.* 2017). Some transcriptional regulators are also exclusively expressed in neurons located in L2/3, such as the transcription factors CUX1 and CUX2, which regulate axonal projections through the corpus callosum (Rodríguez-Tornos *et al.* 2016), dendritic branching, spine formation and synaptogenesis (Cubelos *et al.* 2014), as well as POU3F3 and POU3F2 (BRN1 and BRN2), which are crucial for neuronal positioning (Sugitani *et al.* 2002) and formation of callosal projections (Oishi *et al.* 2016). Similarly, a recent study identified the transcription factor FOXG1 as a major regulation of callosal neuron migration, layering and axonal fasciculation and targeting, possibly via regulation of SATB2 and axon guidance genes such as ROBO1 and SLIT3 (Cargnin *et al.* 2018), further highlighting the roles of transcriptional networks in the control of cortical wiring.

Corticocortical projection neurons	Subcerebral projection neurons	Corticothalamic projection neurons
L2/3 and L5	**L5**	**L6**
Cited2 (Molyneaux *et al.* 2009)	*Bcl6* (Arlotta *et al.* 2005, Leamey *et al.* 2008)	*Cxxc5* (Galazo *et al.* 2016, Kim *et al.* 2016)
Foxg1 (Cargnin *et al.* 2018)	*Bhlhe22* (*Bhlhb5*) (Joshi *et al.* 2008, Molyneaux *et al.* 2015)	*Foxp2* (Hisaoka *et al.* 2010, Molyneaux *et al.* 2015, Galazo *et al.* 2016)
Lhx2 (Molyneaux *et al.* 2015, Muralidharan *et al.* 2017)	*Ctip2* (*Bcl11b*) (Arlotta *et al.* 2005, Chen *et al.* 2008, Srinivasan *et al.* 2012)	*Gse1* (Galazo *et al.* 2016)
Lmo4 (Molyneaux *et al.* 2009, Asprer *et al.* 2011)	*Fezf2* (*Fezl*) (Chen *et al.* 2005, McKenna *et al.* 2011)	*Nfe2l3* (*Nrf3*) (Molyneaux *et al.* 2015)
Ngn2 (Hand and Polleux 2011)	*Sox5* (Arlotta *et al.* 2005, Lai *et al.* 2008)	*Tbr1* (McKenna *et al.* 2011)
Satb2 (Alcamo *et al.* 2008, Britanova *et al.* 2008)	*Tcerg1l* (Molyneaux *et al.* 2015)	*Tle4* (Galazo *et al.* 2016)
Ski (Baranek *et al.* 2012)	*Zfp703* (Molyneaux *et al.* 2015)	*Zfpm2* (*Fog2*) (Galazo *et al.* 2016)
Tle3 (Molyneaux *et al.* 2015)		
L2/3		
Cux1 (Cubelos *et al.* 2014, Rodríguez-Tornos *et al.* 2016)		
Cux2 (Molyneaux *et al.* 2009, Cubelos *et al.* 2014)		
Pou3f2 (*Brn2*) (Molyneaux *et al.* 2009, Oishi *et al.* 2016)		
Pou3f3 (*Brn1*) (Molyneaux *et al.* 2009, Oishi *et al.* 2016)		

Table 1.1: Transcriptional regulators differentially expressed in long-range projection neurons in eutherian mammals.

This table is based on protein and/or mRNA detection. L, neocortical layer. See reference list for citation details. Adapted from Paolino *et al.* 2018.

Knockout/downregulation and overexpression experiments have extensively shown that transcription factors and associated proteins do not exert their effects in isolation, but rather are involved in an intricate regulatory network, with combinatorial expression ultimately specifying guidance factor expression and projection fate determination (Figure 1.3). For instance, the corticocortical transcription factor SATB2, which starts to be expressed as maturing corticocortical projection neurons migrate through the intermediate zone (Lickiss *et al.* 2012, Hatanaka *et al.* 2016) (Figure 1.4), represses the subcerebral gene *Ctip2*, thus inhibiting a subcortical fate in favour of a commissural one (Alcamo *et al.* 2008, Britanova *et al.* 2008). In *Satb2*-knockout mice, CTIP2 expression is expanded to include neurons located in the upper layers of the neocortex, which also project laterally to reach subcortical targets rather than medially (Alcamo *et al.* 2008, Britanova *et al.* 2008, Leone *et al.* 2014) (Figure 1.4, 1.5). In addition to this, ectopic expression of SATB2 achieved with *ex vivo* electroporation in deeper layer neurons shows evident downregulation of CTIP2 (Britanova *et al.* 2008). Moreover, the regulatory protein SKI interacts with SATB2 to form the repressor complex that binds to regulatory regions of the *Ctip2* locus, down-regulating its expression and maintaining corticocortical identity *in vivo* (Baranek *et al.* 2012, Nomura *et al.* 2018). Lack of SKI in SATB2-positive neurons causes these neurons to coexpress CTIP2 and project to subcerebral targets in mice (Baranek *et al.* 2012). Similarly, CTIP2 overexpression in upper layer neurons can also alter their projection fate to include subcortical targets via the internal capsule, such as the thalamus, pons and spinal cord (Chen *et al.* 2008), likely via altered expression of axon guidance genes, such as downregulation of UNC5C, which is crucial for callosal formation (Srinivasan *et al.* 2012, Srivatsa *et al.* 2014).

Finally, the corticothalamic transcription factor TBR1 downregulates the subcerebral transcription factor *Fezf2* (McKenna *et al.* 2011), which in turn acts upstream of *Ctip2* and downregulates *Satb2* to inhibit a corticocortical fate (Chen *et al.* 2005, Chen *et al.* 2008, Srinivasan *et al.* 2012) (Figure 1.3). Moreover, SATB2 has also been shown to upregulate the expression of *Fezf2* (McKenna *et al.* 2015), further regulating subcerebral as well as corticocortical projection fate in a cell context-dependent manner. Indeed, it has been shown that SATB2 plays a crucial role in the formation of subcortical projections when it is coexpressed with CTIP2 during early stages of cortical development (Britanova *et al.* 2008, Lickiss *et al.* 2012, Leone *et al.* 2014, Harb *et al.* 2016).

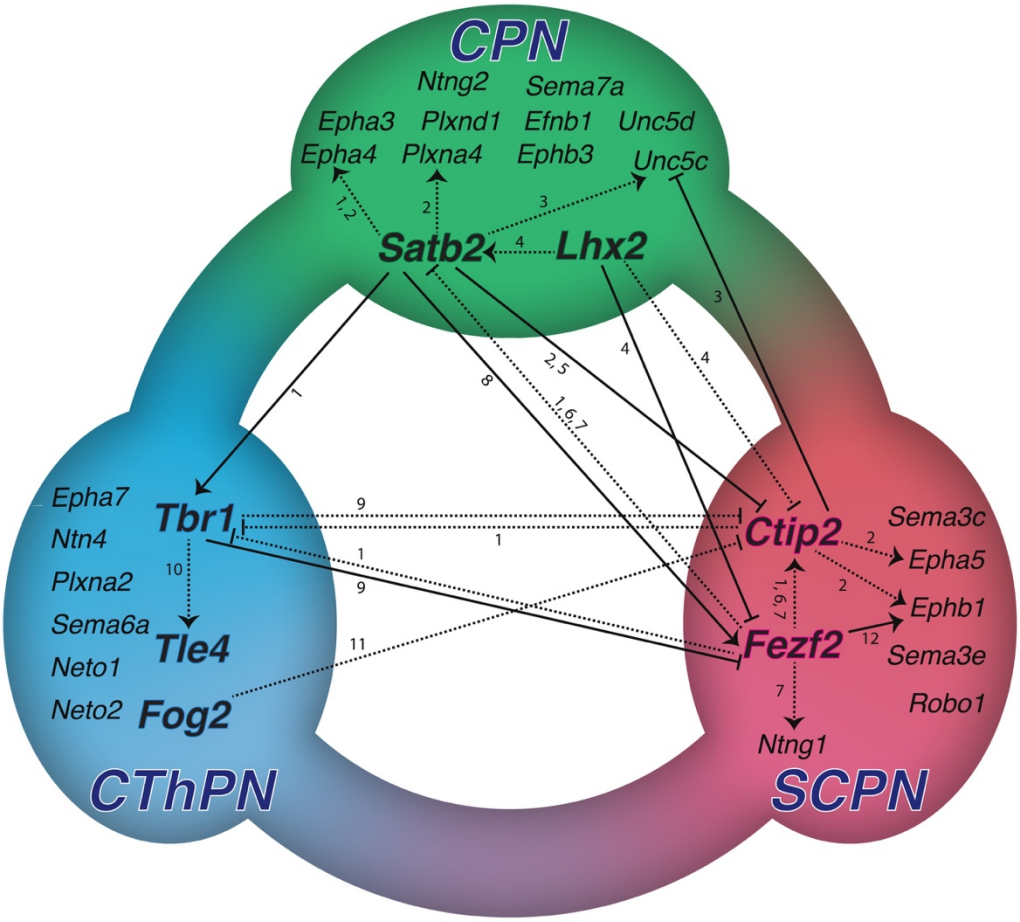

Figure 1.3: Network of transcriptional regulators and axon guidance cue interactions.

Continuous lines represent demonstrated gene interactions, while dashed lines represent suggested interaction based on knockout experiments. Transcriptional regulators in bold. Flat-headed arrows: downregulation; normal arrows: upregulation. CPN = callosal projection neurons, CThPN = corticothalamic projection neurons, SCPN = subcerebral projection neurons. Reference numbers supporting each interaction are indicated: 1) Srinivasan *et al*. 2012; 2) Alcamo *et al*. 2008; 3) Srivatsa *et al*. 2014; 4) Muralidharan *et al*. 2016; 5) Britanova *et al*. 2008; 6) Chen *et al*. 2008; 7) Chen *et al*. 2005; 8) McKenna *et al*. 2015; 9) McKenna *et al*. 2011; 10) Bedogni *et al*. 2010; 11) Galazo *et al*. 2016; 12) Lodato *et al*. 2014. Adapted from Paolino *et al*. 2018.

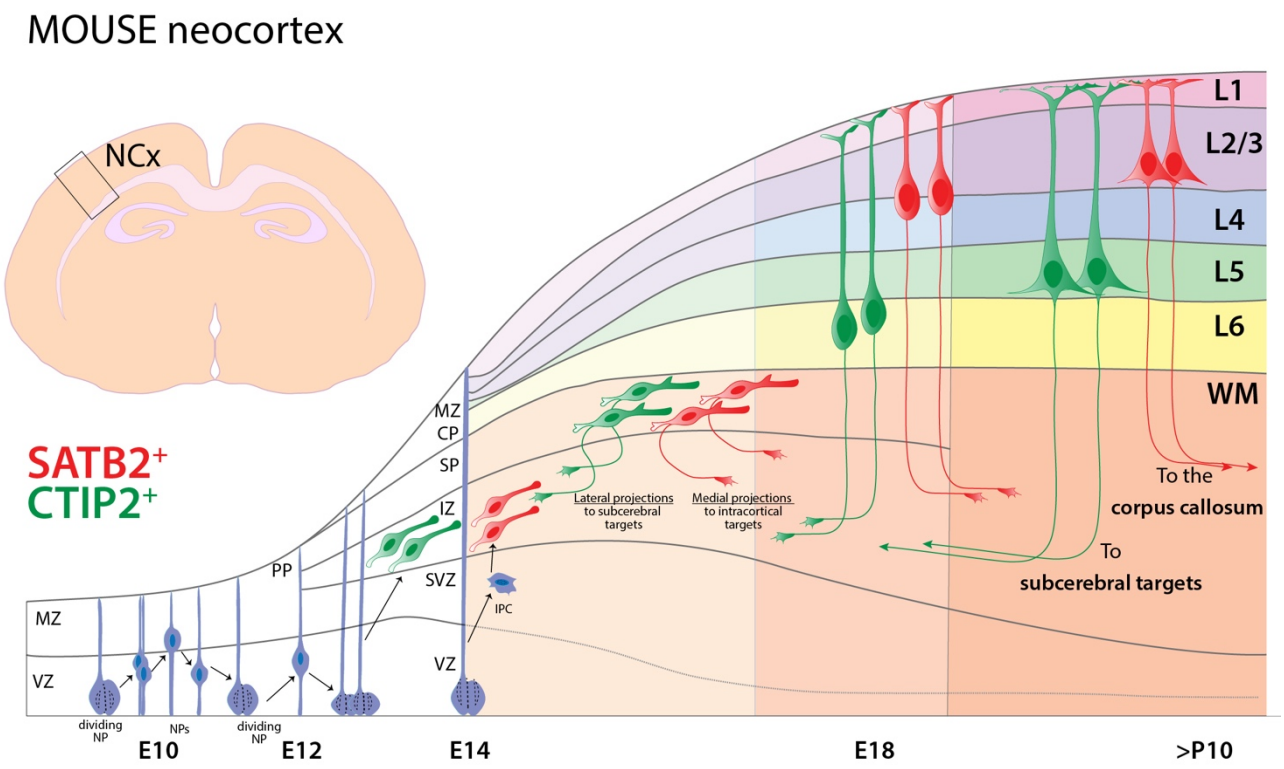

Figure 1.4: During eutherian cortical development, SATB2 and CTIP2 expression coincides with the initial axonal elongation of long-range projection neurons, either medially or laterally, respectively.

In wildtype mice, neurons start to express SATB2 and CTIP2 as they migrate through the intermediate zone, where they start to elongate their axons (Lickiss *et al.* 2012, Hatanaka *et al.* 2016). SATB2-positive neurons will then predominantly target the contralateral hemisphere via the corpus callosum, while CTIP2-positive neurons will project to subcortical targets (Alcamo *et al.* 2008, Arlotta *et al.* 2008, Srinivasan *et al.* 2012, Leone *et al.* 2014, Srivatsa *et al.* 2014). CP = cortical plate, E = embryonic day, IZ = intermediate zone, L = layer, MZ = marginal zone, NCx = neocortex, NP = neural progenitor, PP = preplate, SP = subplate, SVZ = subventricular zone, VZ = ventricular zone, WM = white matter.

This molecular network is precisely regulated to ensure that a correct neuronal fate is imparted to neurons generated at specific stages of development, likely exerting an effect on the initial axonal elongation of long-range projection neurons (Guillemot 2007, Lickiss *et al.* 2012). The expression of some of these markers has been previously shown in different vertebrates (Nomura *et al.* 2018), but it is still unclear whether the same molecular network can regulate the initial axonal elongation and ultimately the projection fate in marsupials and across evolution in general, considering the different commissural strategy. This thesis will address this question, specifically investigating, in marsupials, the expression and function of transcription factors whose role has been already been explored in eutherians. For example, the interactions between SATB2 and CTIP2 are well established in mice, such that in *Satb2*-knockout animals, upper layer neurons project laterally, towards subcortical pathways, as well as towards the contralateral hemisphere via the anterior commissure (Alcamo *et al.* 2008, Britanova *et al.* 2008), resembling the normal phenotype of non-eutherian mammals. Whether these proteins are expressed in the marsupials neocortex and interact during cortical development in non-eutherian species will be investigated in this thesis (Figure 1.5).

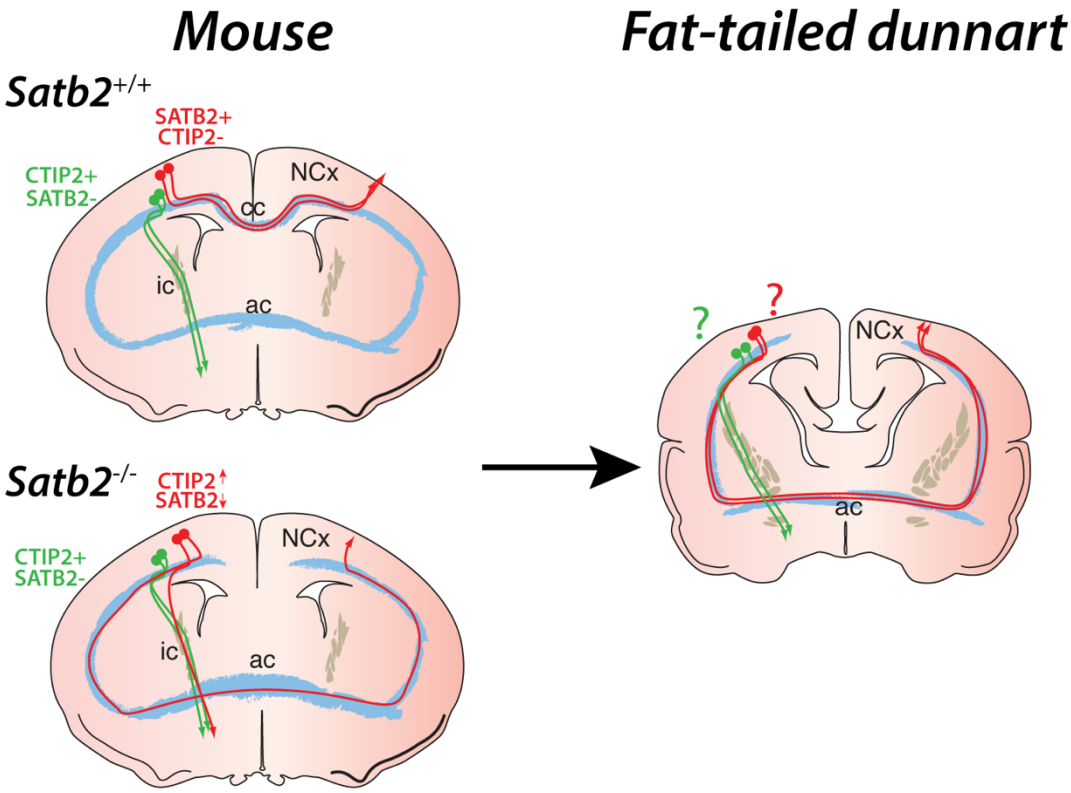

Figure 1.5: Is the molecular network regulating subcortical and commissural fate conserved across mammals?

In wildtype mice, neurons expressing SATB2 mainly extend their axons across the midline to the contralateral hemisphere, thus forming the corpus callosum, while CTIP2-positive neurons project to subcortical targets. When *Satb2* is knocked out, upper-layer neurons project laterally, towards subcortical pathways, as well as towards the contralateral hemisphere via the anterior commissure (Alcamo *et al.* 2008, Britanova *et al.* 2008). This resembles the marsupial phenotype and raises question about the molecular regulation of projection fate determination in these mammalian species. Ac = anterior commissure, cc = corpus callosum, ic = internal capsule, NCx = neocortex.

1.6. Specific aims

Aim 1: To characterise the fat-tailed dunnart as an animal model to study forebrain development (chapter 3). The fat-tailed dunnart is a relatively new model in the field of developmental neuroscience and this aim focuses on its description, with particular attention to the anatomical features of the developing body, head and brain of dunnarts, as well as the birthdate of cortical neurons and the formation of circuits. This knowledge provides a baseline for all subsequent experiments, including investigating the mechanisms regulating the formation of intra- and interhemispheric connectivity.

Aim 2: To investigate the interhemispheric connectome across mammals (chapter 4). Although the pattern of interhemispheric connectivity via the corpus callosum is broadly shared across eutherian species, whether this pattern arose as a consequence of callosal evolution, or instead constitutes a more ancient feature of mammalian brain organisation is unclear. This aim is focused on studying whether the different commissural strategy adopted between marsupials and eutherians has an effect on the organisational principles of interhemispheric connectivity.

Aim 3: To explore the effect of alternative commissural pathway on the dynamics of axonal projection strategies (chapter 5). Commissural axons in eutherian mammals are extended medially in the intermediate zone and cross the midline through the corpus callosum. In marsupials the scenario is different and commissural neurons extend their axons laterally at the intermediate zone to cross the midline via the anterior commissure. In this aim, specific focus will be given to medial versus lateral turning of axons and the mechanisms that regulate this target choice, in order to explore whether the different commissural strategy in marsupials and eutherian species alters the dynamics of initial axonal elongation.

Aim 4: To investigate the molecular mechanisms that regulate corticocortical or subcerebral projection fate in the neocortex of mammals (chapter 6). This section aims to elucidate whether major transcription factors known to direct projection fate in eutherians (i.e. SATB2 and CTIP2) have shared or different roles in marsupials. The transcription factors explored in this chapter have already been shown to play an important role in governing the medial versus lateral turning of the axons at the intermediate zone, ultimately specifying callosal and subcerebral projection fate in mice. The findings of the experiments included in this chapter will elucidate whether the pathways

regulated by specific transcription factors are exclusive to eutherians or instead have a more conserved role in mammalian development.

Chapter 2. Materials and methods

2.1. Animals and tissue collection

2.1.1. Breeding, husbandry and animal transport

The breeding and the husbandry of the fat-tailed dunnart (*S. crassicaudata*; Dasyuridae), an Australian marsupial that breeds prolifically in captivity, have been described in an article that was published during my PhD, where I share co-first authorship with my principal supervisor, Dr Rodrigo Suárez (Suárez, Paolino et al., 2017 attached in chapter 3).

Between June 2012 and December 2013, our team established a breeding colony at the Native Wildlife Teaching and Research Facility, The University of Queensland. The species choice was determined by the fact that fat-tailed dunnarts were already successfully bred in captive colonies at The University of Newcastle (NSW), Remabi Park (SA), and The University of South Australia (SA), and were readily available for the establishment of our new colony. Despite the fact that there is no published brain atlas available in the literature, fat-tailed dunnarts have similar brain size and morphology to the striped-faced dunnart (*Sminthopsis macroura*), a brain atlas for which has been previously published and has been extensively used as reference throughout this thesis (Ashwell *et al.* 2010). This colony produces between 4-12 new litters per month, each with up to 11 pouch-young. The genetic integrity of the colony is kept via rotation of breeders using the Poiley outbreeding system (Poiley 1960). Breeding boxes were set in a male:female ratio of 1:1 (virgin males) to 1:3 (experienced males) per cage, with cage dimensions of 520 x 335 x 95 (mm). Female dunnarts reach sexual maturity at approximately 5 months (average age of females' first-litter is 210 days), and the first females to conceive per litter were kept as new breeders to select for fertility. Weaned and adult dunnarts not included in mating groups were housed individually in cages containing 10 mm corn cob substrate, shredded newspaper, nest boxes (cardboard tubes and boxes), a sand bowl, a water bowl, a 7 ± 12 cm rock, a food bowl, and a drinking bottle. Animals were fed a daily diet consisting of cat biscuits (Adult Cat Total Wellbeing, chicken, Advance) ad libitum, beef mince-mix (w/w, 78% lean beef mince, 5% ground cat kibble, 14% Wombaroo small carnivore food, and 3% of balanced calcium powder; 0.5g for weaners/non-breeders, and 4g lactating females), and live mealworms (*Tenebrio molitor* larva; 3 for weaners/non-breeders, and 6 ± 10 for lactating females). Additionally, once per week, animals received 5-10 g sunflower seeds, 5-10 g hard-boiled egg and 5-10 g apple. The room was maintained on a 16:8h light:dark cycle, humidity between 30 and 60% and temperature between 22 and 26°C. To optimise breeding success, false

winters were set, usually around June and/or December, by gradually reversing the light cycle and dropping temperature by 2 ± 3°C for 2 ± 4 weeks. To check for the presence of joeys, females in breeding cages were gently retrieved from a bottomless hiding box with one hand, allowing gentle inspection of the pouch with the other hand. In non-parous females, the pouch is usually tight and full of pale and dry hair. On the other hand, the pouch of pregnant and oestrous females is easier to open and hairless (Morton 1978). Females with pouch-young can be detected by a moist pouch and presence of joeys attached to the teats. Teats not used by joeys are small and opaque, while the ones with attached young are prominent and highly vascularised. As soon as joeys were detected in the female pouch, the mothers with pouch young were sent via courier from the Native Wildlife Teaching and Research Facility (UQ, Gatton Campus until December 2017, Hidden Vale Wildlife Centre from January 2018) to the Queensland Brain Institute (UQ, St Lucia Campus).

The CD1 wildtype mouse strain was employed for all mouse experiments. This colony is bred at The University of Queensland and time-mated females were obtained by placing male and female mice in the same cage overnight and, in case a vaginal plug was detected, this was considered E0. The day of birth was considered postnatal day (P) 0.

All animal procedures, including laboratory breeding, were approved by The University of Queensland Animal Ethics Committee (AEC approval numbers: QBI/044/18, previous and QBI/045/15/NHMRC) and the Queensland Government Department of Environment and Science (permit number: WA0008250), and were performed according to the current Australian Code for the Care and Use of Animals for Scientific Purposes (NHMRC, 8th edition, 2013), as well as international guidelines on animal welfare.

2.1.2. Intralitter dunnart identification

From developmental stage 18, which corresponds to P0 (day of birth), until the end of stage 27 (P40), dunnart joeys usually remain attached to the same teat, which simplifies the identification of littermates that might have received different treatments, such as electroporation at diverse developmental stages. For joeys to be collected after stage 27, when swapping between teats is more common, a tattooing system was used for their identification. One of the paws and/or the base of the tail of each joey was immobilised with forceps and a small scratch was made on the skin with a fine hypodermic needle (30G) embedded with a green tattoo paste (Ketchum Mfg. Co., NY).

2.1.3. Animal anaesthesia, euthanasia and postmortem collection

Deep anaesthesia of mice for recoverable procedures, such as electroporation, was obtained with an intraperitoneal injection of ketamine/xylazine (120 mg/kg ketamine; Parnell Laboratories; and 10 mg/kg xylazine; Troy Laboratories). For sedation of adult female dunnarts with joeys, they were transferred into a gas anaesthesia induction chamber with isoflurane 5%, delivered in oxygen at a flow rate of 200 mL/Kg/min. The anaesthesia was then maintained by supplying 2-5% isoflurane through a silicone mask (Zero Dead Space MINI Qube Anaesthetic System, AAS, AZ) throughout the procedure. The system connects directly to the vacuum outlet and incorporates an air brake to avoid the risk of lung collapse (Figure 2.1). This allows careful examination and manipulation of joeys localised in the pouch in a minimally invasive manner.

For terminal collection, the joeys were removed from the teat by gently pulling with forceps and anaesthetised with an intraperitoneal injection of 0.05 ± 0.5 mL solution of sodium pentobarbitone (1/50 v/v Lethabarb, Virbac, corresponding to 190 mg Lethabarb per kg body weight), or 5-10 min ice anaesthesia for joeys younger than stage 28 (less than P40). Adult dunnarts and mice, as well as mouse pups, were anaesthetised with intraperitoneal injection of 0.05 ± 0.5 mL solution of sodium pentobarbitone. Following deep anaesthesia, joeys and mouse pups younger than stage 21 (P15 and E13, respectively) were decapitated and drop fixed in 4% paraformaldehyde (PFA; ProSciTech, QLD) in 1X phosphate-buffered saline (PBS; Lonza, Basel), while older joeys and mouse pups, as well as adults were anaesthetised as above and transcardially perfused with 0.9% saline (NaCl), followed by 4% PFA. The brains were post-fixed in 4% PFA for four days before being processed.

2.2. Animal procedures

2.2.1. *In utero* electroporation

Time-mated CD1 pregnant dams were used at E12 (deeper layer neurogenesis in the neocortex) or E15 (upper layer neurogenesis) for all experiments. Deep anaesthesia of mice was obtained as described above. Full anaesthesia was confirmed by toe pinch test, and the dams were placed on a heat pad, which was set at approximately 25°C. The eyes of the dams were covered with Vaseline, in order to prevent drying. Before performing a laparotomy to expose the embryos from the abdominal cavity, the hair covering the abdomen was gently removed using a hair removal cream, the skin was sterilised with chlorohexidine, and gauze was positioned on the skin, leaving a small circular window for the laparotomy. Once the embryos were exposed, each one of them was positioned so that the lateral telencephalic ventricles were visible through the uterine wall. Plasmid DNA with the addition of 0.0025% Fast Green dye (Sigma-Aldrich Co., MO) was then

microinjected with a Picospritzer II (Parker Hannifin) holding a glass pulled pipette, into either the right or left lateral ventricle, depending on the experimental paradigm. The tip of the glass pipette (Thin Wall Glass Capillaries 1.2 mm OD / 0.90 mm ID, WPI, FL), previously prepared using a Flaming/Brown micropipette puller (heat 495, pull 100, vel 100, Sutter Instrument Co., CA), was trimmed obliquely using forceps as previously described (Tabata *et al.* 2008, Matsui *et al.* 2011), before plasmid injection. Individual plasmids used and their respective concentrations are listed in Table 2.1. The plasmids were then electroporated into the presumptive right or left primary somatosensory cortex (S1) with 3 mm diameter microelectrodes (Nepagene) delivering 5 (100 ms, 1 Hz) approximately 36 V square wave pulses from an ECM 830 electroporator (BTX Harvard Apparatus). In general, for intralitter identification, the side of electroporation (left or right) was used to distinguish between control and experimental animals. Once this procedure was completed for each embryo, the uterine horns were replaced inside the abdominal cavity and the incision was sutured closed. Animals were then subcutaneously injected with 1 mL of Ringer's solution (NaCl 135 mM, KCl 5.4 mM, MgCl2 1 mM, CaCl2 1.8 mM, HEPES (Sigma Aldrich) 5 mM) and recovered in a humidified chamber at approximately 28°C. For pain relief, an edible buprenorphine gel pack was positioned next to the recovering dam in the cage. The buprenorphine edible gel pack was prepared before the surgery by injecting MediGel (ClearH2O) with 0.2 ml of edible buprenorphine solution (0.026 mg/ml). Dams were then monitored daily until they gave birth to live pups (at approximately E19/P0). The pups were transcardially perfused between P0 and P10, as described in 2.1.3, depending on the experimental paradigm, and the brightness, size and position of fluorescent patches in S1 of pups were checked under a fluorescence microscope. Those pups that did not have appropriate size or position of fluorescent patches were excluded from further analyses.

2.2.2. In pouch electroporation

Technique of in pouch electroporation in marsupial fat-tailed dunnarts was recently published, where the protocol and the advantages of using this procedure were described in details (Paolino *et al.* 2018). Briefly, once the female dunnart was anaesthetised and placed on its back, the pouch was carefully everted, and the joeys were exposed gently, without detaching them from the teat. The joeys electroporated were from stage 19 (P4-P7) to stage 23 (P20-P23; Figures 3.3-3.4), depending on the experimental paradigm. The joeys were injected with 0.5-1 µl of plasmid DNA in the lateral ventricle using a pulled glass pipette and air pulses delivered via a picospritzer (Parker Hannifin, NH; Figure 2.1D). Similar to *in utero* electroporation, the tip of the glass pipette (Thin Wall Glass Capillaries 1.2 mm OD / 0.90 mm ID, WPI, FL), previously prepared using a

Flaming/Brown micropipette puller (heat 495, pull 100, vel 100, Sutter Instrument Co., CA), was trimmed obliquely using forceps as previously described (Tabata and Nakajima 2008, Matsui *et al.* 2011). The details of the plasmids used can be found in Table 2.1. To visualise the location of the plasmid solution into the lateral ventricle, 0.0025% Fast Green dye (Sigma-Aldrich Co., MO) was added to 1M PBS (PBS; Lonza, Basel) (Tabata and Nakajima 2008, Matsui *et al.* 2011). The 1 mm forcep-type electrodes (Nepa Gene Co., Ichikawa) were positioned on the head of each joey immediately following plasmid injection (Figure 2.1E). Unlike *in utero* electroporation in mice, the marsupial joeys can be directly held with the electrodes, without the barriers of the uterine wall and the amniotic sac, such that it is possible to be more accurate while targeting the area of interest by using smaller electrodes. The spatial orientation depended on the targeted neuronal population (see Figure 3.4). Five 100 ms square pulses of 30-35 V were delivered to specific brain regions via an electroporator system (ECM 830, BTX, Harvard Bioscience, MA). After the completion of the procedure, the joeys were replaced inside the pouch and the mother was recovered.

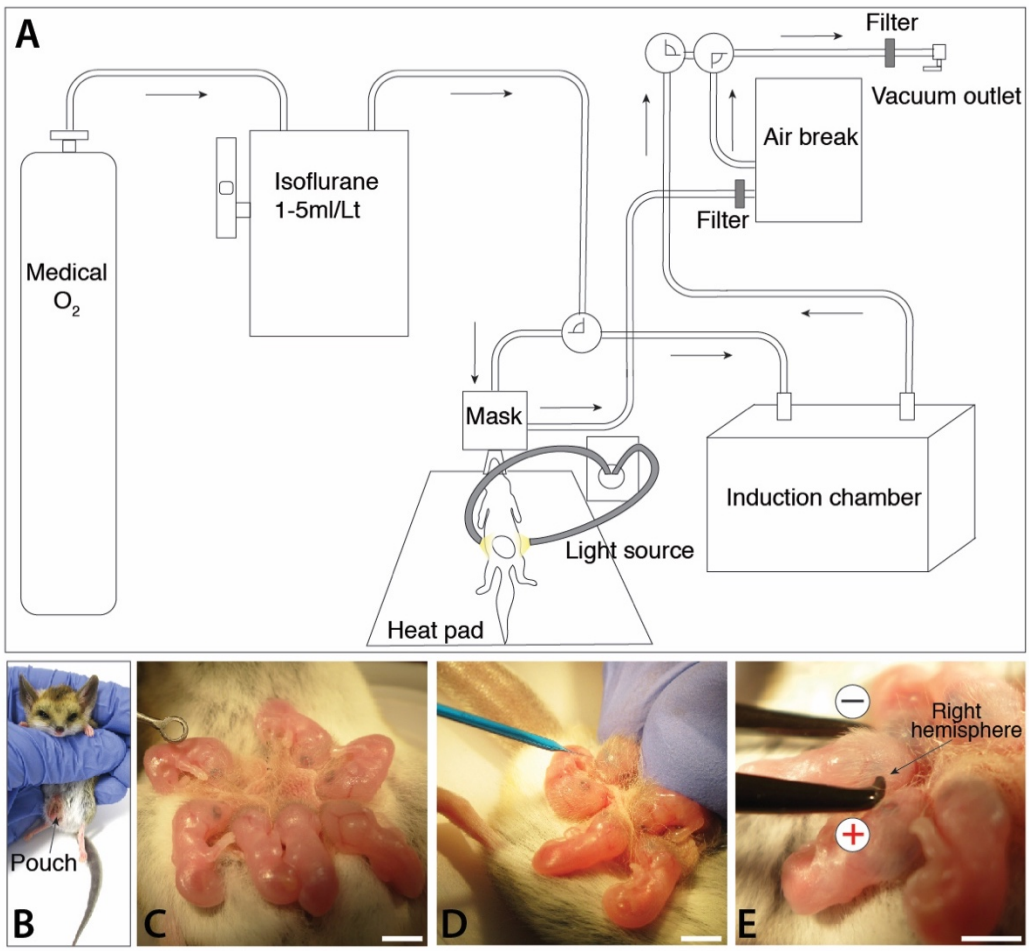

Figure 2.1: Set-up and procedure of in pouch electroporation.

A: Schematic of the set-up required for the anaesthesia of female fat-tailed dunnarts and in pouch electroporation of pouch young. **B**: Female dunnart in supine position with joeys inside the pouch. **C**: Exposure of teat-attached joeys by eversion of the pouch. **D**: The plasmid solution is injected in the lateral ventricle and the dye allows detection of ventricle filling through the skull and skin. **E**: Forceps-like electrodes are positioned across the head of the joeys. The position of the forceps and orientation of the positive electrode allow controlled targeting of selected neuronal population. Scale bars: 4 mm. Taken from Paolino *et al*. 2018.

Plasmid	Concentration	Source
pCAG-eYFP	1 μg/μl	Tetsuichiro Saito, Chiba University, Japan
pPBCAG-GFP	0.75 – 1 μg/μL	Joseph LoTurco, University of Connecticut, USA
pCAG-tdTomato	1 μg/μL	Clontech tdTomato fluorophore subcloned into pCAG by Richards laboratory
pCAG-IRES-GFP-SATB2 (dunnart cDNA)	1 μg/μL	Cloned by Dr Peter Kozulin (Richards lab)
PB-CAG-IRES-GFP-CTIP2 (dunnart cDNA)	1 μg/μL	Cloned by Dr Peter Kozulin (Richards lab)
PB-CAG-IRES-GFP-SKI (dunnart cDNA)	1 μg/μL	Cloned by Dr Peter Kozulin (Richards lab)
pCAG-SATB2 (mouse cDNA)	1 μg/μL	Gift from Prof Victor Tarabykin
pCAG-CTIP2 (mouse cDNA)	1 μg/μL	Gift from Prof Nenad Sestan
pCAG-SKI (mouse cDNA)	1 μg/μL	Gift from Dr Suzana Atanasoski

Table 2.1: List of plasmids used for *in utero* and/or in pouch electroporation.

2.2.3. Stereotaxic surgery

Stereotaxic surgeries were performed on adult dunnarts and joeys between P40 and P50 (stage 28). The animals were anaesthetised with isoflurane as described in section 2.1.3. They were positioned in a stereotaxic apparatus and their head was immobilised with ear-bars. After having removed the fur on the head, a scalp incision was made in the skin, the skin and the muscles were moved aside and a hole was drilled in the skull above the region of interest. Different brain regions were targeted during stereotaxic injections with a pulled glass pipette attached to a picospritzer (Parker Hannifin) and guided by the stereotaxic apparatus. The brain atlas of the stripe-faced dunnart (*Sminthopsis macroura*) was used as an indicative reference (Ashwell *et al.* 2010). The targeted regions were: primary somatosensory cortex (S1), cingulate/motor cortex, and the tectum, depending on the experimental paradigm, which also determined whether the animals were subjected to double or single injections. The tracers used for the experiments were 0.5-1 µl of 0.75-1% cholera toxin subunit B conjugated to a florescent dye (Alexa Fluor 488, Alexa Fluor 647 and Alexa Fluor 555 - CTB 488, CTB 647, CTB 555 Invitrogen) or 1-1.5 µl of 1% fluorescent lipophilic dyes DiI and DiD (Invitrogen). Injected animals were then recovered and euthanised via transcardial perfusion after seven days as described in 2.1.3.

2.2.4. Intraperitoneal injections of EdU in joeys in the pouch

Female dunnarts with pouch young were anaesthetised as described before; the dunnart joeys were exposed carefully and injected intraperitoneally at different postnatal stages (from stage 18, P0-P3; until stage 26, P31-35) with a thymidine analogue, ethynyl deoxyuridine (EdU, 1 µg per 1 g of body weight, diluted in water, Invitrogen). EdU is incorporated into DNA during the S-phase of the cell cycle and allows the labelling of cells that are generated on the day of EdU injection. The solution containing EdU was injected using a pulled glass pipette attached to a picospritzer (Parker Hannifin). The joeys were then euthanised via transcardial perfusion during stage 27 (P35-P40) and the tissue was processed for the detection of EdU using the Click-iT EdU Imaging Assay.

2.2.5. Intraperitoneal injection of EdU in pregnant mice

Time-mated CD1 pregnant dams were injected with EdU (5 µg per 1 g of body weight, diluted in water, Invitrogen) at different stages of embryonic development (from stage 18, E10; until stage 26, E18). The dams were restrained and the solution was injected using a 1 ml 27G syringe. The dams were then repositioned in their cages until giving birth to live pups (at approximately E19/P0).

The pups were then perfused during stage 27 (P4-P5) and the tissue was processed for the detection of EdU using the Click-iT EdU Imaging Assay.

2.3. Histology, image acquisition and analysis

2.3.1. Brain sectioning

For dunnart joeys and mouse pups collected after stage 20 (joeys older than P13 and pups older than E12.5), the brains were dissected out of the skull and sectioned in 50 µm coronal slices using a vibratome (VT1000S, Leica Biosystem, Nussloch). Specifically, the brains were embedded in 3.4% agarose (Difco, Thomas Scientific, NJ) and then glued to a magnetic specimen disk and positioned in the vibratome tray filled with 1X PBS. In order to cut the brain coronally, the brains were oriented so that the olfactory bulbs were facing up and the hindbrain was in contact with the surface of the specimen disk. For dunnart joeys and mouse pups collected before stage 20, the brains were left inside the skull and the whole head was embedded into paraffin to be cut in 12 µm slices using a slicing microtome (RM2235, Leica Biosystem, Nussloch). This procedure reduces the risks of damaging the brains while dissecting them from the skull. Moreover, the slicing microtome allows thinner slices to be collected (between 10 and 20 µm), thus maximising the number of sections collected per each brain. A representative section from each brain region, from rostral to caudal, was mounted onto each slide, which were then placed overnight onto a warm plate, to remove excess moisture and ensure that the sections adhered properly to the glass.

2.3.2. Fluorescent immunohistochemistry

For paraffin-embedded sections, the following dewaxing protocol was used before proceeding to fluorescent immunohistochemistry: the sections were embedded in xylene for ten minutes, twice, to allow dewaxing. A gradual rehydration of the sections was obtained by embedding the sections in 100% ethanol for two minutes, twice, followed by 90% ethanol for one minute, 70% ethanol for three minutes and then 1X PBS for five minutes, before post-fixing with 4% PFA for ten minutes. The brain sections that were embedded in 3.4% agarose (Difco, Thomas Scientific, NJ) and cut with a vibratome (VT1000S, Leica Biosystems, Nussloch) were mounted on slides (Superfrost^{TM} Plus, Thermo Fisher Scientific, MA) and, once dried, incubated in 4% PFA for ten minutes for post-fixation. For both paraffin and agarose-embedded sections, antigen retrieval was performed (when required, depending on the antibody used) in an apposite chamber containing 0.01M Sodium Citrate, 0.05% Tween 20, pH 6.0, reaching 125°C for four minutes, followed by ten minutes at 90°C. Sections from brains injected with CTB conjugated with Alexa Fluor (Invitrogen) were antigen-retrieved at lower temperatures to preserve the fluorescent signal of the retrograde tracer: 20 minutes at 80°C, followed by 40 minutes at room temperature. The slides were then

incubated for two hours in blocking solution of 10% v/v normal donkey serum (NDS; Jackson Immunoresearch Inc., PA) and 0.2% Triton X-100 (TX100, Sigma-Aldrich Co., MO) in PBS (pH 7.4), followed by overnight incubation in 10% normal donkey serum and 0.2% TX100 in PBS with primary antibodies (see table 2.2). After 1X PBS washes (three times for 20 minutes), slides were incubated with appropriate fluorescent secondary antibody; CTIP2 detection sensitivity was improved using a streptavidin-based amplification with donkey anti-rat IgG biotinylated (JIR). The secondary antibodies used were: Alexa Fluor 555 donkey anti-rabbit, Alexa Fluor 488 donkey anti-rabbit, Alexa Fluor 568 donkey anti-goat, Alexa Fluor 488 donkey anti-chicken and Alexa Fluor 647 streptavidin (all 1:500; Invitrogen, Thermo Fisher Scientific, MA). After 1X PBS washes, the slides were stained for ten minutes with 0.1% 4',6-Diamidine-2'-phenylindole dihydrochloride (DAPI; Invitrogen, Thermo Fisher Scientific, MA), then washed and coverslipped with antifade mounting media (ProLong Gold; Invitrogen, Thermo Fisher Scientific, MA). 50 µm brain sections from dunnart joeys and mouse pups injected with EdU (Invitrogen) were processed according to the instructions of the Click-iT EdU imaging kit (Invitrogen) before being incubated with the blocking solution. The detection of EdU is based on a copper-catalysed covalent reaction between an azide and an alkaline.

Antibody	Concentration	Company
Rabbit anti-SATB2	1:500	Abcam 69995
Rat anti-CTIP2	1:500	Abcam 18465
Rabbit anti-TBR1	1:500	Abcam 31940
Chicken anti-GFP	1:750	Abcam 13970
Goat anti-tdTomato	1:1000	Sicgen 8181-200
Rabbit anti-Nurr1	1:500	Santa Cruz Biotech

Table 2.2: List of primary antibodies used for fluorescence immunohistochemistry.

2.3.3. *In situ* hybridisation

Digoxygenin-labelled (DIG RNA labelling Mix; Roche) antisense riboprobes were transcribed from cDNA plasmids. Primers for dunnart probes were designed based on the RNAseq dataset generated in the lab (Kozulin et al., in preparation), while mouse probe primer designs were obtained from the website of the Allen Brain Atlas (Table 2.3). Freshly cut 50 µm coronal brain sections were mounted on to SuperFrost Plus slides in RNAse-free conditions. Once the sections were dried, they were fixed with 4% PFA for ten minutes, followed by three washes of three minutes each with 1X PBS. After fixation, the sections were treated with 10 µg/mL Proteinase K (Roche) in PBS for ten minutes, followed again by three washes of three minutes each with 1X PBS, refixation with 4% PFA for five minutes and three washes of three minutes each with 1X PBS. After these first steps, the slides were incubated for ten minutes in a solution containing 1.33% triethanolamine (Sigma Aldrich), 0.02% hydrochloric acid (37%; LabScan) and 0.35% acetic anhydride (Ajax Finechem) in MilliQ™ H_2O, followed by three washes of three minutes each with 1X PBS. The slides were then incubated in 1 ml of hybridisation buffer for two hours at 68°C, for pre-hybridisation. The hybridisation buffer contained: 50% formamide (Sigma Aldrich), 5X pH 4.5 Standard Saline Citrate buffer (SSC; Invitrogen), 50 µg/mL Bakers'Yeast tRNA (Roche), 5X Denhardt's Solution (Invitrogen) in MilliQ™ H_2O. Then, 1 µg/mL of riboprobe was diluted into 1 ml of hybridisation buffer and incubated at 80°C for five minutes, in order to denature any secondary structures. After the denaturation step, 1 ml of probe solution was applied onto each slide, which were arranged in a chamber humidified with 50% Formamide/5X SCC, and incubated at 68°C overnight. The next day, stringency washes were performed at 68°C. First, the slides were washed in 1% SDS (Sigma Aldrich), 50% formamide in 1X SSC for 30 minutes. The next washes were performed with 2X SSC for 20 minutes and then with 0.2X SSC twice, each for 20 minutes. After the stringency washes, the slides were washed in MABT [0.1M maleic anhydride (MP Biomedicals), 0.15M sodium chloride and 0.1% Tween in MilliQ™ H_2O] three times, five minutes each, at room temperature. The slides were then incubated for two hours in 2% w/v blocking reagent (Roche) in MABT. After the blocking step, the anti-DIG-AP (Roche) was diluted 1:4000 in the same blocking solution, which was re-applied onto each slide (~1 ml) and incubated for two hours at room temperature. Following antibody incubation, the slides were washed with MABT at room temperature three times for five minutes, and then incubated in NTMT solution, which contained 0.1M sodium chloride, 0.1M pH 9.5 Tris hydrochloride (Amresco), 0.05M magnesium dichloride (Ajax Finechem), 0.1% v/v Tween, 2mM imidazole hydrochloride (Sigma Aldrich) in MilliQ™ H_2O, for ten minutes at room temperature. To proceed to the colour reaction, 1 ml of BM purple, which was previously centrifuged to avoid any precipitate, was added onto each slide. The

slides were monitored for between two and 24 hours in order to stop the colour reaction whenever the appropriate staining had developed. The slides were then washed for three times with 1X PBS and then coverslipped with ProLong gold mounting media.

	Forward (5'-3')	Reverse (5'-3')
Mouse-S*atb2*	GCACACAGGGATTATTGTCAGA	GTGGTACCTCTGGTTCTGGAAG
Dunnart-*Satb2*	TCCGAGTCAAAGTAGCATGG,	TGGTTGATGGCTTGAGGGTG
Mouse-*Ctip2*	AGTATGGGGAGAAGCGGG	CTCCTCTCAGCCTGCTCG
Dunnart-*Ctip2*	AATGTCCCGCCGCAAACAG,	GGTTCAAACGCATGACTCTGTC

Table 2.3: List of primers used for the generation of the mouse- and dunnart-specific *in situ* probes.

2.3.4. Image acquisition

Wide-field fluorescence imaging was performed with a Zeiss upright Axio-Imager Z1 microscope fitted with Axio- Cam HRc and HRm cameras and captured with Axio Vision software using MosaicZ. Images were acquired with Zen software (Carl Zeiss AG, Oberkochen). High resolution images were acquired using: 1) 20x/0.75 NA air objective (Nikon) on a Diskovery spinning disk confocal microscope (Spectral Applied Research) built around a Nikon TiE body and equipped with two sCMOS cameras (Andor Zyla 4.2, 2048 x 2048 pixels) and controlled by Nikon NIS software; 2) spinning-disk confocal system (Marianas; 3I, Inc.), consisting of Axio Observer Z1 (Carl Zeiss) equipped with a CSU-W1 spinning-disk head (Yokogawa Corporation of America), ORCA-Flash4.0 v2 sCMOS camera (Hamamatsu Photonics), 20x 0.8 NA PlanApo objectives. Image acquisition was performed using SlideBook 6.0 (3I, Inc). Images were cropped, sized, and enhanced for contrast/brightness with Photoshop, and the figures assembled in Illustrator (Adobe Creative Suite 6, CA).

2.3.5. Cell counting, axonal length analysis and statistical tests

Cell counting analyses in specific regions of interest were performed using an unbiased automatic built-in spot detection algorithm in the software Imaris (Bitplane, Badenerstrasse, Zürich) (Chen *et al.* 2017), or manually with a Fiji (Image J) plugin for manual cell count (Schindelin *et al.* 2012), depending on the experimental paradigm. For example, to count electroporated neurons, or retrogradely labelled cells that incorporated tracers such as CTBs or DiI/DiD, the built-in spot detection algorithm was not ideal because of the pyramidal, and not round, labelling shape of these cells; in these cases, a manual approach using Fiji and visual curation was thus preferable. However, nuclear markers such as transcription factors or EdU allowed the use of automated detection, as spherical shapes were easy to be recognised by the software. For the analysis of commissural axons as they innervate the contralateral hemisphere, described in chapter 3, a region of interest (ROI) was defined in the hemisphere contralateral to the electroporated patch, the ROIs were then rotated so that the pial surface was located on the left. Fiji plugins (Schindelin *et al.* 2012) were then used for axonal length quantification (Suárez *et al.* 2014a). The values of intensity of fluorescence in these ROIs were normalised for the background measured as the fluorescence intensity in the darkest area of each specific brain section, and then reorganised and graphed using Excel.

D'Agostino & Pearson tests were used to assess the normality of the datasets. Mann–Whitney or Kruskal–Wallis non-parametric tests were performed in non-normally distributed data,

while normal datasets were analysed using Student's t-tests or ANOVAs (Prism 7, GraphPad Software Inc., CA). Probability values of $P < 0.05$ were considered significant. All data is presented as mean ± standard error of the mean (SEM). Further details on the number of replicates per experiment and the tests used for all the analysis will be described in more detail in each chapter.

2.4. Generation of dunnart-specific overexpression constructs

For the generation of the dunnart-specific SATB2 overexpression construct, total RNA was obtained from the cortex of dunnart joeys at P25 using TRIzol extraction, and purification with Qiagen Minielute clean-up kit (#74204) followed by DNase treatment (#79254). cDNA was then generated using Superscript III first-strand reverse transcription kit (Invitrogen, #18080-051). Blunt-end PCR products were amplified from P25 dunnart cDNA template using Phusion high-fidelity DNA polymerase (NEB, #M0530), using primers listed in Table 2.4. A single band of ~2.3 kb was visible for *Satb2*. The band was gel-extracted and purified with phenol/chloroform and the PCR product ends were phosphorylated using T4 polynucleotide kinase (NEB, #M0201). The pCAGIG vector was blunt-end digested with EcoRV and the digested plasmid ends were dephosphorylated using Antarctic Phosphatase (NEB, #M0289), for 30 minutes at 37°C. A 1:3, pCAGIG vector : *Satb2* insert blunt-end ligation was setup at 16°C overnight, using a T4 DNA ligation kit (NEB, #M0202). The ligated plasmid was transformed into 20 µl alpha-select competent cells (Bioline, #BIO-85027) and grown overnight at 37°C on LB-agar plates with 100 µg/ml ampicillin. Successful clones were verified with colony PCR (Table 2.4) and Sanger sequencing.

To generate the dunnart-specific CTIP2 overexpression construct, total RNA was obtained from the cortex of adult dunnarts. RNA extraction, purification, DNase treatment, and reverse transcription methods were performed as described for SATB2 above. Nested PCR was used to amplify *Ctip2* product from adult cDNA template with Phusion high-fidelity DNA polymerase, using the primers listed in Table 2.4. First, PCR products (~3.1kb) were gel extracted, and used as a template for the nested PCR, which was also gel extracted (~2.7kb product). PCR product ends were digested with MfeI and NotI, and the pPBCAGIG vector was digested with EcoRI (isoschizimer for MfeI) and NotI. Both digests were purified using Qiagen PCR clean-up kit. A 1:9, pPBCAGIG vector : *Ctip2* insert blunt-end ligation was setup at 16°C overnight, using a T4 DNA ligation kit (NEB, #M0202). The plasmid transformation and colony verification methods were the same as those described for *Satb2* above (Table 2.4).

Dunnart-specific SKI was similarly cloned from the total RNA of P25 dunnart cortex. RNA extraction, purification, DNase treatment, and reverse transcription methods were performed as described for the previous transcription factors, using primers listed in Table 2.4. SKI was amplified with a single PCR from the cDNA template using Phusion. PCR products of ~2.3kb were gel extracted and subjected to polyA-tailing (as per pGEMT protocol, Promega), prior to 1:3 ligation into pGEMT plasmid at 4°C overnight. The ligated plasmid was transformed into alpha-select competent cells, and grown overnight at 37°C on LB-agar plates with 100 µg/ml ampicillin and 80

µg/ml X-gal. Positive colonies were selected and the insert was checked using colony PCR, prior to performing a plasmid miniprep. The SKI insert was digested with AatII, and the DNA ends blunted (NEB, #M1201). The product was column purified and then digested with NotI to fully cut out the insert from pGEMT, followed by gel extraction to isolate the insert. Similarly, pPBCAGIG was digested with XhoI, the DNA ends blunted, then digested with NotI and column purified. A 1:9, pPBCAGIG vector : SKI insert ligation was setup at 16°C overnight, using a T4 DNA ligation kit. The plasmid transformation and colony verification methods were the same as those described for *Satb2* above (Table 2.4).

	Forward (5'-3')	Reverse (5'-3')	Phusion anneal temp and extension time
Satb2	TCCGAGTCAAAGTAGCATGG	CCTGTGCAGCAAAGAAATGTC	56.2°C, 70 sec
Ctip2 1st PCR	CCCAACCGGTACAGCTCTC	TGCTTCTCCCCTACAATGCAA	59.7°C, 120 sec
Ctip2 nested PCR	GGCCGGCAATTGGATGTCAGT GTAAATGCC [adapter contains MfeI restriction site]	ATATATATGCGGCCGCGAATGA GGAGGGAAGG [adapter contains NotI restriction site]	49.3°C (cycles 1-5) then 72°C (cycles 6-35), 110 sec
Ski	GAGCCCGATCGCACCATG	GTTCGAGGCACAGGAAGATG	58.7°C, 120 sec
Satb2 colony PCR	TCCGAGTCAAAGTAGCATGG [Satb2-F]	GTCCAGCTCGACCAGGATG [EGFP-R]	57°C, 120 sec
Ctip2 colony PCR	CAACGTGCTGGTTGTTGTG [pCAG-F]	TTTAGCTTCTTTCGGCCTGC [Ctip2-R]	55°C, 120 sec
Ski colony PCR	CAACGTGCTGGTTGTTGTG [pCAG-F]	TCAGTGCAGGAAGGTGTGTG [Ski-R]	56°C, 45 sec

Table 2.4: List of primers used for the generation of dunnart-specific overexpression constructs.

Chapter 3. Characterising the fat-tailed dunnart as a model system

Most of the results included in this chapter were published in two papers during my PhD:

Suárez R, **Paolino A** (co-first author), Kozulin P, Fenlon LR, Morcom LR, Englebright R, O'Hara PJ, Murray PJ, Richards LJ (2017). Development of body, head and brain features in the Australian fat-tailed dunnart (Sminthopsis crassicaudata; Marsupialia: Dasyuridae); A postnatal model of forebrain formation. PLoS ONE. 12(9): e0184450. doi: https://doi.org/10.1371/journal.pone.0184450
Attached in section 3.2.1:

Contributor	**Statement of contribution**
Rodrigo Suárez	Designed experiments 40% Performed experiments 30% Analysed data 40% Wrote paper 30%
Annalisa Paolino (candidate)	Designed experiments 35% Performed experiments 60% Analysed data 40% Wrote paper 25%
Peter Kozulin	Performed experiments 5% Analysed data 5% Wrote paper 5%
Laura R Fenlon	Designed experiments 10% Analysed data 15% Wrote paper 10%
Laura R Morcom	Performed experiments 5% Wrote paper 5%
Robert Englebright	Wrote paper 5%
Patricia O'Hara	Wrote paper 5%
Peter Murray	Wrote paper 5%
Linda J Richards	Designed experiments 15% Wrote paper 10%

Paolino A, Fenlon LR, Kozulin P, Richards LJ, Suárez R (2018). Multiple events of gene manipulation via in pouch electroporation in a marsupial model of mammalian forebrain development. J Neurosci Methods. 293:45-52. doi: https://doi.org/10.1016/j.jneumeth.2017.09.004

Contributor	**Statement of contribution**
Annalisa Paolino (candidate)	Designed experiments 30% Performed experiments 60% Analysed data 40% Wrote paper 30%
Laura R Fenlon	Designed experiments 30% Analysed data 20% Wrote paper 20%
Peter Kozulin	Wrote paper 5%
Linda J Richards	Designed experiments 10% Wrote paper 20%
Rodrigo Suárez	Designed experiments 30% Performed experiments 40% Analysed data 40% Wrote paper 25%

3.1. Introduction

Understanding the evolution of new anatomical features characterising the mammalian brain can help to elucidate the mechanisms involved in their origin, in their correct formation and in the pathological conditions that arise due to their malformation (Molnár *et al.* 2006, Rakic 2009, Suárez *et al.* 2014b). As detailed in chapter 1, the mammalian brain evolved a six-layered neocortex (Wang *et al.* 2010), with an expansion and diversification of interhemispheric connectivity, culminating with the emergence of the corpus callosum exclusively in eutherian mammals (Suárez *et al.* 2014b). Despite the crucial role played by neocortical circuits in sensory-motor and cognitive function, how they emerged during evolution is still not fully understood (de Sousa *et al.* 2007). A way to investigate the development of new anatomical traits and to identify features that have been conserved, as well as distinction from those that have changed across lineages, is by adopting a comparative approach in extant species (de Sousa and Wood 2007). For this reason, this thesis aims to address evolutionary questions by adopting a comparative approach using the eutherian mouse and the marsupial fat-tailed dunnart.

In order to carry out comparative studies of neuroanatomy, it is crucial to be able to compare the developmental stages in eutherians and marsupials. In this chapter, a standardised staging system for fat-tailed dunnarts is presented to match both human (Carnegie staging system) and mouse development (Thieler staging systems), thus facilitating the use of this animal model for comparative developmental and evolutionary studies. In addition to this, the major developmental milestones of dunnarts based on whole body, craniofacial and brain anatomy features across stages, from birth to weaning, are identified. In the second part of this chapter, cortical neurogenesis and the establishment of cortical circuits are investigated in dunnarts and compared to mice. Specific focus is given to the formation of interhemispheric connections, investigated with the technique of in pouch electroporation (Paolino *et al.* 2018), which allows the independent labelling of deeper and upper layer neurons within the same brain, to explore their interaction during the development of interhemispheric circuits. Throughout this chapter, the advantages of using dunnarts as an experimental model to study specific events of forebrain development and evolution *in vivo* and to address new experimental questions are highlighted.

3.2. Results

3.2.1. Anatomical description of the external features of the body, head and brain in postnatal dunnarts

This section was published during my PhD:

Suárez R, **Paolino A** (co-first author), Kozulin P, Fenlon LR, Morcom LR, Englebright R, O'Hara PJ, Murray PJ, Richards LJ (2017). Development of body, head and brain features in the Australian fat-tailed dunnart (Sminthopsis crassicaudata; Marsupialia: Dasyuridae); A postnatal model of forebrain formation. PLoS ONE. 12(9): e0184450. doi: https://doi.org/10.1371/journal.pone.0184450

Development of body, head and brain features in the Australian fat-tailed dunnart (*Sminthopsis crassicaudata*; Marsupialia: Dasyuridae); A postnatal model of forebrain formation.

Rodrigo Suárez[1¶*], Annalisa Paolino[1¶], Peter Kozulin[1], Laura R. Fenlon[1], Laura R. Morcom[1], Robert Englebright[2], Patricia J. O'Hara[2], Peter J. Murray[2] & Linda J. Richards[1,3*]

[1]The University of Queensland, Queensland Brain Institute, Brisbane, Queensland, Australia.
[2]The University of Queensland, School of Agriculture & Food Science, Gatton, Queensland, Australia.
[3]The University of Queensland, School of Biomedical Sciences, Brisbane, Queensland, Australia.

*Corresponding authors.
E-mails: rsuarezsaa@gmail.com (RS) and richards@uq.edu.au (LJR)
¶These authors contributed equally to this work.

Short title: Development of body, head and brain features in the Australian fat-tailed dunnart.

Abstract

Most of our understanding of forebrain development comes from research of eutherian mammals, such as rodents, primates, and carnivores. However, as the cerebral cortex forms largely prenatally, observation and manipulation of its development has required invasive and/or *ex vivo* procedures. Marsupials, on the other hand, are born at comparatively earlier stages of development and most events of forebrain formation occur once attached to the teat, thereby permitting continuous and non-invasive experimental access. Here, we take advantage of this aspect of marsupial biology to establish and characterise a resourceful laboratory model of forebrain development: the fat-tailed dunnart (*Sminthopsis crassicaudata*), a mouse-sized carnivorous Australian marsupial. We present an anatomical description of the postnatal development of the body, head and brain in dunnarts, and provide a staging system compatible with human and mouse developmental stages. As compared to eutherians, the orofacial region develops earlier in dunnarts, while forebrain development is largely protracted, extending for more than 40 days versus ca. 15 days in mice. We discuss the benefits of fat-tailed dunnarts as laboratory animals in studies of developmental biology, with an emphasis on how their accessibility in the pouch can help address new experimental questions, especially regarding mechanisms of brain development and evolution.
Keywords: Brain development; Carnegie stages; heterochrony; isocortex; model organisms; ontogeny.

Introduction

The six-layered cerebral cortex, also known as isocortex, is a region of the forebrain only present in mammals and participates in daily functions such as sensory integration, motor planning, attention and learning. Comparative studies of brain development across species have provided critical insights not only on the mechanisms of circuit formation, but also on the conservation and change of such mechanisms during evolution. However, a critical challenge in comparative neuroscience is to determine whether and how developmental processes in one species can be compared to those of another species. Direct comparisons of development between species are often obscured by differences in the relative rates of trait formation (heterochrony). For example, the three major mammalian groups, *i.e*., monotremes, marsupials and eutherians, show remarkable heterochronies in face, forelimb and brain formation that likely reflect differences in pre- and postnatal development [1-11]. Therefore, to facilitate our understanding of mechanistic and evolutionary questions about mammalian development we need to integrate the timing of developmental events in different species into a shared scale.

Previous efforts to categorise development as discrete series have helped overcome this issue by establishing comparable stages across model organisms [4, 12-15]. Here, we characterise postnatal development of the Australian marsupial fat-tailed dunnart, *Sminthopsis crassicaudata* (Marsupialia: Dasyuridae), using a standardised staging system that matches human and mouse development (i.e., the Carnegie and Thieler staging systems, respectively). Notably, while most of the neurons and connections of the cerebral cortices form before birth in eutherian species, in marsupials this occurs almost exclusively after birth and during a prolonged period of time, thus offering experimental access to early events of forebrain development *in vivo* [6, 7, 10-20]. We outline our protocols for the breeding and care of this species in captivity to facilitate its use as a laboratory model of developmental biology, and identify its major developmental milestones based on whole body, craniofacial and brain anatomy features across stages, from birth to weaning. Finally, we compare dunnart development with that of other mammals and highlight the advantages of using this species as an experimental model to study specific events of forebrain development *in vivo*.

Materials and methods

Animal welfare

All animal procedures, including laboratory breeding, were approved by The University of Queensland Animal Ethics Committee and the Queensland Government Department of Environment and Heritage Protection, and were performed according to the current Australian Code

for the Care and Use of Animals for Scientific Purposes (NHMRC, 8th edition, 2013), as well as international guidelines on animal welfare.

Breeding colony

We established a breeding colony of fat-tailed dunnarts (*Sminthopsis crassicaudata*) at the Native Wildlife Teaching and Research Facility, The University of Queensland, from founder animals sourced from captive colonies at the University of Newcastle (NSW), Remabi Park (SA), and the University of South Australia (SA), between June 2012 and December 2013. The genetic integrity of our colony is kept via rotation of breeders using the Poiley outbreeding system [21]. Breeding boxes were set in a male:female ratio of 1:1 (virgin males) to 1:3 (experienced males) per cage, with cage dimensions of 520 x 335 x 95 (mm). Female dunnarts reach sexual maturity at approximately 5 months (average age of females' first-litter is 210 days), and the first females to conceive per litter were kept as new breeders to select for fertility. Weaned and adult dunnarts not included in mating groups were housed individually in cages containing 10 mm corn cob substrate, shredded newspaper, nest boxes (cardboard tubes and boxes), a sand bowl, a water bowl, a 7-12 cm rock, a food bowl, and a drinking bottle. Animals were fed a daily diet consisting of cat biscuits (Adult Cat Total Wellbeing, chicken, Advance®) *ad libitum*, beef mince-mix (w/w, 78% lean beef mince, 5% ground cat kibble, 14% Wombaroo© small carnivore food, and 3% of balanced calcium powder; 0.5g for weaners/non-breeders, and 4g lactating females), live mealworms (*Tenebrio molitor* larva; 3 for weaners/non-breeders, and 6-10 for lactating females). Additionally, once per week animals received 5-10g sunflower seeds, 5-10g hard-boiled egg and 5-10g apple. The room was maintained on a 16:8h light:dark cycle, humidity between 30 and 60% and temperature between 22 and 26°C. To optimise breeding success, false winters were set, usually around June and/or December, by gradually reversing the light cycle and dropping temperature by 2-3°C for 2-4 weeks.

To check for joeys presence, females in breeding cages were gently retrieved from a bottomless hiding box with one hand, allowing gentle inspection of the pouch with the other hand. In non-parous females, the pouch is usually tight and full of pale and dry hair. On the other hand, the pouch of pregnant and oestrous females is easier to open and hairless [22]. Females with pouch-young can be detected by a moist pouch and presence of joeys attached to the teats. Teats not used by joeys are small and opaque, while the ones with attached young are prominent and highly vascularised.

Anaesthesia and tissue collection

For temporary sedation, adult female dunnarts with joeys were transferred into a gas anaesthesia induction chamber with isoflurane 5%, delivered in oxygen at a flow rate of 200 mL/Kg/min, followed by isoflurane 2-5% supplied through a rubber mask throughout the procedure (ZDS MINI Qube Anaesthetic System). This allows careful examination of joeys in a non-invasive manner.

Joeys were removed from the teat by gently pulling with forceps and euthanised with an intraperitoneal injection of 0.05-0.5 mL solution of sodium pentobarbitone (1/50 v/v Lethabarb™, Virbac, corresponding to 190 mg Lethabarb per kg body weight), or 5-15 min ice anaesthesia for joeys younger than postnatal day (P) 45, followed by transcardial perfusion of 0.9% NaCl and 4% paraformaldehyde (PFA), or immersion-fixation in 4% PFA for joeys younger than P15.

Histology and microscopy

Following perfusion, joeys younger than 2 weeks of age underwent paraffin embedding and had their heads sectioned in the coronal plane at 12 □m in a sliding microtome (Leica SM 2000R). Sections were mounted, dewaxed and stained with hematoxylin and eosin. Older joeys had their brains dissected, photographed (Lumix DMC-LX7, Panasonic™), embedded in 3.4% agarose blocks and sectioned at 50 □m using a vibratome (Leica VT1000S). These sections were stained for 10 minutes with 0.1% DAPI (Invitrogen), and then washed and coverslipped with ProLong Gold (Invitrogen). Brightfield and fluorescence microphotographs were obtained using a Zeiss upright Axio-Imager microscope fitted with Axio-Cam HRc and HRm cameras, and captured using AxioVision software (Carl Zeiss). Photoshop and Illustrator (Adobe) were used to adjust levels, contrast and prepare figure panels.

Morphometry and statistics

To track joey morphometry, pouches were exposed as described above and the joeys were photographed (Lumix DMC-LX7, Panasonic™) at regular intervals until P45. Crown-rump length, skull width (bi-parietal diameter), and forelimb and hindlimb length were measured from the pictures that included identical calibration tools (Fiji, NIH). Details about the appearance of the joeys were noted across stages, paying particular attention to fur, mouth, eyes, ears, nose, skin, forelimbs, fingers, hindlimbs, and toes. Growth curves and 95% confidence intervals were generated using non-linear semilog fitting of morphometric measurements following the least-squares method. Goodness-of-fit was quantified as R squared (R^2) with 95% confidence intervals and degrees of freedom (d.f.) > 12. Normality tests of residuals were passed in all cases (D'Agostino-Pearson omnibus K2; Prism 7, GraphPad). Measurements are presented as mean ± standard error of the mean.

Results

Developmental morphometry and growth curves of postnatal *S. crassicaudata*

To characterise growth and developmental morphometry of postnatal *S. crassicaudata*, we measured crown-rump length, maximum head width, forelimb length and hindlimb length from at

least 4 different individuals (median 9, mean 14.3) per measurement and age range (see Table 1). Semi-logarithmic relationships between each of these measurements and ages were determined, including best-fit regression curves and 95% confidence intervals (Fig 1). Crown-rump length, skull width and forelimb length showed good non-linear fit ($R^2 \geq 0.985$; Table 2), indicating that morphometry alone can be used to infer developmental age in the case of incomplete data, such as for example from field measurements where date of birth is unknown [22]. Interestingly, however, body size is often more similar between littermates than to age-matched joeys of different sized litters, suggesting that differences in the metabolic/nutritional state of the mothers and/or the number of teats/joeys per litter could be sources of variability [7, 9].

Table 1. Morphometric measurements in postnatal *S. crassicaudata*

Age (days)	Crown-rump length (mm)	Skull width (mm)	Forelimb length (mm)	Hindlimb length (mm)
P2/4	5.32 ± 0.11 *(n= 59)*	1.99 ± 0.05 *(n= 32)*	1.79 ± 0.04 *(n= 58)*	2.01 ± 0.11 *(n= 4)*
P5/7	6.24 ± 0.18 *(n= 19)*	2.57 ± 0.11 *(n= 14)*	2.11 ± 0.10 *(n= 15)*	2.22 ± 0.11 *(n= 4)*
P8/12	7.30 ± 0.20 *(n= 34)*	2.73 ± 0.08 *(n= 15)*	2.51 ± 0.10 *(n= 34)*	2.37 ± 0.18 *(n= 9)*
P13/16	8.46 ± 0.20 *(n= 35)*	3.31 ± 0.07 *(n= 29)*	3.05 ± 0.09 *(n= 34)*	2.85 ± 0.20 *(n= 7)*
P17/19	9.93 ± 0.40 *(n= 14)*	3.34 ± 0.10 *(n= 7)*	3.31 ± 0.10 *(n= 15)*	3.04 ± 0.15 *(n= 9)*
P20/21	11.43 ± 0.56 *(n= 9)*	3.87 ± 0.14 *(n= 8)*	3.79 ± 0.19 *(n= 10)*	3.18 ± 0.15 *(n= 7)*
P22/24	11.80 ± 0.30 *(n= 16)*	4.32 ± 0.15 *(n= 12)*	3.89 ± 0.15 *(n= 16)*	3.74 ± 0.13 *(n= 15)*
P25/26	12.74 ± 0.35 *(n= 18)*	4.50 ± 0.17 *(n= 11)*	4.49 ± 0.15 *(n= 19)*	4.45 ± 0.20 *(n= 13)*
P27/29	13.73 ± 0.51 *(n= 6)*	5.35 ± 0.22 *(n= 7)*	5.09 ± 0.26 *(n= 7)*	5.10 ± 0.43 *(n= 6)*
P30/31	15.50 ± 1.01 *(n= 7)*	5.71 ± 0.21 *(n= 6)*	5.86 ± 0.33 *(n= 7)*	5.87 ± 0.40 *(n= 7)*
P32/35	17.20 ± 0.45 *(n= 23)*	6.04 ± 0.12 *(n= 13)*	6.13 ± 0.18 *(n= 23)*	6.43 ± 0.27 *(n= 20)*
P36/37	19.95 ± 0.79 *(n= 5)*	7.07 ± 0.49 *(n= 4)*	7.84 ± 0.44 *(n= 4)*	7.14 ± 0.13 *(n= 4)*
P38/40	23.62 ± 0.89 *(n= 7)*	8.24 ± 0.26 *(n= 9)*	8.35 ± 0.46 *(n= 9)*	9.32 ± 0.45 *(n= 8)*
P42/45	25.80 ± 1.17 *(n= 4)*	8.80 ± 0.67 *(n= 4)*	10.40 ± 0.74 *(n= 4)*	11.38 ± 0.58 *(n= 4)*

Values indicate mean ± standard error of the mean and sample sizes.

Table 2. Non-linear regression statistics for *S. crassicaudata* growth curves.

Semilog line -- X is linear, Y is log		Crown-rump length (mm)	Head width (mm)	Forelimb length (mm)	Hindlimb length (mm)
Best-fit values					
	Y-intercept	0.6959	0.285	0.188	0.1182
	Slope	0.01709	0.01587	0.01945	0.02188
Std. Error					
	Y-intercept	0.01695	0.01822	0.01753	0.03867
	Slope	0.0005084	0.0005532	0.000515	0.001114
95% CI (profile likelihood)					
	Y-intercept	0.6579 to 0.7323	0.2442 to 0.324	0.1483 to 0.2261	0.0267 to 0.2019
	Slope	0.01599 to 0.01822	0.01468 to 0.0171	0.01832 to 0.02061	0.01943 to 0.02449
Goodness of fit					
	Degrees of Freedom	12	12	12	12
	R squared	0.9916	0.9883	0.9936	0.9769
	Absolute Sum of Squares	4.32	0.681	0.5457	2.4
	Sy.x	0.6	0.2382	0.2132	0.4472
Normality of residuals					
	D'Agostino & Pearson omnibus K2	5.533	1.883	0.9898	1.56
	P value	0.0629	0.3901	0.6096	0.4583
	Passed normality test (alpha=0.05)?	Yes	Yes	Yes	Yes

A postnatal staging system for *S. crassicaudata*

To provide a developmental staging system that would account for inter-individual size variability, while allowing inter-species comparisons, we categorised dunnart development within both the Carnegie staging system for human development [13, 14], and the Thieler staging system for mouse development [15]. We considered formation of the eye as a comparative "anchor point", as its developmental timing is highly conserved from birds to mammals [23]. The Carnegie human system comprises 23 stages from conception to the formation of most adult structures (ca. 60 days/8-9 weeks), after which the embryo is considered a foetus. The Thieler mouse system is based

on milestones that match the Carnegie stages, and includes five additional stages that end postnatally with eye opening. For dunnarts, we have developed a comparable system, whereby embryos are born at equivalent stage 18 and leave the pouch at stage 29, ca. 70 days later (Fig 2). Intrauterine gestation lasts for 13-14 days [24], after which multiple 3-5 mm newborns must reach the pouch and attach to one of the 8-10 teats to complete development. One mother out of 105 in our study had 11 teats and 11 joeys, prompting the speculation that more newborns than teats available might be born and, therefore, that teat number is a limiting factor for litter size. Mothers in our study had an average of six and a mode of seven joeys.

Early postnatal anatomy of newborn *S. crassicaudata* (stage 18)

Newborn dunnarts have translucent and glossy skin. The forelimbs display alternating movements and are larger and more developed than the hindlimbs. The forelimbs have a distinguishable elbow joint and hand digits are partially fused (digital serration), while the forelimbs are proximally fused to the tail, mostly not mobile, and the feet digits are completely fused (paddle shape), although digital grooves are noticeable (Fig 3 and Table 3). The small eyes have a faint but noticeable ring of pigment. While eutherian mammals at equivalent stages have not yet undergone formation of the mouth apparatus, newborn dunnarts have a fully fused palate and well developed tongue (Figs 3 and 4). The lateral margins of the tongue press tightly around the teat and against the palate to allow active milk suckling. The presence of an olfactory and vomeronasal neuroepithelium (Figs 4E and 4F) in newborns raises the question of whether these systems are functional at birth. The olfactory bulb receives sensory axons traversing the cribiform plate, and the telencephalic vesicles include well-developed ganglionic eminences, an olfactory (piriform) cortex and a thin dorsal pallium (presumptive isocortex) that consists of a proliferative ventricular zone and preplate (Fig 4D). Eye development at birth has just undergone closure of the lens vesicle but no lens fibres are present as yet (Fig 4G).

Table 3. Developmental features across postnatal stages of *S. crassicaudata*.

Stage	Age (postnatal days)	Body	Head	Brain
18	0-3	• Hairless, translucent and shiny skin. • Forelimbs with elbow. Mostly fused digits (digital serration). • Hindlimb paddle, partly fused with the tail. Completely fused digits (digital grooves). • Joeys are curled and difficult to stretch. • Milk spot visible. • Little body movement.	• Prominent mandibular prognathism (underbite). • Frontal mouth opening. • Eye pigment slightly visible. • Lens vesicle just closed. • No ear buds. • Large nostrils.	• Telencephalic vesicles present. • Dorsal pallium at stage of preplate and ventricular zone. • Large diencephalon and midbrain.
19	4-7	• Distinct hands. Digits partly fused. • Hindlimbs and tail buds distinguishable, still fused. • Joeys easier to uncurl. • Alternate forelimb movement.	• Darker eye pigment. • No face pigmentation. • Developing lens fibres. • Short and thin hair, only on top of the head.	• Piriform cortex and olfactory tubercle better defined.
20	8-11	• More opaque skin.	• Small ear buds. • Slight pigment on top of snout.	• Prominent lateral olfactory tract,

		• Small claws in separated forelimb digits. • Hindlimb digits mostly fused (digital serration). • Jugular and carotid processes defined.	• Lens epithelium and fibres enlarged. Retinal layers slightly visible. Optic stalk.	endopiriform and piriform regions. • Dorsal pallium without a defined cortical plate.
21	12-15	• Opaque skin. • Hindlimbs and tail unfused and well defined. • Hindlimb digits partly fused. • Joeys can be completely uncurled. • Movement of front-temporal head muscles.	• Underbite less prominent. • Mild pigment on top of snout. • Short, thick hair only on top of the head. • Thicker cornea, lens well developed. Clear retinal layers. Optic nerve.	• Internal, and external capsules clearly defined. • Anterior commissure present. • Cortical plate appears. • Larger subpallium region.
22	16-19	• Large, pigmented forelimb claws. • Hindlimb digits separated, with small claws. • Large jugular and carotid processes visible.	• Larger ear buds. • Darker hair on top of the head. • Darker pigment on top of snout.	• Olfactory tubercle and layer 2 of piriform cortex clearly defined.
23	20-23	• Short, light hair on face and body. • - Hindlimb digits well defined, with small claws.	• Underbite less prominent. • Larger, darker eye pigment. • Larger ear buds.	• Expansion of subventricular and intermediate zones. • Ventralisation of the piriform cortex.

24	24-26	• Short, light hair on face and body. • Darker skin, jugular and carotid processes less visible. • Longer, motile hindlimbs, with clear claws. • Overall body movement increased and responsive.	• Mandibulary and maxillary processes aligned. • Long, thick, dark hair on top of head. • Ear flap is distinguishable. • Small whiskers.	• Hippocampal commissure first visible. • Indentation of piriform and olfactory tubercle cell layers along the lateral olfactory tract. • Superior and inferior colliculi distinguishable.
25	27-30	• Slightly darker body hair. • Legs and tail very well developed. Hindlimb claws slightly pigmented. • Less curved and more motile body.	• Snout progression (slight maxillary overbite). • Mouth still fused. • Larger and darker eye pigment. • Ear lobes better defined.	• Indentation of the rhinal fissure. • Ventral expansion of the developing cortical plate.
26	31-35	• Longer, darker hair on face and body, especially on tail and back. • Large digits with dark and well developed claws. • Jugular and carotid processes less visible.	• Mouth lining visible but still fused. • Eyelid grooves become apparent. • Dark, larger skin pigment patch on top of snout. Larger whiskers.	• Reduction of the subventricular zone. • Cortical layers 5 and 6 are present.
27	36-40	• Longer, darker hair all over body.	• Mouth almost unfused, deep groove.	• Cortical layers 2-4 are defined.

		• Jugular and carotid processes not visible. • Testes/pouch clearly visible. • Fully dependent on their mother, have never left the pouch.	• Eyelid margin is clearly distinct. • Ear canal better defined.	
28	41-50	• Back completely covered with dark and thick hair, abdomen hair lighter colour. • Pups, can detach and switch nipples, as well as leave the pouch temporarily. • Narrower snout.	• Mouth unfused, can be fully opened. • Very pigmented and large, but unopen, eyes. • Fully formed ears with clearly open canal.	• Further indentation of the rhinal fissure. • Further ventral progression of the cortex. • Diencephalon is fully covered by the dorsal cortex.
29	51-70	• Mature-looking fur in head and body. • Mature-looking narrow snout. • Pups often leave the pouch and try solid food.	• Mouth fully open. • Mature-looking whisker pads. • Eyes begin to open.	• Well defined cortical areas and regions, resembling the adult.

Craniofacial and brain development in stages 19-21 of *S. crassicaudata*

Head features of subsequent stages 19, 20, 21 of *S. crassicaudata* (postnatal days 4-7, 8-11, and 12-15, respectively) are presented in Fig 5A-C. Hair follicles can be seen increasing in abundance between these stages (Figs 4 and 5), and subsequent development of thick hair over the parietal scalp remains a salient feature of early-to-mid postnatal development. Telencephalic development includes growth of the piriform cortex and expansion of the lateral olfactory tract, which becomes visible by stage 20 (Fig 5B). The ganglionic eminences are apparent by stage 20 and become striated at stage 21 by axons forming the internal capsule (Fig 5C). The isocortical preplate has split

to form the marginal zone and the subplate by stage 20, followed by the emergence of a thin cortical plate by stage 21. The anterior commissure, carrying olfactory, piriform and temporal isocortical axons appears at stage 21. Eye development shows a similar developmental sequence to stage-matched mice and humans (Fig 5D-F). Stage 19 includes formation of lens fibres, by stage 20 a thin lens epithelium, enlarged lens fibres, and neuroblastic and ganglion cell layers in the retina are apparent, and stage 21 is characterised by a mature-looking lens, a thicker cornea and a distinct optic nerve. Accordingly, pioneering axons of the dunnart optic nerve have been reported to begin growth, cross the midline, and reach their central targets, respectively, during these three stages [25, 26].

Mid and late pouch development: Cortical layering and body changes in stages 22-29 of *S. crassicaudata*

Subsequent stages of *S. crassicaudata* comprise a progressive succession of general body features and brain development. Between stages 22-25, dunnarts undergo changes in facial morphology, with mandibular and maxillar processes progressing from a marked prognathism (underbite), to alignment and progression of the snout (Fig 2 and Table 3). Digit development begins in the forelimbs, and is not evident in the hindlimbs until stage 22.

Principal neuron cell layers of the piriform cortex and olfactory tubercle are evident by stage 22, and become angled by the enlargement of the lateral olfactory tract (Fig 6). This is followed by the expansion of the cortical plate and underlying subplate from latero-ventral to medio-dorsal regions. In fact, the prospective claustrum and endopiriform nuclei, which arise from lateral and ventral pallial derivatives [27, 28], can be distinguished from stage 22 onwards, before the respective enlargement of the overlaying insular/perirhinal and piriform cortices, and formation of the rhinal fissure by stage 25 (Fig 6, arrowheads). In eutherians, most interhemispheric projections from the isocortex and cingulate cortex cross the midline through the corpus callosum, while in non-eutherians these projections course through the anterior commissure. In dunnarts, as in other marsupials, the anterior commissure forms at least one week before the hippocampal commissure, while in eutherians they arise closer in time, with the corpus callosum being the last telencephalic commissure to form [6, 19, 29-31]. Interestingly, dunnarts also lack the astrogliogenic remodelling of the septal midline, a process required for callosal formation in eutherians [32, 33] that could relate to heterochronies in the formation of interhemispheric circuits in the brain of mammals.

A dorsal view of the brain reveals the progressive growth of the isocortical mantle (Figs 6 and 7, green schematics), which does not fully cover the dorsal diencephalon until stage 28. Development of the isocortex is largely protracted in this species, as in other marsupials [7, 8, 10], and isocortical

layers do not become apparent until stage 27 (Fig 7). The piriform/insular cortex boundary (arrowheads in Figs 6 and 7) reveals the ventral expansion of the isocortex, as the rhinal fissure is positioned more ventrally between stages 24-27. Infragranular neurons that give rise to layers 5/6 of the isocortex, as well as subplate neurons, are recognisable superficial to the intermediate zone by stage 26, once supragranular neurons have begun their radial migration towards the cortical plate. The thalamo-recipient cell dense layer 4 as well as upper layers 2/3 become evident by stage 27 onwards (Fig 7). By this time, sensory axons from the thalamus accumulate in layer 4, forming modality-specific sensory areas that subsequently expand tangentially, further displacing the rhinal fissure ventrally (Fig 7).

Pre- and peri-weaning stages are characterised by the formation of the mouth lining from a deep groove, noticeable from stage 26, which allows full opening of the mouth for the first time around stage 28, once isocortical neurons are established in their final layers. After this time, joeys can be observed swapping teats and leaving the pouch temporarily. Fur begins covering the whole body by stage 26 and joeys achieve a mature appearance by stage 29, the last stage of our study, which culminates with eye opening and weaning at around 70 postnatal days.

Discussion

Eutherian mammals, such as rodents and humans, differ from marsupials and monotremes in that they have a prolonged intrauterine period that extends beyond embryonic development (past Carnegie/Thieler stage 23). Non-eutherian mammals, on the other hand, are born at comparatively earlier stages and must complete development by feeding from their mothers' milk, outside the uterus. Accordingly, dunnarts are born with a fully functional mouth apparatus, whereas eutherians at an equivalent stage have unfused pharyngeal arches and orofacial development occurs after the onset of telencephalic development [1, 12, 34]. Another difference is that the anterior skeleton forms much earlier than the posterior skeleton in marsupials, as compared to the more uniform development of eutherians [1, 2, 35-38]. As functional forelimbs are crucial for marsupial embryos to reach the teat, such early behaviour may act as a developmental constraint limiting phenotypic variability of the mouth and forelimbs in marsupials. Accordingly, eutherians display a comparatively larger repertoire of mouth and forelimb morphologies across species than marsupials (e.g. mouth of elephants and star-nosed moles, or forelimbs of bats and dolphins) likely due to the release of such constraints by the extended intrauterine retention of the embryo [34, 39]. Therefore, a major challenge of translating staging systems between species are differences in the relative rates of development between different body parts. However, as the rate of brain development is less variable than that of the body across mammals [11, 40-42], information about the timing of neural structures are optimal for staging purposes. Importantly, later events in brain development are

slower in marsupials than in eutherians [7, 10, 11], possibly due to metabolic differences of lactation versus placentation during development [8, 9], further highlighting their potential as animal models brain wiring.

As compared to eutherians, development of the dunnart isocortex is largely protracted and occurs mostly between the second and the sixth postnatal week. The olfactory cortex, on the other hand, acquires a layered organisation much earlier, along with the growth of the lateral olfactory tract and formation of the anterior commissure. It is not clear whether the olfactory and/or vomeronasal systems of dunnarts are functional at birth, however newborn wallabies orient themselves towards odours from the mother's pouch [43], despite the immature appearance of their olfactory systems [44]. In any case, peripheral and central olfactory structures are present in dunnart newborns, well before the arrival of thalamic inputs from other senses and formation of layers in the isocortex. Whether early olfactory function is related to the subsequent formation of isocortical circuits is a possibility that has ignited recent interest [45-47]. Developmental interactions between the olfactory systems and the rest of the forebrain appear conserved across mammals, even in species whose adults lack functional olfactory systems [48-50]. Moreover, evidence from mice suggest that the olfactory system can influence the cellular and electrical features of isocortical development [51-53], further supporting the hypothesis that the olfactory system could be a driver of mammalian brain development.

The extended period of forebrain formation in marsupials, plus the continuous access to developing joeys inside the pouch, offers promising opportunities to study multiple developmental processes sequentially, and *in vivo*. Such capability cannot be achieved with traditional eutherian models, such as rodents, carnivores and primates, as embryos develop inside the uterus and cannot readily survive if taken prematurely. The excellent breeding under controlled conditions, small body size, large litters, and short life cycles, make dunnarts promising laboratory models to study not only the mechanisms of brain development but also multiple questions of biological relevance.

Acknowledgements

The authors would like to acknowledge the help from staff from The University of Queensland Biological Resources, in particular Kym French, Trish Hitchcock and Cora Lau. Additional thanks to Ilan Gobius, Robert Sullivan, Thomas Pollak, Caitlin Bridges and Ching Moey for their help in experimental and/or animal procedures, and to the reviewers for their helpful suggestions to improve the manuscript.

References

1. Smith KK. Comparative Patterns of Craniofacial Development in Eutherian and Metatherian Mammals. Evolution. 1997;51(5):1663-78. doi: 10.2307/2411218.

2. Smith KK. Heterochrony revisited: the evolution of developmental sequences. Biological Journal of the Linnean Society. 2001;73(2):169-86. doi: 10.1111/j.1095-8312.2001.tb01355.x.

3. Werneburg I, Sánchez-Villagra MR. The early development of the echidna, Tachyglossus aculeatus (Mammalia: Monotremata), and patterns of mammalian development. Acta Zoologica. 2011;92(1):75-88. doi: 10.1111/j.1463-6395.2009.00447.x.

4. Werneburg I, Tzika AC, Hautier L, Asher RJ, Milinkovitch MC, Sanchez-Villagra MR. Development and embryonic staging in non-model organisms: the case of an afrotherian mammal. J Anat. 2013;222(1):2-18. Epub 2012/04/28. doi: 10.1111/j.1469-7580.2012.01509.x. PubMed PMID: 22537021; PubMed Central PMCID: PMCPMC3552411.

5. Jeffery JE, Richardson MK, Coates MI, Bininda-Emonds OR. Analyzing developmental sequences within a phylogenetic framework. Systematic biology. 2002;51(3):478-91. Epub 2002/06/25. doi: 10.1080/10635150290069904. PubMed PMID: 12079645.

6. Ashwell KWS, Waite PME, Marotte L. Ontogeny of the Projection Tracts and Commissural Fibres in the Forebrain of the Tammar Wallaby (*Macropus eugenii*): Timing in Comparison with Other Mammals. Brain, Behavior and Evolution. 1996;47(1):8-22.

7. Darlington RB, Dunlop SA, Finlay BL. Neural development in metatherian and eutherian mammals: variation and constraint. J Comp Neurol. 1999;411(3):359-68. Epub 1999/07/22. PubMed PMID: 10413772.

8. Renfree MB, Holt A, Green S, Carr J, Cheek D. Ontogeny of the brain in a marsupial (Macropus eugenii) throughout pouch life. I. Brain growth. Brain Behav Evol. 1982;20:57-1.

9. Weisbecker V, Goswami A. Brain size, life history, and metabolism at the marsupial/placental dichotomy. Proceedings of the National Academy of Sciences. 2010;107(37):16216-21. doi: 10.1073/pnas.0906486107.

10. Workman AD, Charvet CJ, Clancy B, Darlington RB, Finlay BL. Modeling transformations of neurodevelopmental sequences across mammalian species. J Neurosci. 2013;33(17):7368-83. Epub 2013/04/26. doi: 10.1523/jneurosci.5746-12.2013. PubMed PMID: 23616543; PubMed Central PMCID: PMCPMC3928428.

11. Halley AC. Minimal variation in eutherian brain growth rates during fetal neurogenesis. Proceedings Biological sciences / The Royal Society. 2017;284(1854). Epub 2017/05/12. doi: 10.1098/rspb.2017.0219. PubMed PMID: 28490626; PubMed Central PMCID: PMCPMC5443945.

12. Nelson JE. Developmental staging in a marsupial Dasyurus hallucatus. Anat Embryol (Berl). 1992;185(4):335-54. Epub 1992/01/01. PubMed PMID: 1609962.

13. O'Rahilly R, Müller F. Developmental stages in human embryos: Including a revision of Streeter's "Horizons" and a survey of the Carnegie collection. Connecticut: Merider-Stinehour Press; 1987. 306 p.
14. Streeter G. Developmental Horizons In Human Embryos Description Or Age Groups XIX, XX, XXI, XXII, And XXIII, Being The Fifth Issue Of A Survey Of The Carnegie Collection. Streeter G, editor. Baltimore1957.
15. Thieler K. The House Mouse: Atlas of Embryonic Development. New York: Springer-Verlag; 1989. 178 p.
16. McCrady E. The embryology of the opossum. Am Anat Memoirs. 1938;16:1-233.
17. Rakic P. Specification of cerebral cortical areas. Science. 1988;241(4862):170-6. doi: 10.1126/science.3291116.
18. Cummings DM, Malun D, Brunjes PC. Development of the anterior commissure in the opossum: midline extracellular space and glia coincide with early axon decussation. J Neurobiol. 1997;32(4):403-14. Epub 1997/04/01. PubMed PMID: 9087892.
19. Shang F, Ashwell KWS, Marotte LR, Waite PME. Development of commissural neurons in the wallaby (Macropus eugenii). The Journal of Comparative Neurology. 1997;387(4):507-23. doi: 10.1002/(sici)1096-9861(19971103)387:4<507::aid-cne3>3.0.co;2-6.
20. Molnar Z, Knott GW, Blakemore C, Saunders NR. Development of thalamocortical projections in the South American gray short-tailed opossum (Monodelphis domestica). J Comp Neurol. 1998;398(4):491-514. Epub 1998/08/26. PubMed PMID: 9717705.
21. Poiley S. A systematic method of breeder rotation for non-inbred laboratory animal colonies. Proc Anim Care Panel. 1960;10:159-66.
22. Morton SR. An ecological study of *Sminthopsis crassicaudata* (Marsupialia: Dasyuridae) III. Reproduction and life history. Aust Wildl Res. 1978;5:183-211.
23. Dreher B, Robinson SR. Development of the retinofugal pathway in birds and mammals: evidence for a common 'timetable'. Brain Behav Evol. 1988;31(6):369-90. Epub 1988/01/01. PubMed PMID: 3046710.
24. Godfrey GK, Crowcroft P. Breeding the Fat-tailed marsupial mouse in captivity. International Zoo Yearbook. 1971;11(1):33-8. doi: 10.1111/j.1748-1090.1971.tb01839.x.
25. Dunlop SA, Tee LB, Lund RD, Beazley LD. Development of primary visual projections occurs entirely postnatally in the fat-tailed dunnart, a marsupial mouse, Sminthopsis crassicaudata. J Comp Neurol. 1997;384(1):26-40. Epub 1997/07/21. PubMed PMID: 9214538.
26. Dunlop SA, Lund RD, Beazley LD. Segregation of optic input in a three-eyed mammal. Exp Neurol. 1996;137(2):294-8. Epub 1996/02/01. doi: 10.1006/exnr.1996.0028. PubMed PMID: 8635544.

27. Watson C, Puelles L. Developmental gene expression in the mouse clarifies the organization of the claustrum and related endopiriform nuclei. Journal of Comparative Neurology. 2017;525(6):1499-508. doi: 10.1002/cne.24034.
28. Puelles L. Development and Evolution of the Claustrum. In: John Smythies, Larry Edelstein, Ramachandran VS, editors. The Claustrum: Structural, Functional, and Clinical Neuroscience. San Diego: Academic Press; 2014. p. 119-76.
29. Suárez R. Evolution of Telencephalic Commissures: Conservation and Change of Developmental Systems in the Origin of Brain Wiring Novelties. In: Kaas JH, editor. Evolution of Nervous Systems (Second Edition). Oxford: Academic Press; 2017. p. 205-23.
30. Suárez R, Gobius I, Richards LJ. Evolution and development of interhemispheric connections in the vertebrate forebrain. Frontiers in human neuroscience. 2014;8:497. Epub 2014/07/30. doi: 10.3389/fnhum.2014.00497. PubMed PMID: 25071525; PubMed Central PMCID: PMCPmc4094842.
31. Ashwell KW, Marotte LR, Li L, Waite PM. Anterior commissure of the wallaby (Macropus eugenii): adult morphology and development. J Comp Neurol. 1996;366(3):478-94. Epub 1996/03/11. doi: 10.1002/(SICI)1096-9861(19960311)366:3<478::AID-CNE8>3.0.CO;2-1. PubMed PMID: 8907360.
32. Gobius I, Morcom L, Suarez R, Bunt J, Bukshpun P, Reardon W, et al. Astroglial-mediated remodeling of the interhemispheric midline is required for the formation of the corpus callosum. Cell reports. 2016;17(3):735-47. Epub 2016/10/13. doi: 10.1016/j.celrep.2016.09.033. PubMed PMID: 27732850; PubMed Central PMCID: PMCPMC5094913.
33. Gobius I, Suárez R, Morcom L, Paolino A, Edwards TJ, Kozulin P, et al. Astroglial-mediated remodeling of the interhemispheric midline during telencephalic development is exclusive to eutherian mammals. Neural Development. 2017;12(1):9. doi: 10.1186/s13064-017-0086-1.
34. Goswami A, Randau M, Polly PD, Weisbecker V, Bennett CV, Hautier L, et al. Do developmental constraints and high integration limit the evolution of the marsupial oral apparatus? Integrative and Comparative Biology. 2016;56(3):404-15. doi: 10.1093/icb/icw039.
35. Weisbecker V, Goswami A, Wroe S, Sánchez-Villagra MR. Ossification heterochrony in the Therian postcranial skeleton and the marsupial-placental dichotomy. Evolution. 2008;62(8):2027-41. doi: 10.1111/j.1558-5646.2008.00424.x.
36. Keyte AL, Smith KK. Heterochrony and developmental timing mechanisms: changing ontogenies in evolution. Seminars in cell & developmental biology. 2014;34:99-107. Epub 2014/07/06. doi: 10.1016/j.semcdb.2014.06.015. PubMed PMID: 24994599; PubMed Central PMCID: PMCPMC4201350.

37. Sánchez-Villagra MR. Comparative patterns of postcranial ontogeny in therian Mammals: An analysis of relative timing of ossification events. Journal of Experimental Zoology. 2002;294(3):264-73. doi: 10.1002/jez.10147.
38. Chew KY, Shaw G, Yu H, Pask AJ, Renfree MB. Heterochrony in the regulation of the developing marsupial limb. Developmental Dynamics. 2014;243(2):324-38. doi: 10.1002/dvdy.24062.
39. Kelly EM, Sears KE. Limb specialization in living marsupial and eutherian mammals: constraints on mammalian limb evolution. Journal of Mammalogy. 2011;92(5):1038-49. doi: 10.1644/10-MAMM-A-425.1.
40. Halley AC. Prenatal Brain-Body Allometry in Mammals. Brain Behav Evol. 2016;88(1):14-24. Epub 2016/08/27. doi: 10.1159/000447254. PubMed PMID: 27561684.
41. Passingham RE. Rates of brain development in mammals including man. Brain Behav Evol. 1985;26(3-4):167-75. Epub 1985/01/01. PubMed PMID: 3936591.
42. Sacher GA, Staffeldt EF. Relation of Gestation Time to Brain Weight for Placental Mammals: Implications for the Theory of Vertebrate Growth. The American Naturalist. 1974;108(963):593-615.
43. Schneider NY, Fletcher TP, Shaw G, Renfree MB. The olfactory system of the tammar wallaby is developed at birth and directs the neonate to its mother's pouch odours. Reproduction. 2009;138(5):849-57. doi: 10.1530/rep-09-0145.
44. Ashwell KWS, Marotte LR, Cheng G. Development of the Olfactory System in a Wallaby *(Macropus eugenii)*. Brain, Behavior and Evolution. 2008;71(3):216-30.
45. Rowe TB, Macrini TE, Luo ZX. Fossil evidence on origin of the mammalian brain. Science. 2011;332(6032):955-7. Epub 2011/05/21. doi: 10.1126/science.1203117. PubMed PMID: 21596988.
46. Aboitiz F, Montiel JF. Olfaction, navigation, and the origin of isocortex. Frontiers in Neuroscience. 2015;9. doi: 10.3389/fnins.2015.00402.
47. Rowe TB, Shepherd GM. Role of ortho-retronasal olfaction in mammalian cortical evolution. Journal of Comparative Neurology. 2016;524(3):471-95. doi: 10.1002/cne.23802.
48. Oelschläger HA, Buhl EH, Dann JF. Development of the nervus terminalis in mammals including toothed whales and humans. Annals of the New York Academy of Sciences. 1987;519(1):447-64. doi: 10.1111/j.1749-6632.1987.tb36316.x.
49. Meisami E, Bhatnagar KP. Structure and diversity in mammalian accessory olfactory bulb. Microsc Res Tech. 1998;43(6):476-99. Epub 1999/01/08. doi: 10.1002/(sici)1097-0029(19981215)43:6<476::aid-jemt2>3.0.co;2-v. PubMed PMID: 9880163.

50. Suárez R, García-González D, de Castro F. Mutual influences between the main olfactory and vomeronasal systems in development and evolution. Front Neuroanat. 2012;6:50. Epub 2012/12/28. doi: 10.3389/fnana.2012.00050. PubMed PMID: 23269914; PubMed Central PMCID: PMC3529325.
51. de Frutos Cristina A, Bouvier G, Arai Y, Thion Morgane S, Lokmane L, Keita M, et al. Reallocation of olfactory Cajal-Retzius cells shapes neocortex architecture. Neuron. 2016;92(2):435-48. doi: 10.1016/j.neuron.2016.09.020.
52. Conhaim J, Easton CR, Becker MI, Barahimi M, Cedarbaum ER, Moore JG, et al. Developmental changes in propagation patterns and transmitter dependence of waves of spontaneous activity in the mouse cerebral cortex. J Physiol. 2011;589(Pt 10):2529-41. Epub 2011/04/14. doi: 10.1113/jphysiol.2010.202382. PubMed PMID: 21486817; PubMed Central PMCID: PMCPMC3115823.
53. Easton CR, Weir K, Scott A, Moen SP, Barger Z, Folch A, et al. Genetic elimination of GABAergic neurotransmission reveals two distinct pacemakers for spontaneous waves of activity in the developing mouse cortex. J Neurosci. 2014;34(11):3854-63. Epub 2014/03/14. doi: 10.1523/jneurosci.3811-13.2014. PubMed PMID: 24623764; PubMed Central PMCID: PMCPMC3951690.

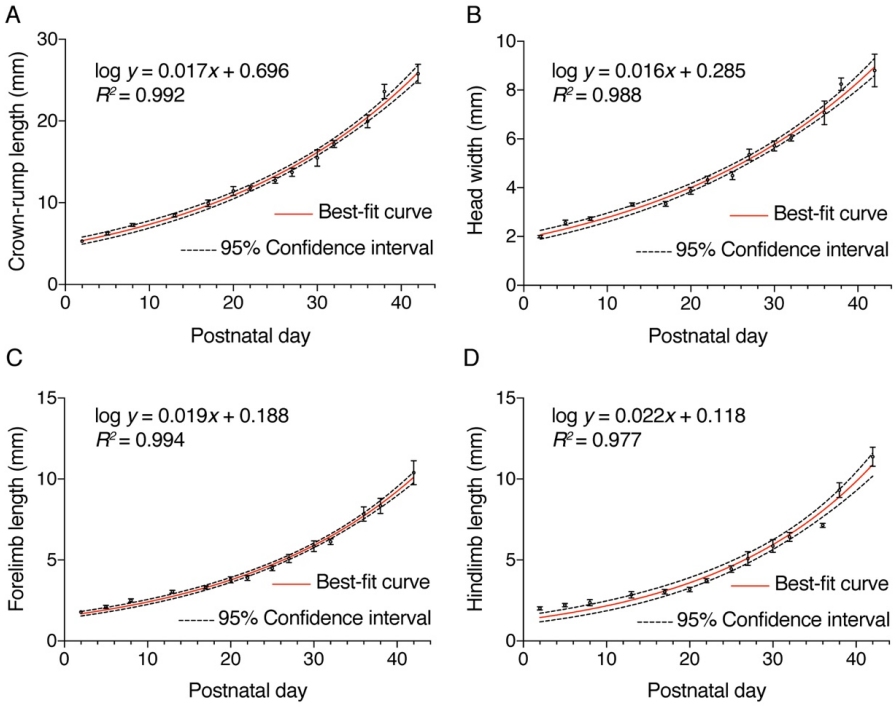

Fig 1. Developmental growth curves of postnatal *S. crassicaudata.*

Semilogarithmic relationships between the postnatal age (in days) and crown-rump length (A), head width (B), forelimb length (C), and hindlimb length (D). Mean ± standard error of the mean, as well as best-fit regression curves (red lines) and 95% confidence intervals (dotted lines) are indicated in each case. Non-linear functions whereby y indicates the corresponding measurements (in mm) and x the age in days, as well as R^2 values are indicated. See Tables 1 and 2 for additional information.

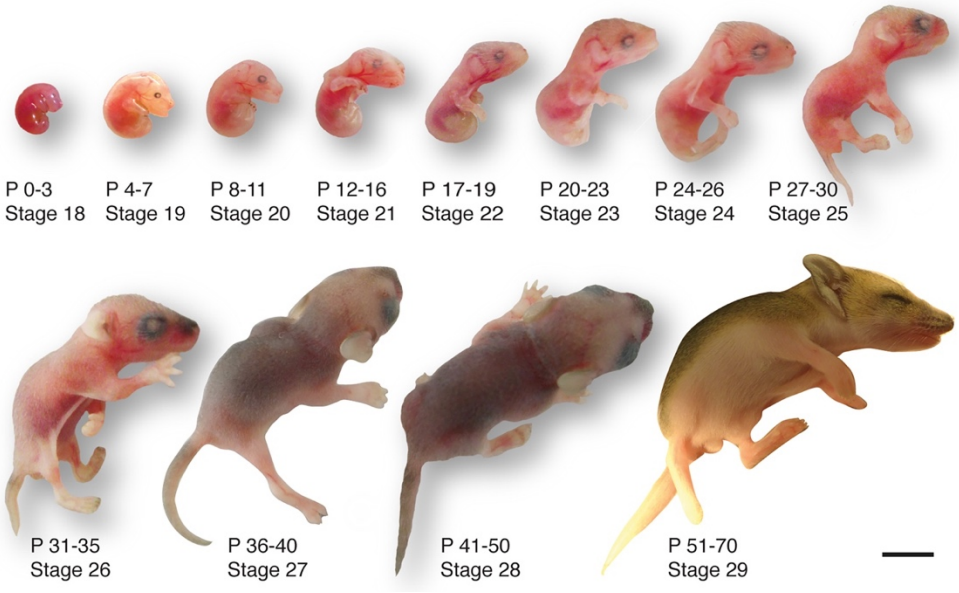

Fig 2. Developmental series of postnatal *S. crassicaudata*.

A system of twenty-nine arbitrary stages from conception to weaning is included to match equivalent stages in human (Carnegie staging system) and mouse (Thieler staging system). Birth occurs at stage 18. Corresponding age of each stage is included as a range of postnatal days (P). See Table 3 for further details. Scale bar: 5 mm.

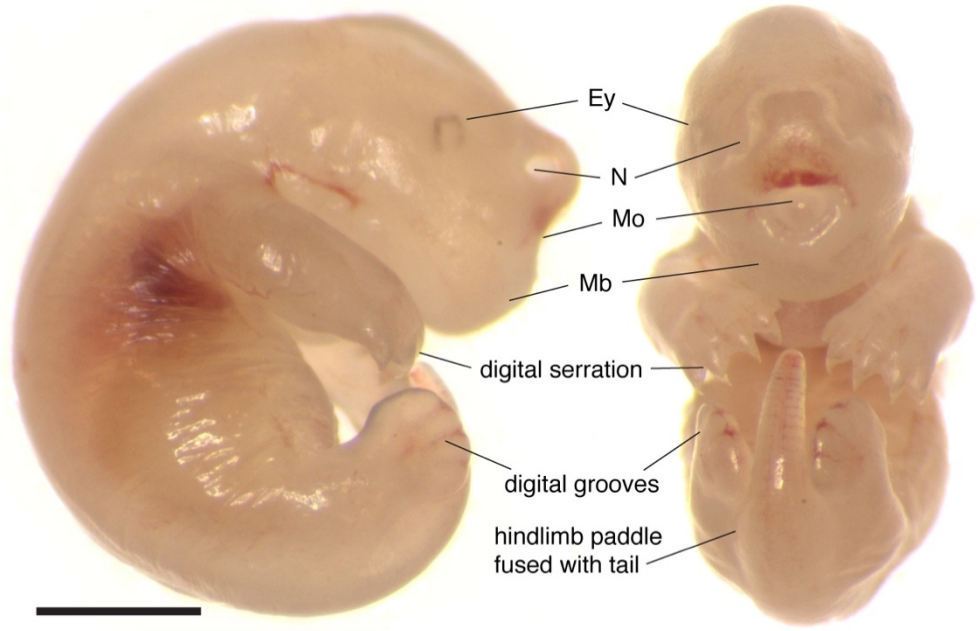

Fig 3. External body features of newborn S. crassicaudata

Microphotograph of a stage 18 newborn dunnart as seen from the right and from the front. Note the prominent orofacial features, including fused mandible (Mb), and wide nostrils (N). The eyes (Ey) are small and lightly pigmented. Forelimbs are more advanced than hindlimbs, with digits serrated as compared to completely fused. Scale bar: 1mm.

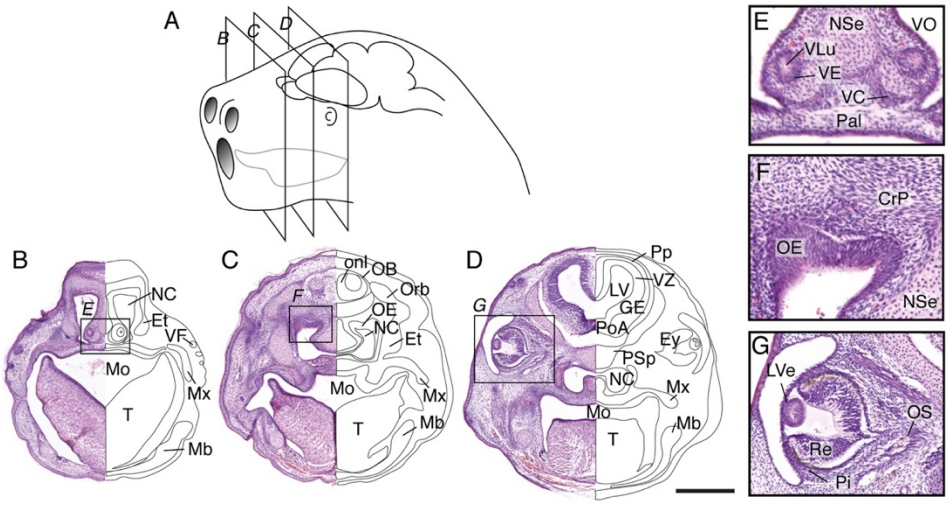

Fig 4. Craniofacial features of newborn *S. crassicaudata*.

(A) Schematic of a stage 18 dunnart head (postnatal day 0-3) indicating the relative size and position of nostrils, mouth, tongue, eyes and brain, as well as the section planes shown in (B-D). (B-D) Hematoxylin/eosin staining of a rostral-caudal series through the planes depicted in panel A reveals orofacial, sensory and brain structures of newborn dunnarts, including a prominent tongue (T) that encloses the teat inside the mouth (Mo) reaching the lateral margins of the palate (Pal). Large nasal cavities (NC) with fused palate (Pal) and nasal septum (NSe) can be seen, including condensation of mandibular (Mb) and maxillary (Mx) processes, eyes (Ey) fully covered by skin, and scattered vibrissal follicles (VF) in the snout. Telencephalic structures include the olfactory bulb (OB), with surrounding olfactory nerve layer (onl), preplate (Pp), ventricular zone (VZ) and ganglionic eminences (GE) as well as a large lateral ventricle (LV). E-F, inset of the regions highlighted in B-D depicting developing sensory structures. E, the vomeronasal organ (VO) includes a lumen (VLu), neuroepithelium (VE) and capsule (VC) at the base of NSe and Pal. F, a thick olfactory neuroepithelium (OE) is located at the roof of the NC, immediately below the presumptive cribiform plate (CrP). G, eye development has just undergone closure of the lens vesicle (LVe), the pigment epithelium (Pi) outlines a dark ring around cells of the retina (Re). Et, ethmoid bone; Orb, orbital bone; PoA, preoptic area; PSp; presphenoid bone. Scale bar: 500 μm.

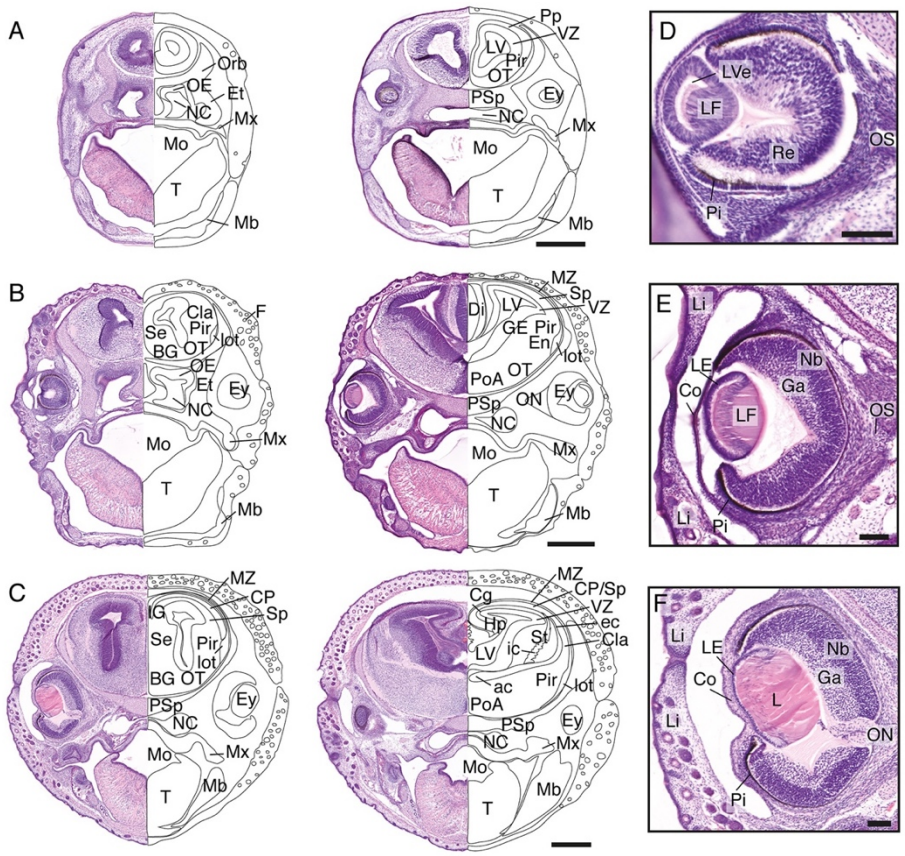

Fig 5. Craniofacial features of stages 19-21 *S. crassicaudata*.

Hematoxylin/eosin staining through rostral (left) and caudal (right) regions of the head of *S. crassicaudata* at stages 19 (A), 20 (B), and 21 (C) in the coronal plane (postnatal days 4-7, 8-11, and 12-15, respectively). Insets of the developing eye at corresponding ages (D-F, respectively). ac, anterior commissure; BG, basal ganglia; Cg, cingulate cortex; Cla, claustrum; Co, cornea; CP, cortical plate; ec, external capsule; En, endopiriform nucleus; Ey, eye; Et, ethmoid bone; F, follicle; Ga, ganglion layer; GE, ganglionic eminence; Hp, hippocampus; ic, internal capsule; IG, indusium griseum; L, lens; LE, lens epithelium; LF, lens fibres; Li, eyelid; lot, lateral olfactory tract; LV, lateral ventricle; LVe, lens vesicle; Mb, mandibulary process; Mo, mouth; Mx, maxillary process; MZ, marginal zone; NC, nasal cavity; Nb, neuroblastic layer; OE, olfactory neuroepithelium; ON, optic nerve; Orb, orbital bone; OS, optic stalk; OT, olfactory tubercle; Pi, pigment epithelium; Pir, piriform cortex; PoA, preoptic area; Pp, preplate; PSp; presphenoid bone; Re, retinal layer; Se, septum; Sp, subplate; St, striatum; SVZ, subventricular zone; T, tongue; VZ, ventricular zone. Scale bars: 500 μm (A-C), 100 μm (E-F).

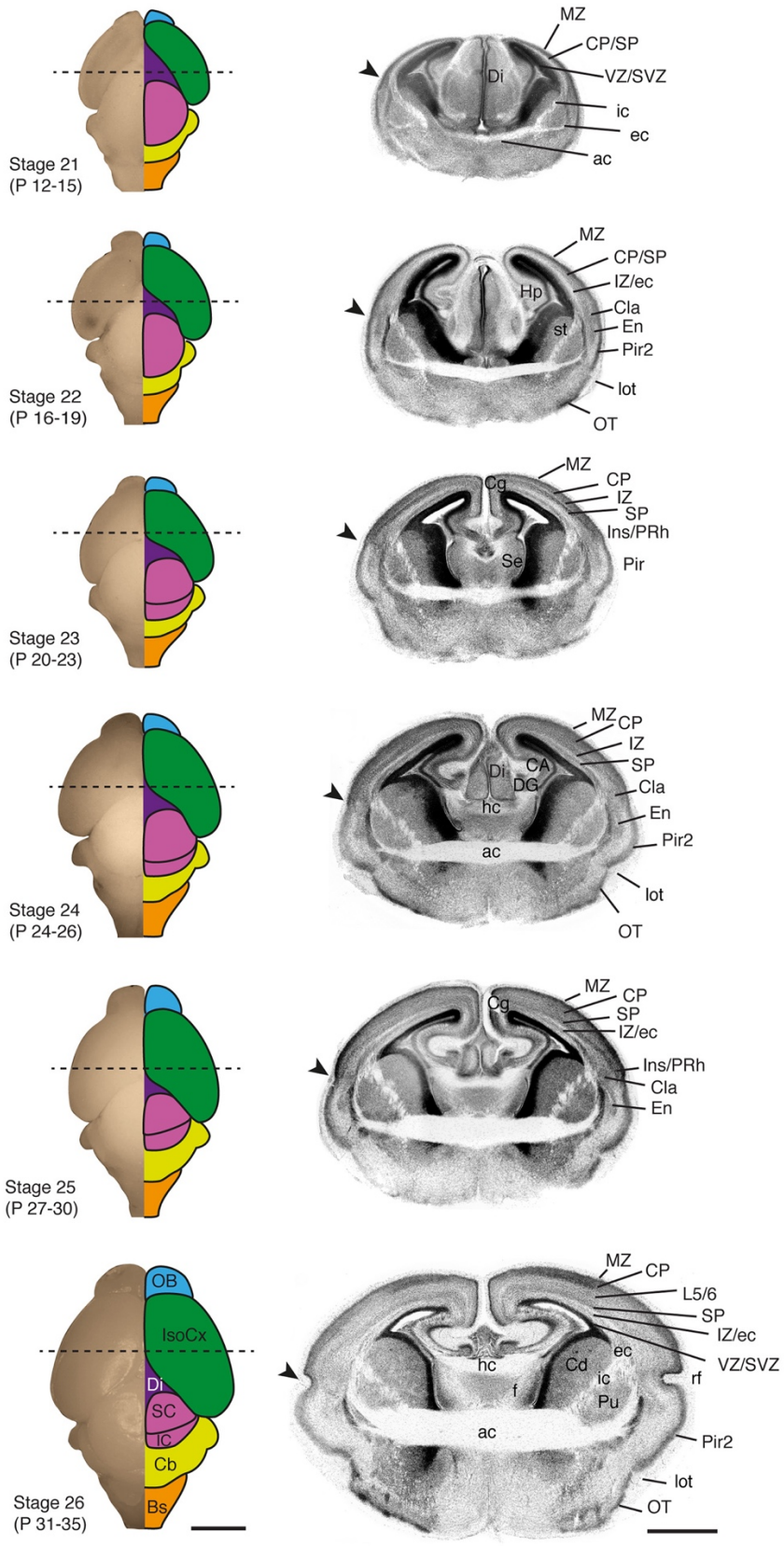

Fig 6. Brain features of *S. crassicaudata* between stages 21 and 26.

Developmental series of fixed dunnart brains showing a dorsal view of the whole brain (left column) and corresponding DAPI-stained coronal section (right column) through the approximate region indicated by dotted lines. The main brain regions are colour-coded, and stages and

approximate postnatal (P) days are indicated. Arrowheads show the prospective rhinal fissure (rf). ac, anterior commissure; BS, brainstem; CA, cornu ammonis hippocampi; Cb, cerebellum; Cd, caudate; Cg, cingulate cortex; Cla, claustrum; CP, cortical plate; DG, dentate gyrus; Di, diencephalon; ec, external capsule; En, endopiriform; f, fornix; hc, hippocampal commissure; Hp, hippocampus; ic, internal capsule; IC, inferior colliculus; Ins, insular cortex; IsoCx, isocortex; IZ, intermediate zone; L5/6, isocortical layers 5/6; lot, lateral olfactory tract; MZ, marginal zone; OB, olfactory bulb; OT, olfactory tubercle; Pir, piriform cortex; Pir2, piriform cortex, layer 2; PRh, perirhinal; Pu, putamen; rf, rhinal fissure; SC, superior colliculus; Se, septum; SP, subplate; SVZ, subventricular zone; VZ, ventricular zone. Scale bars: 2000 μm in whole brains, and 200 μm in coronal sections.

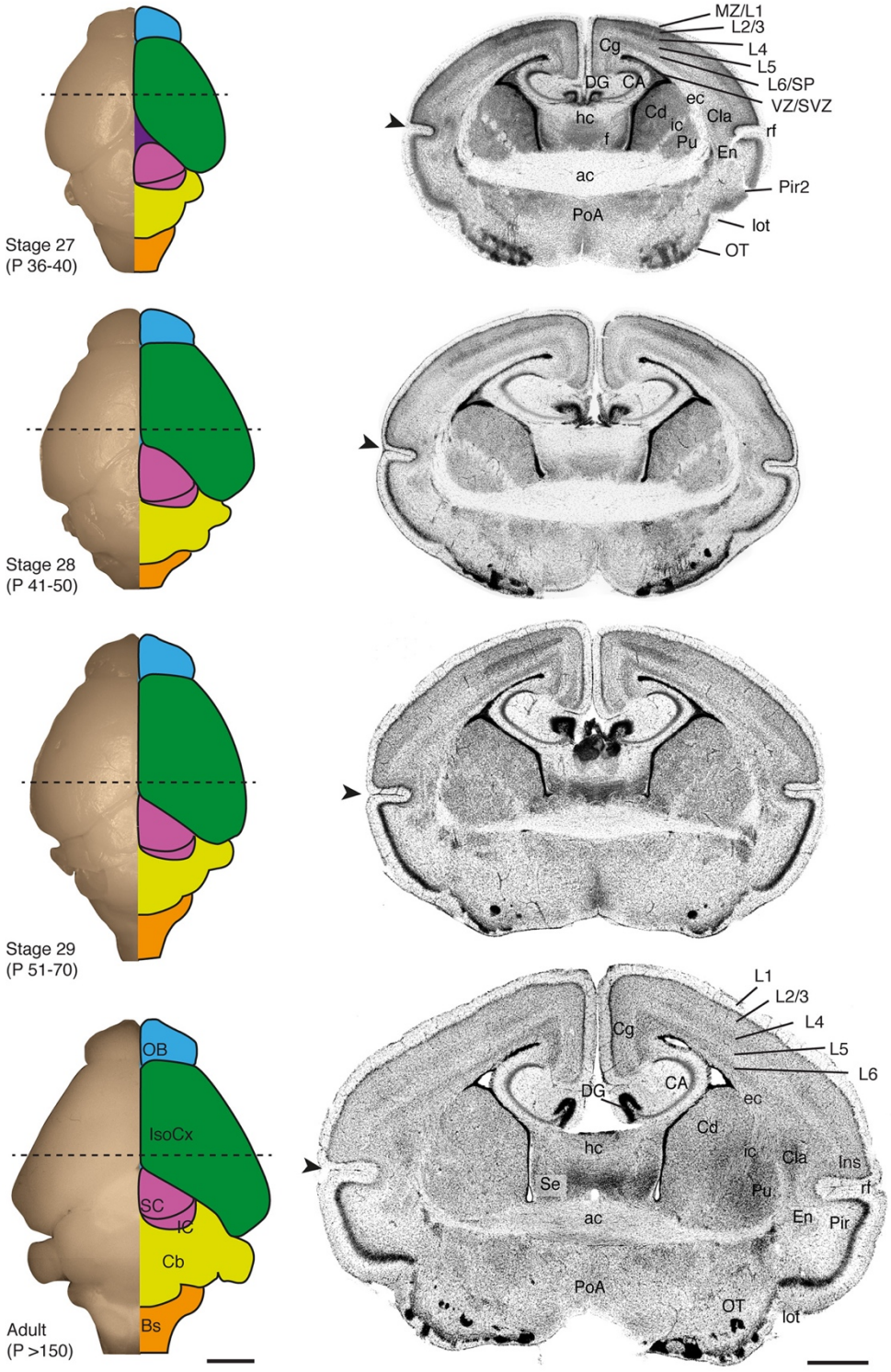

Fig 7. Brain features of *S. crassicaudata* between stages 27 and adulthood.

Developmental series of fixed dunnart brains showing a dorsal view of the whole brain (left column) and corresponding DAPI-stained coronal section (right column) through the approximate region indicated by dotted lines. The main brain regions are colour-coded, and stages and approximate postnatal (P) days are indicated. Arrowheads show the rhinal fissure (rf). ac, anterior commissure; BS, brainstem; CA, cornu ammonis hippocampi; Cb, cerebellum; Cd, caudate; Cg,

cingulate cortex; Cla, claustrum; DG, dentate gyrus; ec, external capsule; En, endopiriform; f, fornix; hc, hippocampal commissure; ic, internal capsule; IC, inferior colliculus; Ins, insular cortex; IsoCx, isocortex; L1-6, isocortical layers 1-6; lot, lateral olfactory tract; MZ, marginal zone; OB, olfactory bulb; OT, olfactory tubercle; Pir, piriform cortex; Pir2, piriform cortex, layer 2; PoA, preoptic area; Pu, putamen; SC, superior colliculus; Se, septum; SP, subplate; SVZ, subventricular zone; VZ, ventricular zone. Scale bars: 2000 μm in whole brains, and 200 μm in coronal sections.

3.2.2. Pattern of neurogenesis of the neocortex and piriform cortex in mouse and fat-tailed dunnart

In contrast with the nuclear arrangement (Karten 1991) and overall pattern of neurogenesis found in the dorsal telencephalon of birds and reptiles (Jarvis *et al.* 2005, Nomura *et al.* 2008), the mammalian neocortex is organised into six layers generated in an inside-out manner (Angevine and Sidman 1961, Smart and Smart 1982, Rakic 1995, Molnár *et al.* 2006, Cheung *et al.* 2010, Puzzolo and Mallamaci 2010). However, precisely how mice and dunnarts compare in terms of the time-points of pyramidal cell neurogenesis and the formation of neocortical layers and circuits, remain largely unknown. The aim of this section of chapter 3 was to determine the developmental stages during which upper and deeper neocortical layers, which include long-range projection neurons, are generated in both dunnart and mouse (Angevine and Sidman 1961, Smart and Smart 1982). Characterising and comparing the birthdate of neurons located in different neocortical layers of dunnart and mouse is crucial to understand aspects of cortical development that are conserved, or not, across therian mammals. For this purpose, dunnart joeys and mouse pups were injected with ethynyl deoxyuridine (EdU) at different stages of development, specifically from stage 18 until stage 26 (from P0/P3 until P31/36 for dunnarts and between E10 and E18 for mice - Figure 3.1), and their brains were collected and examined at stage 27 by the time cortical neurons have reached their final layers (between P36 and P40 for dunnarts and P4-P5 for mice - Figure 3.1). EdU is a thymidine analogue, which is incorporated into the DNA during the S-phase of the cell cycle, so by injecting EdU at different stages of development it is possible to label and quantify the cells that are born during that specific stage.

The analysis of neurogenesis was focused on the neocortex and compared with the piriform (olfactory) cortex, as an example of the three-layered paleocortex. The data collected revealed that, as in mouse (Angevine and Sidman 1961), the dunnart neocortex develops following an inside-out pattern of neurogenesis and it consists of six layers (Figure 3.2A), as previously described in the American opossum (Puzzolo and Mallamaci 2010) and in the tammar wallaby (Reynolds 1985). Specifically in this species, according to the location of cells that incorporated EdU, the deeper layers of the neocortex (L5 and L6) are born from the end of stage 20 until stage 22 (second post-natal week), while the upper layers from stage 23 until stage 24 (third post-natal week, Figure 3.2A). Similarly, the birth of the deeper and upper layers in mice occurred during stage 20 (E12), and stage 23 (E15), respectively, as previously reported (Figure 3.2A) (Smart and Smart 1982), suggesting that the main milestone of neocortical formation might occur at similar stages in mouse

and dunnart, despite the more protracted and postnatal development of the marsupial neocortex as compared to eutherians (Smart and Smart 1982, Cooper 2008, Puzzolo and Mallamaci 2010).

Analysis of neurogenesis in the piriform cortex shows that this brain structure also develops following an inside-out pattern, and it has three main layers in marsupials, as in eutherians (Price 1973, Bayer 1986) (Figure 3.2B). In addition to this, neurogenesis in the dunnart piriform cortex has already started at birth and is more advanced than in the neocortex, such that there is a statistically significant difference in the amount of EdU-positive cells counted in the piriform cortex, compared to the neocortex, in joeys injected with EdU during stage 18 and 19 (Figure 3.2C). Neurogenesis in the piriform cortex then peaks roughly one week before the neocortex, during stage 21 (P12-P16) and sharply declines after stage 22 (P17-P19) (Figure 3.2C). As a result, the majority of dunnart piriform cells that will migrate to L2 are generated between stage 20 and 22 (from P8 until P19 – Figure 3.2B, C). Results in mice suggest a similar pattern, whereby the neurogenesis in the piriform cortex is more advanced compared to the neocortex during stage 18 and 19 (E10-E11), and after stage 22 (E14) only few cells are generated in the piriform cortex, as previously suggested (Smart and Smart 1982) (Figure 3.2B, D). The more advanced stage of neurogenesis in the piriform cortex compared to the neocortex in both species suggests that olfactory structures might be functional at birth, and possibly affect subsequent neocortical development, as explored more extensively in the discussion of this chapter.

The analysis of neurogenesis in both dunnarts and mice allowed us to define and compare the temporal windows of crucial milestones of cortical neurogenesis, thus increasing our understanding of cortical development in therian mammals. In addition to this, this dataset provides fundamental information for the rest of the experiments included in this thesis, such as defining the birthdate of deeper and upper neocortical layers, where most long-range projection neurons reside. This knowledge is an important initial step to be able to manipulate gene expression specifically in these neurons, in order to explore their pattern of axonal elongation, as well as the timeline and the mechanism of cortical circuits formation, as described in the following sections.

Equivalent stages

Stage	Fat-tailed dunnart	Mouse
S18	P 0-3	E 10.5
S19	P 4-7	E 11.5
S20	P 8-11	E 12.5
S21	P 12-16	E 13.5
S22	P 17-19	E 14.5
S23	P 20-23	E 15.5
S24	P 24-26	E 16.5
S25	P 27-30	E 17.5
S26	P 31-35	E 18.5
S27	P 36-40	P0-P4
S28	P 41-50	P4-P10

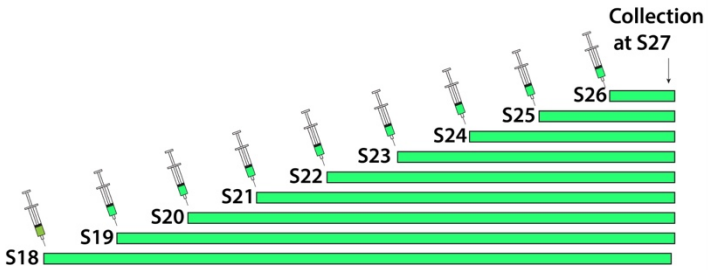

Figure 3.1: Experimental paradigm of EdU study.

Dunnart joeys and mouse pups were injected with EdU at different stages of development, from stage 18 until stage 26, and were then collected during stage 27, when the neocortical layers can be identified. The table shows the equivalent ages per each stage of development in dunnarts and mice, based on Suárez, Paolino *et al*. 2017 and Paolino *et al*. 2018. E = embryonic day, P = postnatal day, S = stage.

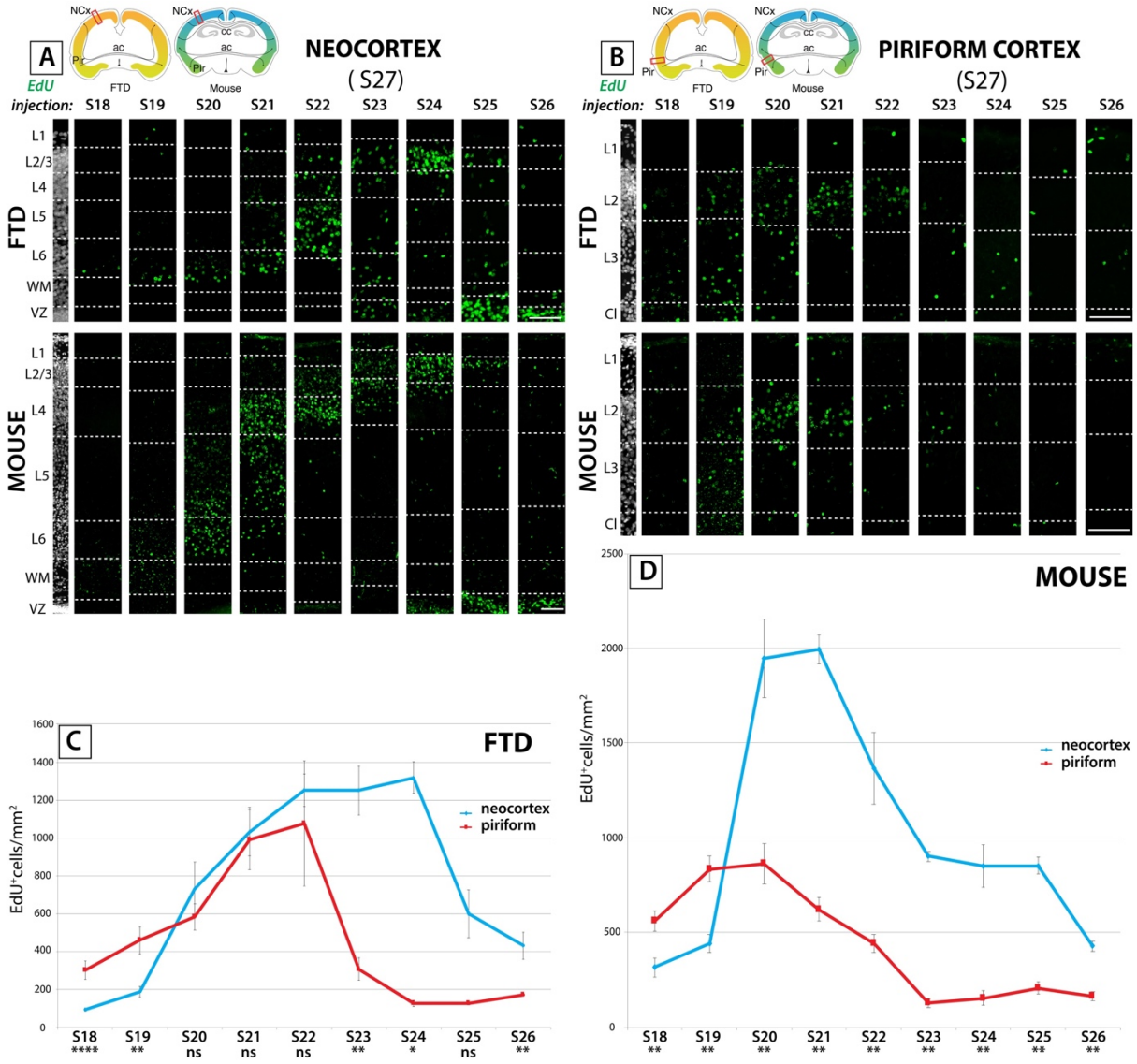

Figure 3.2: Neurogenesis in the dunnart and mouse neocortex and piriform cortex.

A-B: DAPI staining (grey, left) and EdU (green) on stage 27 neocortical (A) and piriform (B) sections of joeys and pups injected with a single pulse of EdU at different stages (S18-26, see Figure 3.1). Scale bars: 100 µm. Note the inside-out pattern of neurogenesis in the neocortex (A) and piriform cortex (B) of both fat-tailed dunnarts (FTD) and mice. Above, schematics of coronal sections showing the region of interests included in the cell count. **C-D**: Graphs representing the result of EdU-positive cells count in the neocortex compared with the piriform cortex, in both dunnart and mouse. Note the advanced stage of neurogenesis of the piriform cortex compared to the neocortex in both species during the first stages of development (S18, S19). Data are represented as mean ± SEM. On the X axis: day of EdU injection, on the Y axis: density of EdU-positive cells. Ac = anterior commissure, cc = corpus callosum, Cl = claustrum, FTD = fat-tailed dunnart, L = layer, NCx = neocortex, ns = non-significant, Pir = piriform cortex, S = stage, VZ = ventricular zone, WM = white matter. * $P < 0.05$, ** $P < 0.01$, *** $P < 0.001$, Mann-Whitney U tests.

3.2.3. Reconstruction of the developmental steps of interhemispheric connections in dunnarts

In section 3.2.2, the timeline of generation of upper and deeper neocortical layers was defined in both dunnart and mouse. These neocortical layers are inhabited by long-range projection neurons; specifically, deeper layer neurons mainly project to subcortical targets, while corticocortical projection neurons are located in both deeper and upper layers of the neocortex and project through the corpus callosum in eutherian mammals and through the anterior commissure in marsupials (Putnam *et al.* 1968, Heath and Jones 1971, Robinson 1982). Taking advantage of the knowledge provided by the EdU analysis of neurogenesis, as well as the innovative technique of in pouch electroporation (Paolino *et al.* 2018), the main goal of this third part of chapter 3 was to explore the sequence of events involved in the establishment of interhemispheric connectivity in dunnarts, with a particular focus on the timing of axonal elongation, midline crossing and contralateral targeting of commissural neurons localised in the upper and deeper layers of the neocortex.

Sections 3.2.3.1-3.2.3-3 contain material that has been published in the following paper:

Paolino A, Fenlon LR, Kozulin P, Richards LJ, Suárez R (2018). Multiple events of gene manipulation via in pouch electroporation in a marsupial model of mammalian forebrain development. J Neurosci Methods. 293:45-52. doi: https://doi.org/10.1016/j.jneumeth.2017.09.004

3.2.3.1. *Independent transfection of distinct neuronal layers with in pouch electroporation*

Previous studies, as well as the results from section 3.2.2, show that the development of the marsupial neocortex is 2-3 times more protracted as compared to similarly sized eutherians (Smart and Smart 1982, Cooper 2008, Puzzolo and Mallamaci 2010) (Figure 3.2), thus offering an extended developmental period for experimental manipulations, including the differential transfection of progenitors that give rise to neurons of distinct neuronal layers.

First, the fluorophore eYFP (Niwa *et al.* 1991, Matsuda *et al.* 2004) was transfected into either deeper or upper layer neocortical neurons by performing in pouch electroporation between stage 19 (P7) and stage 23 (P22) (see chapter 2 for details). The aim of this approach was to ensure the best stage to label long-range projection neurons located in L2/3 and L5, according to the timeline established by the neurogenesis analysis with EdU, as well as to define the success rate of in pouch electroporation when this technique was performed at different stages.

S1 was electroporated across development and the brains examined at stage 27 (P40), when the neurons have reached their final location in the different layers of the neocortex. When the electroporation was performed at stages 19, 20, 21 or 23 (P7, P11, P16 and P22, respectively), transfected neurons were predominantly localised in L5-6, L5-4, L4-3 and L2/3, respectively, corresponding to an inside-out pattern of neurogenesis (Figure 3.3A). These results also suggest that stage 20 and stage 23 were the most accurate to label long-range projection neurons localised in L5 and L2/3, respectively. A high success rate of transfection across developmental stages was obtained with in pouch electroporation (stage 19 = 84.4%, n = 8 litters, 41 total joeys; stage 20 = 89.1% n = 11 litters, 41 total joeys; stage 21 = 86.5%, n = 19 litters, 98 total joeys; stage 22 = 91.5%, n = 11 litters, 50 total joeys, Figure 3.3B). Moreover, transfection success showed no statistically significant difference across stages (Figure 3.3B, Kruskal-Wallis test, $p > 0.99$ for all comparisons), further demonstrating its potential to manipulate gene expression across multiple points of development (Paolino *et al.* 2018).

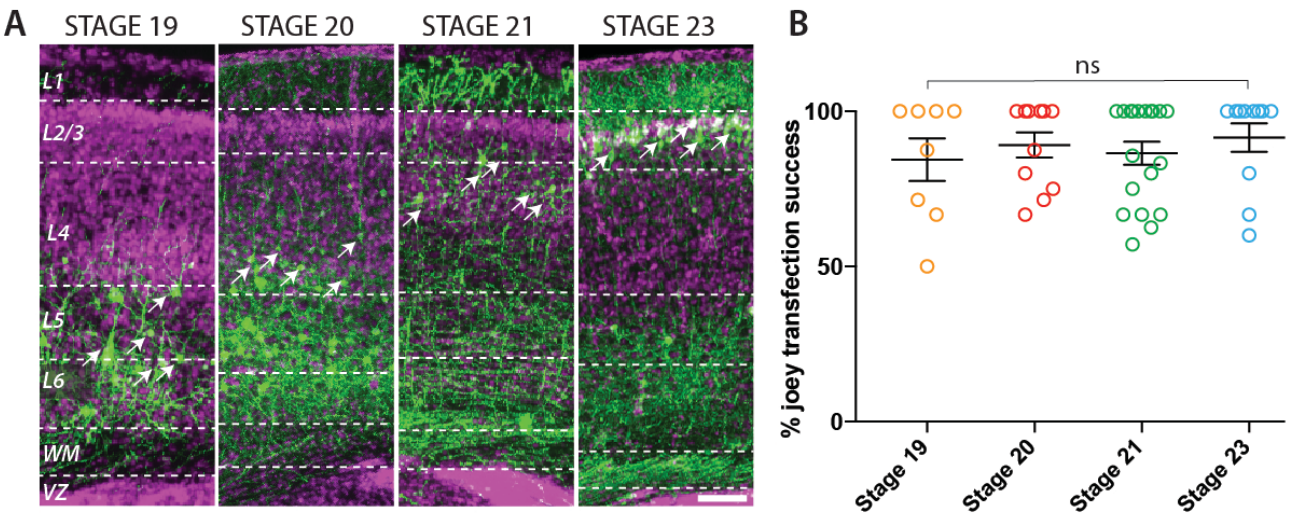

Figure 3.3: In pouch electroporation performed at different developmental stages allows a high transfection efficiency in specific layers of the neocortex.

A: Dunnart joeys were electroporated with eYFP at stages 19 (P7), 20 (P11), 21 (P16) and 23 (P22) and their brains examined at stage 27 (P40). The developmental stage on the day of the electroporation determines the layered position of transfected cells (arrows) within the neocortex, in a protracted inside-out neurogenic fashion. Scale bar: 100 µm. **B**: Scatter plot of transfection success across stages, as indicated by the presence of fluorescent neurons in the brain of electroporated joeys. The results, shown as mean ± SEM, indicate high electroporation efficiency across the developmental stages. L = layers, ns = non=significant, VZ = ventricular zone ,WM = white matter. Taken from Paolino *et al.* 2018.

3.2.3.2. *Different brain regions can be specifically targeted with in pouch electroporation*

The data shown so far described the potential of in pouch electroporation to manipulate gene expression across multiple points of development, aiming specifically at different neocortical layers, thanks to the protracted and *ex utero* neocortical development of the fat-tailed dunnart, which increases the precision of this technique. Another advantage of the postnatal development of the marsupial neocortex is the possibility to precisely target different brain regions, depending on the position of the electrodes and the day in which the procedure was performed.

In mice, *in utero* electroporation has been widely used to transfect numerous brain structures (Taniguchi *et al.* 2012, Baumgart *et al.* 2015, Kozulin *et al.* 2016). However, positioning the electrodes across the uterine wall and amniotic sac can restrict the accuracy and replicability of the electroporated site location. On the other hand, the head of marsupial joeys can be directly held with the electrodes without these barriers, facilitating the precise targeting of the electroporated region. To establish a set of examples of regions that can be reliably transfected in dunnarts, the electrodes were positioned aiming at different forebrain locations and numerous cases of well-confined sites of electroporated neurons were generated. The olfactory bulb and the anterior olfactory nucleus were successfully targeted when the electroporation was performed at stage 18 (corresponding to P0-P3), the thalamus was successfully electroporated during stage 19 (between P4 and P7). The correct timing to target the piriform cortex and the striatum was stage 20 (between P8 and P11), while stage 21 (between P12 and P16) was adequate for the labelling of the entorhinal cortex. During stage 23 (between P20 and P23) it was possible to successfully target the prefrontal cortex, the upper layers of the primary somatosensory cortex, motor cortex and hippocampus, depending on the angle of the electrodes (Figure 3.4).

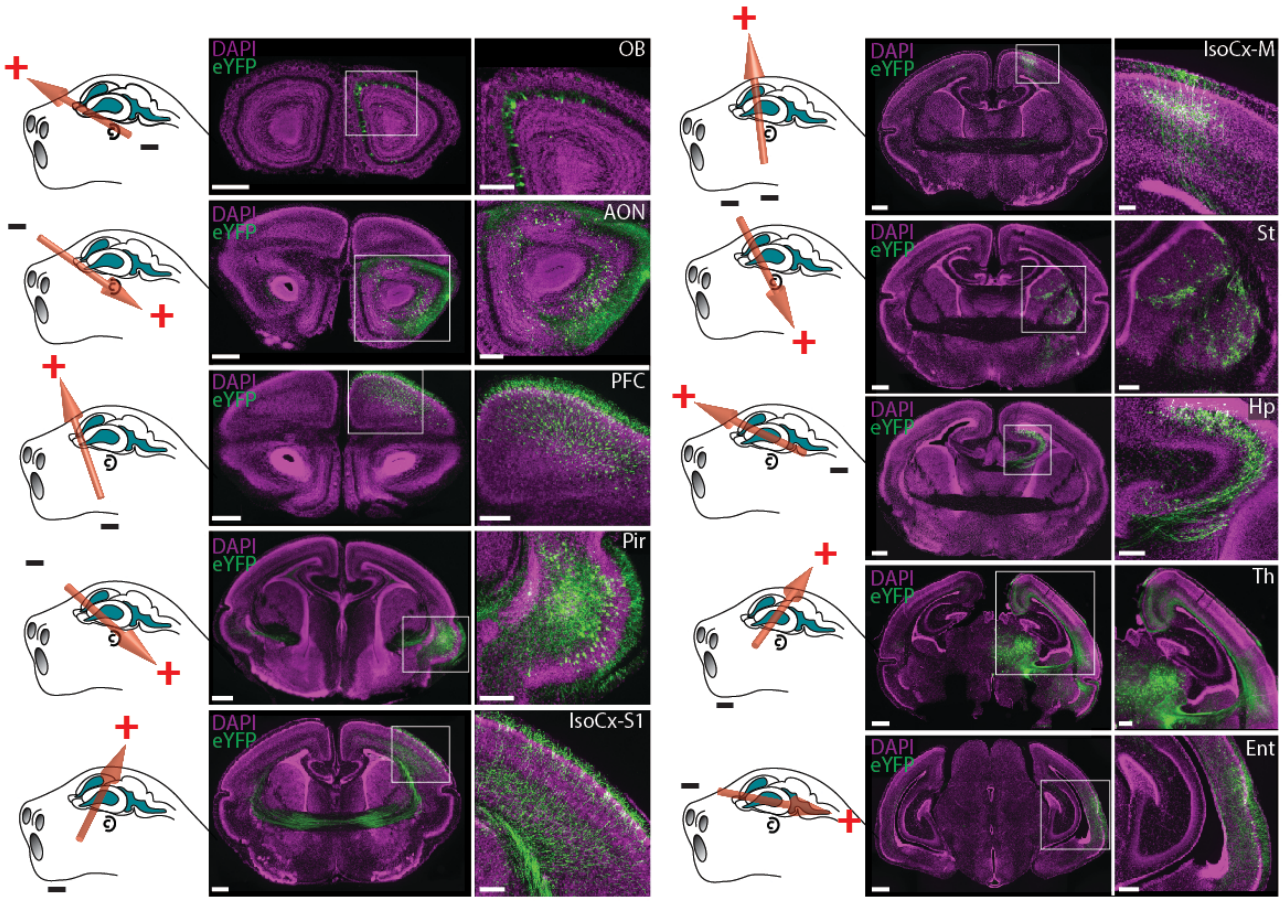

Figure 3.4: High-precision labelling of different forebrain areas with in pouch electroporation in dunnarts.

By combining the timing of electroporation and the position of the electrodes, it is possible to label specific neuronal populations in the dunnart brain. Left schematics indicate the approximate position and direction of current delivered via forceps-type electrodes. The regions labelled were: the olfactory bulb (OB), the anterior olfactory nucleus (AON), prefrontal cortex (PFC), piriform cortex (Pir), primary somatosensory cortex (IsoCx-S1), motor cortex (IsoCx-M), striatum (St), hippocampus (Hp), thalamus (Th), and entorhinal cortex (Ent). Insets of each case are indicated on right panels. Electroporations were performed at stage 18 (between P0 and P3) to label olfactory bulb and anterior olfactory nucleus; stage 19 (between P4 and P7) to label thalamus; stage 20 (between P8 and P11) to label piriform cortex and striatum; stage 21 (between P12 and P16) to label entorhinal cortex; stage 23 (between P20 and P23) to label prefrontal cortex, primary somatosensory cortex, motor cortex and hippocampus. All the joeys were collected at stage 27 (between P36 and P40). Scale bars: 200 µm for whole brain sections, and 100 µm for insets. Taken from Paolino *et al.* 2018.

3.2.3.3. *Different genes can be successfully expressed in different neuronal populations within the same brain*

Using in pouch electroporation, it is possible to precisely target specific populations of pyramidal neurons located in different neocortical layers and then analyse their pattern of projection. Due to the minimal invasiveness of this procedure, which does not require surgery to access the developing joeys, in pouch electroporation can be repeated multiple times in the same litter, thus labelling independently different populations of long-range projection neurons in the same animal and analyse their interaction during the establishment of brain connectivity. As a result, in pouch electroporation allows the analysis of circuits formation with experimental paradigms that would be extremely challenging, if not impossible, in eutherian mammals.

In order to demonstrate the minimal invasiveness of in pouch electroporation, the mortality of animals that undergo this procedure was calculated. The data collected show a 100% survival rate of the mothers of electroporated joeys across different stages of in pouch electroporation (mortality rate 0%, n = 42, Figure 3.5A). The mortality rate of joeys per litter after they received the first electroporation (1.2%, n = 42 litters, 273 total joeys, Figure 3.5A), and after the same joeys were electroporated for the second time, was also calculated (7.4%, n = 42 litters, 269 total joeys, Figure 3.5A). The baseline mortality rate for non-electroporated joeys per litter during the developmental stage in which the first electroporation was performed, i.e. between stage 19 and 21 (P7-P16), was 0% (n = 17 litters, 69 joeys), and during the developmental stage between the second electroporation and collection, i.e. between stage 22 and 28 (P17-P50), was 4.3% (n = 11 litters, 68 joeys). The mortality rate of joeys after one or two electroporations was compared with the baseline of mortality rate of non-electroporated controls of the same age, and the difference was not statistically significant (Figure 3.5A). A Mann-Whitney U test comparing the joeys that died after the first electroporation and the baseline mortality rate between stage 19 and 21 resulted in $P = 0.5827$, and a Mann-Whitney U test comparing the joeys that died after the second electroporation and the baseline mortality rate between stage 22 and 28 resulted in $P = 0.3921$. This data highlight the feasibility of performing multiple electroporation events within single individuals, thus allowing many different experimental approaches to be undertaken in fat-tailed dunnarts.

Given the evidence that in pouch electroporation does not significantly increase the mortality of the joeys or their mothers, even when repeated in the same animals (Figure 3.5A), this technique was then performed twice to differentially manipulate L2/3 and L5 projection neurons in the same joey. Specifically, according to the EdU birthdating results (Figure 3.2), as well as eYFP transfection at different developmental stages (Figure 3.3), electroporating the same neocortical

hemisphere sequentially using two different constructs at stage 20 (P8-P11) and stage 23 (P20-P23) allows to selectively labelled L5 and L2/3 neurons of the dunnart neocortex, respectively (Figure 3.5B) in order to investigate their respective roles in circuit formation. For example, in mammals, the neocortical hemispheres are connected by commissural neurons located in both L2/3 and L5, whose axons cross the midline either across the anterior commissure, as in monotremes and marsupials, or across the corpus callosum, as in eutherian mammals, and target mostly to similar regions of the contralateral cortex (Suárez *et al.* 2018). However, since neurons in these layers are born at different stages of development, whether these axons interact to locate their targets in the contralateral hemisphere is not understood.

In the following section, the technique of in pouch electroporation has been used to label L2/3 and L5 commissural neurons in the same dunnart joeys, in order to analyse the timeline of commissural axons growth and to evaluate whether and how axons extending from the upper and deeper layers of the neocortex interact during circuit formation.

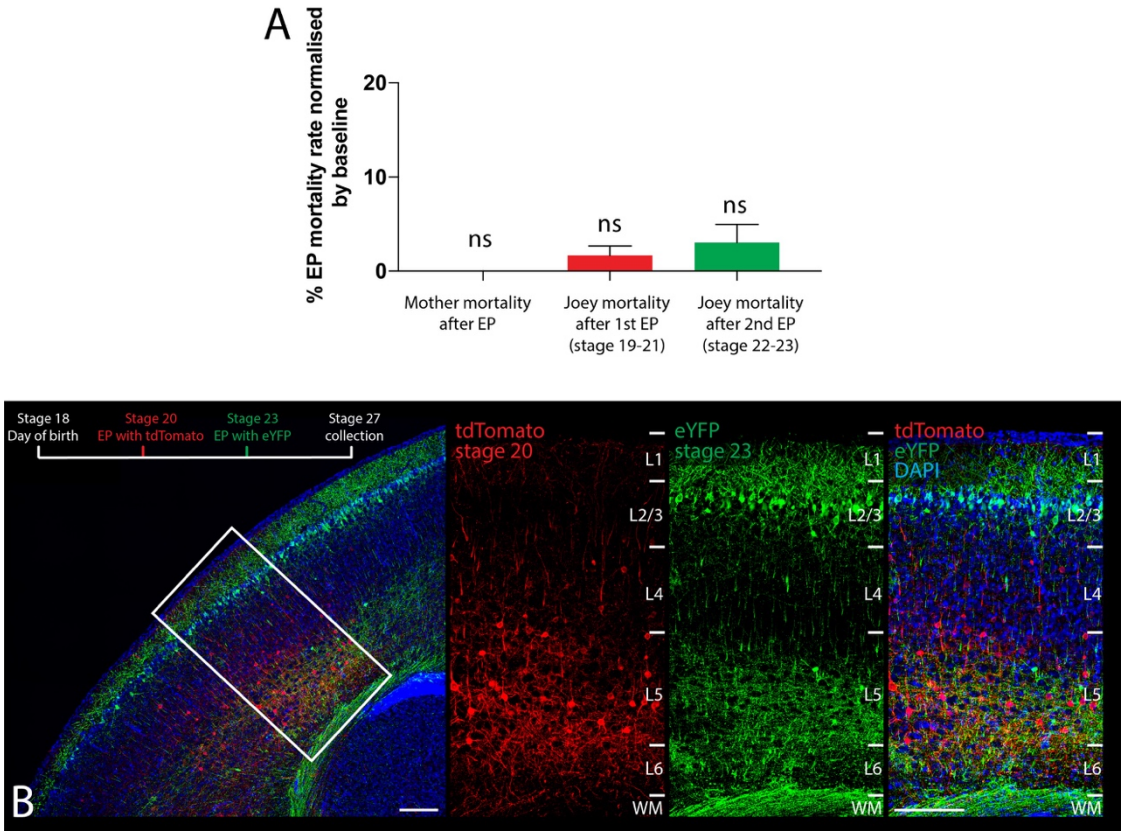

Figure 3.5: In pouch electroporation does not affect dunnart mortality rate and can be performed multiple times in the same individuals to label distinct neuronal populations.

A: The mortality of the mothers and joeys that received either one or two electroporations was compared to non-electroporated controls (mortality baseline). Normalised mortality rate of mothers (0%; n = 42; left), joeys after 1st electroporation (1.2%; control, n = 69; electroporated, n = 273; middle), and joeys after 2nd electroporation (3.1%; control, n = 68; electroporated, n = 269; right) is shown. Differences of mortality rates between non-electroporated controls and electroporated joeys was not statistically significant after either the first or second electroporation (P = 0.5827 and P = 0.3921, respectively; Mann-Whitney U tests). The results are shown as mean ± SEM. **B**: The experimental procedure of the double electroporation is indicated on the top of left panel. The square in the left panel indicates the area of the right insets. Electroporation of tdTomato at stage 20 (P10) resulted in labelling neurons located in the deeper layers (red), while electroporation of eYFP in the same region at stage 23 (P20) labelled the upper layer neurons (green). The last panel on the right shows the distribution of cell layers by including both channels and DAPI staining (blue). EP = electroporation, L = layer, ns = non-significant, WM = white matter. Scale bars: 200 µm. Taken from Paolino *et al.* 2018.

3.2.3.4. *Timeline of growth of commissural axons: contralateral targeting and waiting period*

In order to investigate the dynamics and possible interactions between commissural axons from deeper and upper layer neurons during axon growth and contralateral targeting, double electroporations were performed in individual dunnart joeys (Paolino *et al.* 2018). Based on the results from the EdU birth-date analysis (Figure 3.2), as well as fluorophore transfection at different developmental stages (Figure 3.3), L5 and L2/3 neurons were labelled at stage 20 (P10+/-2) and stage 23 (P20+/-2), respectively, and the brains were then collected at four subsequent stages, stage 24 (P25), stage 26 (P32), stage 27 (P40) and stage 28 (P50). With this protocol it was possible to determine the main milestones of axonal development of both neuronal populations independently.

At stage 24 (P25), the axons projecting from deeper layer neurons have already reached the white matter of the contralateral hemisphere, while upper layer neurons have just started to elongate their axons (Figure 3.6A). Ten days after the second electroporation, during stage 26, axons from the deeper layers have reached the contralateral subplate, while projections from the upper layer neurons have just crossed the midline (Figure 3.6B). Twenty days after the second electroporation, during stage 27, deeper layer axons are still located underneath the contralateral cortical plate, and axons from the upper layers have now also reached this position (Figure 3.6C). At the end of stage 28 (after P45), axons emerging from deeper and upper layer neurons innervate the contralateral cortical plate simultaneously (Figure 3.6D). These results constitute the first evidence of a waiting period during which axons of deeper layer neurons wait for the axons extending from later-born upper layer neurons to collectively innervate the contralateral cortical plate, in a manner similar to the waiting period of thalamic axons in the subplate before they innervate specific cortical areas (Rakic 1977, Molnár *et al.* 1995, Grant *et al.* 2012, Deck *et al.* 2013). This also suggests that the process of contralateral axon targeting might occur in sequential steps. Whether this phenomenon is also present in eutherians is currently unknown and would require double surgeries of *in utero* electroporation.

Interestingly, commissural axons innervating the contralateral cortical plate often presented axonal varicosities in close apposition to those axons extending from different neuronal populations, suggesting that physical interactions of axons from upper and deeper layer neurons may be necessary for correct contralateral targeting (Figure 3.7). Pairs of axons from each neuronal population, which colocalised within 8 µm from each other for at least 80 µm, were examined. Within each pair, the distance between one axonal varicosity and the closest one on the same or paired axon was determined (Figure 3.7). This analysis revealed that the distance between

varicosities of paired axons (in blue) was shorter than that within axons (in yellow), suggesting a spatial correlation of axonal varicosities between paired axons (Figure 3.7). It is still unclear what kind of interaction, if any, these varicosities might establish. Further experiments, such as manipulating the axonal elongation of either deeper or upper layer neurons, or altering the expression of cell adhesion molecules to see if the varicosities still form would be required to elucidate this phenomenon that has never been described before, as well as to define whether an interaction between commissural neurons located in deeper and upper layers might be necessary for correct contralateral targeting.

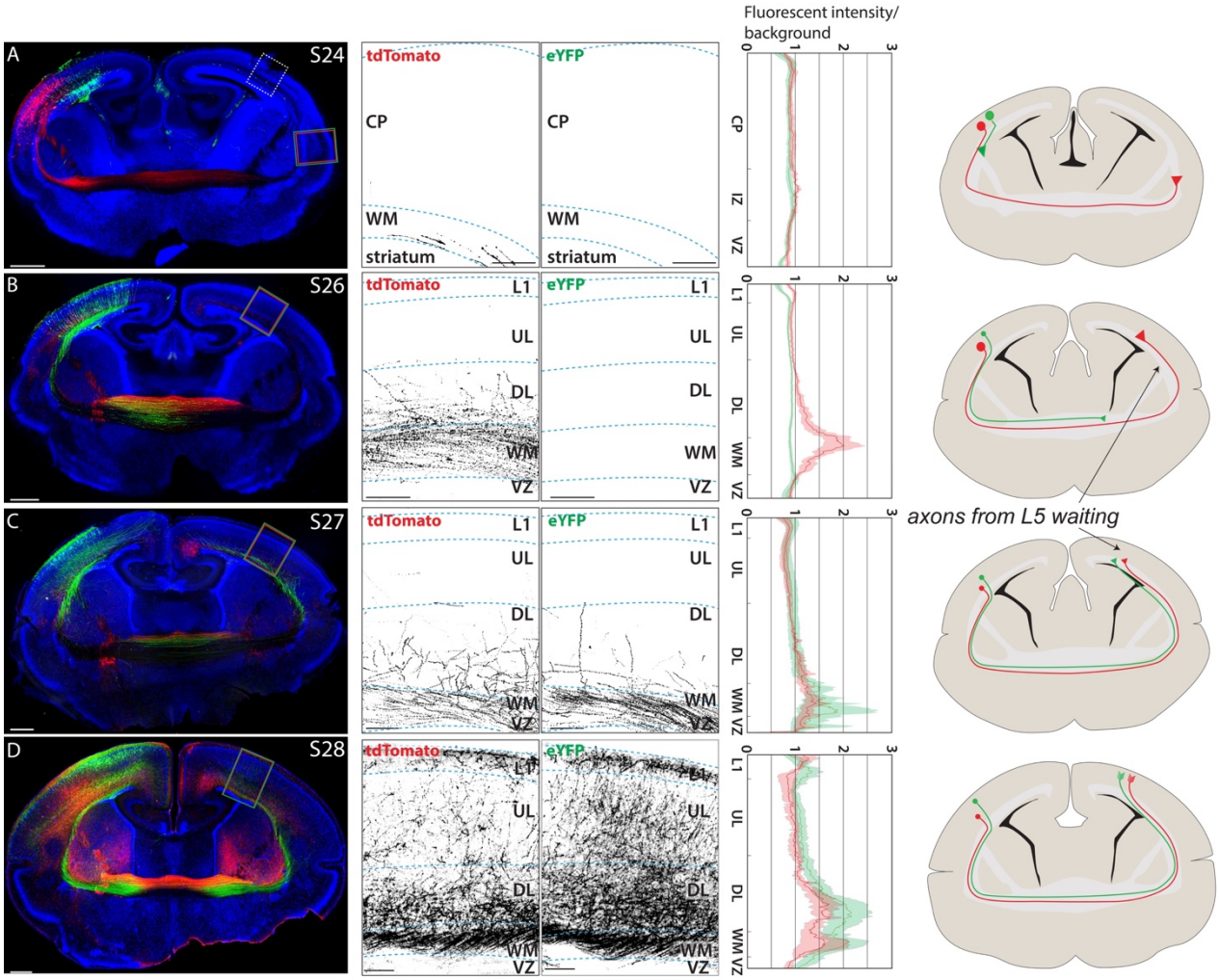

Figure 3.6: Time course of axonal development, analysis of contralateral projections.

A: Coronal section of dunnart brain collected at stage 24, after electroporation with tdTomato at stage 20 and eYFP at stage 23: axons extending from the DL have already reached the contralateral hemisphere, where they localised in the white matter, while the majority of UL neurons have not extended any process yet. **B**: Coronal section of dunnart joey collected at stage 26: axons extending from the DL neurons have reached the contralateral cortical plate, while axons from the UL have crossed the midline. **C**: Coronal section of dunnart joey collected at stage 27: axons extending from the DL neurons are still localised in the DL of the contralateral hemisphere, same location as previous stage. Axons extending from the UL neurons have now reached the DL of the contralateral hemisphere, in the same location as the axons from the DL. **D**: Coronal section of dunnart joey collected at stage 28: axons extending from the DL and UL neurons fully arborise the contralateral hemisphere, reaching the pial surface. Quantification was obtained by measuring the intensity of florescence in the homotopic region of the contralateral hemisphere, normalised for the background. Cp = cortical plate, DL = deeper layers, IZ = intermediate zone, L = layer, S = stage, UL = upper

layers, VZ = ventricular zone, WM = white matter. Scale bars 400 and 100 μm for whole brains and insets, respectively.

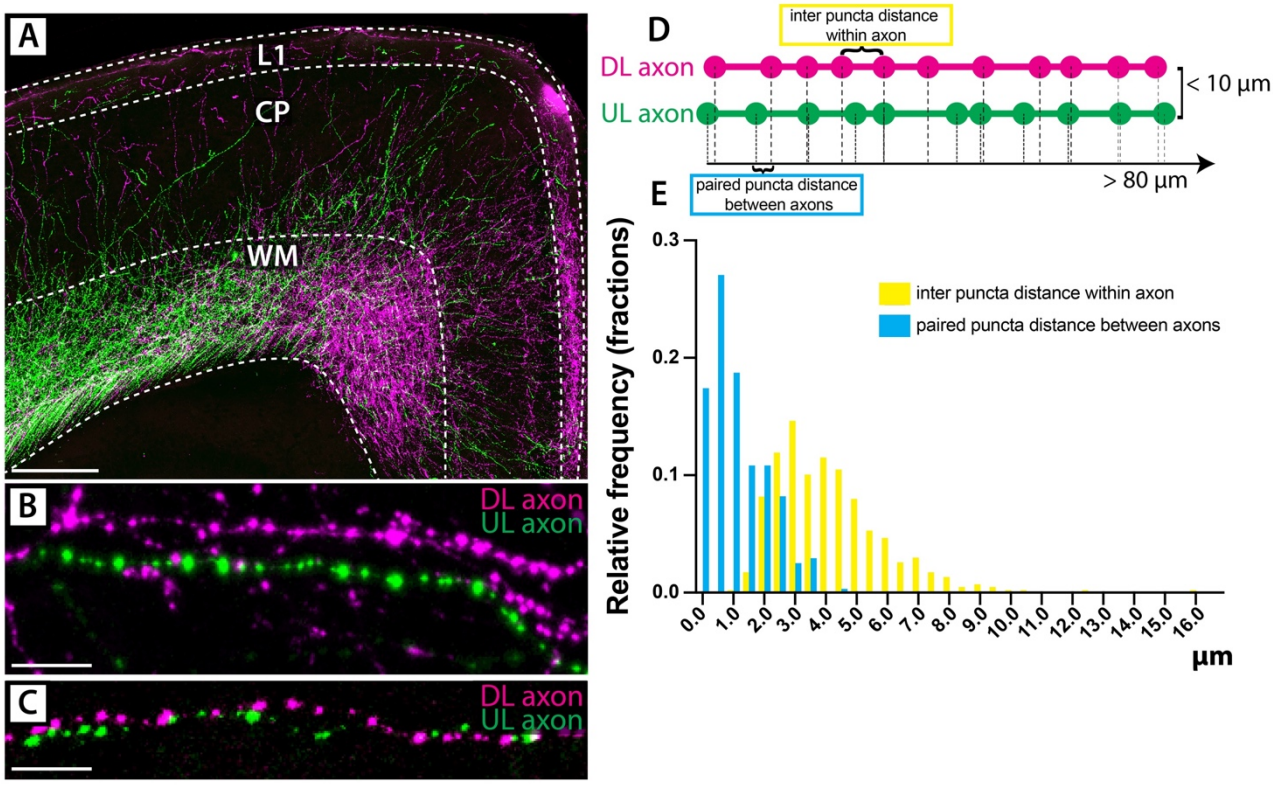

Figure 3.7: Close location of varicosities on axons extending from deeper and upper layer neurons during contralateral targeting.

A: Axons extending from DL (magenta) and UL (green) neurons seem to spatially interact as they reach the upper layers of the cingulate cortex at stage 28 (P50). **B-C**: High power images of varicosities on coupled DL (magenta) and UL (green) axons with bigger (B) or shorter (C) inter-axonal distance. **D**: Schematics of the puncta distance measurements within and between axons. **E**: Graph showing the shape of the distribution of the minimal distance of each varicosity from its nearest varicosity on a paired axon (in blue) or within a single axon (yellow). The data show that the distance between paired varicosities on coupled axons is shorter than the distance between puncta within a single axon. Cp = cortical plate , DL = deeper layers, L = layer, UL = upper layers, WM = white matter. Scale bars 250 and 25 µm.

3.3. Discussion

The aim of this chapter was to define a developmental staging system for the fat-tailed dunnart, as well as to study the timing of corticogenesis and circuit formation in fat-tailed dunnart compared to mouse, as an established eutherian model of brain development. The goal was, first of all, to define whether major differences exist in terms of cortical development of species with different commissural strategies, and also to provide information that is crucial for the use of fat-tailed dunnart as an innovative experimental model to study brain development and evolution.

By describing and comparing the rate of development of the eutherian mouse and the marsupial fat-tailed dunnart, specific heterochronies (differences in the relative timing or speed of developmental features in distinct species) were revealed that characterise the development of body parts and facial structures in these species. The different timing of development of specific anatomical features, which is due to the different gestational length and survival requirements of eutherian and marsupial new-borns, is a major challenge for directly translating developmental stages between species, thus careful comparative studies throughout development are required to address evolutionary questions. Despite these differences, some anatomical structures, such as the eye and its components, have been shown to have a conserved timing of formation across vertebrates, and can thus be employed as developmental "anchor points" in the comparison of different species during development (Dreher *et al.* 1988). Based on this knowledge, a developmental staging system of the fat-tailed dunnart was proposed that matches the Thieler (mouse) and the Carnegie (human) staging systems, thus allowing the analyses of comparative neuroanatomy that are included in the rest of this thesis.

Throughout the first part of chapter 3, the advantages of employing the fat-tailed dunnart as an animal model to study brain development and evolution are highlighted. The postnatal and protracted telencephalic development allows experimental manipulations of the developing mammalian brain with high temporal and spatial resolution, as well as experiments that would not be feasible in traditional eutherian species, such as rodents or primates. In order to plan such manipulatory experiments, further information about cortical neurogenesis in fat-tailed dunnarts, such as the timing of cortical layer formation, was required. Sections 3.2.2 and 3.2.3 thus complement the paper attached as section 3.2.1, as they are dedicated to a detailed comparative analysis of neurogenesis between mouse and fat-tailed dunnart, followed by the characterisation of the main milestones of commissure development.

Dunnart joeys, like every marsupial, are born extremely immature, after a short gestation and a particularly short period of organogenesis (Smith 2001), such that by birth (P0) they resemble mice at E10 (Thieler stage 18) and human foetuses at gestational week 7 (Carnegie stage 18) (Suárez *et al.* 2017) and their neocortex is an undifferentiated neuroepithelium during the first postnatal days (Reynolds 1985). The analysis of neurogenesis with EdU injections at different developmental stages in dunnart and mouse provided a temporal scale of cortical formation and showed that, despite the protracted and postnatal cortical development in this marsupial species, the main milestones of cortical development, such as the generation of deeper and upper layers and the formation of the piriform cortex, occur at comparable developmental stages across therian mammals (Angevine and Sidman 1961, Smart and Smart 1982, Rakic 1995, Molnár *et al.* 2006, Cheung *et al.* 2010, Puzzolo and Mallamaci 2010) (Figure 3.2). Moreover, the data shown in this chapter revealed that in both dunnarts and mice neuronal production in the piriform context begins, peaks and declines earlier than the neocortex (Figure 3.2C-D). This result supports the hypothesis that the development of olfactory brain areas precedes and might influence the formation of the neocortex across mammals, and further adds to anatomical and behavioural evidence indicating that the olfactory system could be functional during the first postnatal hours, and help marsupial joeys to locate the nipples inside the pouch (Schneider *et al.* 2009, Schneider 2011). Further evidence linking olfactory cortex development with neocortical formation come from *in vitro* studies in embryonic and newborn mice showing that patterned waves of activity of the neocortex are initiated at the olfactory cortices (Namiki *et al.* 2013, Easton *et al.* 2014) as well as from studies demonstrating Cajal-Retzius cells that migrate towards the neocortex after patterning the olfactory cortex (de Frutos *et al.* 2016).

The temporal definition of the generation of deeper and upper layer neurons with EdU analysis was essential to study the pattern of axonal elongation and the timeline of circuits formation, as it defined the specific stages in which it is possible to transfect and label long-range projection neurons located in L2/3 and L5 with in pouch electroporation (Paolino *et al.* 2018). By collecting joeys at different stages of development after a double electroporation paradigm to label deeper and upper layer neurons, at P10 and P20 respectively, it was possible to define a timeline of commissure formation, according to which commissural neurons cross the midline one week after birth and reach the contralateral hemisphere after two weeks (Figure 3.6). In addition to this, this experimental paradigm unveiled a waiting period of axons from deeper layer neurons that reach the contralateral hemisphere at stage 26 and then wait in L5/6 for few days, until the axons extending from the upper layers reach the same position at stage 27, to then complete the innervation of the cortical plate at stage 28 (Figure 3.6). Waiting periods, as defined by periods spent by a growth

cone in the proximity of its specific target before accessing it (O'Leary *et al.* 1988, Hedin-Pereira *et al.* 1999), are common yet complex phenomena during brain development, and they have been observed in many different systems in vertebrates, including mammals. For example, in the formation of interhemispheric projections, visual callosal axons reach the contralateral cortex and enter a "waiting" phase in the cortical subplate in monkey, cat, and rodents (Rakic 1977, Olavarria *et al.* 1985, Innocenti 1990, Mizuno *et al.* 2007). Due to the challenge of performing two surgeries in few days to electroporate deeper and upper layer neurons in the same animal, usually only the upper layer neurons are labelled to study the time course of callosal formation (Mizuno *et al.* 2007, Wang *et al.* 2007, Fenlon *et al.* 2017); it is thus unclear whether, during the development of the corpus callosum, the commonly labelled upper layer axons reach the axons extending from the deeper layer neurons, which may be waiting at the contralateral hemisphere before completing contralateral targeting. Another example of axons waiting at the subplate is during the development of the thalamocortical tract, when thalamic projections wait in this cortical region before innervating the cortical layers (Wise *et al.* 1978, Ghosh and Shatz 1993, Allendoerfer 1994, Molnár and Blakemore 1995, López-Bendito *et al.* 2003, Grant *et al.* 2012). The signals that might trigger the completion of cortical targeting are still not known, but it has been previously suggested that the maturation of the target region might be important for its appropriate innervation (O'Leary and Terashima 1988, Wang *et al.* 2000). Previous studies of thalamocortical innervation in marsupials, such as the wallaby (Marotte *et al.* 1997) and the opossum (Molnár *et al.* 1998) showed no evidence of a waiting period of thalamocortical projection in the subplate (Marotte *et al.* 1997, Molnár *et al.* 1998). Instead, the thalamocortical axons invaded the developing cortical layers as they began to form. This difference in the waiting period of thalamocortical axons in the subplate might be related to the different developmental dynamics and architectural structure of subplate cells in marsupials as compared to eutherians, as described in section 1.3.1 (Reynolds 1985, Marotte *et al.* 1997, Molnár *et al.* 1998). Although the contralateral projections were the main focus of this analysis, preliminary qualitative observations of ipsilateral projections, such as the ones reaching the cingulate cortex, suggest that axons extending from the deeper layer neurons reach the pial surface before the axons extending from the upper layer neurons, without an evident waiting period. Specifically, axons from the deeper layers can be seen reaching the pial surface of the ipsilateral cingulate as early as P32 (stage 26), which is before the upper layer neurons extend their medial projection to this brain region, as further described in section 5.2.1. Additional experiments and a more accurate analysis of the ipsilateral neocortex and projections to other regions of the brain, including subcerebral targets as well as the thalamus, would be required to fully elucidate whether different mechanisms and waiting periods are in place for the correct targeting of different neuronal populations.

The data shown in this chapter suggest the existence of a waiting period during the development of neocortical interhemispheric projections in marsupials, and the analysis of proximity of varicosities of paired deeper and upper layer axons suggest that a physical interaction between these neuronal population might occur during this process. It is unclear whether this waiting period might be crucial for the correct establishment of contralateral targeting, or whether the correlation of puncta has any functional relevance. For example, possible areas of future investigation might address whether they contain sites of axon-axonal synapses, or synapses onto intermediary cells, contact points by glial cells, or any other process which may or may not convey interdependent communication between the two populations of commissural neurons as they innervate the contralateral cortex.

Overall, the results of this chapter show that, despite the postnatal and protracted development of the neocortex in marsupials and the different commissural strategy adopted in these species, the main pattern and milestones of neurogenesis are conserved across therian mammals. In the next chapter, the question of whether the different commissural system in marsupials, monotremes and eutherian resulted in the different pattern of brain connectivity is investigated.

Chapter 4. Investigating the interhemispheric connectome across mammals

4.1. Introduction

The experiments performed in chapter 3 suggest that, despite the different commissural strategy in marsupial and monotremes, the neocortex is generated according to an inside-out pattern, with the peak of deeper and upper layer neurons generation occurring during stage 20 and 23, respectively, in both species. This evidence indicates that the main patterns and milestones of neocortical neurogenesis are broadly conserved across therian mammals, but whether the emergence of an additional commissure in eutherians led to major differences in the organisational principles of the adult neocortical commissures still remains to be determined.

Previous studies have shown that the interhemispheric projections crossing the midline via the corpus callosum in eutherians are arranged within the tract in a topographic manner and that they broadly connect to homotopic regions of the contralateral hemisphere (de Lacoste *et al.* 1985, Zhou *et al.* 2013, Suárez *et al.* 2018). It is still unclear whether these characteristics are typical of this novel eutherian trait or are instead conserved in mammalian lineages with different commissural routes and therefore may predate the evolution of the corpus callosum. In order to address this question, in this chapter, the fat-tailed dunnart is used as animal model to study the differences and similarities in the organisational principles of interhemispheric connectivity in marsupials, which did not evolve a corpus callosum, and eutherians. This study combines histological evidence of axonal tracts with a diffusion MRI technique known as HARDI (High Angular Resolution Diffusion Imaging). HARDI is an advantageous technique, as its higher angular resolution allows the discrimination of multiple fibre bundles that cross within the same voxel, which would not be possible with classical DTI (Diffusion Tensor Imaging) approaches. As a result, compared to DTI, HARDI can allow a more accurate analysis of 3D patterns of brain connectivity (Berman *et al.* 2013, Mori and Tournier 2014).

4.2. Results

This chapter is based on the publication:

Suárez R, **Paolino A**, Fenlon LR, Morcom LR, Kozulin P, Kurniawan ND, and Richards LJ (2018). A pan-mammalian map of interhemispheric connections predates the evolution of the corpus callosum. Proc Natl Acad Sci U S A. 115(38): 9622-9627 doi: https://doi.org/10.1073/pnas.1808262115

Contributor	**Statement of contribution**
Rodrigo Suárez	Designed experiments 40% Performed experiments 30% Analysed data 20% Wrote paper 50%
Annalisa Paolino (candidate)	Designed experiments 30% Performed experiments 25% Analysed data 20% Wrote paper 20%
Laura R Fenlon	Designed experiments 20% Analysed data 20% Wrote paper 10%
Laura R Morcom	Performed experiments 15% Analysed data 10% Wrote paper 5%
Peter Kozulin	Performed experiments 20% Analysed data 10% Wrote paper 5%
Kurniawan ND	Performed experiments 10% Analysed data 10%
Linda J Richards	Designed experiments 10% Analysed data 10% Wrote paper 10%

Biological Sciences: Neuroscience, Evolution

Title: A pan-mammalian map of interhemispheric brain connections predates the evolution of the corpus callosum

Short title: Ancient mammalian interhemispheric connectome

Authors: Rodrigo Suárez[a,1], Annalisa Paolino[a], Laura R. Fenlon[a], Laura R. Morcom[a], Peter Kozulin[a], Nyoman D. Kurniawan[b], and Linda J. Richards[a,c,1]

Author affiliations: The University of Queensland, [a]Queensland Brain Institute, [b]Centre for Advanced Imaging, [c]School of Biomedical Sciences, Brisbane QLD 4070, Australia.

[1]To whom correspondence may be addressed: r.suarez@uq.edu.au or richards@uq.edu.au.

Keywords: diffusion tensor MRI, cortical evolution, connectivity, homotopy, neocortex.

Author contributions R.S., L.R.F., and L.J.R. designed research; R.S., A.P., L.R.F., L.R.M., P.K., and N.D.K. performed research; R.S., A.P., L.R.F., L.R.M., P.K., N.D.K., and L.J.R. analyzed results; and R.S. wrote the paper. All authors contributed to data interpretation and revision of the article.

Abstract

The brain of mammals differs from that of all other vertebrates in having a six-layered neocortex, extensively interconnected within and between hemispheres. Interhemispheric connections are conveyed through the anterior commissure in egg-laying monotremes and marsupials, whereas eutherians evolved a separate commissural tract, the corpus callosum. Although the pattern of interhemispheric connectivity via the corpus callosum is broadly shared across eutherian species, it is not known whether this pattern arose as a consequence of callosal evolution, or instead corresponds to a more ancient feature of mammalian brain organization. Here we show that, despite cortical axons using an ancestral commissural route, monotremes and marsupials share features of interhemispheric connectivity with eutherians that likely predate the origin of the corpus callosum. Based on *ex vivo* MRI and tractography, we found that connections through the anterior commissure in both fat-tailed dunnarts (Marsupialia) and duck-billed platypus (Monotremata) are spatially segregated according to cortical area topography. Moreover, cell-resolution retrograde and anterograde interhemispheric circuit mapping in dunnarts revealed several features shared with callosal circuits of eutherians. These include the layered organization of commissural neurons and terminals, a broad map of connections between similar (homotopic) regions of each hemisphere, and regions connected to different areas (heterotopic) including hyperconnected hubs along the medial and lateral borders of the cortex, such as the cingulate/motor cortex and claustrum/insula. We therefore propose that an interhemispheric connectome originated in early mammalian ancestors, predating the evolution of the corpus callosum. Since these features have been conserved throughout mammalian evolution, they likely represent key aspects of neocortical organization.

Significance statement

The neocortex is a hallmark of mammalian evolution, and connections between both hemispheres integrate bilateral functions. In eutherians (*e.g.*, rodents and humans), interhemispheric circuits course via the corpus callosum and share a similar connectome throughout species. Non-eutherian mammals (*i.e.*, monotremes and marsupials), however, did not evolve a corpus callosum; therefore, whether the eutherian connectome arose as consequence of callosal evolution, or instead it reflects ancient connectivity principles remains unknown. We studied monotreme and marsupial interhemispheric neocortical connectomes and compared these with eutherian datasets. This revealed interhemispheric connectivity features shared across mammals, with or without a corpus callosum, suggesting that an ancient connectome originated at least 80 million years before callosal evolution.

Introduction

The vertebrate nervous system is organized into functional modules of spatially arranged neurons and fibers (1), where topographic maps shared between peripheral and central circuits mediate sensory-motor behaviors (2). Although such maps are abundant in the spinal cord, hindbrain and midbrain, they are less evident in the telencephalic pallium of non-mammalian vertebrates, such as birds (3, 4). Mammals, on the other hand, evolved a highly topographic six-layered neocortex that recapitulates the peripheral sensory maps via point-to-point connections with subcortical regions (5-7). Moreover, the left and right cortical hemispheres of mammals are heavily interconnected, as compared to fewer such connections in birds where sensory-motor and associative regions of the telencephalic pallium receive limited input from the contralateral hemisphere (8, 9) (Fig. 1). A second key evolutionary innovation was the origin of the corpus callosum exclusively in eutherian (placental) mammals (10-12). Such event likely involved re-routing neocortical axons medially to the dorsal region of the embryonic commissural plate, coupled with a process of midline tissue remodeling by embryonic astroglia (13), which is exclusively present in eutherians (14). The evolution of the corpus callosum as a distinct tract allowed a significant expansion of the number of interhemispheric neocortical connections in species with large brains (15). The corpus callosum carries fibers topographically arranged according to the position of their cell bodies (16-18) and connect mostly similar (homotopic) but also different (heterotopic) regions in each hemisphere (Fig. 1*B*). However, although the map of callosal fibers in eutherians is well- established, and includes connectivity features that are highly conserved across species, such as the presence of bilateral hubs (19-25), it remains unclear whether such features depend on the route taken by commissural axons or instead they reflect more ancient organizational principles of neocortical connectivity.

To address these questions, here we studied the main connectivity features of interhemispheric cortical circuits in non-eutherian mammals and compared these with known eutherian connectomes. We found that the spatial segregation of interhemispheric axons across the anterior commissure in marsupials and monotremes resembles the arrangement of fibers across the callosal tract in eutherians, including the presence of point-to-point homotopic circuits. Furthermore, single cell-level circuit mapping via *in vivo* retrograde and anterograde tracer injections in marsupials revealed a highly conserved layer distribution of contralaterally projecting neurons, as well as homotopic, heterotopic and hyperconnected circuits through the anterior commissure that strongly suggest an ancient pre-callosal origin.

Results

We first performed magnetic resonance imaging (MRI) and tractography on fixed brains of fat-tailed dunnarts (*Sminthopsis crassicaudata*: Marsupialia, Dasyuridae), by placing spherical regions-of-interests (ROIs) at several cortical regions and an inclusion ROI at the anterior commissure (Fig. 2*A*). This revealed that interhemispheric cortical fibers are spatially segregated within the anterior commissure according to the three-dimensional arrangement of cortical areas, similar to the topographic segregation of callosal axons in humans and rodents (16-18) (Fig. 2*A*, Fig. S1, and Video S1). We then examined whether the relative position of fibers within the anterior commissure midline was sufficient to recapitulate cortical area topography, by manually drawing two-dimensional ROIs at the mid-sagittal plane (Fig. 2*B*). Color-coded tractographic reconstructions of fibers crossing through each territory of the mid-sagittal anterior commissure revealed a highly topographic interhemispheric map of connections between at least five well-defined homotopic bilateral domains (*i.e.*, olfactory, frontal, cingulate/motor, neocortical and entorhinal cortices; Fig. 2 *B* and *C,* and Fig. S2). To validate these MRI reconstructions with histology, we then performed double injections of carbocyanine fluorescent tracers (DiI and DiD) into separate regions of the same hemisphere of fixed adult dunnart brains (neocortex and cingulate/motor cortex, Fig. 2*D,* and neocortex and anterior olfactory nucleus Fig. 2*E*). This resulted in segregated fibers along the anterior commissure, similar to previous reports in wallabies (26). Notably, experiments of neuronal tracer injections closely recapitulated the segregation of fibers using MRI tractography and seeding ROIs in equivalent areas (Fig. 2*F*). Similarly, an equivalent cortical-area segregation was observed in axons within the internal capsule, which carries cortical-subcortical connections, using both histology (Fig. 2*D*) and MRI (Fig S1*D*), suggesting that similar developmental mechanisms of axon guidance may direct the areal topography of intra- and extra-cortical connections (12, 17).

Pan-mammalian commissural axon segregation. To elucidate whether the topographic segregation of interhemispheric axons based on cortical area position is a feature exclusive to the Therian clade (Metatheria + Eutheria), or instead they can be traced back to more evolutionarily distant mammals, we then performed brain tractography in an egg-laying monotreme mammal (Prototheria), the duck-billed platypus (*Ornithorhynchus anatinus*: Monotremata, Ornithorhynchidae). We examined MRI tractography of fixed platypus brains and found that well defined, three-dimensionally adjacent and homotopic commissural tracts were evident by placing small adjacent regions of interest within the mid-sagittal anterior commissure, along antero-posterior, dorso-ventral, and an oblique axis (antero-dorsal to postero-ventral; Fig. S3 and Video S2). Similar to dunnarts and eutherians, placing ROIs in well-defined cortical areas of the platypus brain (5) resulted in fibers that crossed the midline in spatially segregated topographic domains

(Fig. 3 *A* and *B*). Moreover, this arrangement could be reconstructed by manual parcellation of the mid-sagittal anterior commissure, which resulted in at least five broadly homotopic interhemispheric subsystems that include the olfactory/piriform, rostral cortical, neocortical, and entorhinal cortices (Fig. 3 *C* and *D*, and Video S3). The similar patterns of commissural fiber topography within the white matter tract, with shared spatial arrangement relative to each other and recapitulating the position of cortical areas, in species from all extant mammalian subclasses strongly suggest the ancient origin of neocortical axon guidance principles in the common ancestors of all modern mammals.

Single cell-level circuit mapping in dunnarts. Although these results demonstrate conserved features that suggest a pan-mammalian topography of interhemispheric cortical connections at the macro- and meso-scale levels, features of micro-anatomy connectivity, such as neuronal projection diversity within areas, as well as branching, fasciculation or crossing of axons, cannot be readily revealed via magnetic resonance imaging. To investigate whether and which features of the callosal connectome at the cellular level are present in marsupials, we performed retrograde interhemispheric circuit mapping in dunnarts. Stereotaxic injections of retrograde fluorescent tracers (carbocyanines and/or cholera toxin b subunit) into distinct cortical regions in 13 dunnarts *in vivo* revealed that, similar to callosal neurons in eutherians, contralaterally projecting neurons are located in regions that are broadly homotopic to the injection sites (Fig. 4 *A* and *B*, and Table S1). Moreover, the distribution of commissural projecting neurons, particularly within primary sensory areas, differed across cortical layers ($P < 0.0001$, one-way ANOVA), whereby they are located primarily in layers 2/3 (65.3 $\pm$ 2.2 %), followed by layer 5 (24.3 $\pm$ 1.6 %), and to a lesser extent in layer 4 (7.6 $\pm$ 1.4 %; Fig. S4). These ratios closely resemble that of eutherian callosal neurons in primary sensory cortices (27-29). However, in both eutherian and non-eutherian mammals, the layer distribution of commissural neurons is largely variable across cortical areas (Figs. 4 and 5). Notably, we found that the medial and caudal portions of the cerebral cortex of dunnarts (*i.e*., motor and cingulate/retrosplenial cortices) receive contralateral inputs not only from homotopic areas, but also from several heterotopic regions of the contralateral hemisphere (*e.g.,* site 6; Fig. 4*B*). Such heterotopic inputs included lateral regions of the cortex at similar rostro-caudal levels (Fig. S5), as well as long-range contralateral projections from neurons located at more rostral regions, including the claustrum, a non-layered derivative of the pallial subplate, and lateral portions of the frontal and orbital cortices (Fig. 5).

Similar long-range interhemispheric connections from the claustrum to heterotopic contralateral targets, including the dorso-medial portions of the cortex, have been previously described in rodents (19-21), and can be revealed after retrograde tracer injections in the posterior

cingulate/retrosplenial or motor cortices (Figs. S6 and S7, respectively). Moreover, the long-range contralateral projection neurons in the dunnart claustrum were topographically organized according to the medio-lateral position of their termination sites (Fig. S8), further resembling the ipsilateral and contralateral topography of the eutherian claustrum (19-23).

Anterograde circuit mapping via in-pouch electroporation in dunnarts. We next examined the patterns of contralateral axon innervation via in-pouch electroporation of fluorescent reporters in dunnarts during cortical development (30), followed by collection after completion of corticogenesis (31). We found that, whereas commissural neurons project largely to homotopic targets (Fig. 6, arrowheads), most neocortical regions, but not the olfactory or piriform areas, also send heterotopic axonal projections that terminate in the contralateral motor and cingulate areas (Fig. 6, insets), consistent with the anterograde tract-tracing results and further demonstrating that the cingulate, restrosplenial and motor cortices receive long-range interhemispheric connections from multiple heterotopic regions.

We next investigated whether projections from one cortical area to two or more different targets arise from the collateral branches of homogeneous neuronal populations, or instead from distinct neurons with independent projection profiles. To elucidate between these scenarios, we performed injections of retrograde tracers into the medial and lateral portions of the same hemisphere of the dunnart cortex *in vivo* and counted neurons that incorporated either one or both tracers at the medial and lateral cortices contralateral to the injection sites (Fig. 7 *A* and *B*). We found that the majority of neurons incorporated only one of the dies, with less than 3% neurons incorporating both dies (Fig. 7 *C* and *D*, arrowheads). Moreover, both homotopic and heterotopic neurons were arranged in an intermingled, salt-and-pepper fashion, and their relative proportion differed across cortical areas (Fig. 7 *C-E*). The lateral regions of the cortex, including the insula, contained more homotopic neurons than the medial regions, including cingulate and motor cortices (80.8 ± 2.7 % vs. 62.6 ± 5.7 %, respectively). On the other hand, these medial cortical regions had more heterotopic and branched (both tracers) contralaterally-projecting neurons than the lateral cortex (heterotopic: 35.2 ± 5.5 % medial vs. 18.8 ± 2.5 % lateral; both: 2.2 ± 0.5 % medial vs. 0.5 ± 0.3 % lateral; $P < 0.026$, $df = 8$, $N = 5$, Student's t-test; Fig. 7*E*). Importantly, such arrangement of intermingled commissural neurons with homotopic and heterotopic targets, with only few cells that demonstrate long-range contralateral branches, has also been reported in callosal neurons of rodents and primates (32-34). These findings, together with anterograde evidence of contralateral axons terminating in both homotopic and heterotopic targets in both marsupials and eutherians, suggest that the mechanisms of contralateral axon targeting include both positional and non-positional cues (35).

Finally, to get a better understanding of the homologies between the marsupial and eutherian commissural connectomes, we examined the general distribution and bilateral symmetry of heterotopic circuits in dunnarts, particularly within known interhemispheric hubs in eutherians such as the claustrum (Figs. S9 and 8). Similar to eutherians, the claustrum of dunnarts was distinguished from the surrounding striatum and deep insular cortex by Nurr1+ and Ctip2- expression (Fig. 8*A*), resembles the eutherian claustrum in that it is differentially interconnected with contralateral areas (19-23). For example, while the dunnart claustrum receives dense projections from heterotopic regions in the contralateral hemisphere, such as the perirhinal cortex (Fig. 8*B*), it is also largely avoided by axons from the contralateral primary somatosensory sensory cortex (Fig. 8*C*). Furthermore, the overall pattern of neocortical contralateral projections closely resembled the pattern of projections within the same hemisphere, in a mirrored fashion (Fig. S9). A similar pattern of ipsilateral and contralateral symmetry of pyramidal neuron projections has been widely reported in the better studied neocortex of rats (25), further suggesting the deep-time evolutionary conservation of cortical connectivity rules throughout mammals.

Discussion

In all eutherians studied to date, including rodents, carnivores, monkeys and humans, the axons that form the corpus callosum are spatially segregated within the tract into rostro-caudal and dorso-ventral topographies that represent the broad position of neuronal cell bodies across the different cortical areas (16-18). Callosal circuits include connections between largely homotopic regions, as well as heterotopic circuits that importantly include the medial (*i.e.*, cingulate, motor and retrosplenial cortex) and lateral (*i.e.,* perirhinal cortex, insula and claustrum) borders of the neocortical sheet (25, 32-37). These medial and lateral regions also represent hyperconnected hubs within and between hemispheres, and form part of the task-negative (also known as default mode) network (25, 38). Notably, despite its relatively small size, the non-layered claustrum is a central contributor to large-scale neocortical networks in rodents (21) and humans (23). Our findings of the dunnart claustrum as a major component of long-range heterotopic and hyperconnected contralateral circuits suggest its early origin. Indeed, despite reports of the apparent absence of the claustrum in platypus (39), cytoarchitectonic and neuroanatomical studies in the claustrum of the short-beaked echidna (*Tachyglossus aculeatus*; Monotremata) suggest that Therian-like circuits including the claustrum/insula and the medial/frontal cortices may have originated early in mammalian evolution, possibly as a central hub of long-range heterotopic connectivity between and within neocortical hemispheres (40-42).

Previous studies in marsupials have described several features of cortical intra- and interhemispheric organization that are shared with eutherians. These include similar developmental sequence of neuronal generation (26, 30, 31, 43, 44), expression of cell type- and layer-specific genetic markers (44-46), and patterns of connections within and between cortical hemispheres, including homotopic and heterotopic circuits (26, 47-50), which laid the groundwork for the present study. Taken together, our findings in platypus and dunnarts further suggest the early origin and conservation of an interhemispheric cortical connectome that pre-dates the evolution of the corpus callosum. The main features of such an ancient connectome are summarized in Fig. 8*D* and include: 1) co-existence of homotopic and heterotopic circuits, 2) topographic segregation of commissural axons within the tract according to the position of cell bodies, and 3) hyperconnected hubs at the medial (cingulate/motor) and lateral (claustrum/insula) borders of the cortex. In conclusion, our results suggest that the origin of the corpus callosum in early eutherian ancestors likely included the conservation of pre-existing features of intra- and interhemispheric connectivity. Notably, humans with congenital absence of the corpus callosum but with preserved interhemispheric integrative functions often show compensatory wiring through the anterior commissure that resembles the non-eutherian connectome (51). This suggests that, under certain unknown conditions, neocortical commissural neurons may exploit developmental plasticity of ancient mechanisms of axon guidance resulting in functional interhemispheric circuits. Our findings provide a comparative framework to further elucidate the molecular underpinnings of interhemispheric wiring in individuals with and without a corpus callosum, as well as to investigate developmental hypotheses concerning the evolution of homologous circuits in the vertebrate brain.

Materials and Methods

Animal ethics

This study was approved by The University of Queensland Animal Ethics Committee, and followed international guidelines on animal welfare.

Magnetic resonance imaging and tractography

Fixed brains of adult platypus (n = 2) and dunnarts (n = 3) were scanned at 16.4 T or 9.4 T (Bruker Ultrashield Plus Avance I, 89 mm bore, or Bruker Biospec Avance III, 300 mm bore, respectively; Paravision 5.1). Diffusion MRI datasets were processed using HARDI/Q-ball reconstruction, and tractography was generated using Fiber Assignment by Continuous Tracing in TrackVis (www.trackvis.com).

In-pouch electroporation of dunnart joeys

Electroporation of cortical neurons in dunnarts attached to the mother's teat was performed as described (30). Briefly, 0.5-1 μL of a 1 mL/mg DNA solution of pCAG-eYFP plasmid was injected into the lateral ventricle, followed by delivery of five 100 ms square pulses of 30-35 V at 1Hz (ECM 830, BTX, Harvard Bioscience).

Histology and cell counts

Double injections of fine carbocyanine crystals (DiI and DiD) were done in fixed dunnart brains using a pulled-glass micropipette. Brains were kept from light in formalin at 4°C for 7 days, and then at 38°C for 7 months for transport. *In vivo* stereotaxic injections (Table S1) were done under 2-5% isoflurane, using a reference atlas of the stripe-faced dunnart (*S. macroura*) (52). Brains were collected after 7 days, and histological images obtained with confocal microscopy. Cell-counts were made blind to the injection sites. Statistically significant differences were considered as $P < 0.05$ using two-tailed Student's t-test (Fig. 7*E*), or one-way ANOVA (Fig. S*4*) (Prism 7).

Supplementary Information

Supplementary material and full methods provided in *SI Appendix.*

Acknowledgements

We thank the Queensland Nuclear Magnetic Resonance Network and the Australian National Imaging Facility for the operation of the scanners, the Queensland Brain Institute's Advanced Microscopy Facility for histology imaging, and the University of Queensland Biological Resources and the Native Wildlife Teaching and Research Facility for all animal help. This work was supported by the Australian Research Council (DP160103958 to L.J.R. and R.S., and DE160101394 to R.S.), the National Health and Medical Research Council (APP1120615 to L.J.R., and APP1035093 to P.K.), the Australian Postgraduate Award (L.R.F., L.R.M.) and the UQ-QBI Doctoral Scholarship (A.P.).

Figures

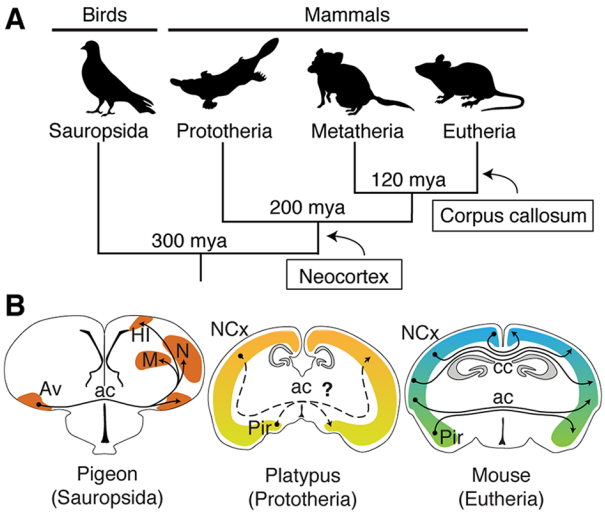

Fig. 1.

Evolution of cortical commissures. (*A*) Cladogram of birds and mammals showing the origin of the neocortex (NCx) and the corpus callosum (cc). (*B*) Coronal brain schematics. The anterior commissure (ac) of pigeons contains mostly unidirectional projections from the ventral arcopallium (Av) to contralateral homotopic and heterotopic targets, including the mesopallium (M), nidopallium (N) and hyperpallium intercalatum (HI). In eutherians, callosal axons are topographically segregated and connect mostly homotopic regions, while the ac carries axons from the piriform cortex (Pir) and lateral NCx. Homologous circuits in non-eutherians are carried exclusively through the ac. Mya, million years ago.

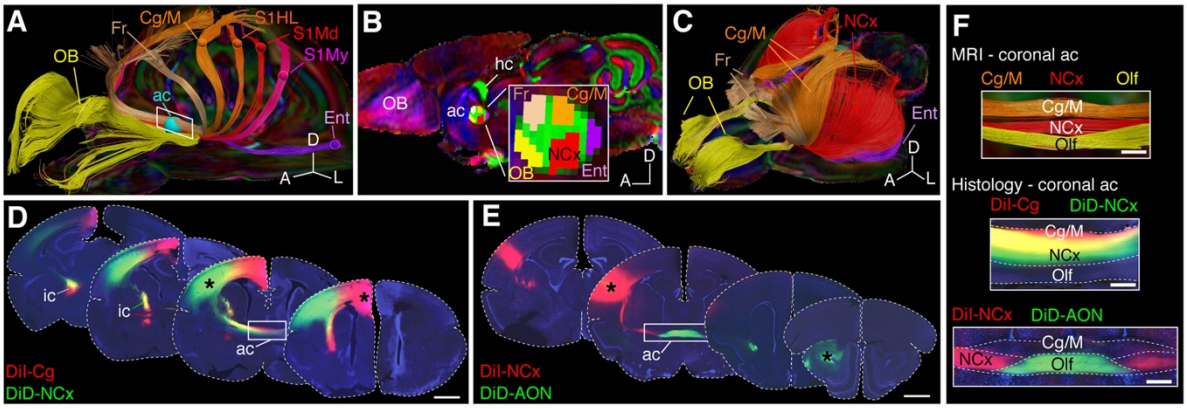

Fig. 2.

Segregation of commissural fibers by cortical areas in marsupials. (*A*) HARDI tractography of the dunnart brain (marsupial) using a spherical region of interest (ROI) at the anterior commissure (ac, cyan) and inclusion ROIs at seven cortical regions (spheres), reveal segregated tracts into color-coded homotopic domains. (*B*) Mid-sagittal dunnart MRI scan showing five hand-drawn ROIs within the anterior commissure (inset) that generate the color-coded tracts in *C*. (*C*) Tracts generated by ROIs in *B* reveal contralateral homotopy of the main cortical areas. (*D* and *E*) Coronal sections of dunnart brains after *ex vivo* injections of DiI (red) and DiD (green) in the regions indicated by asterisks. (*F*) Comparable coronal views of fiber segregation within the ac, as revealed by MRI and histology (from top to down, high-magnification views of the areas shown in *A*, *D* and *E*, respectively). AON, anterior olfactory nucleus; Cg/M, cingulate/motor cortex; Ent, entorhinal cortex; Fr, frontal cortex; ic, internal capsule; NCx, neocortex; OB, olfactory bulb; Olf, olfactory branch; Pir, piriform cortex; S1, primary somatosensory cortex; S1HL, S1 hindlimb; S1Md, S1 mandible; S1My, S1 mystacial whiskers. Scale bars: 1 mm in *D* and *E*, and 200 μm in *F*.

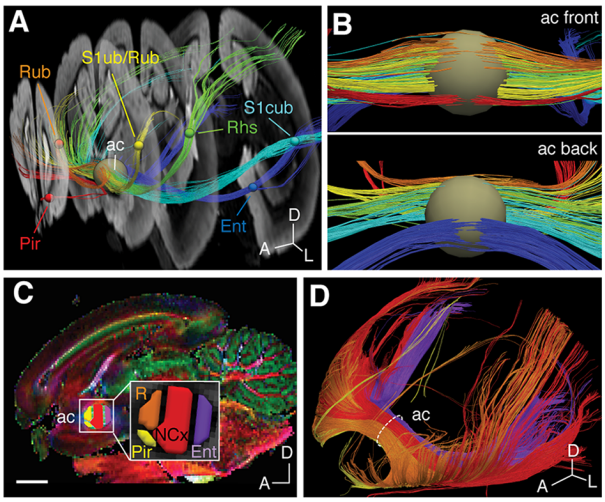

Fig. 3.

Topography of the anterior commissure of the platypus. (*A*) T1-weighted coronal series of a fixed platypus brain showing color-coded tracts between cortical regions of interest (ROIs, small spheres) and the anterior commissure (ac, large sphere). (*B*) Higher magnification coronal views of the tracts generated in *A* as viewed from the front (top) and the back (bottom). (*C*) Mid-sagittal view of the platypus brain and the anterior commissure (inset) showing the parcellation of ROIs that generate the tracts in *D*. (*D*) Interhemispheric tracts across ROIs of *C*, showing color-coded homotopic domains. A, anterior; D, dorsal; Ent, entorhinal cortex; L, lateral; NCx, neocortex; Pir, piriform cortex; R, rostral somatosensory cortex; Rhs, R head-shield; Rub, R upper-bill; S1cub, primary somatosensory cortex central upper-bill; S1ub, primary somatosensory cortex upper-bill. Scale bar: 4 mm.

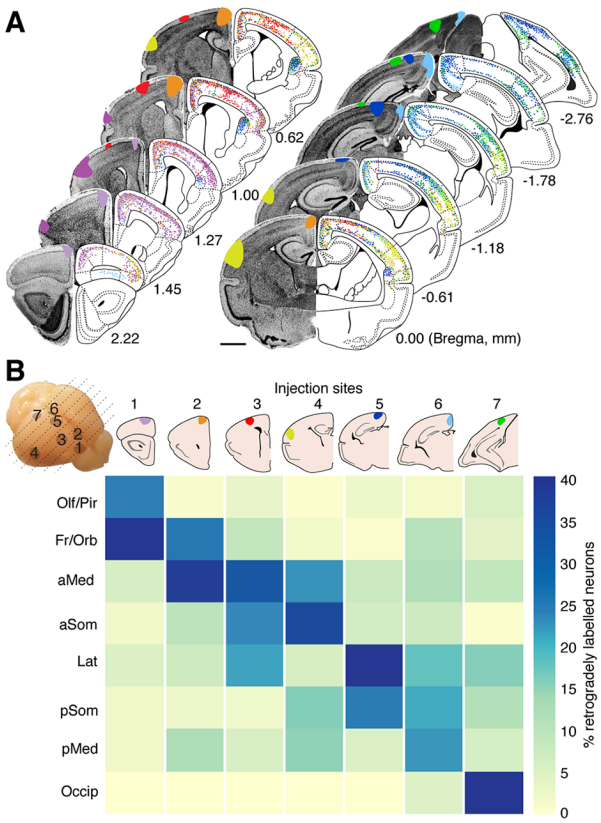

Fig. 4.

Homotopic and heterotopic commissural neurons in marsupials resemble the callosal connectome of eutherians. (*A*) Coronal sections of dunnart brains showing a summary of retrograde tracer injection sites (DAPI and color-coded in the left) and the contralateral position of cell bodies (dots). (*B*) Connectivity matrix combining injection sites (columns; approximate brain positions on top left) and percentage of labeled neurons per brain area (rows). aMed, anterior medial cortex; aSom, anterior somatosensory cortex; Fr/Orb, frontal/orbital cortices; Lat, lateral cortex; pMed, posterior medial cortex; pSom, posterior somatosensory cortex; Olf/Pir, olfactory/piriform cortices; Occip, occipital cortex. Scale bar: 1 mm.

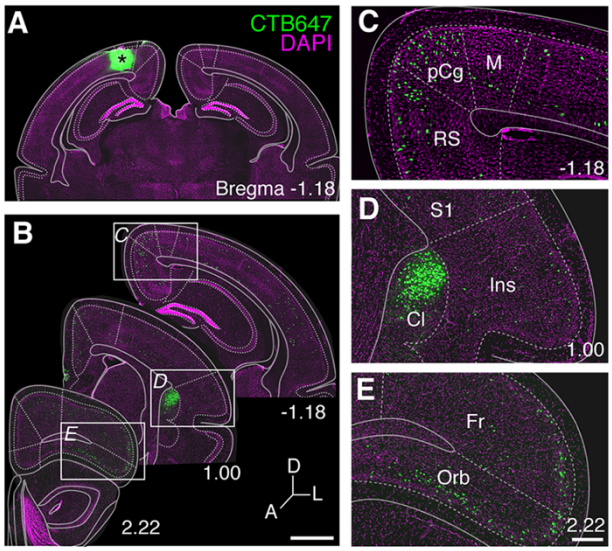

Fig. 5.

Heterotopic claustro-cortical commissural connections in dunnarts. (*A*) A posteromedial CTB injection and contralaterally projecting neurons across the rostro-caudal extent (*B*) in mm from Bregma. (*C-E*) Insets of the regions highlighted in *B* include neurons in the posterior cingulate (pCg), retrosplenial (RS) and motor (M) cortices in *C*, the claustrum (Cl) and insula (Ins) in *D*, and the frontal (Fr) and orbital cortices (Orb) in *E*. A, anterior; D, dorsal; L, lateral; S1, primary somatosensory cortex; Occip, occipital cortex. Scale bars: 1 mm in *B*, and 250 μm in *C-D*.

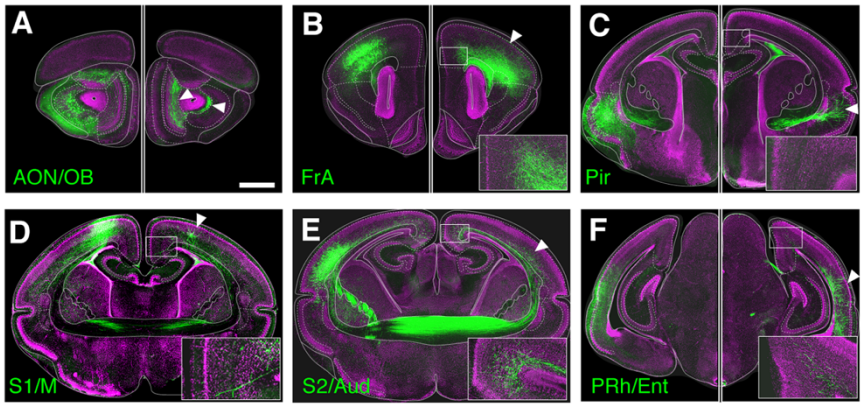

Fig. 6.

Anterograde mapping of contralateral projections in dunnarts reveals a conserved interhemispheric connectome. (*A*-*F*) In-pouch electroporated neurons are shown in the left hemisphere and their axon terminals in the right hemisphere in six different cases. Homotopic targets are shown with arrowheads, and insets show heterotopic terminals in the contralateral motor/cingulate cortex. To reveal the cell bodies and their axons, the hemispheres have different brightness/contrast levels in *A*-*C* and *F*. AON/OB, anterior olfactory nucleus/olfactory bulb; FrA, anterior frontal cortex; Pir, piriform cortex; PRh/Ent, perirhinal/entorhinal cortex; S1/M, primary somatosensory/motor cortex; S2/Aud, secondary somatosensory/auditory cortex. Scale bar, 1 mm.

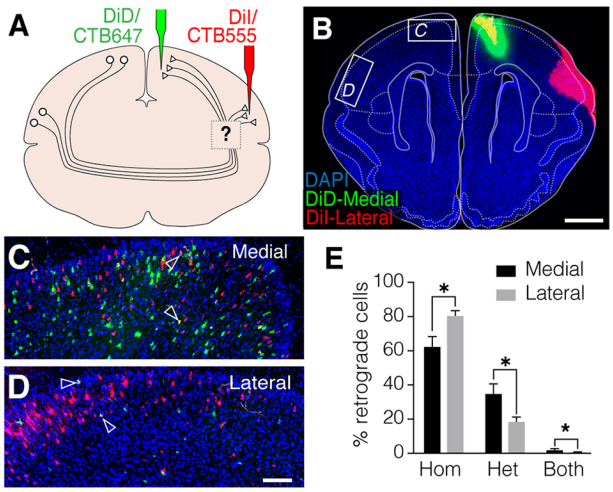

Fig. 7.

Intermingled populations of homotopic and heterotopic commissural neurons in dunnarts. (A-B) Double retrograde injections with CTB647 and CTB555 and/or DiI and DiD in the medial and lateral cortices result in intermingled cell bodies in the contralateral homotopic cortices (C and D) with very few double-labeled cells (arrowheads). (E) The proportion of cells that project exclusively to homotopic (Hom), heterotopic (Het) and to both targets differ between the medial and lateral cortices (mean + SEM, N = 5, *P < 0.026). Scale bars, 1 mm in *B*, 100 μm in *H*.

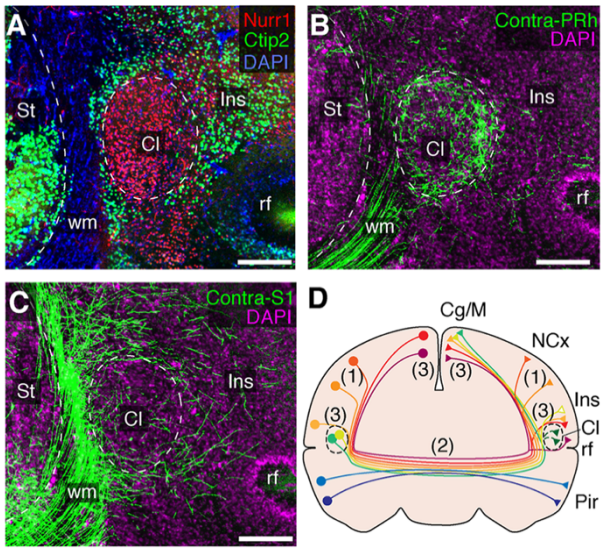

Fig. 8.

Heterotopic circuits and a pan-mammalian connectome. (*A*) Coronal dunnart brain section stained against Nurr1 (red), Ctip2 (green) and DAPI (blue) outline the claustrum (Cl) from the striatum (St), white matter (wm) and insula (Ins). (*B*-*C*) Axon terminals in the claustrum (Cl) were differentially found after electroporations in the perirhinal (PRh, *B*) or somatosensory (S1, *C*) cortices of the contralateral hemisphere. (*D*) Schematic of a coronal brain section representing the features of an interhemispheric connectome likely conserved by all mammals. Neocortical (NCx) neurons from layers 2/3 and 5 project to contralateral homotopic regions (1), following a topographic arrangement of axons across the midline (2), whereas hyperconnected and heterotopic circuits include the cingulate-motor (Cg/M) and insular (Ins) cortices, as well as the claustrum (3). Pir, piriform cortex; rf, rhinal fissure. Scale bars, 250 μm.

References

1. Ramón y Cajal S (1904) *Histología del Sistema Nervioso del Hombre y de los Vertebrados* (Boletín Oficial del Estado, Madrid).
2. Sperry RW (1945) Restoration of vision after crossing of optic nerves and after contralateral transplantation of eye. *Journal of Neurophysiology* 8(1):15-28.
3. Fredes F, Tapia S, Letelier JC, Marin G, & Mpodozis J (2010) Topographic arrangement of the rotundo-entopallial projection in the pigeon (Columba livia). *J Comp Neurol* 518(21):4342-4361.
4. Elliott KC, Wu W, Bertram R, Hyson RL, & Johnson F (2017) Orthogonal topography in the parallel input architecture of songbird HVC. *J Comp Neurol* 525(9):2133-2151.
5. Krubitzer L, Manger P, Pettigrew J, & Calford M (1995) Organization of somatosensory cortex in monotremes: In search of the prototypical plan. *The Journal of Comparative Neurology* 351(2):261-306.
6. Oh SW*, et al.* (2014) A mesoscale connectome of the mouse brain. *Nature* 508(7495):207-214.
7. Kaas JH (1997) Topographic Maps are Fundamental to Sensory Processing. *Brain Research Bulletin* 44(2):107-112.
8. Letzner S, Simon A, & Güntürkün O (2016) Connectivity and neurochemistry of the commissura anterior of the pigeon (Columba livia). *Journal of Comparative Neurology* 524(2):343-361.
9. Paterson AK & Bottjer SW (2017) Cortical inter-hemispheric circuits for multimodal vocal learning in songbirds. *Journal of Comparative Neurology* 525(15):3312-3340.
10. Owen R (1837) On the Structure of the Brain in Marsupial Animals. *Philosophical Transactions of the Royal Society of London* 127:87-96.
11. Suárez R (2017) Evolution of Telencephalic Commissures: Conservation and Change of Developmental Systems in the Origin of Brain Wiring Novelties. *Evolution of Nervous Systems (Second Edition)*, ed Kaas JH (Academic Press, Oxford), pp 205-223.
12. Suárez R, Gobius I, & Richards LJ (2014) Evolution and development of interhemispheric connections in the vertebrate forebrain. *Frontiers in human neuroscience* 8:497.
13. Gobius I*, et al.* (2016) Astroglial-mediated remodeling of the interhemispheric midline is required for the formation of the corpus callosum. *Cell reports* 17(3):735-747.
14. Gobius I*, et al.* (2017) Astroglial-mediated remodeling of the interhemispheric midline during telencephalic development is exclusive to eutherian mammals. *Neural Development* 12(1):9.

15. Ashwell KW (2016) Anterior commissure versus corpus callosum: A quantitative comparison across mammals. *Zoology (Jena, Germany)* 119(2):126-136.
16. de Lacoste MC, Kirkpatrick JB, & Ross ED (1985) Topography of the Human Corpus Callosum. *Journal of Neuropathology & Experimental Neurology* 44(6):578-591.
17. Zhou J*, et al.* (2013) Axon position within the corpus callosum determines contralateral cortical projection. *Proc Natl Acad Sci U S A* 110(29):E2714-2723.
18. Tovar-Moll F*, et al.* (2007) Neuroplasticity in human callosal dysgenesis: a diffusion tensor imaging study. *Cereb Cortex* 17(3):531-541.
19. Sloniewski P, Usunoff KG, & Pilgrim C (1986) Retrograde transport of fluorescent tracers reveals extensive ipsi- and contralateral claustrocortical connections in the rat. *J Comp Neurol* 246(4):467-477.
20. Smith JB & Alloway KD (2014) Interhemispheric claustral circuits coordinate sensory and motor cortical areas that regulate exploratory behaviors. *Frontiers in systems neuroscience* 8:93.
21. Wang Q*, et al.* (2017) Organization of the connections between claustrum and cortex in the mouse. *Journal of Comparative Neurology* 525(6):1317-1346.
22. Patzke N, Innocenti GM, & Manger PR (2014) The claustrum of the ferret: afferent and efferent connections to lower and higher order visual cortical areas. *Frontiers in systems neuroscience* 8:31.
23. Torgerson CM, Irimia A, Goh SYM, & Van Horn JD (2015) The DTI Connectivity of the Human Claustrum. *Human brain mapping* 36(3):827-838.
24. Zingg B*, et al.* (2014) Neural Networks of the Mouse Neocortex. *Cell* 156(5):1096-1111.
25. Swanson LW, Hahn JD, & Sporns O (2017) Organizing principles for the cerebral cortex network of commissural and association connections. *Proceedings of the National Academy of Sciences*.
26. Ashwell KW, Marotte LR, Li L, & Waite PM (1996) Anterior commissure of the wallaby (Macropus eugenii): adult morphology and development. *J Comp Neurol* 366(3):478-494.
27. Jacobson S & Trojanowski JQ (1974) The cells of origin of the corpus callosum in rat, cat and rhesus monkey. *Brain research* 74(1):149-155.
28. Wise SP & Jones EG (1976) The organization and postnatal development of the commissural projection of the rat somatic sensory cortex. *The Journal of Comparative Neurology* 168(3):313-343.

29. Granger EM, Masterton RB, & Glendenning KK (1985) Origin of interhemispheric fibers in acallosal opossum (with a comparison to callosal origins in rat). *J Comp Neurol* 241(1):82-98.
30. Paolino A, Fenlon LR, Kozulin P, Richards LJ, & Suárez R (2018) Multiple events of gene manipulation via in pouch electroporation in a marsupial model of mammalian forebrain development. *Journal of neuroscience methods* 293:45-52.
31. Suárez R*, et al.* (2017) Development of body, head and brain features in the Australian fat-tailed dunnart (Sminthopsis crassicaudata; Marsupialia: Dasyuridae); A postnatal model of forebrain formation. *PLOS ONE* 12(9):e0184450.
32. Fenlon LR, Suárez R, & Richards LJ (2017) The anatomy, organisation and development of contralateral callosal projections of the mouse somatosensory cortex. *Brain and Neuroscience Advances* 1:1-9.
33. Lanz F*, et al.* (2017) Distant heterotopic callosal connections to premotor cortex in non-human primates. *Neuroscience* 344:56-66.
34. Olavarria JF & Safaeian P (2006) Development of callosal topography in visual cortex of normal and enucleated rats. *The Journal of comparative neurology* 496(4):495-512.
35. Fenlon LR & Richards LJ (2015) Contralateral targeting of the corpus callosum in normal and pathological brain function. *Trends in Neurosciences* 38(5):264-272.
36. Suárez R*, et al.* (2014) Balanced interhemispheric cortical activity is required for correct targeting of the corpus callosum. *Neuron* 82(6):1289-1298.
37. De Benedictis A*, et al.* (2016) New insights in the homotopic and heterotopic connectivity of the frontal portion of the human corpus callosum revealed by microdissection and diffusion tractography. *Human Brain Mapping* 37(12):4718-4735.
38. Stafford JM*, et al.* (2014) Large-scale topology and the default mode network in the mouse connectome. *Proceedings of the National Academy of Sciences* 111(52):18745-18750.
39. Butler AB, Molnar Z, & Manger PR (2002) Apparent absence of claustrum in monotremes: implications for forebrain evolution in amniotes. *Brain Behav Evol* 60(4):230-240.
40. Ashwell KW, Hardman C, & Paxinos G (2004) The claustrum is not missing from all monotreme brains. *Brain Behav Evol* 64:223-241.
41. Divac I, Holst MC, Nelson J, & McKenzie JS (1987) Afferents of the Frontal Cortex in the Echidna (*Tachyglossus aculeatus*). Indication of an Outstandingly Large Prefontal Area. *Brain, Behavior and Evolution* 30(5-6):303-320.

42. Divac I, Pettigrew JD, Holst MC, & McKenzie JS (1987) Efferent Connections of the Prefrontal Cortex of Echidna (*Tachyglossus aculeatus*). *Brain, Behavior and Evolution* 30(5-6):321-327.
43. Ashwell KWS, Waite PME, & Marotte L (1996) Ontogeny of the Projection Tracts and Commissural Fibres in the Forebrain of the Tammar Wallaby (*Macropus eugenii*): Timing in Comparison with Other Mammals. *Brain, Behavior and Evolution* 47(1):8-22.
44. Puzzolo E & Mallamaci A (2010) Cortico-cerebral histogenesis in the opossum Monodelphis domestica: generation of a hexalaminar neocortex in the absence of a basal proliferative compartment. *Neural Development* 5:8-8.
45. Cheung AF*, et al.* (2010) The subventricular zone is the developmental milestone of a 6-layered neocortex: comparisons in metatherian and eutherian mammals. *Cereb Cortex* 20(5):1071-1081.
46. Wang WZ*, et al.* (2011) Comparative aspects of subplate zone studied with gene expression in sauropsids and mammals. *Cereb Cortex* 21(10):2187-2203.
47. Bravo H, Olavarria J, & Martinich S (1990) Patterns of interhemispheric and striate-peristriate connections in visual cortex of the South American marsupial Marmosa elegans (mouse opossum). *Anat Embryol (Berl)* 182(6):583-589.
48. Dooley JC, Franca JG, Seelke AM, Cooke DF, & Krubitzer LA (2013) A connection to the past: Monodelphis domestica provides insight into the organization and connectivity of the brains of early mammals. *J Comp Neurol*.
49. Martinich S, Pontes MN, & Rocha-Miranda CE (2000) Patterns of corticocortical, corticotectal, and commissural connections in the opossum visual cortex. *J Comp Neurol* 416(2):224-244.
50. Sheng XM, Marotte LR, & Mark RF (1990) Development of connections to and from the visual cortex in the wallaby (Macropus eugenii). *J Comp Neurol* 300(2):196-210.
51. Tovar-Moll F*, et al.* (2014) Structural and functional brain rewiring clarifies preserved interhemispheric transfer in humans born without the corpus callosum. *Proceedings of the National Academy of Sciences* 111(21):7843-7848.
52. Ashwell KWS, McAllan BM, & Mai JK (2010) Atlas of the brain of the stripe-faced dunnart (*Sminthopsis macroura*). *The Neurobiology of Marsupials*, ed Ashwell KWS (Cambridge University Press, New York), p 241.

PNAS
www.pnas.org

Supplementary Information for

A pan-mammalian map of interhemispheric brain connections predates the evolution of the corpus callosum

Rodrigo Suárez[a,1], Annalisa Paolino[a], Laura R. Fenlon[a], Laura R. Morcom[a], Peter Kozulin[a], Nyoman D. Kurniawan[b], and Linda J. Richards[c,1]

Rodrigo Suárez and Linda Richards
Email: r.suarez@uq.edu.au or richards@uq.edu.au.

This PDF file includes:

Other supplementary materials for this manuscript include the following:

Materials and Methods

Animals

All animal procedures, including breeding in captivity, were approved by The University of Queensland Animal Ethics Committee and the Queensland Government Department of Environmental and Heritage Protection, and followed the Australian Code for the Care and Use of Animals for Scientific Purposes (National Health and Medical Research Council, 8th edition, 2013), as well as international guidelines on animal care and welfare to minimize animal discomfort. Two adult platypus brains (*Ornithorhynchus anatinus*) fixed in formalin (i.d. 819 and 918) came from the collection of Prof. John Nelson held in the Australian National Wildlife Collection, Commonwealth Scientific and Industrial Research Organisation (CSIRO, Canberra). Fat-tailed dunnarts were bred in captivity, as described previously (48). Brains were collected after transcardial perfusion of saline (0.9%) and formalin (4% paraformaldehyde, PFA).

Ex vivo magnetic resonance imaging

Fixed brains of platypus (n = 2) and dunnarts (n = 3) were incubated for four days in the contrast agent gadopentetate dimeglumine (Magnevist, Bayer) at 0.25% v/v in 1M phosphate buffer saline (PBS), pH 7.4. For dunnart brains, magnetic resonance imaging was performed using a 16.4 T micro-imaging spectrometer (Bruker Ultrashield Plus Avance I; 89 mm bore diameter, Paravision 5.1) and a 15 mm surface acoustic wave coil (M2M Imaging). Three-dimensional high-resolution structural images were acquired using fast low angle shot (FLASH) with the following parameters: echo time (TE)/repetition time (TR) = 12/50 ms, flip angle (FA) = 30°, one excitation, field of view (FOV) = 1.74 x 1.2 x 0.8 cm, 30 μm isotropic resolution, and acquisition time of 40 min. High angular resolution diffusion imaging (HARDI) was acquired with the same FOV, using three-dimensional diffusion-weighted spin echo sequence of TE/TR = 20/400 ms, diffusion gradient ∂/Δ = 2.5/12.5 ms, b-value = 5000 s/mm^2, 30 diffusion encoding directions, 100 μm isotropic resolution, and acquisition time of 16 hours. For platypus brains, one sample was acquired at 16.4T using 3D FLASH with TE/TR = 6/50 ms, FA = 30^o, four excitations, FOV = 3.24 x 2.77 x 2.30 cm, 80 μm isotropic resolutions, and acquisition time of 2.5 h. Three-dimensional HARDI was acquired with the same FOV using TE/TR = 21/200 ms, ∂/Δ = 2.5/12.5 ms, b-value = 3000 s/mm^2, 30 diffusion encoding directions at 180 μm isotropic resolution. A second, slightly larger platypus brain sample was scanned at 9.4 T (Bruker Biospec Avance III, 300 mm bore diameter, Paravision 5.1) using a 40 mm rat head volume coil. Structural imaging was acquired using a three-dimensional rapid acquisition with relaxation enhancement (RARE) sequence, with TE/TR = 24/400 ms, RARE factor = 4, one excitation, FOV = 4.2 x 3.3 x 3.6 cm at 150 μm isotropic

resolution, and acquisition time of 52 min. Three-dimensional HARDI was acquired using TE/TR = 250/30 ms, ∂/Δ = 4/20 ms, b-value = 4000 s/mm^2, 30 diffusion encoding directions at 300 μm isotropic resolution, and acquisition time of 13.5 h.

Tractography reconstructions

Diffusion MRI datasets were processed using HARDI/Q-ball reconstruction and tractography streamlines were generated using the fiber assignment by continuous tracing (FACT) method within the diffusion toolkit of TrackVis program (www.trackvis.com). Briefly, dunnart brain structural scans were examined in the three planes and a spherical region of interest (ROI) was placed within the center of the anterior commissure and used as a seeding point to visualize interhemispheric tracts (radius = 4.75, corresponding to 142.5 μm, and coordinates = 50, 89, 157), and inclusion tracts were generated with smaller color-coded ROIs (radius = 2, *i.e*. 60 μm) at the following coordinates: olfactory bulb (56, 109, 186), entorhinal cortex (47, 26, 121), frontal cortex (85, 76, 187), cingulate/motor cortex (90, 77, 156), primary somatosensory cortex (S1) hindlimb field (90, 77, 156), S1 mandible field (89, 58, 138), and S1 mystacial whisker field (78, 46, 139), as shown in Fig. 2*A*. The same procedure was done in platypus with the following parameters: anterior commissure (radius = 6, *i.e*. 480 μm, coordinates = 77, 82, 126) and inclusion ROIs (radius = 1.5, *i.e*. 120 μm) in the piriform cortex (85, 92, 151), rostral somatosensory cortex (R) upper-bill (70, 104, 148), S1 upper-bill (85, 111, 134), R head-shield (85, 123, 119), S1 central upper-bill (75, 129, 103), and entorhinal cortex (93, 106, 86), as shown in Fig. 3 *A* and *B*. Confirmation of segregated domains was done by generating color-coded tracts after drawing individual, non-contiguous, two-dimensional ROIs with the hand-draw function in TrackVis, at the midsagittal plane of different dunnart and platypus brains (Figs. 2 *B* and *C*, and 3 *C* and *D*). Supplementary figures S1-S3 and videos S1-S3 of HARDI tractography in both species were made following the aforementioned methods.

***Ex vivo* carbocyanine injections**

For histological confirmation of segregated tracts, we performed double injections with carbocyanine crystals, DiI and DiD (1,1'-dioctadecyl-3,3,3',3'-tetramethylindocarbocyanine perchlorate, and 1,1'-dioctadecyl-3,3,3',3'-tetramethylindocarbocyanine, 4-chlorobenxenesulfonate salt, respectively; Invitrogen, Thermo Fisher Scientific) in formalin-fixed dunnart brains. Briefly, carbocyanine crystals were sonicated and small fragments were placed into one of two regions within the same hemisphere using a pulled glass micropipette. Brains were incubated in 4% PFA at 4°C for one week, and then transferred to a 38°C oven for at least 7 months to ensure axonal

transport. We then embedded the brains in 3.4% agarose and obtained 50 □m coronal sections using a vibratome (VT1000S, Leica Biosystems). Sections were mounted, stained for 10 min with DAPI (0.1% 4',6-Diamidine-2'-phenylindole dihydrochloride; Invitrogen, Thermo Fisher Scientific), washed in 1M PBS, cover slipped and imaged within 48 h.

In-pouch electroporation of dunnart joeys

Female dunnarts were anaesthetized as described above, and joeys examined inside the pouch. Electroporation of cortical neurons in postnatal dunnarts attached to the teat was performed inside the pouch as described previously (34). A small amount (0.5-1 μL) of a 1 mL/mg DNA solution of pCAG-eYFP plasmid was injected into the lateral ventricle, followed by electroporation with forceps-type electrodes (Nepa Gene), which delivered five 100 ms square pulses of 30-35 V at 1Hz (ECM 830, BTX, Harvard Bioscience). Joeys were collected around 50 postnatal days, and perfused as described above.

Immunofluorescence and microscopy

Brains sections were mounted and stained for DAPI alone (dye injections), or combined with immunohistochemistry. The primary antibodies were chicken anti-Gfp (1:750, ab13970, Abcam), goat anti-TdTomato (1:1000, AB8181-200, SICGEN), rabbit anti-Nurr1 (1:500, sc-991, Santa Cruz Biotech), rat anti-Ctip2 (1:500, ab18465, Abcam), with the corresponding secondary fluorescent antibodies (Alexa Fluor 488/555/568/647; Invitrogen, Thermo Fisher Scientific). Images were obtained using an upright microscope (Axio-Imager Z1, Zeiss) fitted with an AxioCam MRm camera, and captured with Zen software (Zeiss). Higher magnification images were obtained using an inverted microscope (TiE, Nikon) with a spinning disk confocal module (Diskovery, Andor), fitted with a sCMOS camera (Andor Zyla 4.2) and captured with NIS software (Nikon).

***In vivo* stereotaxic injections of retrograde tracers**

We performed 17 injections of retrograde tracers (DiI and/or DiD, 10 mg/mL dissolved in dimethyl sulfoxide, and/or cholera toxin beta-subunit conjugated with Alexa Fluor 555 or 647, 5 mg/mL in PBS; Invitrogen, Thermo Fisher Scientific) in 13 dunnarts *in vivo*. Animals were anaesthetized with 5% isoflurane in medical oxygen, delivered at 200mL/kg/min, placed in a mouse stereotaxic apparatus (Stoelting) and kept under 2-5% isoflurane through a nose mask. A pulled glass pipette was used to inject the dyes via a picospritzer (Parker Hannifin). Coordinates with respect to Bregma were recorded and cortical areas were assessed by comparing a brain atlas of the stripe-faced dunnart (*Sminthopsis macroura*) (52) with histology. Brains were collected after 7 days by

transcardial perfusion of 0.9% NaCl followed by 4% PFA, and sectioned coronally as indicated above.

Cell-level circuit mapping

The pattern of contralateral connections was mapped at single-cell resolution in dunnart brains after injections of retrograde tracers into the opposite hemisphere. To detect the injection sites, coronal sections of dunnart brains were visualized and imaged using an upright microscope (Axio-Imager Z1, Zeiss) fitted with an AxioCam MRm camera and captured with Zen software (Zeiss). The hemispheres contralateral to the injection sites were then imaged at high resolution using an inverted Nikon TiE microscope (Nikon) with a Diskovery spinning disk confocal module (Spectral Applied Research), fitted with a sCMOS camera (Andor Zyla 4.2) and captured with NIS software (Nikon). Experiments in which the injection sites penetrated the white matter or the ventricles, as well as cases where fewer than 80% of brain areas could be quantified, were excluded from the analyses. We manually curated, based on fluorescent cell body morphology, and counted a total of 34,005 contralaterally projecting neurons from 17 well-defined injections in 13 animals. Coronal sections counterstained with DAPI were mapped onto a 10 section template, including all cortical regions, based on an atlas of a related species (*S. macroura*) (52). Labeled cells were counted per area and section by investigators blind to the position of the contralateral injections. A summary of individual experiments is presented in supplementary Table S1. To generate the connectivity matrix in Fig. 4*B*, we calculated the percentage of retrogradely labeled cells across eight regions per experiment, and averaged experiments with comparable injection sites grouped into seven sites as indicated. In double-injection experiments (Fig. 7), cells were counted at the medial and lateral extents of the contralateral hemisphere having incorporated either one or both tracers. Statistically significant differences were considered as $P < 0.05$, using two-tailed Student's t-tests (for cortical area differences in homotopic, heterotopic and branched projections, Fig. 7*E*), and one-way ANOVA (for inter-layer differences in commissural neuron cell counts, Fig. S*4*) using Prism 7 (GraphPad).

Supplementary Figures

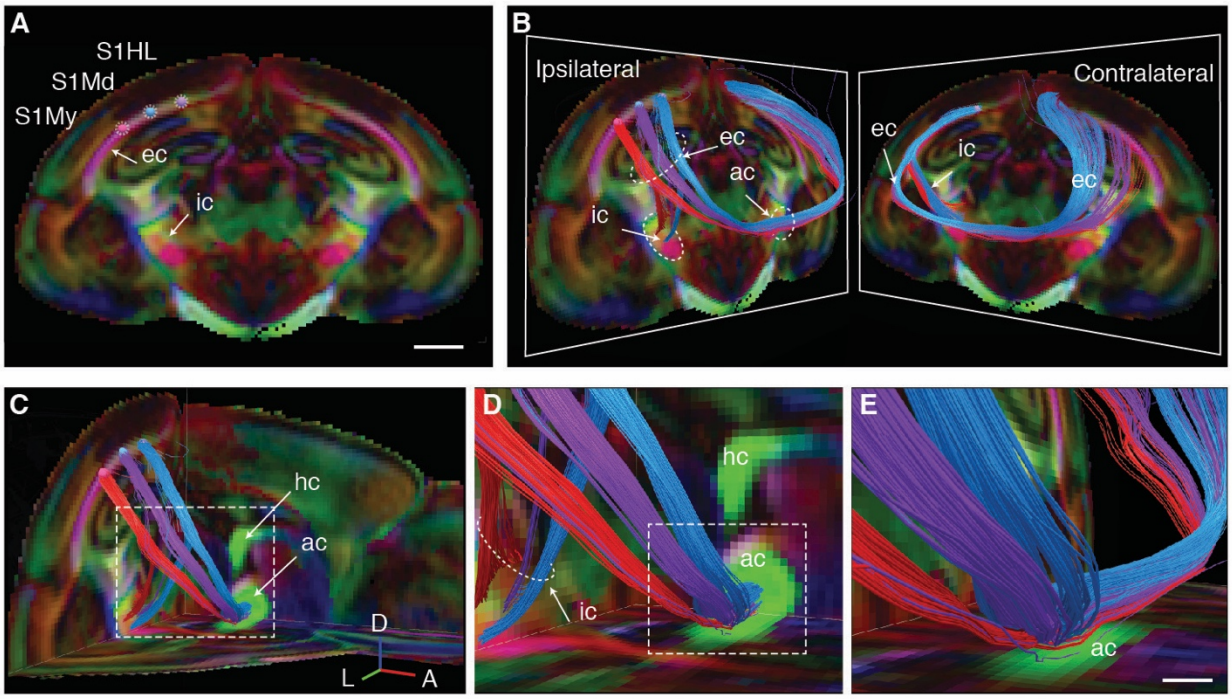

Fig. S1.

Intra- and extra-cortical fibers are topographically arranged in dunnarts. (*A*) Diffusion tensor imaging of a fixed dunnart brain showing three adjacent regions of interest (ROIs) within the primary somatosensory cortex (S1) hindlimb (S1HL), mandibular (S1Md), and mystacial (S1My) subfields. ec, external capsule; ic, internal capsule. (*B*) Color-coded tracts generated from the ROIs in **A** seen from ipsilateral and contralateral views reveal axonal segregation of homotopic circuits between hemispheres via the anterior commissure and external capsules, as well as cortical-subcortical topography via the internal capsule. (*C* and *D*) The same brain viewed with coronal, horizontal and midsagittal planes showing the point of crossing within the anterior commissure (ac), segregation of fibers within the internal capsule (ic), and the relative position of the hippocampal commissure (hc). (*E*) Inset from *D* without the mid-sagittal plane, showing the contralateral topography of fibers. Scale bars: 1 mm in *A*, 200 µm in *E*.

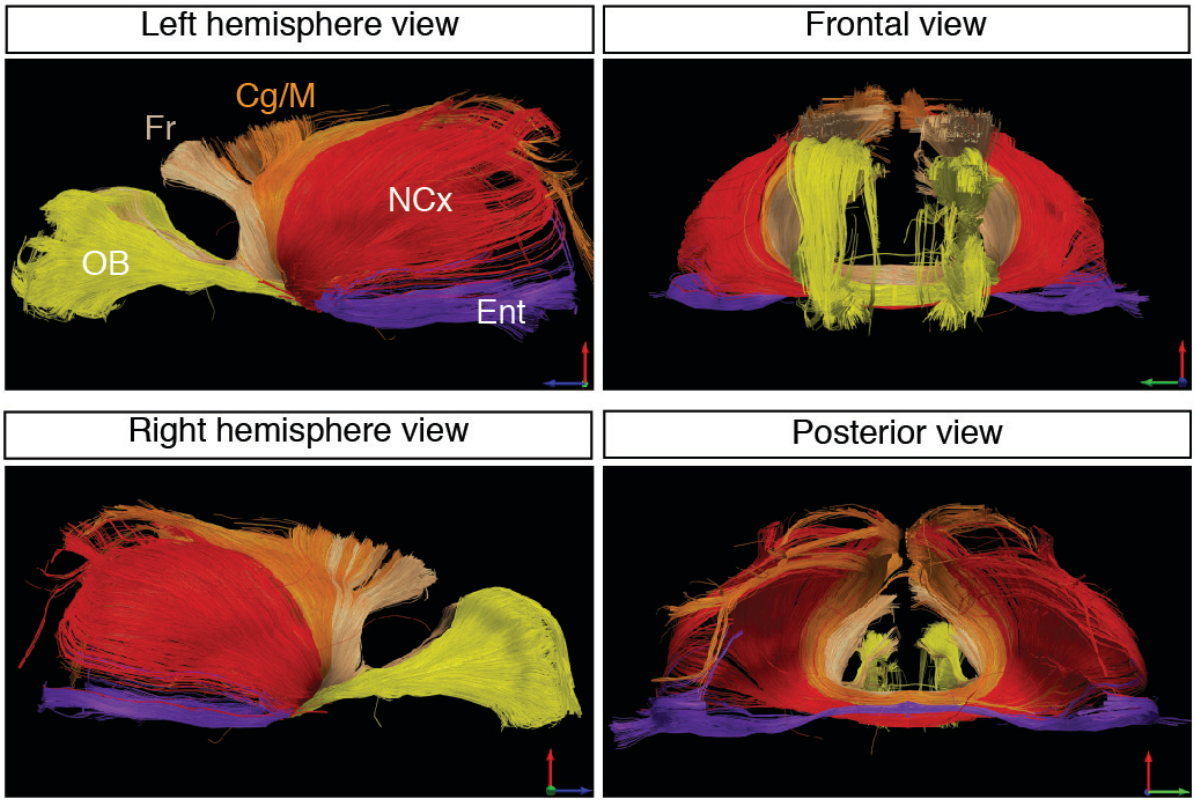

Fig. S2.

Homotopic fields can be reconstructed from the mid-sagittal anterior commissure in dunnarts. At least five color-coded homotopic domains can be generated by parcellation of the mid-sagittal anterior commissure as shown in Fig. 1*D*, including the olfactory bulbs (OB, yellow), frontal cortices (Fr, beige), cingulate and motor regions (Cg/M, orange), and bulk neocortical (NCx, red) and entorhinal cortices (Ent, purple). Views from the left, front, right and back.

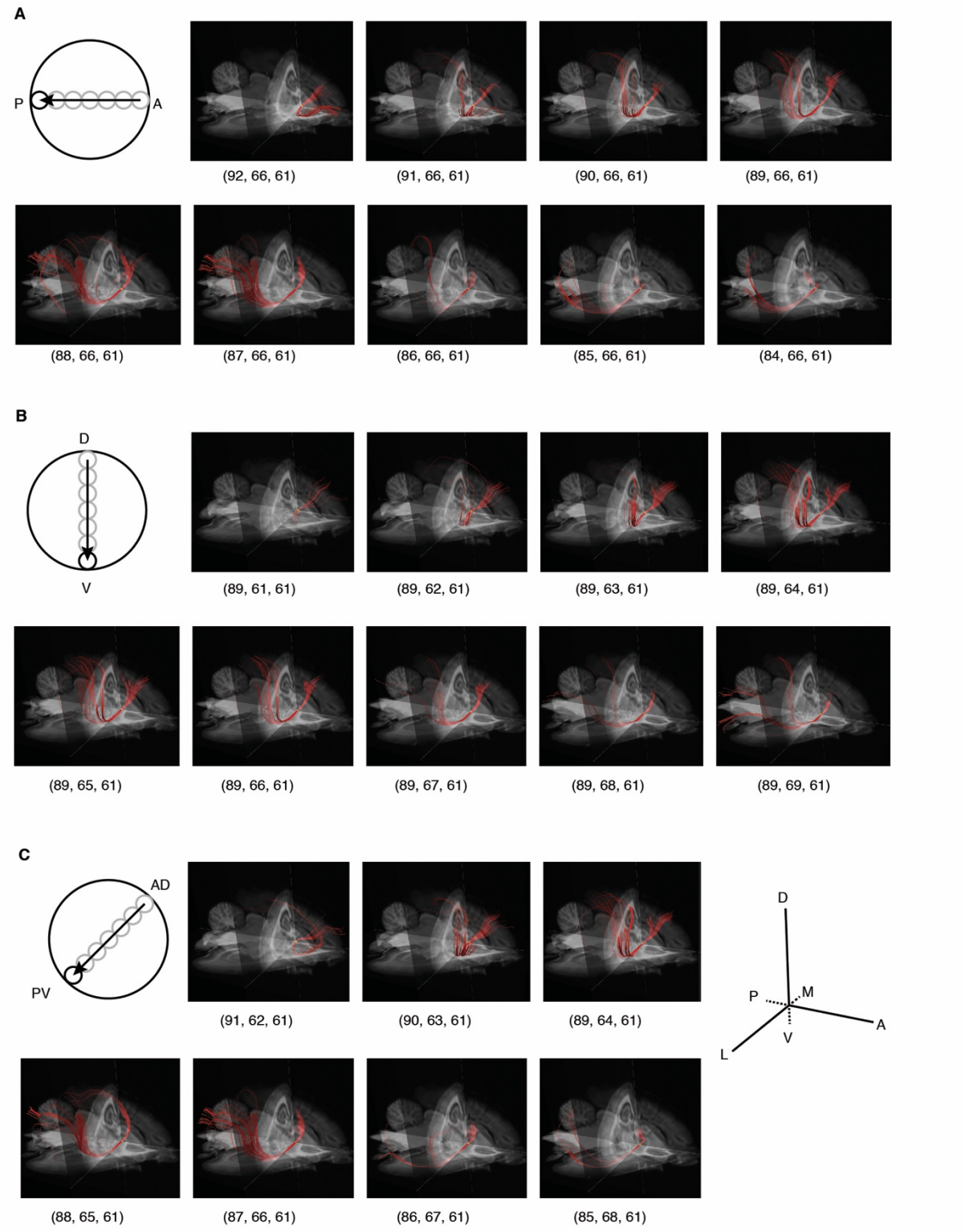

Fig. S3.

Segregation of homotopic of fibers within the anterior commissure of platypus. (*A*) Movement of a small region of interest (ROI) in seven steps along the antero-posterior axis (schematics on left) generates tracts in red in the corresponding images on the right (ROI in yellow, coordinates below each panel, see axes in *C*). (*B*) Same procedure as in *A*, but moving the ROI along dorso-ventral

equidistant steps. (*C*) Movement of the ROI in the oblique antero-dorsal (AD) to postero-ventral (PV) axis generates the tracts shown on the right. A, anterior; D, dorsal; L, lateral; M, medial; P, posterior; V, ventral.

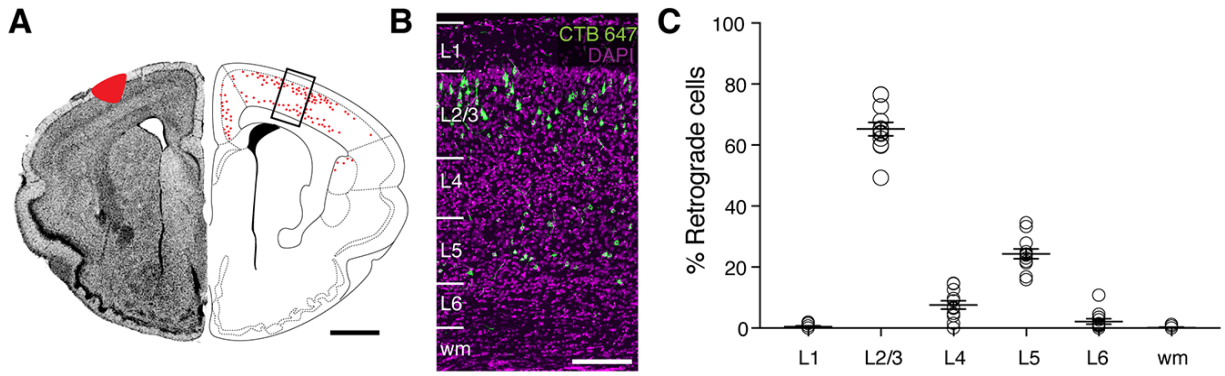

Fig. S4.

Layer distribution of commissural neurons in dunnarts. (*A*) Injections of retrograde tracers into primary sensory areas (e.g., S1 and V1) result in contralaterally labelled neurons located prominently in layers (L) 2/3 and 5 (*B*). (*C*) Quantification of the relative percentages of retrogradely labelled neurons across cortical layers after injections in homotopic contralateral areas in four animals. Data indicated as mean ± SEM. Scale bar: 1 mm in *A*, 200 µm in *B*.

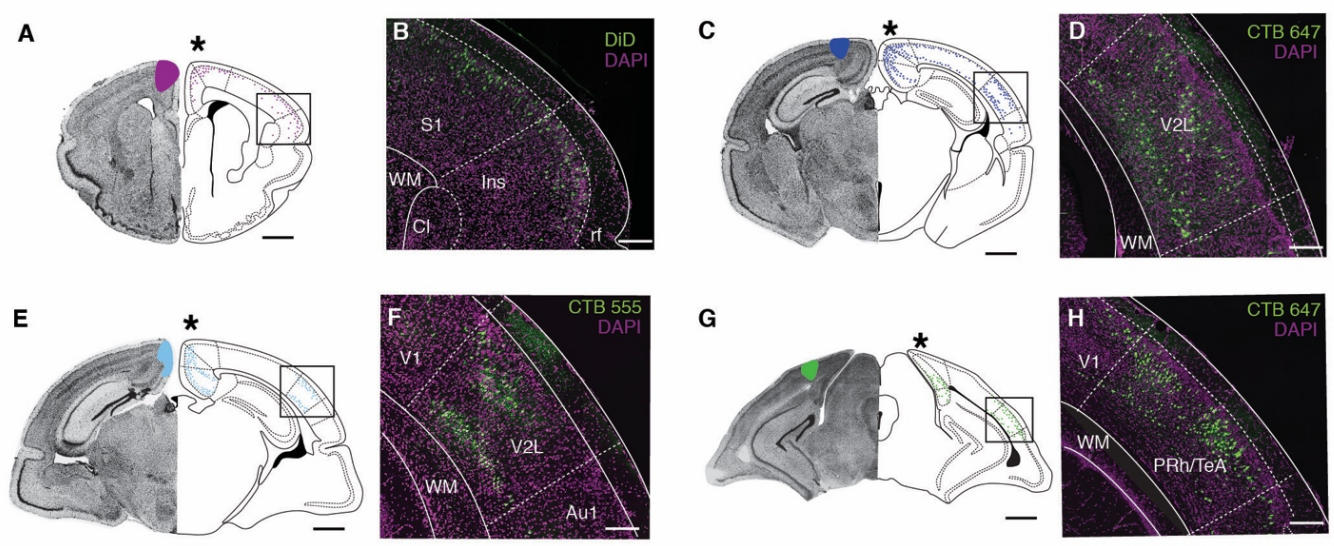

Fig. S5.

The medial cortices of dunnarts receive inputs from heterotopic regions of the contralateral neocortex. Four representative cases of medial injections at different antero-posterior extents are shown in *A*, *C*, *E*, and *G*, and insets of the contralateral neocortex in *B*, *D*, *F* and *H*. Homotopically projecting neurons are indicated by asterisks. Cl, claustrum; Ins, insular cortex; PRh/TeA, perirhinal/temporal association cortex; rf, rhinal fissure; S1, primary somatosensory cortex; V1, primary visual cortex; V2L, lateral field of the secondary visual cortex; WM, white matter. Scale bars: 1 mm in *A*, *C*, *E*, and *G*; 250 μm in *B*, *D*, *F* and *H*.

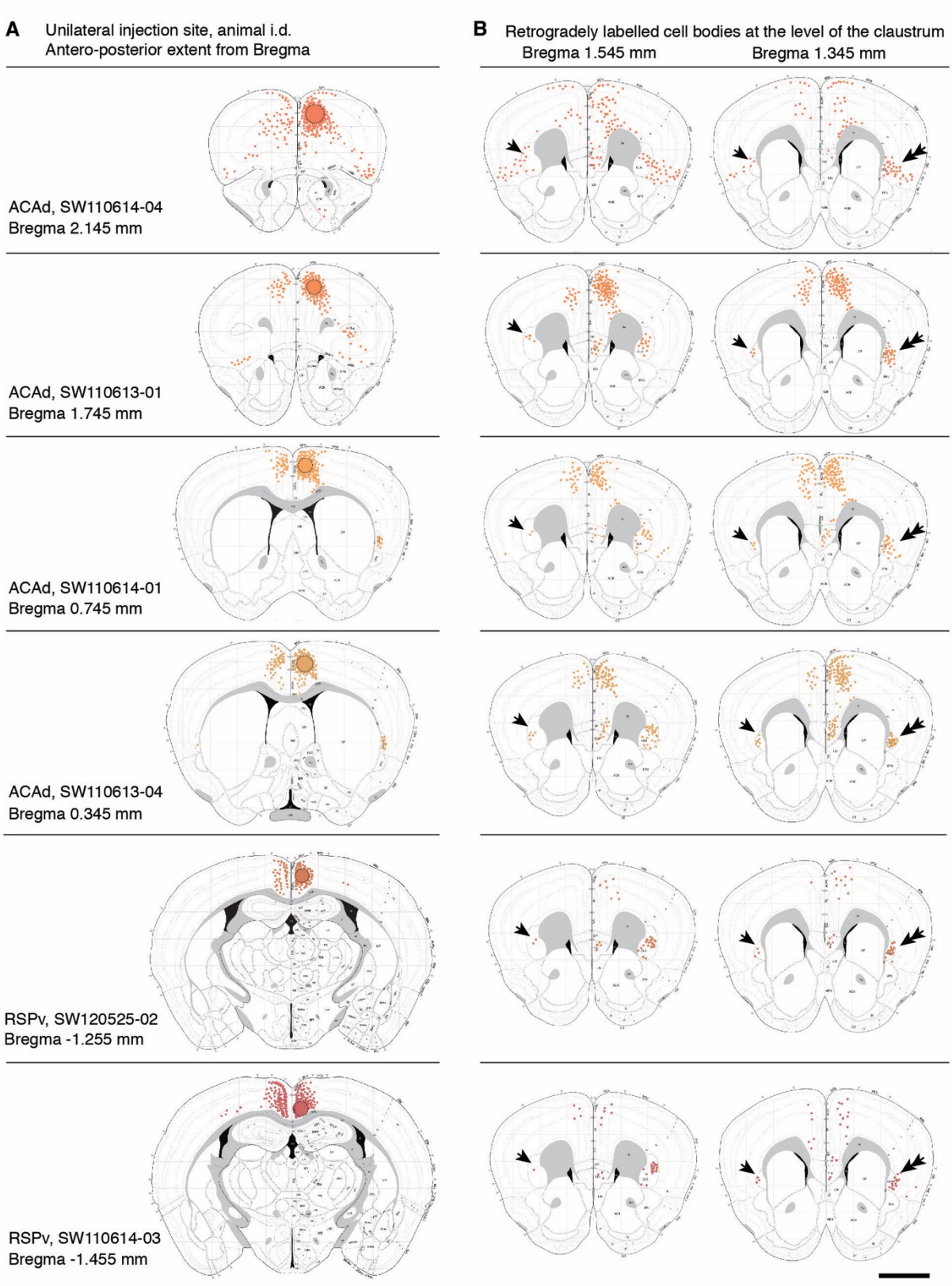

Fig. S6.

The claustrum of mice sends ipsilateral and contralateral long-range projections to the medial cortices. (*A*) Six representative cases of retrograde tracer injection experiments (Fluorogold or

cholera toxin B) into the medial cortices (ACAd, anterior cingular area dorsal; RSPv, retrosplenial cortex ventral) of mice along the antero-posterior axis (injection sites circled and color-coded). (*B*) Retrogradely labeled cell bodies from each experiment in *A*, at the level of the claustrum showing contralateral (arrowheads) and ipsilateral (double arrowheads) heterotopic circuits. Courtesy of www.mouseconnectome.org. Scale bar 2 mm.

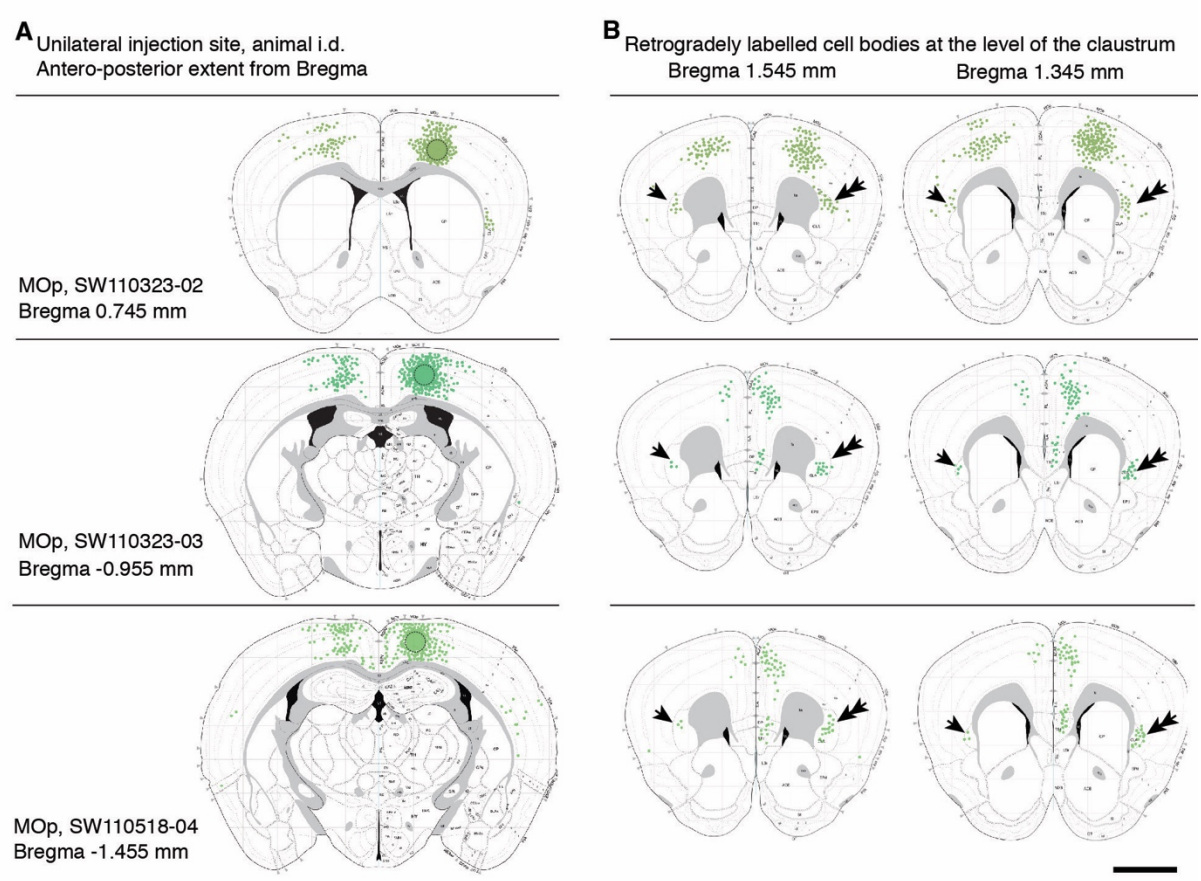

Fig. S7.

Long-range heterotopic projections from the mouse claustrum include both motor cortices. (*A*) Three representative cases of retrograde tracer injections (Fluorogold or cholera toxin B) into the motor cortices (MOp, posterior motor cortex) of mice along the antero-posterior axis (injection sites circled and color-coded). (*B*) Retrogradely labeled cell bodies from each experiment in *A*, at the level of the claustrum showing contralateral (arrowheads) and ipsilateral (double arrowheads) heterotopic circuits. Courtesy of www.mouseconnectome.org. Scale bar 2 mm.

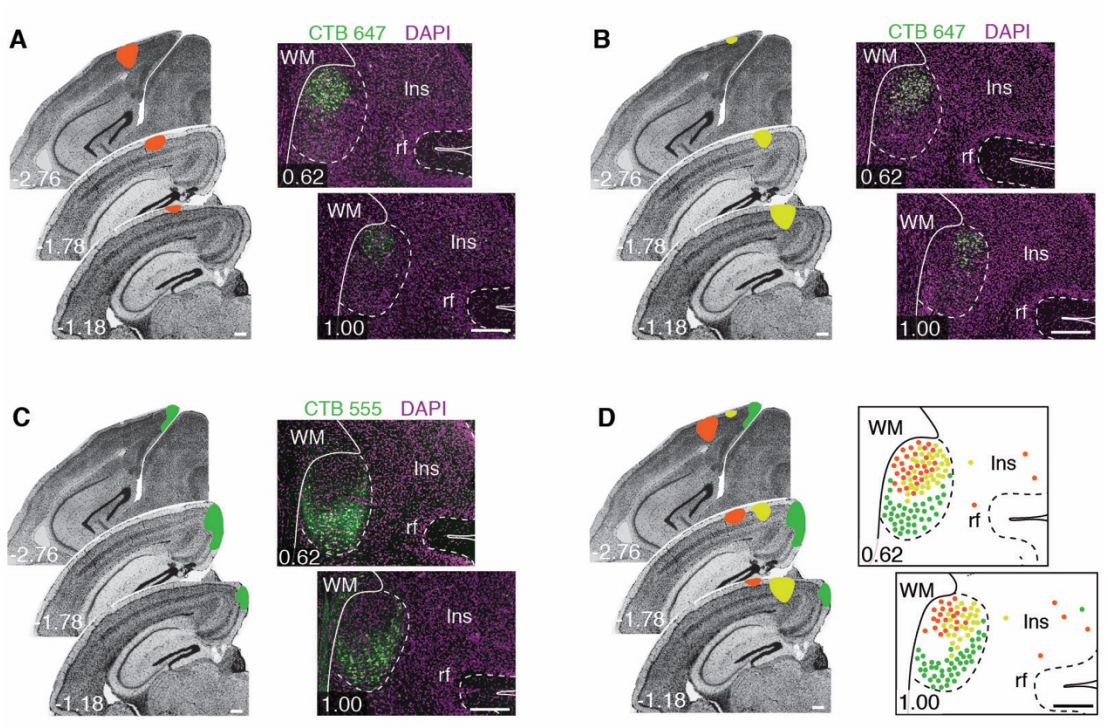

Fig. S8.

Contralateral claustro-cortical circuits in dunnarts are topographically organized according to cell body position. (*A* to *C*) *In vivo* injections of retrograde tracers (cholera toxin B, CTB) into the postero-medial cortex of dunnarts, left panels, and insets of the contralateral claustrum on right panels at defined Bregma coordinates (in mm, bottom left). (*A*) Superposition of the experiments in *A* to *C*, indicating the approximate position of topographically segregated cell bodies in the contralateral claustrum (right panel). Ins, insular cortex; rf, rhinal fissure; WM, white matter. Scale bars: 250 µm.

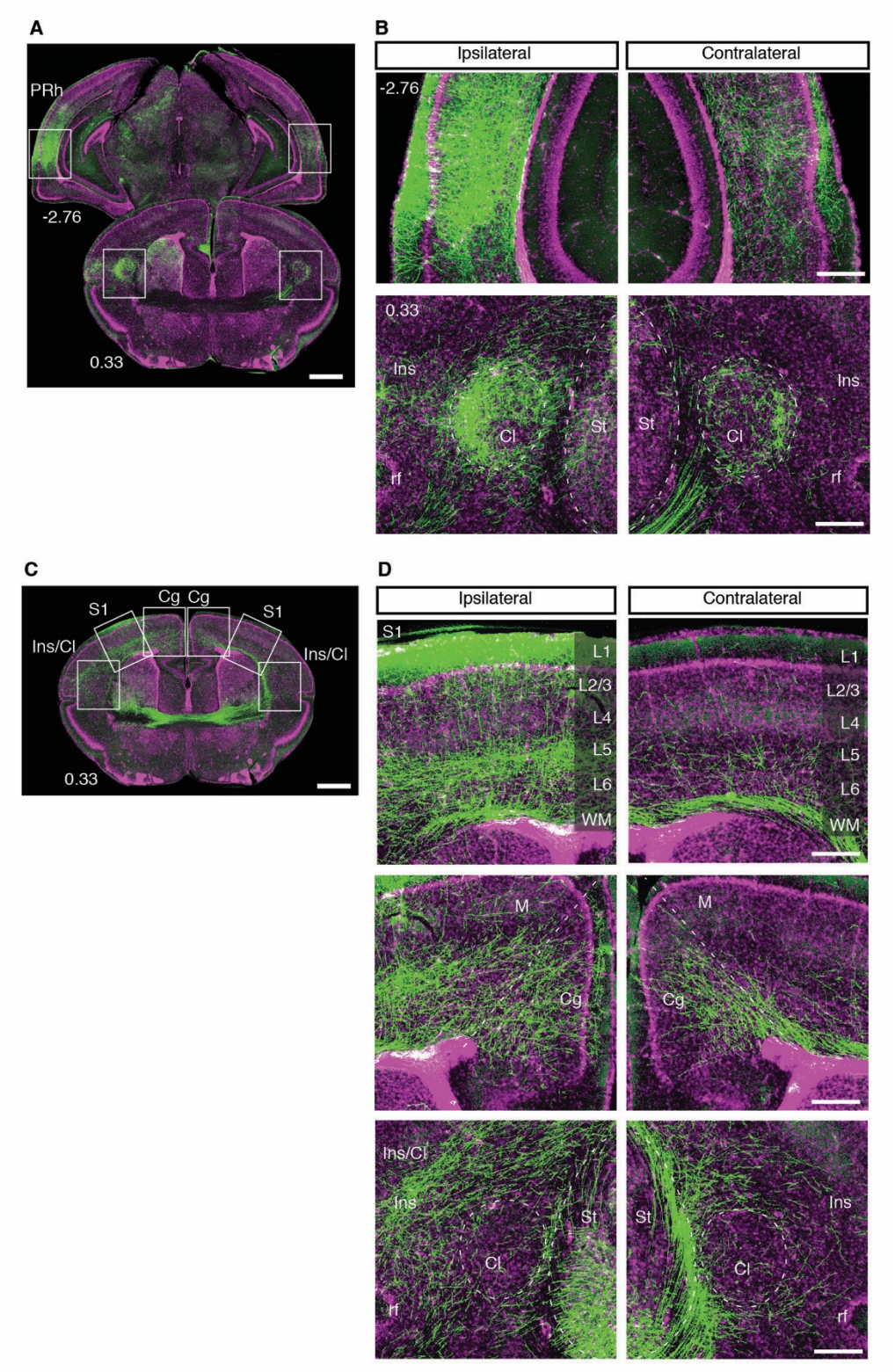

Fig. S9.

Mirror ipsilateral and contralateral projections in dunnarts reveal hyperconnected hubs in medial and lateral regions of the cortex. (*A*) In-pouch electroporated neurons in the perirhinal cortex (PRh, Bregma -2.76 mm) result in contralateral projections to the homotopic region (*B*, top panels), as well as heterotopic ipsi- and contralateral projections to the claustrum (Cl, Bregma 0.33 mm; *B*,

bottom panels). (*C*) Electroporation in the primary somatosensory cortex (S1, Bregma 0.33 mm) labels axonal terminals in the contralateral homotopic S1 (*D*, top panels), as well as bilateral projections to the cingulate cortices (Cg, *D*, middle panels) and insular (Ins) region, while avoiding the claustrum in both hemispheres (*D*, bottom panels). rf, rhinal fissure; St, striatum. Scale bars: 1 mm in *A*, and *C*; 250 μm in *B* and *D*.

Areas	Individual experiments (animal id-dye)																
	393-DI	613-C5	486-C5	610-C5	534-C5	467-DD	476-DD	534-C6	610-C6	403-DI	415-DI	465-DI	451-DI	579-C6	580-C6	486-C6	613-C6
aPir	51	4	18	26	371	13	11	6	0	1	6	10	10	61	2	166	0
pPir	0	4	0	9	50	0	24	12	0	12	7	11	17	9	27	75	0
Orbl	98	55	69	92	216	54	23	13	11	0	25	0	0	82	333	88	7
Orbv	20	176	244	44	220	13	28	0	1	0	1	0	0	34	119	53	0
Orbm	8	356	120	45	211	8	9	0	0	0	5	0	0	5	3	288	0
Fr	149	280	260	343	341	88	9	7	32	0	11	0	0	76	173	17	4
aCg	2	246	35	95	755	175	129	75	61	156	49	15	16	186	96	32	2
aM	19	717	546	296	748	214	107	28	48	15	3	0	0	93	91	74	0
cM	0	4	0	65	411	175	87	248	300	22	50	12	24	215	116	2	0
aS1	7	14	21	406	1438	115	167	145	107	47	10	5	17	130	72	10	1
cS1	3	2	0	272	245	96	268	580	359	131	65	4	28	171	128	3	2
aS2	2	2	0	34	20	30	82	9	14	244	176	82	109	19	60	1	12
aIns	6	46	43	113	457	76	230	36	5	98	32	11	30	38	52	27	0
aCl	6	94	28	16	43	44	17	5	22	8	7	7	9	90	121	40	5
pCl	0	5	3	13	5	6	6	5	13	8	72	12	4	187	185	141	10
aEnd	7	2	28	2	59	12	15	1	5	1	1	3	10	19	4	10	1
pEnd	0	3	0	1	0	2	5	0	0	2	13	3	2	0	0	3	0
pCg	10	424	83	159	444	48	15	107	130	43	37	32	22	459	350	61	1
RSP/Sub	0	107	0	6	6	8	3	2	1	4	0	3	6	76	118	187	269
pM	1	0	25	69	299	15	3	149	122	8	17	20	7	325	205	19	0
pS1	11	5	0	147	118	30	24	229	257	29	162	53	74	617	699	199	25
pS2	0	3	0	44	33	9	4	7	41	39	237	198	67	15	162	224	18
pIns	4	6	1	51	218	74	122	45	31	708	235	197	65	21	80	138	15
A1/Tea	0	3	0	0	7	5	0	4	1	0	0	0	0	4	353	148	58
PRh/Ect	0	1	0	0	24	0	7	4	7	2	0	0	3	26	78	4	0
V2/Ent	0	12	0	0	1	0	0	0	1	0	0	0	0	0	119	57	403
V1	0	0	0	0	2	5	0	0	0	0	0	0	0	0	285	40	422

Injection site coverage per area:
< 20%
20-50%
> 50%

Table S1. Contralateral circuit mapping in dunnarts demonstrate homotopic and heterotopic circuits.

Total count of retrogradely labeled neurons per experiment (columns) and brain areas (rows). Site and extent of contralateral injections are shown in green per experiment (animal number and dye used; *i.e.*, DI/DD, DiI/DiD; C5/C6, CTB 555/CTB 647). Horizontal bars (magenta) show the relative proportion of commissural neuron count per experiment. A1/TeA, auditory cortex/ temporal association area; aCg, anterior cingulate cortex; aCl, anterior claustrum; aEnd, anterior endopiriform nucleus; aIns, anterior insular cortex; aM, anterior motor cortex; aPir, anterior piriform cortex; aS1, anterior primary somatosensory cortex; aS2, anterior secondary somatosensory cortex; cM, central motor cortex; cS1, central primary somatosensory cortex; Ent, entorhinal cortex; Fr, frontal cortex; Orbl, lateral orbital cortex; Orbm, medial orbital cortex; Orbv, ventral orbital cortex; pCg, posterior cingulate cortex; pCl, posterior claustrum; pEnd, posterior endopiriform nucleus; pIns, posterior insular cortex; pM, posterior motor cortex; pPir, posterior piriform cortex; PRh/Ect, perirhinal/ectorhinal area; pS1, posterior primary somatosensory cortex; pS2, posterior secondary somatosensory cortex; RSP, retrosplenial complex; Sub, subiculum; V1, primary visual cortex; V2L, secondary visual cortex lateral; V2M, secondary visual cortex medial.

Movie S1. Segregation of homotopic domains along the anterior commissure in dunnarts. Three-dimensional animation of tractography using inclusion regions of interest (ROIs) between the anterior commissure (cyan ball) and seven small ROIs placed in different cortical areas, as indicated in Fig. 2*A*.

Movie S2. Topography of homotopic fibers along the platypus anterior commissure. Movement of a small region of interest (ROI; yellow sphere) within the mid-sagittal anterior commissure along the antero-posterior, dorso-ventral and oblique antero-posterior/dorso-ventral axes, as detailed in Fig. S3, results in topographic homotopic bilateral tracts (red). Coronal, horizontal and sagittal planes are shown intersecting at corresponding points of ROI movement.

Movie S3. Segregation of homotopic fibers in the anterior commissure of platypus. Three-dimensional animation of a platypus brain tractography after parcellating the mid-sagittal anterior commissure at equivalent regions to those described in Fig. 3*C*. Homotopic contralateral fibers include the olfactory/piriform (red), rostral cortical (orange), bulk neocortical (yellow) and entorhinal cortex (green) domains.

4.3. Discussion

In all eutherians, callosal axons project medially while their cell bodies are still migrating through the intermediate zone and cross the midline in a highly topographic pattern, such that medially positioned neurons extend their axons in the dorsal portion of the corpus callosum, while neurons that are located in more lateral areas of the neocortex project more ventrally (Tovar-Moll *et al.* 2007, Zhou *et al.* 2013). Once they have crossed the midline, callosal axons reach broadly homotopic contralateral cortical regions, but also heterotopic areas, such as the cingulate/motor and retrosplenial cortex, as well as the insula and claustrum (Bravo *et al.* 1990, Sheng *et al.* 1990, Martinich *et al.* 2000, Smith and Alloway 2014, De Benedictis *et al.* 2016, Fenlon *et al.* 2017, Swanson *et al.* 2017). It is still unclear whether these characteristics are typical of the medially projecting callosal neurons of eutherians or whether they are shared by commissural neurons of marsupials.

The data presented in this paper, obtained using MRI, as well as single cell-level circuit mapping via *in vivo* retrograde and anterograde tracing systems in marsupials, revealed an early origin and conservation of the organisational principles characterising the mature interhemispheric cortical connectome, which predates the evolution of the corpus callosum. Specifically, despite the different commissural strategy adopted by marsupials, this article demonstrates a highly conserved layer distribution of contralaterally projecting neurons, as well as a topographic arrangements of the axons in the anterior commissure and homotopic, heterotopic and hyperconnected circuits through this interhemispheric tract. The mechanisms that might be involved in the formation of this highly organised interhemispheric map across mammals are still unclear. In the previous chapter, spatially correlated varicosities on axons extending from commissural neurons located in the deeper and the upper layers of the dunnart neocortex were suggested to be a site of direct or indirect physical axonal interaction, which might be required for correct contralateral targeting to homotopic or heterotopic regions of the contralateral hemisphere (3.2.3.4).

Combined with chapter 3, these findings collectively show a surprisingly conserved timing of major brain events, such as neurogenic order, commissural projection order and adult principles of organisation within these neocortical commissural tracts, despite the alternative route taken by their axons to cross the midline. The results from the following chapters 5 and 6 aim to characterise and investigate the developmental dynamics and mechanisms underlying the earliest difference in neocortical commissural development between marsupials and eutherian mammals, which is the

medial versus lateral turning of commissural axons in the intermediate zone of the cortical plate, as well as the role of transcription factors in specifying these projections.

Chapter 5. Exploring the effect of alternative commissural pathway on the dynamics of axonal projection strategies

5.1. Introduction

In chapter 4, monotreme and marsupial interhemispheric neocortical connectomes were analysed and compared with eutherian datasets, revealing broad features of interhemispheric connectivity that are shared across mammals. These results suggest that ancient rules of interhemispheric cortical connectivity originated at least 80 million years before the evolution of the corpus callosum (Suárez *et al.* 2018). Despite this conservation of the organisational principles of the mature commissural tracts across mammals, it is possible that the emergence of the corpus callosum in eutherians might result in a difference in the initial axonal elongation of commissural axons. In fact, in eutherians, commissural neurons extend their axons medially to form the corpus callosum as they migrate through the intermediate zone of the developing cortex, while in non-eutherian mammals, the adult pattern of commissural projections suggests that commissural axons project laterally, to reach the anterior commissure (Heath and Jones 1971, Robinson 1982, Richards *et al.* 1997, Lickiss *et al.* 2012). In addition to this, a sequential order of axonal elongation, during cortical development has been described in neurons located in the deeper layers of the eutherian neocortex, with laterally projecting axons that reach subcortical targets being extended before medially projecting axons that target the contralateral hemisphere (Richards *et al.* 1997). In the marsupial neocortex, the scenario might be different, as the adult pattern of connectivity suggests that both commissural and subcortical neurons extend their axons laterally, to then reach the external or the internal capsule, respectively. Altogether, it is thus unclear to which extent cortical neurons extend medial projections in the marsupial neocortical context, whether the mature pattern of marsupial connectivity is a result of axonal branching followed by pruning and/or whether this different connectivity pattern is a reflection of a different order of axonal elongation during early stages of cortical development.

In this chapter, the early dynamics of initial axonal elongation are explored in fat-tailed dunnarts, with a specific focus on the initial medial versus lateral extension of axons. Investigating these aspects of cortical circuits formation using anterograde and retrograde tracing systems *in vivo* can help to elucidate whether different strategies of initial axonal elongation occur in the commissural systems of marsupials and eutherians, and whether the early dynamics of medial versus lateral axonal extension relate to the evolution of neuronal projection fate across mammals.

5.2. Results

5.2.1. Laterally projecting commissural axons are extended before axons projecting medially to the ipsilateral cingulate in the dunnart neocortex

In order to investigate the order and timing of medial versus lateral axonal elongation, as the first step of circuit formation, in pouch electroporation was performed twice, at stage 20 and again at stage 23, within the same joeys, to label the deeper and upper layer neurons, respectively, using different fluorophores (e.g., eYFP and tdTomato, Figure 3.5). Electroporated brains were then collected at different intervals after the electroporations, more specifically at stages 21 (P16), 24 (P25), 26 (P32), 27 (P40) and 28 (P50), to analyse the first steps of circuit formation in the ipsilateral hemisphere. At stage 21, which is five-to-six days after the first electroporation with tdTomato, all the axons extending from deeper layer neurons have turned laterally to project either subcerebrally via the internal capsule and cerebral peduncle or to the contralateral hemisphere via the external capsule and anterior commissure (Figure 5.1A-C), while no axons turning medially were identified at this stage. After two weeks from deeper layer neurons generation, a few axons coming from this neuronal population start to project medially towards the ipsilateral cingulate cortex (Figure 5.1E). After 20 days from the first electroporation, the number of medially projecting axons from neurons located in the deeper layers increases drastically and is maintained in later stages (Figure 5.1H, K, N). Interestingly, a similar pattern is followed a few days later by the axons extending from the upper layer neurons, which were electroporated at stage 23 and which are a more homogeneous population of corticocortically projecting neurons. Initially, axons turn laterally to reach the external capsule and anterior commissure (Figure 5.1G, I) and after three weeks from neuronal generation, medially projecting axons innervate the ipsilateral cingulate cortex (Figure 5.1J, L). The number of medially projecting axons increase by stage 28 (Figure 5.1M, O). These data clearly show a specific timing of initial axonal elongation, where laterally projecting axons are extended before medially projecting ones in both deeper and upper layer neurons of the neocortex, which resembles the order of axonal elongation described in the deeper layers of the mouse neocortex (Richards *et al.* 1997), regardless of the different commissural strategy in these two species.

Whether laterally and medially projecting axons correspond to branches extended from the same neurons, or instead whether specific neuronal populations project either ipsilaterally or contralaterally, could not be determined with this experimental paradigm due to the high density of electroporated cells, which challenges the visualisation of single axons for their entire length. This

question is addressed in the next section, using double retrograde tracer injections in the regions targeted by the axons (ipsilateral cingulate and contralateral S1), followed by cell count analyses of neurons incorporating either one (non-branching neurons) or both tracers (branching neurons).

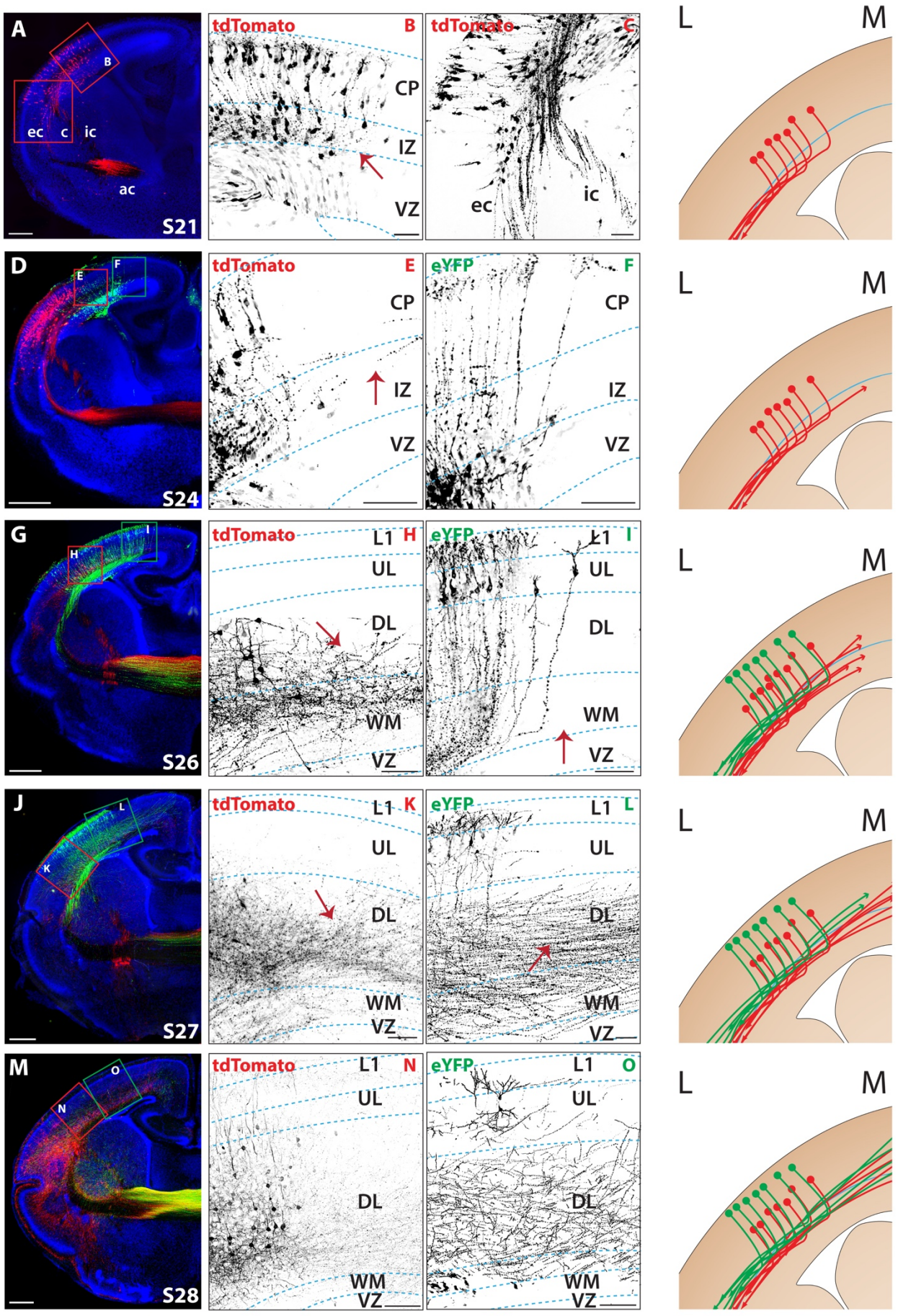
A
B
ec
c
ic
ac
S21
tdTomato
B
CP
IZ
VZ
tdTomato
C
ec
ic
L
M
D
E
F
S24
tdTomato
E
CP
IZ
VZ
eYFP
F
CP
IZ
VZ
L
M
G
H
I
S26
tdTomato
L1
H
UL
DL
WM
VZ
eYFP
L1
I
UL
DL
WM
VZ
L
M
J
K
L
S27
tdTomato
L1
K
UL
DL
WM
VZ
eYFP
L1
L
UL
DL
WM
VZ
L
M
M
N
O
S28
tdTomato
L1
N
UL
DL
WM
VZ
eYFP
L1
O
UL
DL
WM
VZ
L
M

Figure 5.1: Time course of axonal development.

A-C: Coronal section of dunnart brain collected at stage 21, after electroporation with tdTomato at stage 20. DL neurons electroporated with tdTomato are migrating within the cortical plate. Arrow showing axons turning laterally towards the internal capsule (ic) or external capsule (ec). There are no labelled axons turning medially. **D-F**: Coronal section of dunnart brain collected at stage 24. E: DL neurons electroporated with tdTomato, arrow showing few axons turning medially toward the cingulate. F: UL neurons labelled with eYFP are still located in the germinative zone. No medial axon is visible. **G-I**: Coronal section of dunnart brain collected at stage 26. H: DL neurons electroporated with tdTomato, arrow showing many more axons turning medially toward the cingulate, compared with the previous stage. I: UL neurons labelled with eYFP have reached their position in L2/3. No medial axon is visible. **J-L**: Coronal section of dunnart brain collected at stage 27. K: DL neurons electroporated with tdTomato, arrow showing a lot of intermingled axons turning medially toward the cingulate. L: UL neurons labelled with eYFP are localised in L2/3 of the neocortex and send extensive projections towards the cingulate (arrow). **M-O**: Coronal section of dunnart joey collected at stage 28. Axons extending from the DL (tdTomato) and UL (eYFP) are projecting medially towards the cingulate and are intermingled. The schematic summarises the main findings of this experiment: it represents a region of interest from a coronal section of the brain, with deeper layer neurons (in red) and upper layer neurons (in green) projecting their axons laterally (L) at first, and then medially (M). Ac = anterior commissure, ec = external capsule, DL = deeper layers, ic = internal capsule, UL = upper layers, VZ = ventricular zone, WM = white matter. Schematics on the right. Scale bars 400 μm and 100 μm.

5.2.2. Different corticocortical neuronal populations project predominantly laterally/commissurally or medially/ipsilaterally in adult and juvenile dunnarts

The data presented in the previous section show that, in dunnart, commissural axons projecting laterally to the anterior commissure are extended before axons projecting medially to the cingulate/motor cortex within the same hemisphere, which appear 15-20 days after neuronal generation (Figure 5.1). The results suggests the following possible scenarios that might explain how axonal specificity arises: 1) interhemispheric projecting neurons have two axonal branches that form sequentially, first the lateral branch projecting to the anterior commissure and then the medial ipsilateral branch to the cingulate/motor cortex, which suggest that branching might be an important mechanism of circuit formation; 2) there are two sub-populations of neocortical neurons that project predominantly either laterally to the anterior commissure or medially towards the midline, which suggest a transcriptional regulation of projection fate from early stages of development; 3) both mechanisms contribute, whereby initially branched neurons lose one of their branches to retain one principal projection. In order to investigate this, double injections with retrograde tracers (DiD and DiI) in the ipsilateral medial cortex (cingulate/motor cortex) and contralateral neocortex (S1) were performed in adult dunnarts (Figure 5.2A-E). The cingulate cortex was selected as area of injection as the results from the experiment in section 5.2.1 show that this region receives several projections from both deeper and upper layer neurons, and is thus an example of a hyperconnected hub (chapter 4 and Suárez *et al.* 2018). Retrogradely labelled cells located laterally to the cingulate/motor cortex injection were analysed and quantified in order to establish whether they incorporated either DiI alone (commissural neurons, Figure 5.2C), DiD alone (ipsilaterally projecting neurons, Figure 5.2D), or both (branching neurons projecting to both sites, Figure 5.2E). The data show that 98.8% of the retrogradely traced neurons counted in the region of interest incorporated only one tracer and 1.2% were labelled with both tracers in the adult (Figure 5.2K, mean = 1.2%, SEM = 0.25%, n = 3), indicating that distinct subpopulations of neurons predominantly project medially towards the cingulate/motor cortex or laterally towards the contralateral hemisphere (Figure 5.2A-E). To evaluate whether this pattern arises from differential exuberance/pruning of branched axonal terminals during development (Garcez *et al.* 2007), the same DiI/DiD injections were repeated in juvenile dunnarts at stage 28 of development (Figure 5.2F-J). At this age the cytoarchitecture typical of adult neocortex is established, but not yet fully mature, and the commissural axons have just reached the contralateral hemisphere, thus allowing retrograde tracing experiments at a time when neocortical and commissural development is still in progress. For this reason, at this stage, it is more likely that a definitive pruning process has not taken place yet, in which case, if there is exuberant branching followed by pruning, more double-labelled cells would be observed in

juveniles than in adults. Surprisingly, the results showed a statistically non-significant difference in the percentage of single- or double-labelled neurons between adult and juvenile dunnarts (Figure 5.2K: mean = 0.677%, SEM = 0.29%, n = 4). Therefore, exuberance and pruning of axons reaching the selected brain areas may be negligible, if present at all, and axons may reach specifically either ipsilateral or contralateral targets by stage 28, which is the earliest stage at which retrograde tracing experiments can be performed, as before this stage not enough commissural axons have reached the contralateral hemisphere to take up retrograde label. Another possible scenario is that at least two different neuronal populations exist, which may have different branches but incorporate one dye over the other because of one prevailing branch in terms of extension of the arborisation (Economo *et al.* 2016). The following experiment aims to clarify this and to investigate whether this specific axonal elongation, either laterally towards the contralateral hemisphere or medially towards the cingulate, occurs from the very beginning of axonal growth, without branching.

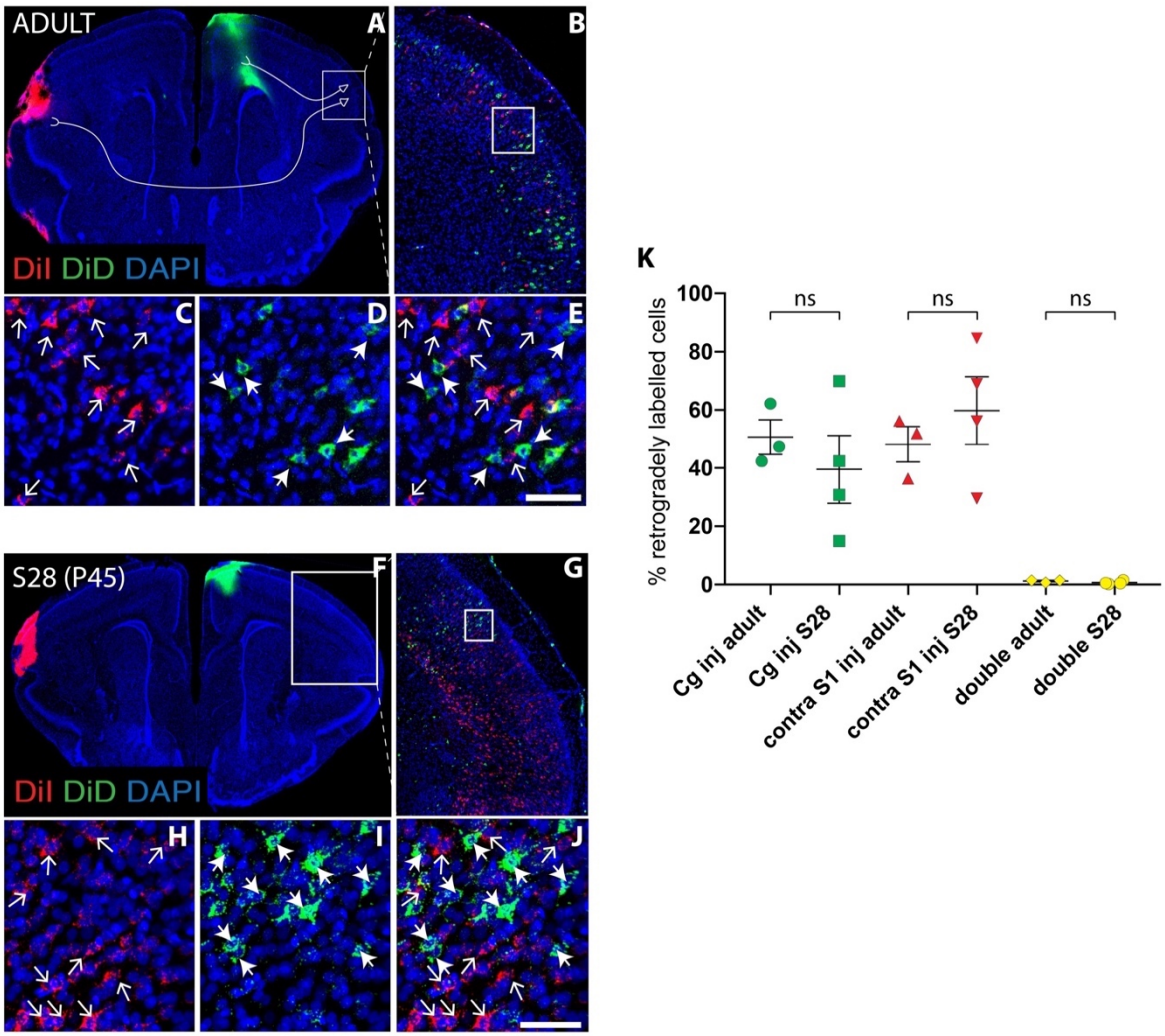

<u>Figure 5.2:</u> Different neuronal populations project predominantly to the contralateral hemisphere or to the ipsilateral cingulate cortex in both adult and juvenile dunnarts.

A, **F**: Injection of DiI in the lateral neocortex and DiD in the cingulate/motor cortex of adult and joey at stage 28 (older than P45), respectively. **B-E**, **G-J**: Neuronal subpopulations mostly project laterally to the anterior commissure or medially to the cingulate (arrows and arrowheads). Only few neurons project to both targets (in yellow). Scale bar: 50 µm. **K**: Statistically non-significant difference was found, between adults and S28 joeys, in the percentage of cells retrogradely labelled from the cingulate, from the contralateral S1 or from both sites. Gc = cingulate cortex, ns = non-significant, S = stage, S1 = primary somatosensory cortex. Adult: n = 3, joeys at stage 28: n = 4 * $P < 0.05$, ** $P < 0.01$, *** $P < 0.001$, Mann-Whitney U tests.

5.2.3. Neocortical commissural neurons have a different direction of initial axonal elongation in mouse and fat-tailed dunnart

The experiments performed in section 5.2.2 suggest that by stage 28 (> P45), when axons have just reached the contralateral hemisphere, two different neuronal populations exist in the dunnart neocortex that have predominantly extended their axons either laterally or medially, to reach either contralateral or ipsilateral targets, respectively. It is still unclear whether, in dunnarts, this specific axonal elongation occurs from the very beginning of axonal growth. Moreover, in contrast with the laterally projecting commissural neurons in the dunnart neocortex, neocortical commissural neurons in eutherian mammals extend their axons predominantly medially to cross the midline via the corpus callosum. In order to understand whether this different direction of axonal elongation between commissural neurons in marsupials and eutherians occurs during early stages of development, the upper layers neurons were labelled with *in utero* and in pouch electroporation in mice and dunnarts, respectively, and their projections were analysed at subsequent stages. The analysis was restricted to upper layer neurons as they are a more homogeneous population of corticocortical projection neurons than deeper layers commissural neurons, which are intermingled with subcortical projection neurons.

According to the experiments in sections 3.2.2 and 3.2.3, upper layer neurons were electroporated at stage 23, which correspond to E15 in mice and P20-22 in dunnarts, and the animals were collected three days after the electroporation. At this stage, it is possible to visualise neurons migrating in the cortical plate that have already begun to elongate their axons medially within the intermediate zone of mice (Figure 5.3A-B), while they had begun projecting laterally in dunnarts (Figure 5.3C-D). This phenotype becomes more striking a few more days after electroporation, such as P3 in mice and P32 in dunnarts (Figure 5.3E-H). This result further supports the hypothesis that a molecular mechanism that regulates medial versus lateral axonal projection in these two species might be in place during early stages of cortical development.

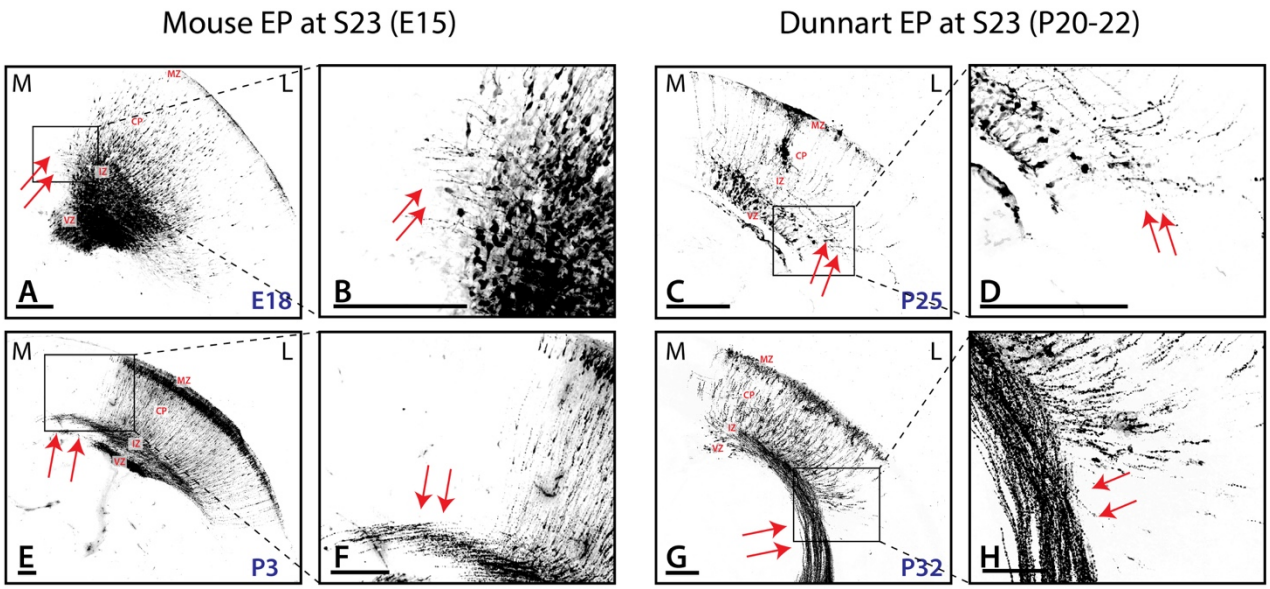

Figure 5.3: Different axonal elongation in neocortical commissural neurons of mouse and dunnart.

Upper layer neurons were electroporated at stage 23 in mouse (E15) and dunnart (P20-22). Mouse pups were then collected at E18 (**A-B**) and P3 (**E-F**), dunnart joeys at P25 (**C-D**) and P32 (**G-H**), showing a clear difference in the initial axonal elongation in these two species, whereby commissural neurons turn medially in mice and laterally in dunnarts, from early stages of development (arrows). Cp = cortical plate, EP = electroporated, IZ = intermediate zone, L = lateral M = medial, MZ = marginal zone, P = postnatal day, VZ = ventricular zone. Scale bars: 200 µm.

5.3. Discussion

The deeper layers of the mammalian neocortex are comprised of heterogenous neuronal populations that project to both subcortical and cortical targets, and previous studies in eutherian mammals have described a precise order of axonal elongation, whereby subcortical projection neurons extend their axons laterally, before corticocortical projection neurons elongate their axons medially (Richards *et al.* 1997). This suggests that the timing of axonal elongation might be relevant for projection fate determination. Despite the different commissural strategy adopted by marsupials, analysis of the timing of initial axonal elongation with in pouch electroporation of deeper and upper layer neurons in dunnarts showed that laterally projecting axons are extended before medially projecting axons, in both neuronal populations. This evidence suggests a conserved order of initial axonal elongation at least in the deeper layers of therian mammals.

In contrast, the scenario is different for pyramidal neurons of the upper layers, which are comprised of corticocortical projection neurons. In fact, in mouse, upper layer neurons initially project their axons medially, and lateral axonal projections appear only at later stages of cortical development (Hand and Polleux 2011, Hand *et al.* 2015). The opposite scenario occurs in dunnarts, where commissural neurons project all of their axons laterally at first, followed by medially projecting processes. Moreover, retrograde tracer injections *in vivo* have shown that, in developing as well as in adult dunnarts, different neuronal population project either laterally to cross the midline at the anterior commissure and reach the homotopic contralateral hemisphere, or medially to reach the cingulate cortex, with only a negligible percentage of retrogradely labelled neurons projecting to both sites. The lack of evident axonal branching, as well as the clear unidirectionality of the axons extended as the neurons are migrating through the cortical plate, suggest that the molecular regulation of initial axonal elongation, and consequently projection fate determination, might differ between mice and dunnarts.

The genes that might be involved in such differential targeting are currently unknown, and it also remains unclear what the function of neurons projecting ipsilaterally to the dunnart cingulate cortex might be. An interesting future direction of these findings would be to analyse the molecular profile of these medially projecting neurons to evaluate whether they express similar genes to eutherian callosal neurons. Such a molecular analysis would enable the investigation of the existence of marsupial neurons with similar features to that of callosal neurons, with axons that turn medially at the intermediate zone, like callosal neurons, but cannot cross the midline due to a lack of substrate, as midline remodelling does not occur in non-eutherian species (Gobius *et al.* 2016,

Gobius *et al.* 2017). Experiments that are currently in progress in the lab, which combine retrograde labelling of medially (intrahemispherically) and laterally (commissurally) projecting neurons, with fluorescence-activated cell sorting (FACS) followed by RNAseq, aim to identify the molecular profile of these two population of neurons in order to address this question. The future data obtained with these experiments will likely yield exciting results that build upon the foundations presented in this thesis.

As the major difference in terms of medial versus lateral initial axonal elongation between eutherians and marsupials occurs early during development, and several transcription factors have been associated with this step of circuit formation in eutherians (Hand and Polleux 2011, Lickiss *et al.* 2012, Hatanaka *et al.* 2016), the next chapter investigates the expression and the function of the candidate transcription factors SATB2 and CTIP2. These two proteins are known to regulate commissural and subcerebral projection fate, respectively, in mouse (Alcamo *et al.* 2008, Britanova *et al.* 2008, Molyneaux *et al.* 2009, Srinivasan *et al.* 2012, Leone *et al.* 2014, Srivatsa *et al.* 2014), by specifying medial versus lateral axonal projections (Figure 1.4) (Lickiss *et al.* 2012, Hatanaka *et al.* 2016).

Chapter 6. Investigating the transcriptional specification of interhemispheric and subcerebral projection neurons in the mammalian neocortex

6.1. Introduction

The expression of specific transcription factors in pyramidal neurons affects their initial axonal elongation and projection fate, and they can therefore be used as markers to differentiate the heterogeneous neuronal populations that comprise the neocortex (Molnár *et al.* 2006). In mice, for example, several transcription factors have been shown to be expressed in corticocortical, and specifically callosal neurons (Molyneaux *et al.* 2009, Hisaoka *et al.* 2010, Fame *et al.* 2011, Rodríguez-Tornos *et al.* 2016) (Table 1.1). Among these, *Satb2* has often been regarded as a "callosal gene" in the literature because of its crucial role in specifying callosal fate during brain development (Alcamo *et al.* 2008, Britanova *et al.* 2008, Molyneaux *et al.* 2009, Srinivasan *et al.* 2012) by directly repressing *Ctip2*, which is expressed in deeper layer neurons and specifies corticospinal and corticotectal projection identity (Alcamo *et al.* 2008, Arlotta *et al.* 2008, Srinivasan *et al.* 2012, Leone *et al.* 2014, Srivatsa *et al.* 2014).

Previously, it has been shown that the peaks of expression of SATB2 and CTIP2 temporally coincides with the initial axonal elongation of pyramidal neurons, either medial or lateral, respectively, while they are migrating towards their appropriate neocortical layers (Lickiss *et al.* 2012, Hatanaka *et al.* 2016) (Figure 1.4). In addition to this, when *Satb2* is knocked out in mice, CTIP2 is overexpressed and commissural axons fail to project medially to form the corpus callosum (Alcamo *et al.* 2008, Britanova *et al.* 2008, Leone *et al.* 2014), but instead project laterally towards the internal capsule to reach subcortical targets, or towards the external capsule to innervate the contralateral hemisphere via the anterior commissure (Alcamo *et al.* 2008, Britanova *et al.* 2008, Leone *et al.* 2014). This phenotype resembles the connectivity of non-eutherian mammalian brains, where commissural neocortical axons turn laterally in the intermediate zone and cross the midline via the anterior commissure (Figure 1.5). Therefore, this evidence suggests a role for SATB2 and CTIP2 in regulating the medial and lateral axonal extension, respectively, in mice (Lickiss *et al.* 2012, Hatanaka *et al.* 2016), as it has also been suggested for other transcription factors, such as NGN2 (Hand and Polleux 2011), and raises the question about the role that these transcription factors play in the specification of long-range projection fate in marsupials and across evolution in general (Figure 1.5).

In this chapter, the pattern of expression and the function of SATB2 and CTIP2 are investigated during neocortical fate determination and commissure development in mice and dunnarts, with the aim of elucidating their role in regulating medial versus lateral projections, and ultimately in fate-specification of corticocortical versus subcerebral connections, respectively.

Due to the different commissural strategies employed by cortical axons of eutherians and marsupials (Putnam *et al.* 1968, Heath and Jones 1971, Robinson 1982), comparing the function of SATB2 and CTIP2 in these species can help us to better understand the developmental and evolutionary processes involved in the specification of cortical circuits. Interestingly, mice and humans with agenesis of the corpus callosum can display functional connections between cortical hemispheres through an enlarged anterior commissure (Barr and Corballis 2002, Sarnat 2007, Alcamo *et al.* 2008, Britanova *et al.* 2008, Tovar-Moll *et al.* 2014), resembling the ancestral pattern of interhemispheric integration of non-eutherian mammals. This evidence suggests that there might be a rerouting through the evolutionary older anterior commissure in some cases of corpus callosum malformation that can lead to functional interhemispheric integration, thanks to developmental plasticity (including possible reversion to ancestral states, a process known as atavism) of ancient developmental mechanisms. Therefore, understanding the development and evolution of cortical wiring can also impact biomedical research on brain plasticity in pathological conditions.

6.2. Results

6.2.1. Similarities and differences in the pattern of expression of SATB2 and CTIP2 in marsupials and eutherians

6.2.1.1. *The functional domains of SATB2 and CTIP2 predicted proteins are highly conserved in therian mammals*

The corpus callosum evolved exclusively in eutherian mammals, it is thus unclear whether SATB2, previously regarded as a "callosal gene" (Alcamo *et al.* 2008, Britanova *et al.* 2008), and CTIP2, which is under SATB2 regulation, are expressed in a similar pattern and/or play similar roles in neuronal fate-specification in the marsupial brain, where the major interhemispheric tract is the anterior commissure. The mRNA sequence for SATB2 and CTIP2 has been previously predicted in some species of marsupials, such as the American grey short-tailed opossum (*Monodelphis domestica* - NCBI Reference Sequence: XM_001379413.3), the Tasmanian devil (*Sarcophilus harrisii* - NCBI Reference Sequence: XM_012544916.1), and more recently the koala (*Phascolarctos cinereus* – NCBI Reference Sequence: XM_020993639.1). However, the patterns of protein expression and their function have not been studied in the brain of these species. The first step in a SATB2/CTIP2 comparative analysis was thus to evaluate the degree of homology of the predicted proteins across therian mammals, specifically including the marsupials opossum (NCBI Reference Sequence: XP_007494637.1 for SATB2, XP_007473667.1 for CTIP2), Tasmanian devil (NCBI Reference Sequence: XP_012400370.1 for SATB2, XP_012405905.1 for CTIP2), and fat-tailed dunnart, whose developmental cortical transcriptome was recently sequenced by other members of our laboratory (Kozulin et al., in preparation), and the eutherians rat (NCBI Reference Sequence: XP_017452092.1 for SATB2, NP_001264216.1 for CTIP2), mouse (NCBI Reference Sequence: NP_001345509.1 for SATB2, NP_001073352.1 for CTIP2), human (Reference Sequence: NP_001165980.1, NP_612808.1 for CTIP2) and dog (NCBI Reference Sequence: XP_013966583.1 for SATB2, XP_005623848.1 for CTIP2 - Figure 6.1). Using mouse SATB2 protein as a reference, which is composed of 733 amino acids, the analysis of homology revealed that 9 amino acid substitutions (1.2 % of the whole protein) were marsupial-specific, while 11 amino acids substitutions were inconsistent between the two lineages (1.5%). CTIP2 mouse protein is 766 amino acids long and it shows more variability between marsupials and eutherians than SATB2, with 119 amino acids located outside the functional domains being marsupial-specific (15.5%) and 115 amino acids showing inconsistency between marsupials and eutherians (15%). Restricting the analysis of homology to the functional domains of the two transcription factors, as

major variations in these regions may be more likely to change protein function, revealed a remarkable degree of conservation across therian mammals, with only one amino acid differing between marsupials and eutherians in the second DNA-binding domain of SATB2. Specifically, the eutherian SATB2 protein has an aspartic acid (D) in position 477, while marsupials have a glutamic acid (E) (Figure 6.1). As these are both amino acids with an acidic side chain, it is possible that this change might not have any effect on functionality. The machine learning trained classifier SNAP2 (Screening for Non-Acceptable Polymorphisms, version 2) (Hecht *et al.* 2015) was employed to predict the effects of this point mutation in the SATB2 mouse protein. The results showed that a substitution of aspartic acid with glutamic acid in position 477 produced a low score (< 0), predicting this substitution has a weak effect on any change in SATB2 protein function. As for CTIP2, its functional domains are completely conserved across therian mammals at the protein level (Figure 6.1). Given that the predicted protein analysis suggested that SATB2 and CTIP2 proteins may exist with a predominantly conserved structure in the marsupial brain, the next sections are focused on investigating the temporal and spatial patterns of their expression in this species compared to mouse.

SATB2 analysis of homology

First DNA binding domain (350-437)

Tasmanian devil	KPEPTNSSVEVSPDIYQQVRDELKRASVSQAVFARVAFNRTQGLLSEILRKEEDPRTASQSLLVNLRAMQNFLNLPEVERDRIYQDER
fat-tailed dunnart	KPEPTNSSVEVSPDIYQQVRDELKRASVSQAVFARVAFNRTQGLLSEILRKEEDPRTASQSLLVNLRAMQNFLNLPEVERDRIYQDER
opossum	KPEPTNSSVEVSPDIYQQVRDELKRASVSQAVFARVAFNRTQGLLSEILRKEEDPRTASQSLLVNLRAMQNFLNLPEVERDRIYQDER
rat	KPEPTNSSVEVSPDIYQQVRDELKRASVSQAVFARVAFNRTQGLLSEILRKEEDPRTASQSLLVNLRAMQNFLNLPEVERDRIYQDER
mouse	KPEPTNSSVEVSPDIYQQVRDELKRASVSQAVFARVAFNRTQGLLSEILRKEEDPRTASQSLLVNLRAMQNFLNLPEVERDRIYQDER
human	KPEPTNSSVEVSPDIYQQVRDELKRASVSQAVFARVAFNRTQGLLSEILRKEEDPRTASQSLLVNLRAMQNFLNLPEVERDRIYQDER
dog	KPEPTNSSVEVSPDIYQQVRDELKRASVSQAVFARVAFNRTQGLLSEILRKEEDPRTASQSLLVNLRAMQNFLNLPEVERDRIYQDER

Second DNA binding domain (473-560)

Tasmanian devil	PIKVDGANVNITAAIYDEIQQEMKRAKVSQALFAKVAANKSQGWLCELLRWKENPSPENRTLWENLCTIRRFLNLPQHERDVIYEEES
fat-tailed dunnart	PIKVDGANVNITAAIYDEIQQEMKRAKVSQALFAKVAANKSQGWLCELLRWKENPSPENRTLWENLCTIRRFLNLPQHERDVIYEEES
opossum	PIKVDGANVNITAAIYDEIQQEMKRAKVSQALFAKVAANKSQGWLCELLRWKENPSPENRTLWENLCTIRRFLNLPQHERDVIYEEES
rat	PIKVDGANINITAAIYDEIQQEMKRAKVSQALFAKVAANKSQGWLCELLRWKENPSPENRTLWENLCTIRRFLNLPQHERDVIYEEES
mouse	PIKVDGANVNITAAIYDEIQQEMKRAKVSQALFAKVAANKSQGWLCELLRWKENPSPENRTLWENLCTIRRFLNLPQHERDVIYEEES
human	PIKVDGANVNITAAIYDEIQQEMKRAKVSQALFAKVAANKSQGWLCELLRWKENPSPENRTLWENLCTIRRFLNLPQHERDVIYEEES
dog	PIKVDGANVNITAAIYDEIQQEMKRAKVSQALFAKVAANKSQGWLCELLRWKENPSPENRTLWENLCTIRRFLNLPQHERDVIYEEES

Third DNA binding domain (615-674)

Tasmanian devil	PRSRTKISLEALGILQSFIHDVGLYPDQEAIHTLSAQLDLPKHTIIKFFQNQRYHVKHHG
fat-tailed dunnart	PRSRTKISLEALGILQSFIHDVGLYPDQEAIHTLSAQLDLPKHTIIKFFQNQRYHVKHHG
opossum	PRSRTKISLEALGILQSFIHDVGLYPDQEAIHTLSAQLDLPKHTIIKFFQNQRYHVKHHG
rat	PRSRTKISLEALGILQSFIHDVGLYPDQEAIHTLSAQLDLPKHTIIKFFQNQRYHVKHHG
mouse	PRSRTKISLEALGILQSFIHDVGLYPDQEAIHTLSAQLDLPKHTIIKFFQNQRYHVKHHG
human	PRSRTKISLEALGILQSFIHDVGLYPDQEAIHTLSAQLDLPKHTIIKFFQNQRYHVKHHG
dog	PRSRTKISLEALGILQSFIHDVGLYPDQEAIHTLSAQLDLPKHTIIKFFQNQRYHVKHHG

CTIP2 analysis of homology

First zinc finger domain (221-251)

Tasmanian devil	YICTTCKQPFNSAWFLLQHAQNTHGFRIYLE
fat-tailed dunnart	YICTTCKQPFNSAWFLLQHAQNTHGFRIYLE
opossum	YICTTCKQPFNSAWFLLQHAQNTHGFRIYLE
rat	YICTTCKQPFNSAWFLLQHAQNTHGFRIYLE
mouse	YICTTCKQPFNSAWFLLQHAQNTHGFRIYLE
human	YICTTCKQPFNSAWFLLQHAQNTHGFRIYLE
dog	YICTTCKQPFNSAWFLLQHAQNTHGFRIYLE

Second zinc finger domain (426-453)

Tasmanian devil	KSCEFCGKTFKFQSNLIVHRRSHTGEKP
fat-tailed dunnart	KSCEFCGKTFKFQSNLIVHRRSHTGEKP
opossum	KSCEFCGKTFKFQSNLIVHRRSHTGEKP
rat	KSCEFCGKTFKFQSNLIVHRRSHTGEKP
mouse	KSCEFCGKTFKFQSNLIVHRRSHTGEKP
human	KSCEFCGKTFKFQSNLIVHRRSHTGEKP
dog	KSCEFCGKTFKFQSNLIVHRRSHTGEKP

Third zinc finger domain (454-481)

Tasmanian devil	YKCQLCDHACSQASKLKRHMKTHMHKAG
fat-tailed dunnart	YKCQLCDHACSQASKLKRHMKTHMHKAG
opossum	YKCQLCDHACSQASKLKRHMKTHMHKAG
rat	YKCQLCDHACSQASKLKRHMKTHMHKAG
mouse	YKCQLCDHACSQASKLKRHMKTHMHKAG
human	YKCQLCDHACSQASKLKRHMKTHMHKAG
dog	YKCQLCDHACSQASKLKRHMKTHMHKAG

Fourth zinc finger domain (786-813)

Tasmanian devil	DTCEYCGKVFKNCSNLTVHRRSHTGERP
fat-tailed dunnart	DTCEYCGKVFKNCSNLTVHRRSHTGERP
opossum	DTCEYCGKVFKNCSNLTVHRRSHTGERP
rat	DTCEYCGKVFKNCSNLTVHRRSHTGERP
mouse	DTCEYCGKVFKNCSNLTVHRRSHTGERP
human	DTCEYCGKVFKNCSNLTVHRRSHTGERP
dog	DTCEYCGKVFKNCSNLTVHRRSHTGERP

Fifth zinc finger domain (814-843)

Tasmanian devil	YKCELCNYACAQSSKLTRHMKTHGQIGKEV
fat-tailed dunnart	YKCELCNYACAQSSKLTRHMKTHGQIGKEV
opossum	YKCELCNYACAQSSKLTRHMKTHGQIGKEV
rat	YKCELCNYACAQSSKLTRHMKTHGQIGKEV
mouse	YKCELCNYACAQSSKLTRHMKTHGQIGKEV
human	YKCELCNYACAQSSKLTRHMKTHGQIGKEV
dog	YKCELCNYACAQSSKLTRHMKTHGQIGKEV

Sixth zinc finger domain (844-874)

Tasmanian devil	YRCDICQMPFSVYSTLEKHMKKWHGEHLLTN
fat-tailed dunnart	YRCDICQMPFSVYSTLEKHMKKWHGEHLLTN
opossum	YRCDICQMPFSVYSTLEKHMKKWHGEHLLTN
rat	YRCDICQMPFSVYSTLEKHMKKWHGEHLLTN
mouse	YRCDICQMPFSVYSTLEKHMKKWHGEHLLTN
human	YRCDICQMPFSVYSTLEKHMKKWHGEHLLTN
dog	YRCDICQMPFSVYSTLEKHMKKWHGEHLLTN

Figure 6.1: Analysis of homology of SATB2 and CTIP2 functional domains between marsupials and eutherian mammals.

The DNA-binding domains of SATB2 and CTIP2 proteins were compared in marsupials (Tasmanian devil, fat-tailed dunnart, opossum – green) and eutherian mammals (rat, mouse, human and dog – yellow). This analysis shows that the sequence of amino acids of the SATB2 DNA binding domains are broadly conserved, a part from one amino acid in the second DNA binding domain that is different in marsupials (glutamic acid) compared to eutherian mammals (aspartic acid). For CTIP2, the six zinc finger domains are 100% conserved across therian mammals.

6.2.1.2. *The pattern of expression of SATB2 and CTIP2 is broadly conserved in the neocortex of adult mouse and dunnart*

After having defined the high degree of homology of SATB2 and CTIP2 protein across therian mammals, the next step was to analyse their pattern of expression, to evaluate whether this homology is also reflected in the location in similar neuronal populations, perhaps subserving similar roles, as it has recently been demonstrated that both genes have different functions in pallial development of birds and reptiles (Nomura *et al.* 2018). First, *in situ* hybridisation was performed on adult mouse and dunnart brain sections, using species-specific probes, in order to detect the presence of mRNA encoding for SATB2 and CTIP2 proteins. As described in chapter 2, the dunnart riboprobes were designed based on the fat-tailed dunnart sequence (Kozulin et al., in preparation), while the mouse riboprobes were cloned with primers from the Allen Brain Atlas website. Surprisingly, despite the lack of a corpus callosum in marsupials, *Satb2* and *Ctip2* mRNAs were detected in brain sections of adult fat-tailed dunnarts, with a pattern of expression broadly comparable to the mouse, with *Ctip2* mRNA highly expressed in the deeper layers of the neocortex of both species, especially in L5, while *Satb2* mRNA can be detected in both deeper and upper layers, with a particularly strong labelling in L2/3 (Figure 6.2). Despite these similarities, there are also some differences in *Satb2* mRNA localisation between these two species. Specifically, *in situ* hybridisation for *Satb2* shows a strong band of mRNA in L4, L5b and L6 in mouse, while in dunnart the expression is more homogenous in L4 and L5 and less strong in L6 compared to mouse (Figure 6.2).

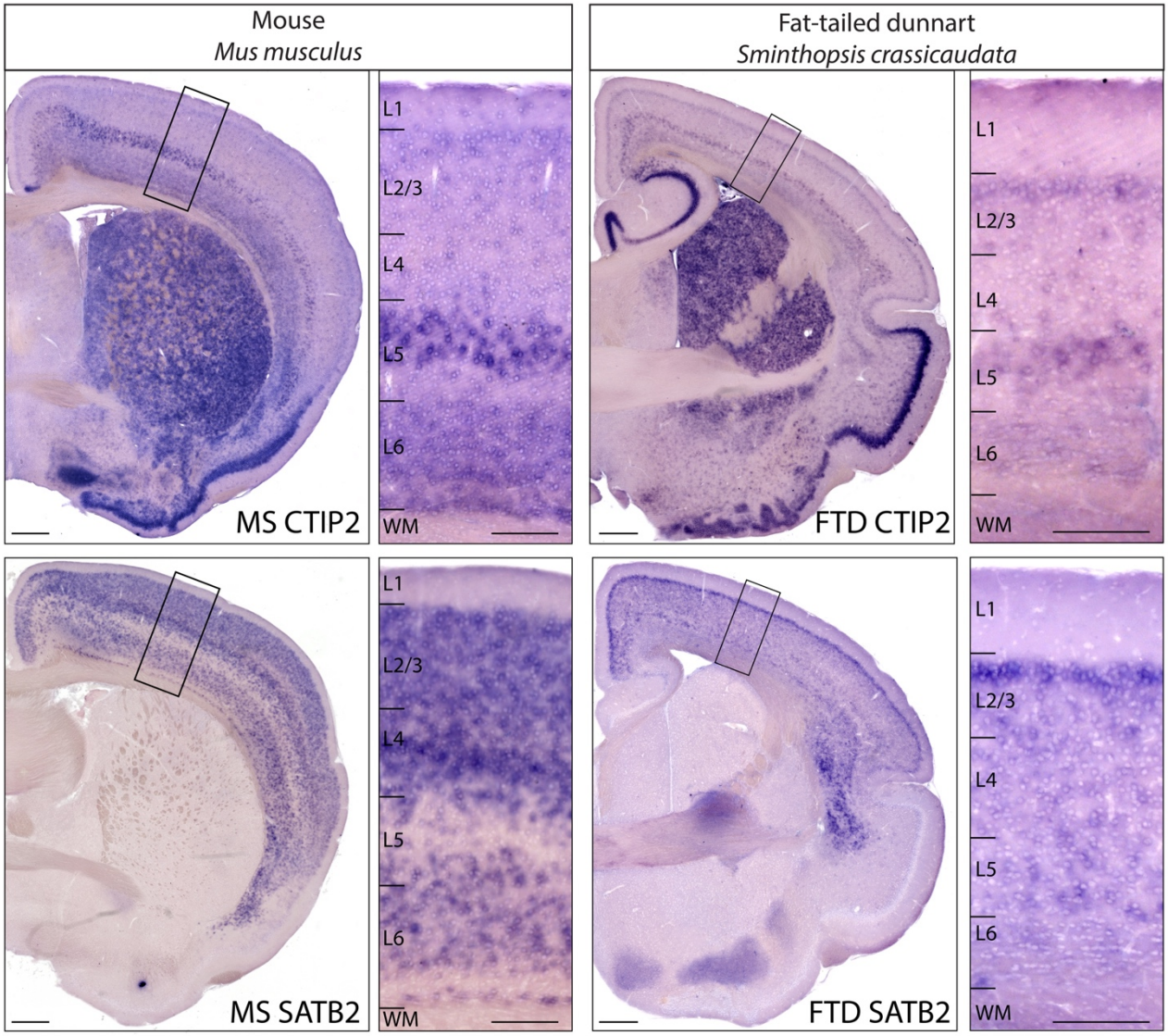

Figure 6.2: *In situ* hybridisation of SATB2 and CTIP2 in adult fat-tailed dunnart and mouse.

Coronal brain sections of adult mouse and fat-tailed dunnart were incubated with species-specific riboprobes, which were cloned with primers from the Allen Brain Atlas for mouse or designed based on the dunnart transcriptome for dunnart (Kozulin et al., in preparation). Note that in both species, CTIP2 is expressed in deeper neocortical layers, striatum and piriform cortex, while SATB2 is mostly expressed in neocortical upper layers as well as in the claustrum/endopiriform nuclei. FTD = fat-tailed dunnart, L = layer, MS = mouse, WM = white matter. Scale bar: 400 µm and 200 µm for wide-field images and insets, respectively.

After having demonstrated adult marsupial expression of mRNA encoding for SATB2 and CTIP2, immunohistochemistry was performed against these two transcription factors in mouse and dunnart adult brain sections, in order to investigate whether and where SATB2 and CTIP2 proteins are expressed. The general pattern of expression of SATB2 and CTIP2 proteins in the neocortex of dunnart was found to be very similar to mouse, with SATB2 being highly expressed in the upper and deeper layers of the neocortex, while CTIP2 is mainly confined to the deeper layers, with scattered cells expressing this protein in the upper layers (Figure 6.3). Despite this similar general pattern of expression of these two transcription factors in mouse and dunnart, the percentage of SATB2 and CTIP2-positive cells per layer, obtained by manually counting cells expressing SATB2 and/or CTIP2 divided by the total number of DAPI-positive cells, revealed some differences in transcription factor expression between these two species. Specifically, the percentage of SATB2-positive cells was surprisingly higher in dunnart in L2/3, and lower in L6, compared to mouse, where it is possible to identify a band of SATB2-positive cells in L6b (Figure 6.3). On the other hand, the percentage of CTIP2-positive cells was significantly higher in mice than in dunnarts in all the layers of the neocortex (Figure 6.3). Finally, the percentage of cells that coexpress SATB2 and CTIP2 was also significantly higher in mice than in dunnarts, particularly in L2/3 and L6, suggesting that the main differences in gene expression between lineages might be in the relative proportions, rather than just the presence or absence of any transcription factor alone in each cortical layer.

The timing of transcription factor expression is also essential for neuronal fate-specification (Lickiss *et al.* 2012, Hatanaka *et al.* 2016). To account for potential differences in gene expression timing between species, immunohistochemistry against SATB2 and CTIP2 was performed on mouse and dunnart brain sections collected at different developmental stages, in order to detect the temporal dynamics (i.e., beginning, peak and decline) of their expression, and the results are presented in the next section. Any difference in the timing of SATB2 and CTIP2 expression in these two mammalian species could be mechanistically related to the different wiring strategies, such as the initial axonal elongation of commissural neurons in mice and dunnarts.

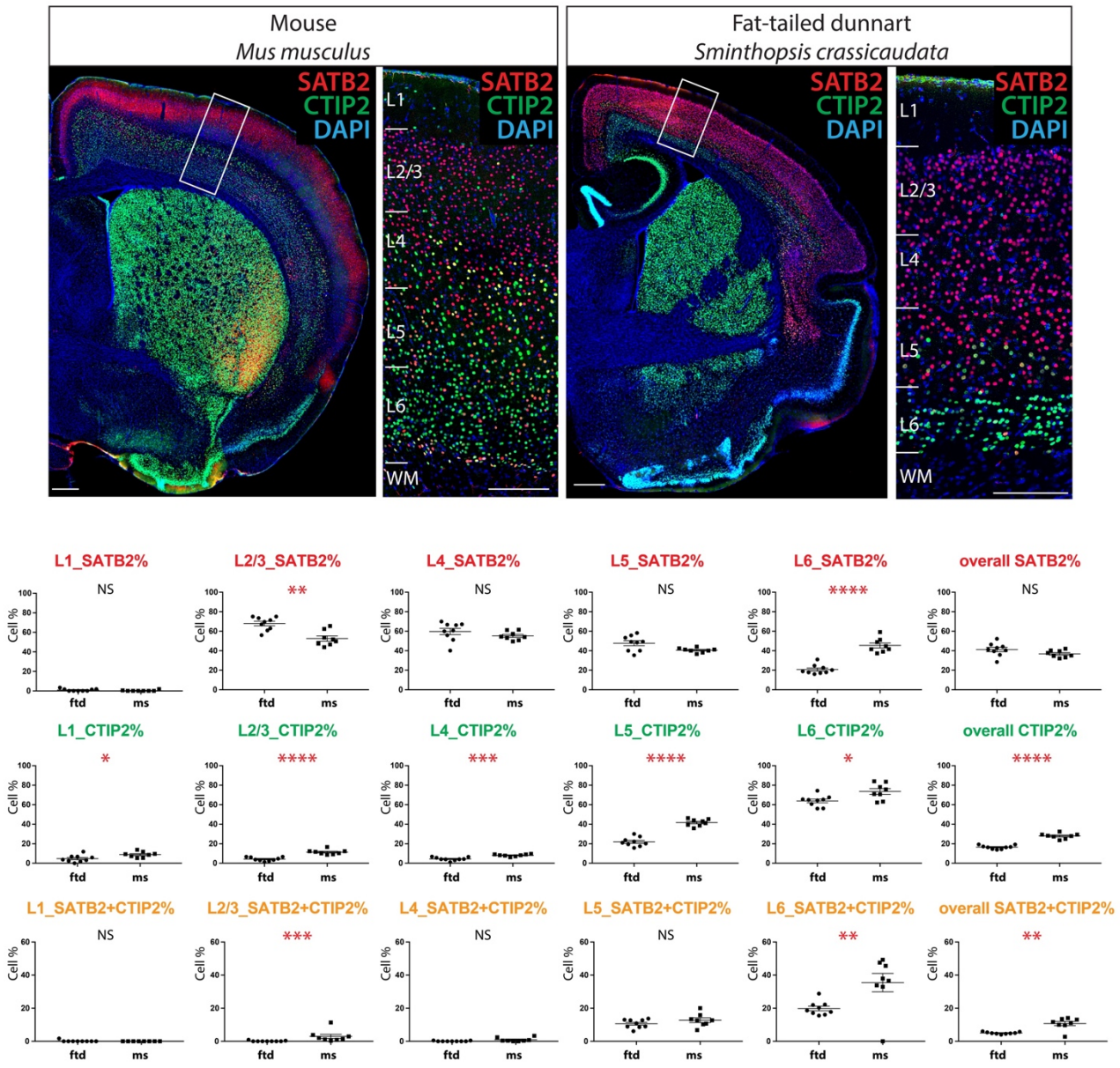

Figure 6.3: SATB2 and CTIP2 expression in adult fat-tailed dunnart and mouse.

DAPI staining (blue), as well as SATB2 (red) and CTIP2 (green) immunofluorescence on coronal sections of adult mouse and fat-tailed dunnart. The percentage of cells expressing SATB2, CTIP2, or both, was obtained by manually counting SATB2, CTIP2, and SATB2/CTIP2-positive cells, and this value was divided for the number of DAPI-positive cells in each layer. A total of 8 adult mice and 9 dunnarts were examined. Data are presented as mean ± SEM. Scale bars: 400 µm and 200 µm for wide-field images and insets, respectively. Ftd = fat-tailed dunnart, L = layer, ms = mouse, NS = non-significant, WM = white matter, * $P < 0.05$, ** $P < 0.01$, *** $P < 0.001$ Mann-Whitney U tests.

6.2.1.3. *The pattern of expression of SATB2 and CTIP2 is broadly conserved in the neocortex of mouse and dunnart throughout development*

Despite some differences in the percentage of SATB2 and CTIP2-positive cells detected in adult mice and dunnarts, the overall pattern of expression of these transcription factors is broadly similar in the adults of these two mammalian lineages (Figure 6.3). In this section of chapter 6, the expression of SATB2 and CTIP2 is examined across neocortical development in order to investigate whether the temporal dynamics of their expression differs between species.

Immunohistochemistry against SATB2 and CTIP2 on mouse and dunnart brains collected at different stages of development (from stage 18 until stage 28) (Thieler 1989, Suárez *et al.* 2017) showed that the pattern of expression in these species is broadly shared throughout development (Figure 6.4). In both mice and dunnarts, L2/3 and L4 are predominantly populated by SATB2-positive cells, L5 is characterised by intermingled cells expressing SATB2 and/or CTIP2, while L6 is predominantly CTIP2-positive, with the exception of a band of SATB2-positive cells localised in the lower part of L6 in mouse, which has been previously described in adult immunohistochemistry (Figure 6.3-6.4). In dunnarts, it is possible to first detect SATB2 protein in the neocortex at stage 20, whereas in similarly-staged mice this transcription factor has not yet started to be expressed in neocortical neurons. Regarding CTIP2 expression, CTIP2-positive cells are already localised in the thin neuroepithelium at stage 18, in both species. A clear distinction of SATB2-positive cells in the upper layers and CTIP2 in the deeper layers becomes visible at stage 23 in both species. Altogether, these results suggest a surprising conservation in the pattern of SATB2 and CTIP2 expression across development. A slightly earlier detection of SATB2 protein in dunnarts compared to mice, as well as differential percentage expression per cortical layer evidenced in the adult neocortex, could be either incidental or may be an important mechanism underlying the different commissural strategies between species. Whether this earlier timing of SATB2 expression is a result of an earlier generation of SATB2-positive cells in marsupials compared to eutherian mammals is investigated and discussed in the following sections.

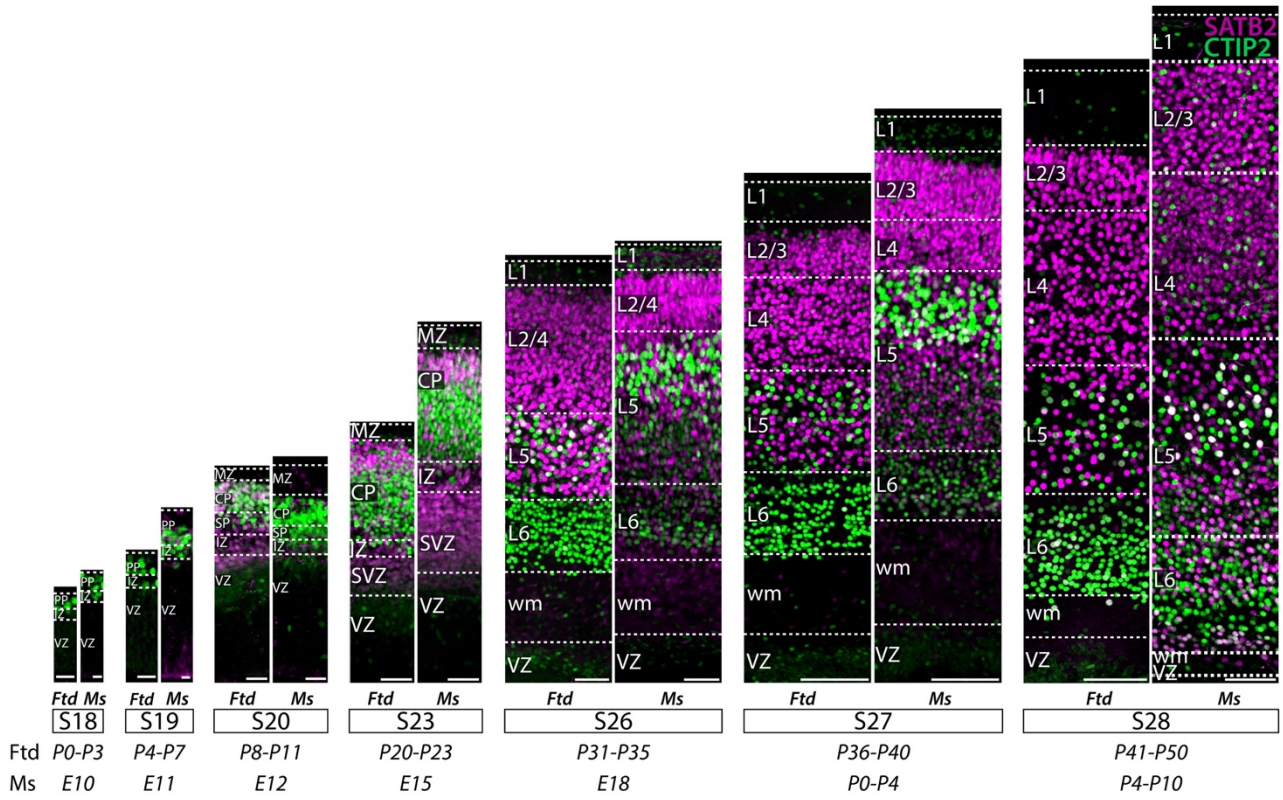

Figure 6.4: SATB2 and CTIP2 expression throughout development in fat-tailed dunnart and mouse.

SATB2 (purple), and CTIP2 (green) immunofluorescence on coronal sections of the brain of fat-tailed dunnarts (Ftd) and mice (Ms) at different stages of development, from stage 18 until stage 28. Scale bars: 25 µm for stages 18, 19 and 20; 50 µm for stages 23 and 26; 100 µm for stages 27 and 28. CP = cortical plate, DL = deeper layers, E = embryonic day, IZ = intermediate zone, L = layer, MZ = marginal zone, P = postnatal day, PP = preplate, S = stage UL = upper layers, VZ = ventricular zone, wm = white matter.

6.2.1.4. *Similarities and differences in the pattern and timing of neurogenesis of neurons expressing SATB2 and/or CTIP2 in mouse and fat-tailed dunnart*

Together with the description of SATB2 and CTIP2 patterns of expression throughout development, defining the developmental stages in which SATB2- and CTIP2-positive cells are born in dunnarts and mice is crucial in order to understand which aspects of cortical development are conserved, and which are not, across mammals. In order to analyse the birthdate of cells expressing SATB2 and CTIP2 during development, immunohistochemistry was performed against these two transcription factors on coronal brain sections of dunnart joeys and mouse pups that also received an injection of EdU at one of the different stages of development, and collected at the end of stage 27 (Figure 6.5A), when it is possible to identify the layers of the neocortex (Thieler 1989, Suárez *et al.* 2017). The analysis of neuronal identity revealed that, in dunnarts, the peak of neurogenesis of cells expressing the deep layer marker CTIP2 is during stages 20-21 (between P8 and P16, Figure 6.5B, D) (Suárez *et al.* 2017) and are located in L5 and L6 (Figure 6.5B, D). The peak of production of neurons expressing the upper layer marker SATB2 is during stages 22-24 (between P17 and P26, Figure 6.5B, D) (Suárez *et al.* 2017). Dunnart SATB2-positive cells are located mainly in L2/3, but also in L5, similar to callosal projection neurons in eutherian mammals, which express SATB2 (Britanova *et al.* 2008) (Figure 6.5B, D). In mice, the peak of CTIP2-positive cell generation occurs during stage 20 (E12, Figure 6.5C, E), while the neurogenesis of cells expressing SATB2 peaks at the end of stage 21 (E13-E14, Figure 6.5C, E), which is interestingly earlier than in dunnarts, in contrast with the earlier detection of SATB2 protein in this marsupial species compared to mice. The SATB2-positive cells generated from stage 19 (Figure 6.5C, E) are likely the ones that will then migrate to L6, forming the SATB2-positive band in the lower part of this layer, which is not detected in dunnarts (Figure 6.3-6.5), and might be the origin of the wider timing overlap (relative to stages) in the generation of cells that express SATB2 and/or CTIP2 in mouse, compared to dunnarts (Figure 6.5C, E).

Despite these differences in the timing and overlap of SATB2 and CTIP2 generation between mouse and fat-tailed dunnart, overall the data collected show that the order, the migration and the layering distribution of cells expressing SATB2 and CTIP2 is broadly conserved in marsupials and eutherians, with the peak of birth of deeper layer-CTIP2-positive cells occurring before SATB2-positive cells, which populate both upper and deeper layers (Arlotta *et al.* 2005, Alcamo *et al.* 2008, Britanova *et al.* 2008, Chen *et al.* 2008, Srinivasan *et al.* 2012, Srivatsa *et al.* 2014) (Figure 6.4-6.5). Whether these two transcription factors label neuronal populations with similar projection patterns in both species is still unclear and this will be addressed in the next section using circuit-mapping experiments.

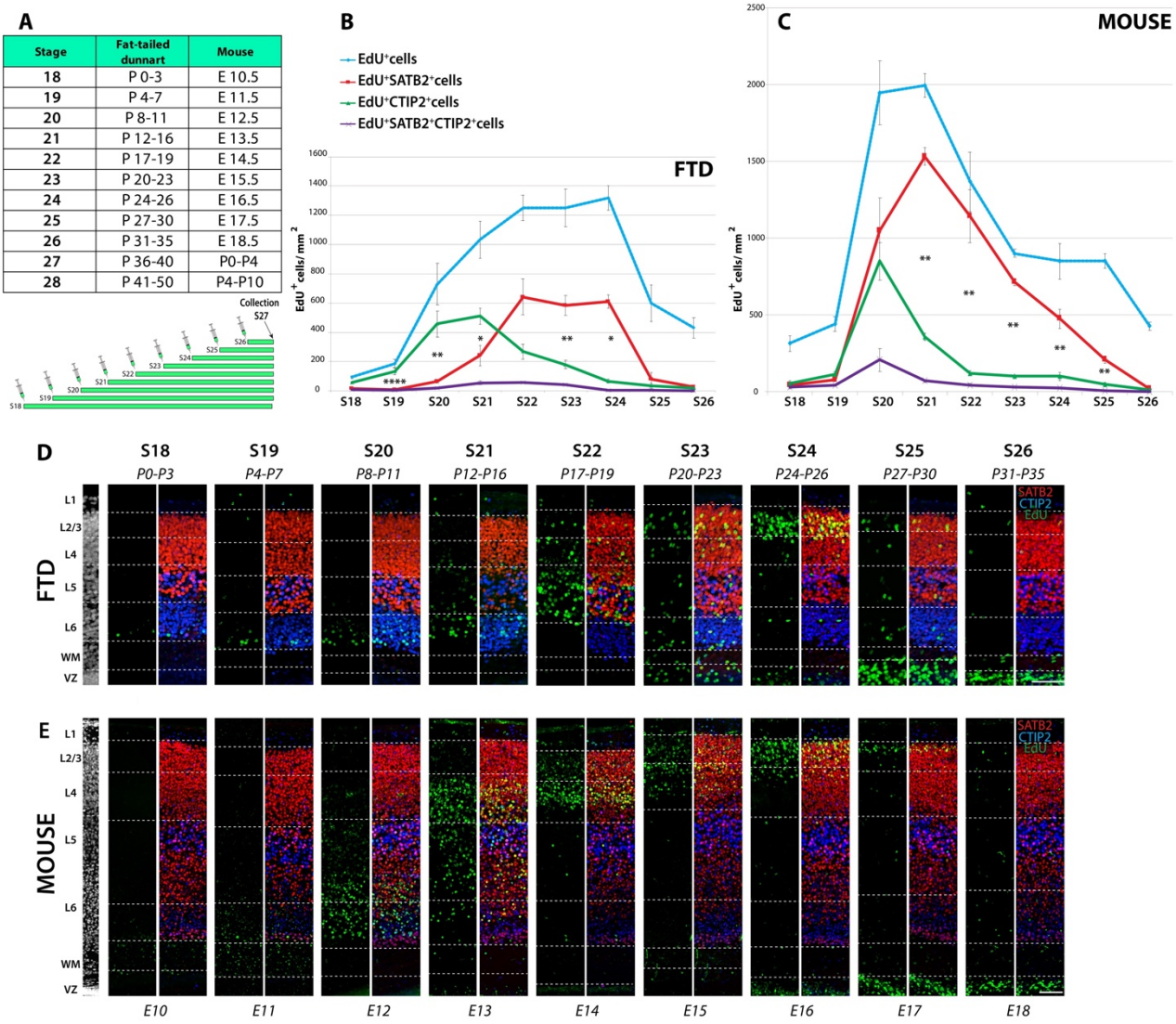

Figure 6.5: Reconstruction of neuronal birthdate and cell identity in the dunnart and mouse neocortex.

A: Paradigm of EdU injection experiment. **B-C**: Graphic presentation of neurogenesis in the neocortex of the fat-tailed dunnart (B) and mouse (C), where the change in density of cortical EdU-positive cells during postnatal development and colocalisation of specific layer markers (SATB2 and CTIP2) is shown. On the X axis: developmental stages of EdU injection, on the Y axis: cell density expressed as cell/mm^2. **D-E**: DAPI staining (grey) and EdU (green), SATB2 (red), CTIP2 (blue) immunofluorescence on S27 coronal neocortical sections of dunnart joeys and mouse pups injected with a single pulse of EdU at different ages. E = embryonic day, FTD = fat-tailed dunnart, L = layer, P = postnatal day, S = stage, VZ = ventricular zone, WM = white matter. Scale bar: 100 µm. Data are presented as mean ± SEM. Comparison between EdU+ cells expressing SATB2 or CTIP2: * $P < 0.05$, ** $P < 0.01$, *** $P < 0.001$, Mann-Whitney U tests.

6.2.2. SATB2 and CTIP2 define commissural and subcerebral populations respectively in dunnarts

So far, the analyses performed in this chapter have revealed a broadly conserved pattern of expression, distribution and order of generation in neurons expressing SATB2 and CTIP2 in marsupial and eutherian mammals. The next step was to determine whether these two transcription factors also have a broadly conserved function across mammals, thereby specifying a commissural and subcerebral projection fate, respectively (Alcamo *et al.* 2008, Britanova *et al.* 2008, Leone *et al.* 2008, Srivatsa *et al.* 2014). In order to address this, the retrograde neuronal tracer cholera toxin B-subunit, conjugated with Alexa Fluor 488 (CTB488, Invitrogen), was injected into either the S1 (Figure 6.6) or the superior colliculus (Figure 6.7) of adult fat-tailed dunnarts *in vivo,* and immunohistochemistry against SATB2 and CTIP2 was performed on coronal brain sections collected after seven days, to allow for dye transport. Injections in the contralateral S1 were performed to analyse the expression pattern of commissural neurons, while the ipsilateral superior colliculus was injected to retrogradely label corticotectal neurons, as a sub-population of subcerebral projection neurons.

When CTB was injected in the dunnart S1 (Figure 6.6A), retrogradely labelled cells in the contralateral S1 were located in L2/3, and also in L5 (Figure 6.6B-D, n = 3), as in eutherian mammals (Ramos *et al.* 2008). Surprisingly, the results show that all retrogradely labelled neurons projecting contralaterally express SATB2, but not CTIP2 (Figure 6.6C-D and pie chart, n = 3), as is also the case for the majority of callosal neurons in mice (Alcamo *et al.* 2008, Srivatsa *et al.* 2014, Harb *et al.* 2016).

Next, corticotectal projection neurons were labelled with CTB injections in the superior colliculus (Figure 6.7A). Retrogradely labelled corticotectal neurons were mainly located in L5 (Figure 6.7B), as in rodents (Hallman *et al.* 1988), and all labelled neurons expressed CTIP2, with a majority coexpressing SATB2 as well (Figure 6.7B, C n = 3). In particular, 95% of the analysed corticotectal neurons retrogradely labelled with CTB488 express both SATB2 and CTIP2, while only 5% express CTIP2 without SATB2 (Figure 6.7, pie chart). This result suggests that CTIP2 has a broadly conserved role across mammals in specifying a subcerebral projection fate (Arlotta *et al.* 2008, Chen *et al.* 2008), while SATB2 might regulate the development of commissural projections, rather than only callosal, as well as subcerebral tract formation, likely in a context dependent manner, just as previously shown in mouse (Leone *et al.* 2014, McKenna *et al.* 2015).

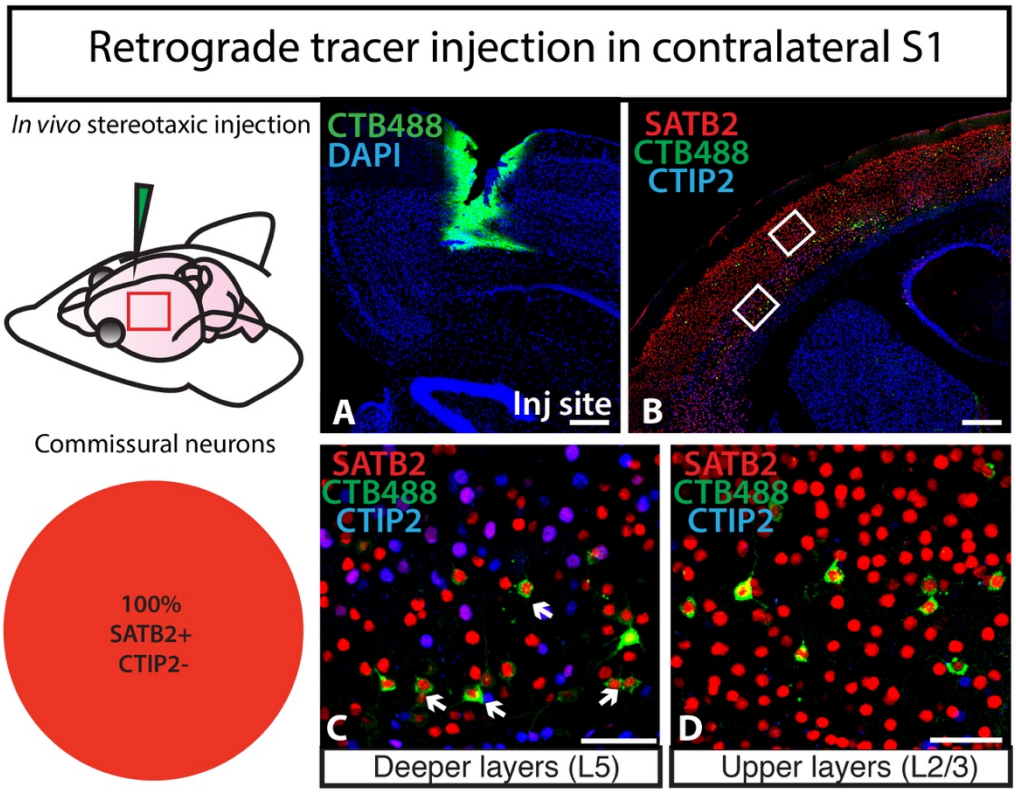

Figure 6.6: Contralaterally projecting neurons in the dunnart neocortex express SATB2, but not CTIP2.

A: CTB Alexa Fluor 488 was injected in S1. **B**: Retrogradely labelled cells (green) in the contralateral hemisphere are located both in deeper (L5) and upper layers (L2/3). **C, D**: Retrogradely labelled cells (green) express SATB2 (red), but not CTIP2 (blue), both in the deeper (L5) and upper layers (L2/3). Inj = injection, L = layer, S1 = primary somatosensory cortex. Scale bars: 250 µm and 50 µm for wide-field images and insets, respectively (n = 3).

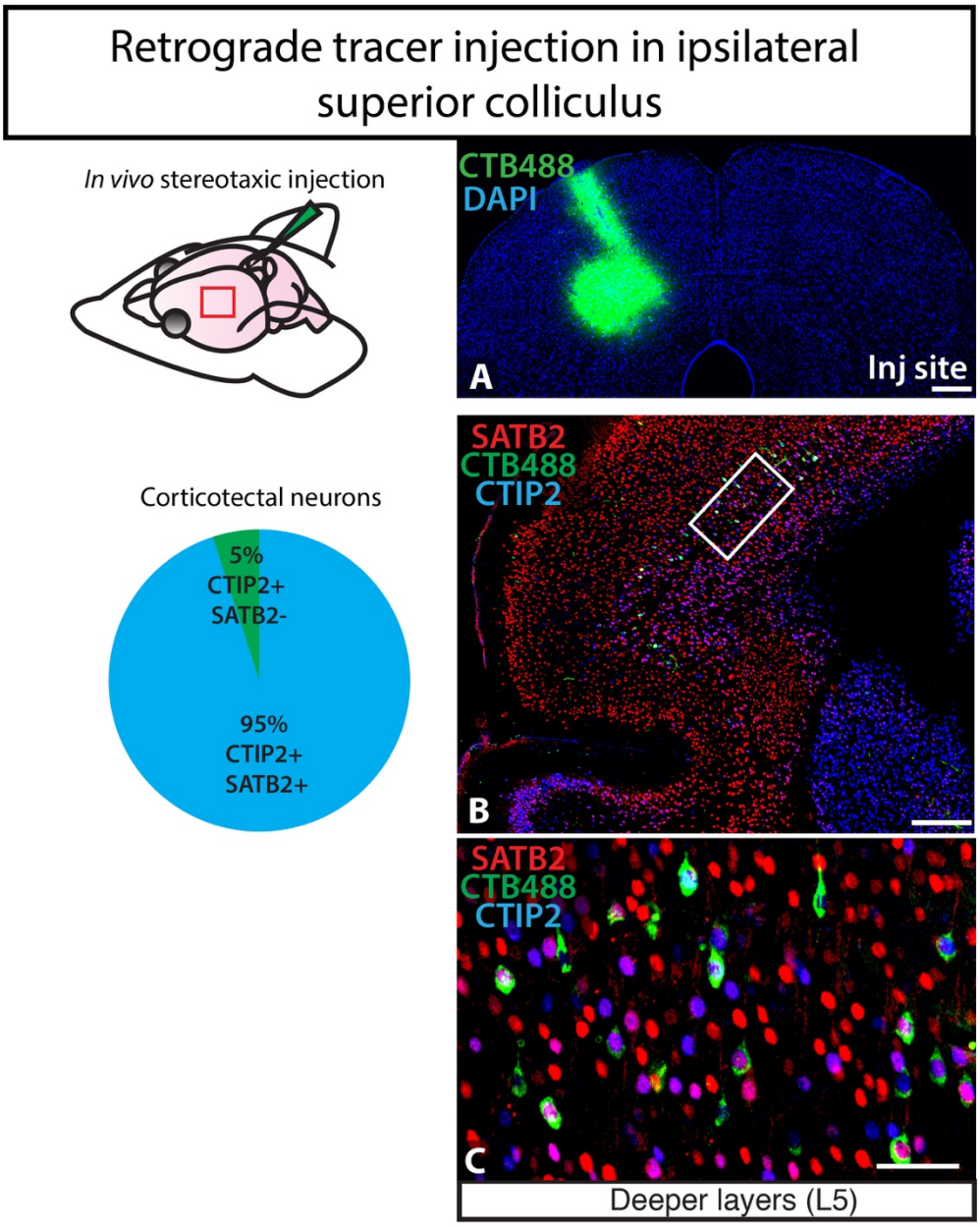

Figure 6.7: Corticotectal projection neurons in the dunnart neocortex express CTIP2, as well as SATB2.

A: CTB Alexa Fluor 488 was injected in the superior colliculus. **B**: Retrogradely labelled cells in the lateral neocortex (green) are located in deeper layers (L5). **C**: 95% of the retrogradely labelled cells (green) examined in the lateral neocortex express both SATB2 (red) and CTIP2 (blue), while only 5% express only CTIP2. Inj = injection, L = layer, Scale bar: 250 μm and 50 μm for wide-field images and insets, respectively (n = 3).

In summary, retrograde tracing experiments combined with immunohistochemistry against SATB2 and CTIP2 suggest that these transcription factors might have a broadly conserved role in the regulation of neuronal projection fate across mammals. To further explore which developmental programs are a consequence of their expression, the next section describes manipulatory experiments that were performed to ectopically overexpress these transcription factors and analyse the pattern of projection of manipulated neurons in both mice and dunnarts.

6.2.3. *In vivo* assays of commissural versus subcerebral fate determination

The data presented in sections 6.2.1 and 6.2.2 suggest that, in fat-tailed dunnarts, the transcription factors SATB2 and CTIP2 might be involved in specifying a corticocortical and subcerebral projection fate, respectively, similar to eutherians, despite the alternative commissural route present in this species. The aim of this section is to experimentally probe the role of SATB2 and CTIP2 in determining different neuronal fates in early-and later-born neurons, as well as to unveil the molecular mechanisms behind developmental programs regulated by specific genes in different cortical evolutionary contexts. This was achieved by experimentally altering the expression of SATB2 and CTIP2 by overexpressing these two transcription factors in ectopic cortical layers using *in utero* and in pouch electroporation in mice and dunnarts, respectively (see sample size used for quantification in Table 6.1). Despite the almost complete homology of the DNA-binding functional domains of SATB2 and CTIP2 across therian mammals, some differences outside the functional domains were identified in both proteins, which could account for additional functions, such as folding or binding of co-factors. For this reason, both the mouse- and the dunnart-specific cDNA sequences were employed for the overexpression experiments in both species (results summarised in Figure 6.17), in order to define whether any difference in the results might be due to the species-specific proteins or to the cortical context in which these proteins were overexpressed. Specifically, dunnart-specific cDNA overexpression constructs for CTIP2 and SATB2 were designed based on the dunnart cortical transcriptome (section 2.4, chapter 2, Kozulin et al., in preparation), while the mouse-specific constructs were a gift from the lab of Prof Victor Tarabykin (SATB2), Prof Nenad Sestan (CTIP2) and Dr Suzana Atanasoski (SKI, SATB2 cofactor). In all the experiments presented in this chapter, the overexpression constructs were co-electroporated with the fluorophore tdTomato and the analysis of the axonal projections was performed by quantifying the intensity of fluorescence of tdTomato-positive axons in different cortical region, depending on the experimental paradigm. As described in Chapter 2, the overexpression constructs were cloned into pCAG-IRES-GFP, but GFP was not highly expressed in the axons of manipulated neurons, hence TdTomato was co-electroporated to improve the visualisation and analysis of axonal projections, as well as to serve as a single fluorophore used in both experimental and control animals that would be highly comparable between the two conditions in analyses of fluorescence intensity.

CTIP2 overexpression						
	Mouse control	Mouse EP with ms-CTIP2	Mouse EP with ftd-CTIP2	Dunnart control	Dunnart EP with ms-CTIP2	Dunnart EP with ftd-CTIP2
Cell count: SATB2 and CTIP2 IHC	13	11	13	10	4	8
Cell count: TBR1 IHC	14	11	9	12	4	10
FI: ipsi and contra thalamus	11	11	10	9	4	9
FI: ipsi and contra corticoth projection	11	11	10	10	4	8
FI: ipsi and contra cp	10	11	14	10	4	7
FI: cc	11	11	10	n/a	n/a	n/a
FI: ipsi and contra ec/ic	n/a	n/a	n/a	12	4	9
SATB2 overexpression						
	Mouse control	Mouse EP with ms-SATB2-SKI	Mouse EP with ftd-SATB2-SKI	Dunnart control	Dunnart EP with ms-SATB2-SKI	Dunnart EP with ftd-SATB2-SKI
Cell count: SATB2 and CTIP2 IHC	9	10	8	7	4	7
Cell count: EP cells in VZ	9	10	8	7	4	7
FI: ipsi cp	10	3	7	8	4	7
FI: ipsi and contra med/lat striatum	10	3	7	8	4	7
FI: ac/(ac+cc)	10	3	7	n/a	n/a	n/a
FI: ipsi cingulate	10	3	7	8	4	7
FI: ec/ic	n/a	n/a	n/a	8	4	7

Table 6.1: Sample size for quantification of *in vivo* assays.

Cc = corpus callosum, contra = contralateral, cp = cerebral peduncle, ec = external capsule, EP = electroporation, FI = fluorescence intensity, ftd = fat-tailed dunnart, ic = internal capsule, IHC = immunohistochemistry, ipsi = ipsilateral, lat = lateral, med = medial, ms = mouse, n/a = not applicable, VZ = ventricular zone.

6.2.3.1. *CTIP2 overexpression in the upper layer neurons of the mouse neocortex elicits a subcortical projection fate*

In mouse, upper layer neurons are generated during stage 23 (E15) and predominantly express the transcription factor SATB2, with the peak of CTIP2-positive cell generation occurring earlier, during stage 20 (E12, Figures 3.2 and 6.5). The ectopic expression of CTIP2 mouse- and dunnart-specific construct, together with the fluorophore tdTomato, was thus achieved by *in utero* electroporation of the upper layers of the neocortex during stage 23 (E15). TdTomato alone was electroporated in the same area (S1) and at the same stage in control animals. Mouse pups were then collected at the end of stage 28 (P10), when it is possible to analyse the projections of electroporated neurons. Immunohistochemistry against SATB2 and CTIP2 was performed on coronal brain sections to confirm the overexpression of CTIP2 and to evaluate its effect on SATB2 expression (Figure 6.8).

The results show that, in control animals, neurons electroporated with tdTomato were located in the upper layers of the neocortex and the majority of them expressed SATB2 (93.53% of the electroporated cells, Figure 6.8A, D, G). Of these electroporated cells, only a few expressed the transcription factor CTIP2 in control animals (2.33%, Figure 6.8A, D, H). On the other hand, in experimental joeys that were transfected with both tdTomato and the construct overexpressing mouse-specific CTIP2, 93% of the electroporated cells express SATB2 and 90% expressed CTIP2, with 87% coexpressing both these transcription factors (Figure 6.8B, E, G, H). Cell count analysis demonstrated a statistically significant difference in the percentage of electroporated cells that express CTIP2 in the control versus experimental animals, with a higher number of tdTomato-CTIP2-positive cells in the latter group (Figure 6.8D, E, H), confirming the efficacy of the transfection of the mouse-specific CTIP2 overexpression construct in mice. On the other hand, the difference in the expression of SATB2 in control versus experimental animals was not significant (Figure 6.8 D, E, G), supporting existing evidence that, in mouse, SATB2 can regulate the expression of CTIP2, but not *vice versa* (Alcamo *et al.* 2008, Britanova *et al.* 2008). Similar results were obtained when the dunnart-specific CTIP2 overexpression construct was electroporated in mice (Figure 6.8C, F). Specifically, 93% of the electroporated cells express SATB2 and 86% expressed CTIP2 (Figure 6.8C, F, G, H), with 85% coexpressing both these transcription factors. The comparison of the percentages of CTIP2 expressing cells in the animals that were electroporated with the mouse- or the dunnart-specific construct did not show statistically significant differences between the two groups, suggesting that the mouse- and the dunnart-specific CTIP2 overexpression constructs are equally efficient in terms of protein production (Figure 6.8D, E, H).

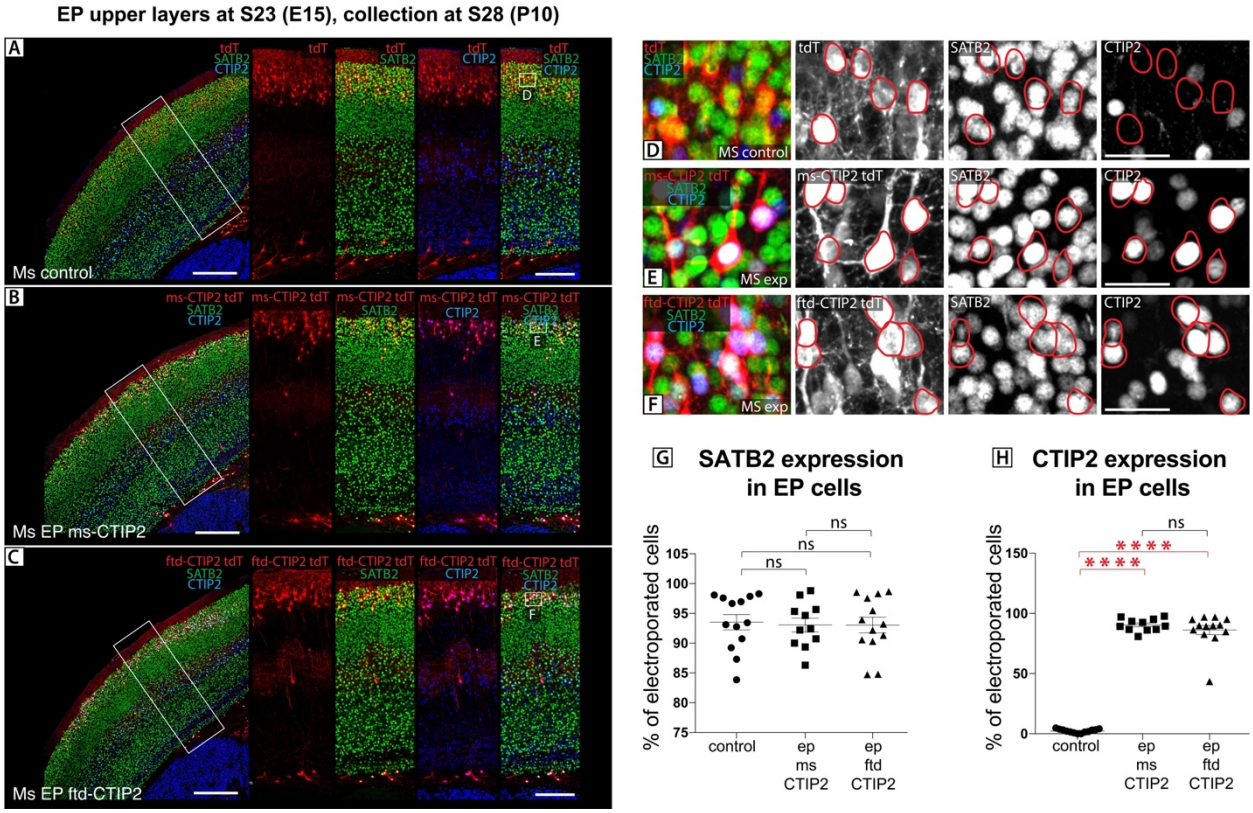

Figure 6.8: Ectopic overexpression of either mouse- or dunnart-specific CTIP2 in the upper layers of the mouse neocortex.

Mouse embryos were electroporated during stage 23 (E15) to overexpress tdTomato alone in control (**A** and inset **D**, in red), with mouse-specific CTIP2 (**B** and inset **E**, in red) or with dunnart-specific CTIP2 (**C** and inset **F**, in red) in the upper layers of the neocortex. Pups were collected at stage 28 (P10). Coronal brain sections were stained for SATB2 (green) and CTIP2 (blue) to evaluate the effects of the genetic manipulation. **G-H**: Cell count analysis in the neocortex of tdTomato-positive cells expressing SATB2 or CTIP2 shows an increase in CTIP2 expression in experimental animals, compared to controls, confirming the efficacy of the manipulation for both the overexpressing constructs (n > 10 animals per treatment, see also Table 6.1). No difference was detected in the percentage of electroporated cells expressing SATB2 in both the experimental groups versus control animals. E = embryonic age, EP = electroporated, exp = experimental, ftd = fat-tailed dunnart, Ms = mouse, ns = non-significant, P = postnatal day, S = stage, tdT = tdTomato. Scale bars: 500 µm in A, B and C; 250 µm in right panels; 50 µm in D, E and F. Data are presented as mean ± SEM. * $P < 0.05$, ** $P < 0.01$, *** $P < 0.001$, **** $P < 0.0001$, Mann-Whitney U tests.

In order to evaluate whether the mouse and dunnart proteins were able to elicit a similar phenotype in manipulated neurons, the projections of neurons electroporated with the mouse- or dunnart-specific constructs were analysed. In line with previous studies using the mouse-specific construct (Chen *et al.* 2008), our results showed that ectopically overexpressing both species-specific CTIP2 constructs in the upper layers of the mouse neocortex was sufficient to alter the pattern of axonal projections, such that some of the axons extending from the upper layer neurons project to the contralateral hemisphere through the corpus callosum, but also to subcerebral targets (Figure 6.9). Specifically, the analysis of the intensity of fluorescence performed on control (Figure 6.9A) and experimental animals (Figure 6.9B, C), normalised for the intensity of the background, showed that cells that were electroporated with the CTIP2 mouse- or dunnart-specific overexpression constructs extend their axons through the cerebral peduncle (Figure 6.9A-D). Interestingly, data from fluorescence analysis revealed an increase in projections through the contralateral cerebral peduncle of both experimental groups, as well as the ipsilateral cerebral peduncle, possibly suggesting that some axons cross the midline through the corpus callosum, and then project to subcerebral targets in the contralateral hemisphere (Figure 6.9A-D). In addition to the axons extending towards subcerebral targets, ectopic projections reaching the ipsilateral thalamus via the corticothalamic projection were also identified in both group of experimental animals receiving either the mouse- or the dunnart-specific construct (Figure 6.9A-C, E). Interestingly, the data collected suggest that, despite eliciting a similar outcome in manipulated neurons, the mouse-specific construct seems to have a more striking effect on the alteration of the projection fate, compared to the dunnart- specific construct, as there is a statistically significant difference in the intensity of fluorescence measure in the ipsilateral thalamus and the ipsilateral corticothalamic projection (Figure 6. 9A-C, E), between the two experimental manipulations. Moreover, axons in the contralateral thalamus were detected in most of the experimental animals electroporated with both constructs (Figure 6. 9A-C, E), further suggesting that some axons extending from manipulated upper layer neurons might project to ectopic subcerebral targets after having crossed the midline via the corpus callosum.

Analysis of fluorescence intensity was also performed in the corpus callosum of both experimental and control animals to detect any difference in the amount of axons projecting to the contralateral hemisphere. When the mouse construct was electroporated in the upper layers of the mouse neocortex, no statistically significant difference was found in the analysis of intensity of fluorescence in the corpus callosum of control versus experimental animals, even if the data show a trend towards a reduction of axons crossing the midline via the corpus callosum, possibly in favour of a subcortical projection fate, in the experimental group. In mice that were electroporated with the

dunnart-specific CTIP2, a statistically significant difference was found in the experimental versus the control animals (Figure 9A-C, F).

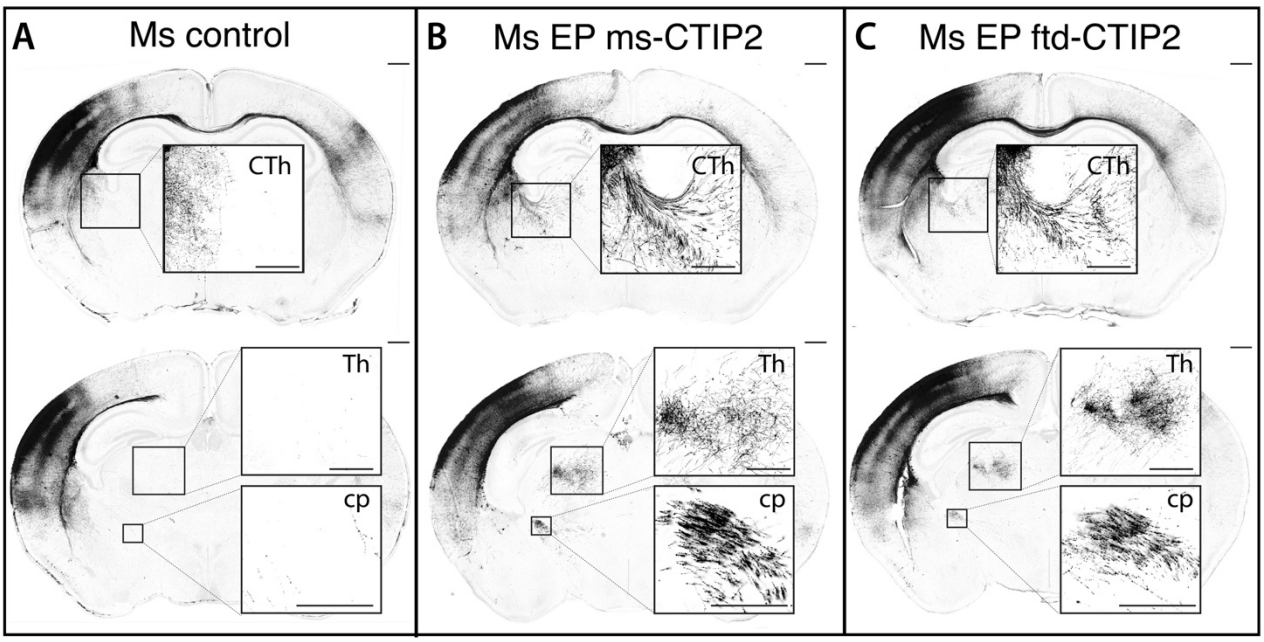
A
Ms control
CTh
Th
cp
B
Ms EP ms-CTIP2
CTh
Th
cp
C
Ms EP ftd-CTIP2
CTh
Th
cp

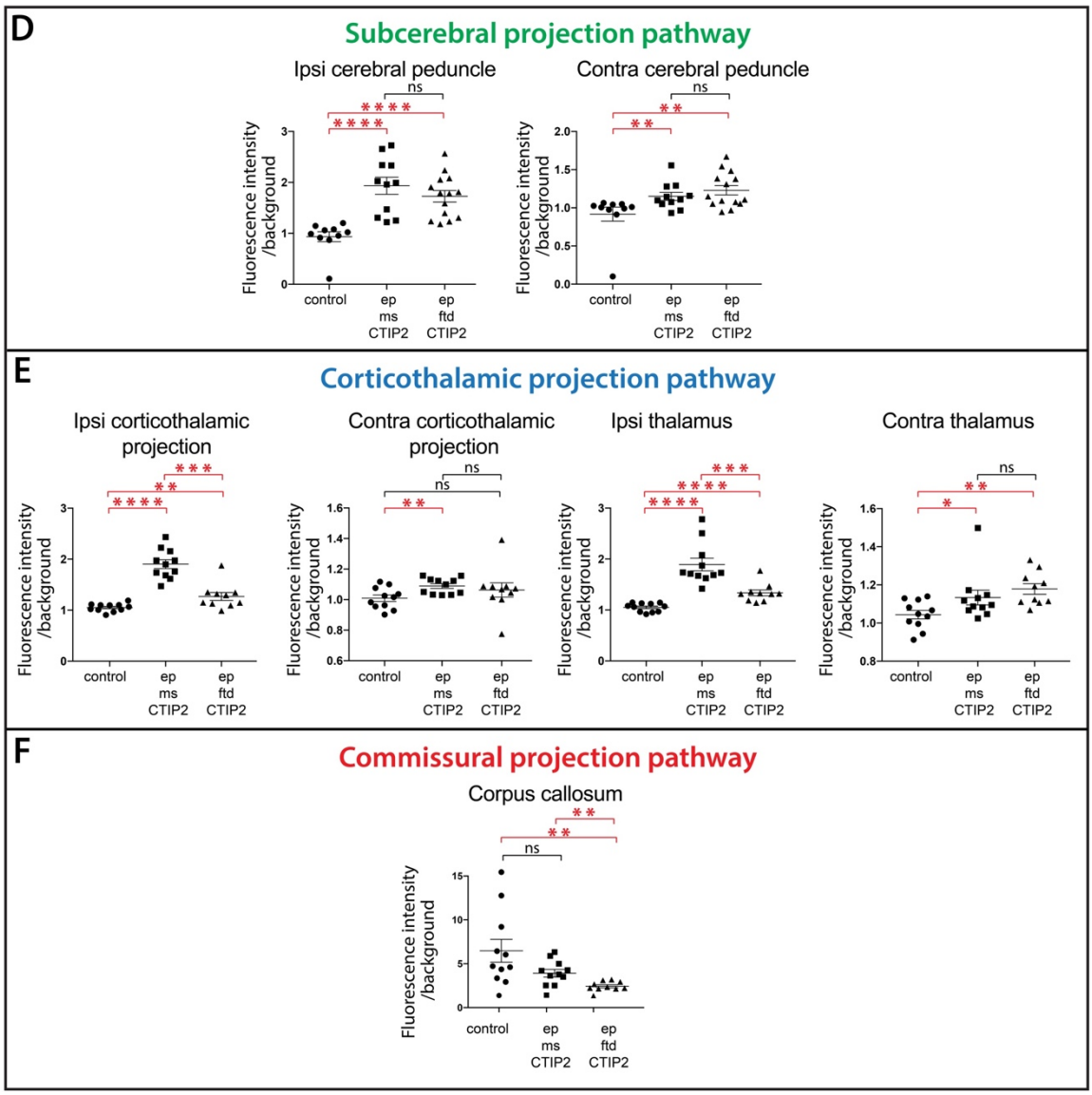
D
Subcerebral projection pathway
Ipsi cerebral peduncle
Contra cerebral peduncle
Fluorescence intensity /background
control
ep ms CTIP2
ep ftd CTIP2
E
Corticothalamic projection pathway
Ipsi corticothalamic projection
Contra corticothalamic projection
Ipsi thalamus
Contra thalamus
F
Commissural projection pathway
Corpus callosum

Figure 6.9: Ectopic overexpression of either mouse- or dunnart-specific CTIP2 in the upper layers of the mouse neocortex can alter the pattern of axonal projection.

Coronal brain sections of mouse pups electroporated with tdTomato alone (**A**) or with CTIP2 mouse-specific (**B**) or dunnart-specific (**C**) overexpression construct. **D**: Analysis of the intensity of fluorescence, normalised for the intensity of the background, showed that cells that were electroporated with the CTIP2 mouse- or dunnart-specific overexpression constructs extend their axons to subcerebral targets through the ipsilateral and contralateral cerebral peduncles. **E**: Ectopic projections also reached the ipsilateral thalamus via the corticothalamic projection in both experimental groups. In experimental animals, axons were also detected in the contralateral thalamus. **F**: Analysis of intensity of fluorescence in the corpus callosum of control versus experimental animals revealed a trend towards a reduction of axons crossing the midline via this commissural tract in experimental animals. Contra = contralateral, cp = cerebral peduncle, CTh = corticothalamic projection, EP = electroporated, FTD = fat-tailed dunnart, ipsi = ipsilateral, Ms = mouse, ns = non-significant, Th = thalamus. Scale bars: 500 μm in panels with whole brain sections, as well as insets of Th and CTh; 50 μm for insets of cp ($n > 10$ animals per treatment, see also Table 6.1). Data are presented as mean ± SEM, *$P < 0.05$, ** $P < 0.01$, *** $P < 0.001$, **** $P < 0.0001$, Mann-Whitney U tests.

6.2.3.2. *CTIP2 overexpression in the upper layer neurons of the dunnart neocortex elicits a subcortical projection fate*

In dunnart, comparably to mouse, neocortical neurons generated during stage 23 migrate through the cortical plate towards the upper layers of the neocortex and mainly express the transcription factor SATB2. In this species, the peak of generation CTIP2-positive cells occurs at stage 20-21 (Figures 3.2 and 6.5). To investigate the effect of overexpressing mouse- or dunnart-specific CTIP2 constructs, together with the fluorophore tdTomato, in pouch electroporation was performed in S1 during stage 23, which in dunnarts corresponds to P20. TdTomato alone was electroporated in the same area (S1) and the same stage in control animals. Dunnart joeys were then collected at the end of stage 28 (P50), when it is possible to analyse the projections of the electroporated neurons. Immunohistochemistry against SATB2 and CTIP2 was performed on coronal brain sections to confirm the overexpression of CTIP2 and determine whether it has any effect on the expression of SATB2 (Figure 6.10).

The data collected show that, in control animals, tdTomato-positive neurons were located in the upper layers of the neocortex and most of them expressed SATB2 (97% of electroporated cells, Figure 6.10A, D, G). Of these electroporated cells, only a few expressed the transcription factor CTIP2 (4.21% of electroporated cells, Figure 6.10A, D, H). On the other hand, electroporated cells in experimental joeys that were transfected with tdTomato and mouse-specific CTIP2 construct, 95% expressed SATB2, 82.75% expressed CTIP2 and 77.75% coexpressed both transcription factors (Figure 6.10B, E, G, H). Cell count analysis confirmed a statistically significant difference in the percentage of electroporated cells that express CTIP2 in the experimental animals versus the controls, with a higher number of tdTomato-CTIP2-positive cells in the former group (Figure 6.10D, E, H), which confirms the efficacy of the transfection of the mouse-specific CTIP2 overexpression construct in dunnart joeys. The difference in the number of electroporated cells that expressed SATB2 in the control versus experimental animals transfected with the mouse-specific CTIP2 was not significant (Figure 6.10D, F, G). When the dunnart-specific overexpression construct was electroporated in dunnart joeys, 88.81% of electroporated cells expressed SATB2, 94.07% expressed CTIP2, 86,1% expressed both transcription factors (Figure 6.10C, F, G, H). Cell count analysis confirmed that there is a statistically significant difference in the amount of electroporated cells that express CTIP2 in the control group versus the group that was transfected with the dunnart-specific CTIP2 overexpression construct (Figure 6.10D, F, H). Interestingly, a statistically significant difference was also detected in the percentage of electroporated cells that express SATB2 in controls versus experimental animals, with a slight decrease of SATB2 expression in manipulated neurons (Figure 6.10D, F, G). This is particularly interesting as SATB2

has already been suggested to directly regulate the expression of CTIP2 (Alcamo *et al.* 2008, Britanova *et al.* 2008), while the opposite has never been shown in mice or even in dunnart when the mouse-specific CTIP2 protein was overexpressed. The comparison of the percentage of CTIP2 expressing cells in the animals that were electroporated with the mouse- or the dunnart-specific construct show statistically non-significant difference between the two experimental groups, suggesting that the mouse- and the dunnart-specific CTIP2 overexpression constructs are equally efficient when they are electroporated in dunnarts (Figure 6.10D, E, F, H).

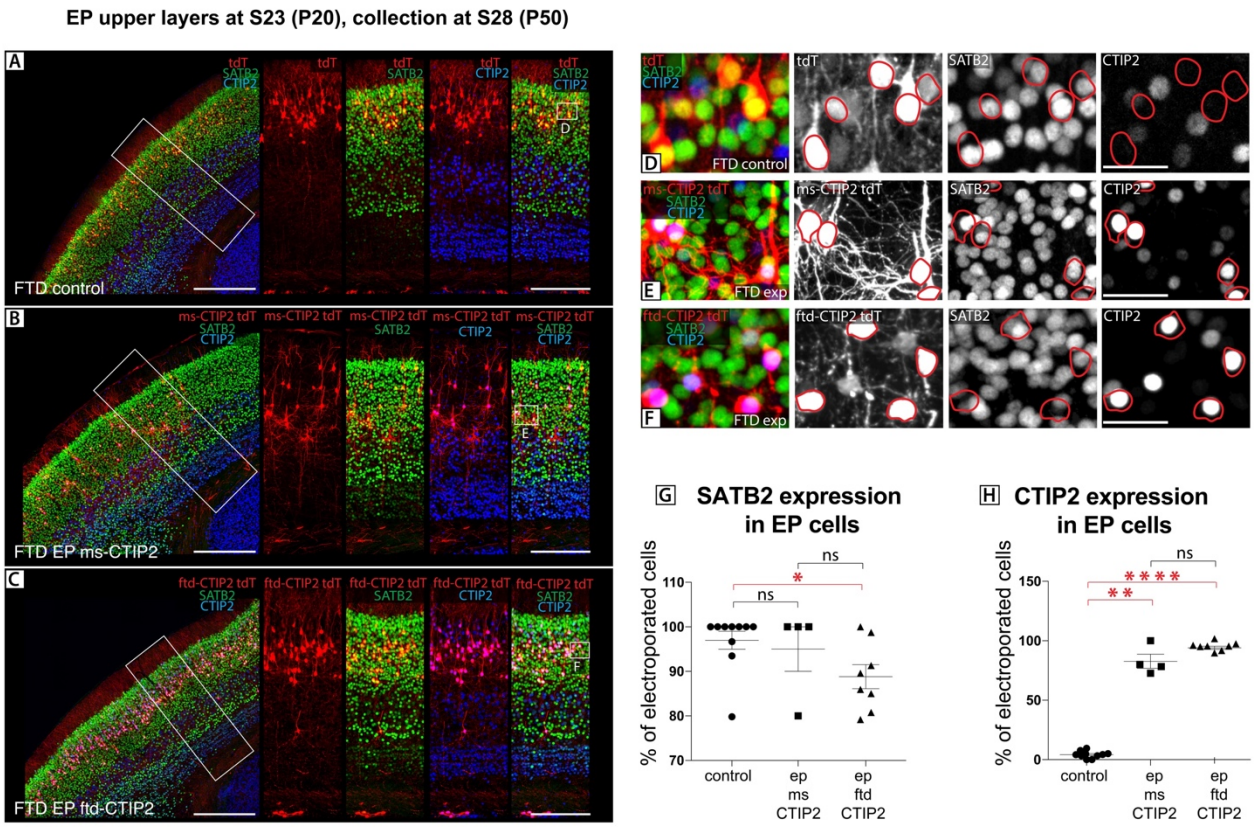

Figure 6.10: Ectopic overexpression of either mouse- or dunnart-specific CTIP2 in the upper layers of the dunnart neocortex.

Dunnart joeys were electroporated during stage 23 (P20) to overexpress tdTomato alone in control (**A** and inset **D** in red), with mouse-specific CTIP2 (**B** and inset **E**, in red) or dunnart-specific CTIP2 (**C** and inset **F**, in red) in the upper layers of the neocortex. Joeys were collected at stage 28 (P50). Coronal brain sections were stained for SATB2 (green) and CTIP2 (blue) to evaluate the effects of the genetic manipulation. **G, H**: Cell count analysis in the cortical plate of tdTomato-positive cells expressing SATB2 or CTIP2 clearly shows an increase in CTIP2 expression in experimental animals confirming the efficacy of the manipulation for both the overexpressing constructs ($n \geq 4$ animals per treatment, see also Table 6.1). A slight decrease of SATB2 expression was detected when the dunnart-specific CTIP2 overexpression construct was electroporated. EP = electroporated, exp = experimental, FTD = fat-tailed dunnart, Ms = mouse, ns = non-significant, P = postnatal day, S = stage, tdT = tdTomato. Scale bars: 250 µm in A, B and C, 50 µm in D, E, F. Data are presented as mean ± SEM. * $P < 0.05$, ** $P < 0.01$, *** $P < 0.001$, **** $P < 0.0001$, Mann-Whitney U tests.

The axons of manipulated neurons were analysed to evaluate whether the ectopic expression of the mouse- or the dunnart-specific CTIP2 could alter their projection fate. Similar to the results obtained in mice, the data collected in dunnarts show that overexpressing CTIP2 in upper layer neurons of the dunnart neocortex was sufficient to dramatically alter the pattern of axonal projections, such that, similar to manipulations in mice, some of the axons extending from the upper layer neurons project to ectopic subcortical targets (Figure 6.11). Specifically, the analysis of the intensity of fluorescence performed on control (Figure 6.11A) and experimental animals (Figure 6.11B, C) showed that cells that were electroporated with either the CTIP2 mouse- or dunnart-specific overexpression construct extend their axons to the contralateral hemisphere through the anterior commissure, but also to subcerebral targets through the cerebral peduncle (Figure 6.11A-D). Interestingly, in both experimental groups, some axons extending from manipulated neurons were also extending towards the thalamus via the corticothalamic projection (Figure 6.11A-C, E). Differently from mouse, the analysis of the intensity of fluorescence in the thalamus, both ipsilateral and contralateral, as well as the contralateral corticothalamic projection, did not result in statistically significant difference between both groups of experimental animals and controls, as axons reaching the thalamus were often not abundantly stained (Figure 6. 11A-C, E). A possible reason for this could be that, in this species, more time is required for the axons to reach the ipsilateral and the contralateral thalamus, as axons were detected in the corticothalamic projection.

The intensity of fluorescence was also measured in the external capsule of both groups of experimental animals and controls, and divided for the value measured in the internal capsule to detect any difference in the ratio of axons projecting to the contralateral hemisphere or to subcortical targets. Our results show a trend towards a reduction of the amount of axons projecting via the external capsule to the contralateral hemisphere, possibly in favour of a subcortical projection fate via the internal capsule, and the difference was statistically significant when the mouse-specific construct was overexpressed (Figure 6. 11A-C, F) It should be noted, however, that some of these effects might be masked by the high level of fasciculation of axons within white matter tracts, suggesting that some phenotypes might be even more striking than what we quantify here.

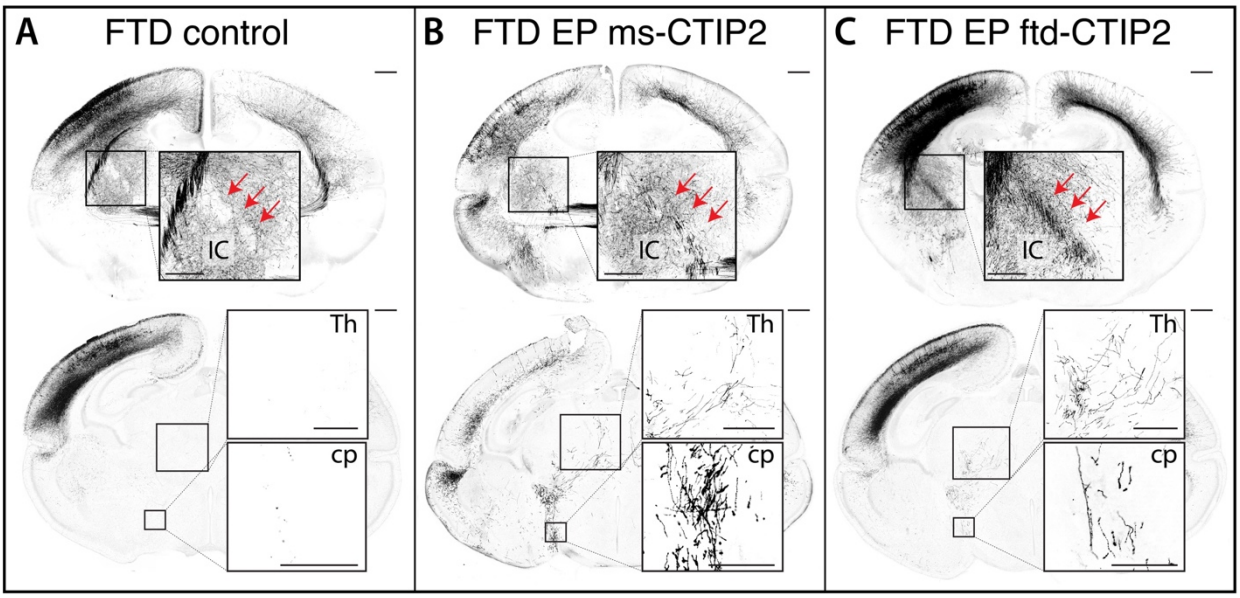
A FTD control
B FTD EP ms-CTIP2
C FTD EP ftd-CTIP2
IC
Th
cp

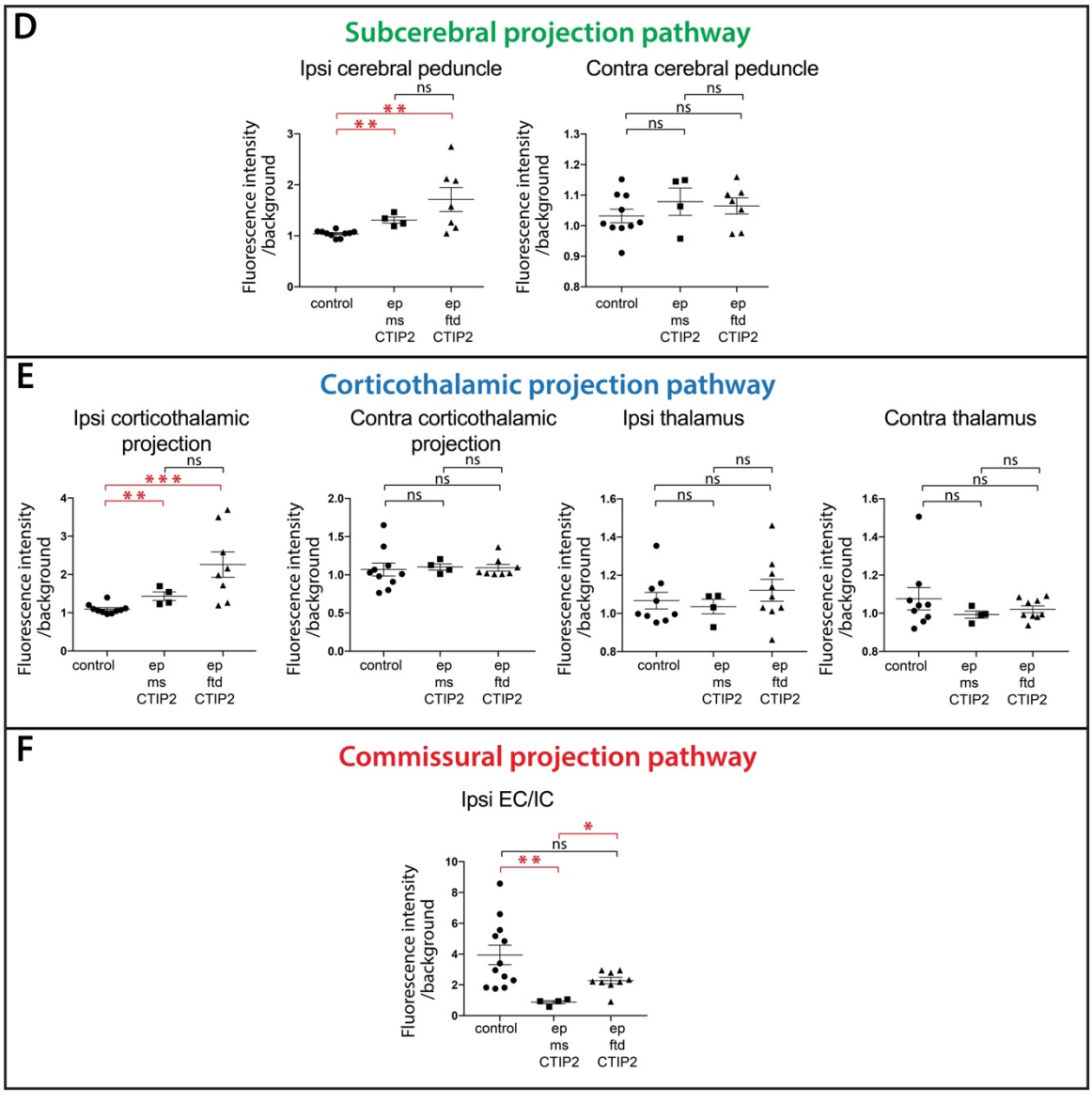
D
Subcerebral projection pathway
Ipsi cerebral peduncle
Contra cerebral peduncle
Fluorescence intensity /background
control
ep ms CTIP2
ep ftd CTIP2
E
Corticothalamic projection pathway
Ipsi corticothalamic projection
Contra corticothalamic projection
Ipsi thalamus
Contra thalamus
F
Commissural projection pathway
Ipsi EC/IC

Figure 6.11: Ectopic overexpression of either mouse- or dunnart-specific CTIP2 in the upper layers of the dunnart neocortex can alter the pattern of axonal projection.

Coronal brain sections of dunnart joeys electroporated with tdTomato alone (**A**) or with CTIP2 mouse-specific (**B**) or dunnart-specific (**C**) overexpression construct. **D**: Analysis of the intensity of fluorescence, normalised for the intensity of the background, showed that cells that were electroporated with the CTIP2 mouse- and dunnart-specific overexpression construct extend their axons to subcerebral targets through the cerebral peduncle. **E**: Axons from neurons electroporated with CTIP2 mouse- or dunnart-specific overexpression construct were also extending towards the ipsilateral thalamus via the corticothalamic projection. The analysis of intensity of fluorescence in the thalamus did not result in statistically significant difference. Corticothalamic axons might need more time to reach their final target in this species. **F**: Analysis of intensity of fluorescence in the external capsule, divided for the value in the internal capsule of control versus experimental animals revealed a trend towards a reduction of the ratio of axons reaching the contralateral hemisphere via the external capsule. Contra = contralateral, cp = cerebral peduncle, CTh = corticothalamic projection, EC = external capsule, EP = electroporated, FTD = fat-tailed dunnart, IC = internal capsule, ipsi = ipsilateral, Ms = mouse, ns = non-significant, Th = thalamus. Scale bars: 500 μm in panels with whole brain sections, as well as insets of IC and Th; 50 μm in panel with insets of cp ($n \geq 4$ animals per treatment, see also Table 6.1). Data are presented as mean ± SEM. * $P < 0.05$, ** $P < 0.01$, *** $P < 0.001$, Mann-Whitney U tests.

6.2.3.3. *Influence of CTIP2 overexpression on TBR1*

In both mice and dunnarts, the overexpression of the mouse- or dunnart-specific CTIP2 in the upper layers of the neocortex elicited the formation of ectopic projections from electroporated neurons that reached the thalamus. As the transcription factor TBR1, which is part of the same transcriptional network involving CTIP2 and SATB2 (Figure 1.3), is known to specify a corticothalamic projection fate in L6 postmitotic neurons (Hevner *et al.* 2001, Bedogni *et al.* 2010, McKenna *et al.* 2011) (Figure 1.3), its expression was investigated in control and experimental animals, to establish whether there is any change in its expression that might be related to the ectopic projections of the electroporated neurons to the thalamus. Interestingly, immunohistochemistry followed by cell count analysis revealed a decrease of TBR1 expression in L2/3 mouse neurons electroporated with the dunnart-specific but not the mouse-specific CTIP2, as compared to controls (Figure 6.12A-D). Moreover, the opposite effect was found in dunnarts, whereby both constructs resulted in an increase of TBR1 expression (Figure 6.12E-H). This evidence suggests that there might be some differences, between marsupials and eutherian mammals, in the molecular network regulating projection fate.

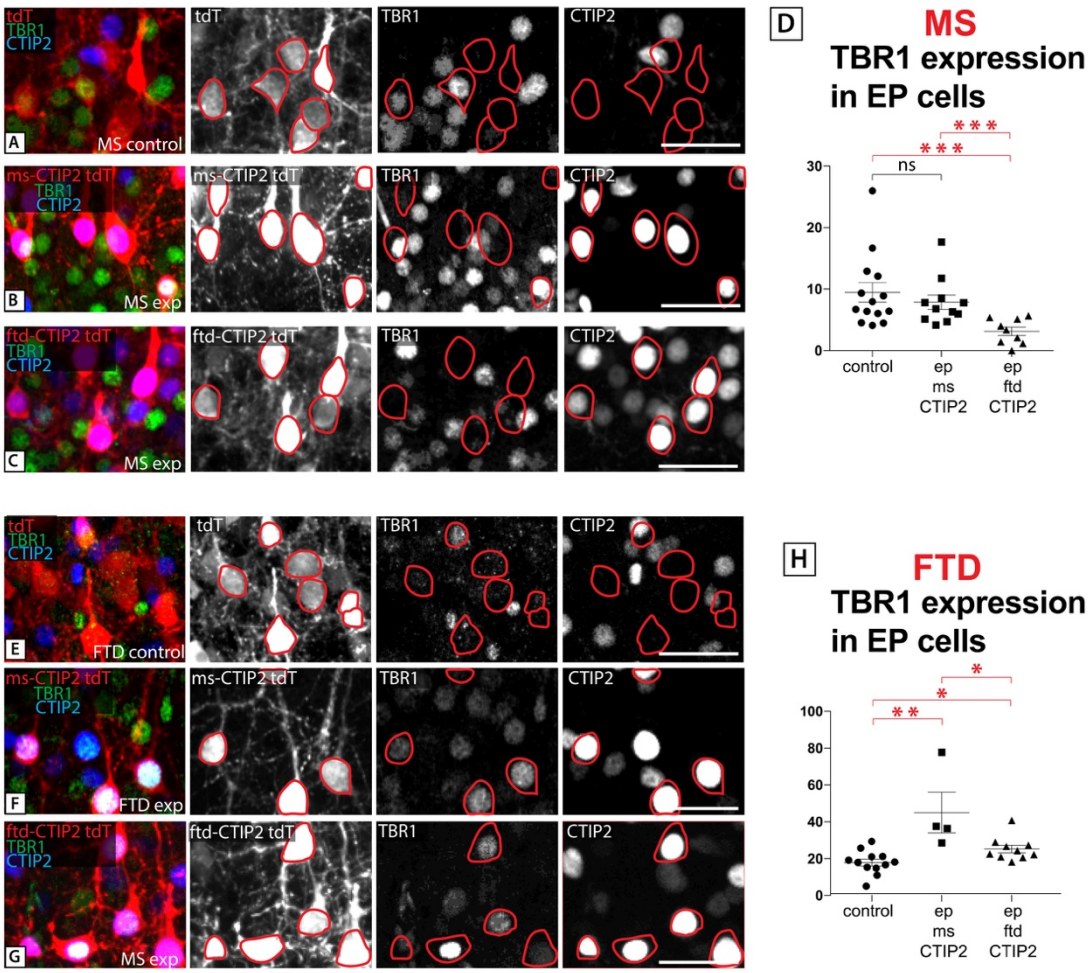

Figure 6.12: Ectopic overexpression of either mouse- or dunnart-specific CTIP2 in the upper layers of the mouse and dunnart neocortex can alter the pattern of expression of TBR1.

Mouse embryos and dunnart joeys were electroporated during stage 23 (E15 and P20, respectively) with tdTomato alone in control (**A** and **E**, in red), or with CTIP2 mouse-specific (**B** and **F**, in red) or dunnart-specific overexpression constructs (**C** and **G**, in red) in the upper layers (L2/3) of the neocortex. Pups and joeys were collected at stage 28 (P10 and P50, respectively). Coronal brain sections were co-stained for TBR1 (green) and CTIP2 (blue) to evaluate the effects of the genetic manipulation. **D**, **H**: Cell count analysis in the neocortex of tdTomato-positive cells expressing TBR1 or CTIP2 shows a clear reduction of TBR1 expression in mice that were electroporated with the dunnart-specific construct (n ≥ 9 animals per treatment, see also Table 6.1). The opposite result was found in fat-tailed dunnarts, with an increase in TBR1 expression in electroporated cells transfected with either the mouse- or the dunnart-specific CTIP2 overexpression construct. EP = electroporated, exp = experimental, FTD = fat-tailed dunnart, Ms = mouse, tdT = tdTomato. Scale bars: 250 μm in all the panels. Data are presented as mean ± SEM. * $P < 0.05$, ** $P < 0.01$, *** $P < 0.001$, Mann-Whitney U tests.

6.2.3.4. *SATB2 overexpression in the deeper layer neurons of the mouse neocortex elicits a commissural projection fate, through the anterior commissure*

In mouse, deeper layer neurons are generated during stage 20 (E12) and predominantly express the transcription factor CTIP2, and the peak of generation of SATB2-positive cells occurs in the following stage (Figures 3.2 and 6.5). Ectopic overexpression of either SATB2 mouse- or dunnart-specific constructs, together with the fluorophore tdTomato, was therefore performed at stage 20 (E12). As the cofactor SKI has been previously shown to be crucial for the role of SATB2 in transcriptional regulation of projection fate (Baranek *et al.* 2012), SATB2 was electroporated with the addition of the mouse- or dunnart-specific SKI overexpression construct. TdTomato alone was electroporated in the same area (S1) and at the same stage in control animals. Mouse pups were then collected at the end of stage 28 (P10), when it is possible to analyse the projections of electroporated neurons. Immunohistochemistry against SATB2 and CTIP2 was performed on coronal brain sections to confirm the overexpression of SATB2 and evaluate its effect on CTIP2 expression (Figure 6.13).

The first striking result was a clear migration defect of manipulated neurons, such that 11.75% of the electroporated cells that received the mouse-specific SATB2 overexpression construct, and 15.56% of electroporated cells transfected with the dunnart-specific construct, in mice, did not migrate properly into the cortical plate and were localised in the white matter/germinative zone area, in contrast to the 0.99% of cells electroporated with tdTomato localised in this area in control animals (Figure 6.13A-C, G). In some experimental animals transfected with the mouse-specific SATB2-SKI constructs, in addition to the impaired migration, some electroporated cells form aggregates in the cortical plate, further demonstrating an altered neuronal localisation following SATB2-SKI overexpression (not shown).

For the expression of SATB2 in electroporated cells, there was a statistically significant increase in the percentage of cells expressing this transcription factor in both groups of experimental animals, compared to controls. Specifically, 93.8% of cells transfected with the mouse-specific construct and 94.9% of cells electroporated with the dunnart-specific cDNA express SATB2, versus 82.2% of electroporated cells in control animals (Figure 6.13D-F, H). These results confirm the efficiency of the transfection of both mouse- and dunnart-specific SATB2 overexpression constructs in the deeper layers of the mouse neocortex. However, overexpression of SATB2 and SKI from either species produced no change in the number of CTIP2-expressing neurons (Figure 6. 13D-F, I).

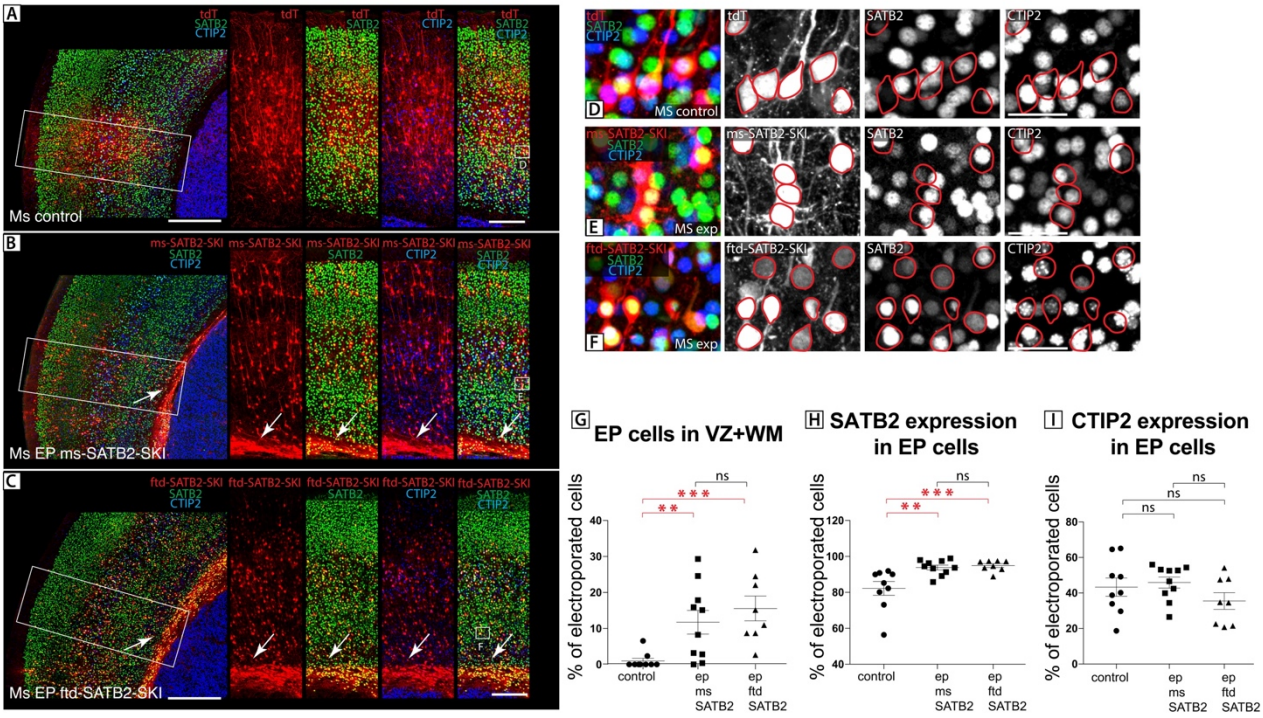

Figure 6.13: Ectopic overexpression of either mouse- or dunnart-specific SATB2-SKI in the deeper layers of the mouse neocortex.

Mouse embryos were electroporated during stage 20 (E12) to overexpress tdTomato alone in control (**A** and inset **D**, in red), with SATB2 and SKI mouse-specific (**B** and inset **E**, in red) or dunnart-specific constructs (**C** and inset **F**, in red) in the deeper layers of the neocortex. Pups were collected at stage 28 (P10). Coronal brain sections were stained for SATB2 (green) and CTIP2 (blue) to evaluate the effects of the genetic manipulation. Clear impaired migration of manipulated neurons, which are located in the area of the germinative zone and white matter in both experimental groups (white arrows). **G-I**: Cell count analysis of tdTomato-positive cells expressing SATB2 or CTIP2 in the neocortex shows an increase in SATB2 expression in both groups of experimental animals, compared to controls, confirming the efficacy of the manipulation ($n \geq 8$ animal per treatment, see also Table 6.1). No difference was detected in the percentage of electroporated cells expressing CTIP2 in experimental groups versus control animals. E = embryonic age, EP = electroporated, exp = experimental, ftd = fat-tailed dunnart, Ms = mouse, ns = non-significant, P = postnatal day, S = stage, tdT = tdTomato. Scale bars: 500 µm in A, B and C, 250 µm in right panels, 50 µm in D, E, F. Data are presented as mean ± SEM. * $P < 0.05$, ** $P < 0.01$, *** $P < 0.001$, Mann-Whitney U tests.

In order to evaluate whether the mouse and dunnart proteins were able to elicit similar axonal phenotypes in manipulated neurons, the projections of neurons electroporated with the mouse- or dunnart-specific SATB2 and SKI constructs were analysed. Previous studies overexpressing mouse-specific SATB2 ectopically in mouse deeper layer neocortical neurons reported that axons were found in the corpus callosum, in the anterior commissure and in the internal and external capsule, while no axons projecting to the cerebral peduncle were detected, suggesting a reduction in the amount of axons projecting to subcerebral targets (Britanova *et al.* 2008). Our data show that some of the manipulated neurons transfected with the mouse- or dunnart-specific SATB2-SKI overexpression constructs still project subcerebrally through the cerebral peduncle and, even though the analysis of intensity of fluorescence measured in the cerebral peduncle show a general trend towards a reduction of axons taking this projection fate in manipulated neurons, the difference with control animals was not statistically significant (Figure 6.14A-D).

Despite this, ectopically overexpressing either SATB2-SKI mouse- or dunnart-specific constructs in the deeper layer of the mouse neocortex was sufficient to alter the pattern of axonal projections. Surprisingly, the analysis of the intensity of fluorescence in the anterior commissure and in the corpus callosum revealed an increase in the amount of axons crossing the midline via the evolutionary older anterior commissure in both group of experimental animals compared to controls. This analysis was expressed as intensity of fluorescence measured in the anterior commissure, normalised for the total amount of intensity of fluorescence in the anterior commissure and the corpus callosum [AC/(AC+CC)], in experimental both experimental group of animals versus controls (Figure 6.14A-C, E), when the patch of electroporated cells was localised in a similar neocortical region and was of a comparable size.

Further intensity of fluorescence analysis showed that, in mice that received either the mouse- or the dunnart-specific overexpression constructs, more axons reached the medial part of the striatum (Figure 6.14A-C, F). In fact, the ratio between the intensity of fluorescence measured in the medial striatum and the lateral striatum, both ipsilateral and contralateral to the patch, was higher in both groups of experimental animals compared to controls (Figure 6.14A-C, F). Ectopic projections in the experimental animals that were electroporated with the dunnart-specific SATB2 and SKI overexpression constructs were also reaching the ipsilateral cingulate cortex (Figure 6.14A-C, G), while no difference in the amount of axons projecting towards the ipsilateral cingulate was found when the experimental animals were electroporated with the mouse-specific constructs.

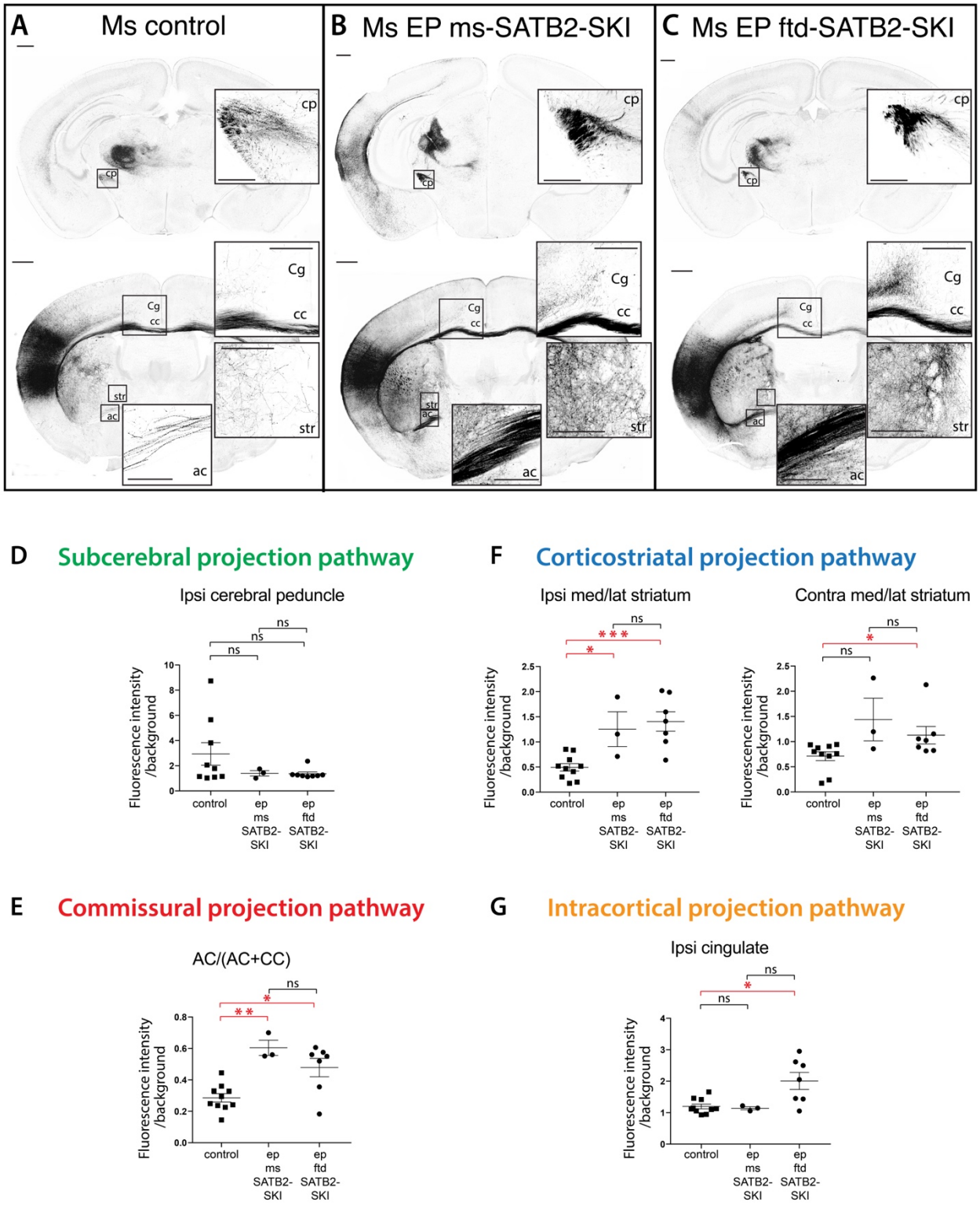

Figure 6.14: Ectopic overexpression of either mouse- or dunnart-specific SATB2-SKI in the deeper layers of the mouse neocortex can alter the pattern of axonal projection.

Coronal brain sections of mouse pups electroporated with tdTomato alone (**A**) or with either SATB2-SKI mouse-specific (**B**) or dunnart-specific (**C**) overexpression constructs. **D**: Analysis of the intensity of fluorescence, normalised for the intensity of the background, showed that there was

no statistically significant difference in the amount of projections to the cerebral peduncle from cells electroporated with the SATB2-SKI mouse-specific or dunnart-specific overexpression constructs, compared to control animals. **E**: Analysis of the intensity of fluorescence in the anterior commissure, divided for the total of intensity of fluorescence in the anterior commissure and in the corpus callosum, suggest that more axons might be crossing the midline via the anterior commissure in both group of experimental animals compared to controls with equivalent electroporated patches. **F**: More axons were projecting to the medial-ipsilateral portions of the striatum, such that the ratio between the intensity of fluorescence in the medial versus lateral ipsilateral striatum was higher in both experimental groups compared to controls. A similar trend was observed in the contralateral striatum. **G**: More axons were detected in the ipsilateral cingulate of experimental animals that received the dunnart-specific constructs. Ac = anterior commissure, cc = corpus callosum, contra = contralateral, Cg = cingulate cortex, cp = cerebral peduncle, EP = electroporated, FTD = fat-tailed dunnart, ipsi = ipsilateral, Ms = mouse, ns = non-significant, str = striatum. Scale bars: 500 μm in panels with whole brain sections; 250 μm in panels with insets of ac, ipsi and contra str; 50 μm in panel with insets of cp ($n \geq 3$ animal per treatment, see also Table 6.1). Data are presented as mean ± SEM, * $P < 0.05$, ** $P < 0.01$, *** $P < 0.001$, Mann-Whitney U tests.

6.2.3.5. *SATB2 overexpression elicits a commissural fate in the deeper layers of the dunnart neocortex*

In fat-tailed dunnart, deeper layer neurons are generated during stage 20 (P10-P12) and predominantly express the transcription factor CTIP2, as the peak of SATB2-positive cell generation occurs between stage 22 and 24 (Figures 3.2 and 6.5). The electroporation of SATB2 mouse- and dunnart-specific construct, together with the fluorophore tdTomato, was thus performed during stage 20 (P10-P12), as all SATB2-overexpression experiments in mice. As in mice, the mouse- and dunnart-specific SKI overexpression constructs were electroporated together with the species-specific SATB2. TdTomato alone was electroporated in the same area (S1) and at the same stage in control animals. Dunnart joeys were then collected at the end of stage 28 (P50), when it is possible to analyse the projections of electroporated neurons. Immunohistochemistry against SATB2 and CTIP2 was performed on coronal brain sections to confirm the overexpression of SATB2 and evaluate its effect on CTIP2 expression (Figure 6.15).

In contrast to the results in mice, manipulated neurons in dunnarts do not accumulate at the ventricular zone but migrate to the cortical plate. The percentage of electroporated cells that were localised in the germinative zone/white matter area in experimental animals and controls was not statistically different (Figure 6.15A-C, G). Interestingly, however, in dunnart joeys electroporated with the mouse-specific SATB2-SKI constructs, an abnormal aggregation of electroporated cells was evident throughout the different layers of the neocortex (Figure 6.15B, white arrows). This kind of aggregation was not present when the dunnart-specific constructs were transfected, and is similar to what was observed in mouse when the mouse-specific SATB2-SKI overexpression plasmids were electroporated, suggesting that this might be a particular effect of the mouse-specific proteins.

As expected, there was a statistically significant increase in the percentage of electroporated cells expressing SATB2 in both groups of experimental animals as compared to controls. Specifically, 97% of cells transfected with the mouse-specific construct and 98.9% of cells electroporated with the dunnart-specific cDNAs express SATB2, versus 89.75% of electroporated cells in control animals (Figure 6.15D-F, H). These results confirms the efficacy of the transfection of the mouse- and dunnart-specific SATB2 overexpression construct in the deeper layers of the dunnart neocortex. As in mice, SATB2-SKI overexpression does not affect the number of cells expressing the subcerebral marker CTIP2 (Figure 6. 15D-F, I).

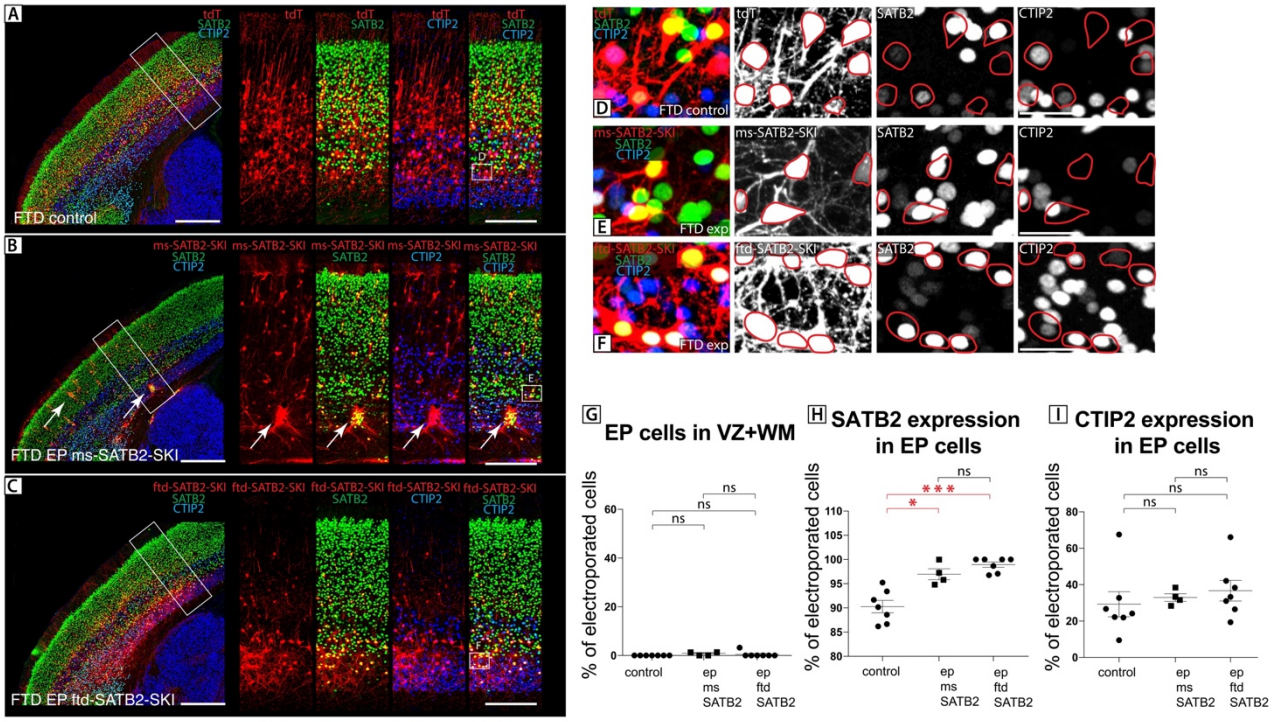

Figure 6.15: Ectopic overexpression of either mouse- or dunnart-specific SATB2-SKI in the deeper layers of the dunnart neocortex.

Dunnart joeys were electroporated during stage 20 (P10-P12) to overexpress tdTomato alone in control (**A** and inset **D**, in red) or with SATB2 and SKI mouse-specific (**B** and inset **E**, in red) or dunnart-specific constructs (**C** and inset **F**, in red) in the deeper layers of the neocortex. Dunnart joeys were collected at stage 28 (P50). Coronal brain sections were stained for SATB2 (green) and CTIP2 (blue) to evaluate the effects of the genetic manipulation. Neurons that were electroporated with the mouse-specific construct create cellular aggregates (white arrows in B). **G**: Cell count analysis of tdTomato-positive cells in the ventricular zone/white matter area shows that there is no defect of migration. **H-I**: Cell count analysis of tdTomato-positive cells expressing SATB2 or CTIP2 in the neocortex shows an increase in SATB2 expression in both groups of experimental animals, compared to controls, confirming the efficacy of the manipulation ($n \geq 4$ animals per treatment, see also Table 6.1). No difference was detected in the percentage of electroporated cells expressing CTIP2 in experimental groups versus control animals. EP = electroporated, exp = experimental, FTD = fat-tailed dunnart, Ms = mouse, ns = non-significant, P = postnatal day, S = stage, tdT = tdTomato, VZ = ventricular zone, WM = white matter. Scale bars: 500 µm in A, B and C, 250 µm in right panels, 50 µm in D, E, F. Data are presented as mean ± SEM. * $P < 0.05$, ** $P < 0.01$, *** $P < 0.001$, Mann-Whitney U tests.

After confirming the efficacy of SATB2 overexpression in dunnart joeys, using both the mouse- and dunnart-specific constructs, the next step was to evaluate whether these species-specific constructs have the same effect on the axonal projection pattern of manipulated neurons in dunnarts. SATB2 had previously been identified to play an important role in specifying a commissural fate across therian mammals in previous chapters of this thesis. Therefore, the intensity of fluorescence at the level of the cerebral peduncle was analysed, to establish whether overexpressing this transcription factor would reduce subcerebral projections. As in mice, some of the manipulated neurons transfected with the mouse- or dunnart-specific SATB2-SKI overexpression constructs still project subcerebrally through the cerebral peduncle and the analysis of intensity of fluorescence measured in the cerebral peduncle of experimental and control dunnart joeys showed no difference between experimental and control animals (Figure 6.16A-D).

Interestingly, the analysis of the intensity of fluorescence in the external and internal capsules, expressed as a ratio between these two measurements, indicates that there is an increase in the amount of axons that undertake a commissural fate extending through the external capsule. A significant difference between experimental and control animals was observed when the mouse-specific overexpression construct was electroporated (Figure 6.16A-C,E), but not with the dunnart-specific construct.

Electroporating the dunnart deeper layers with tdTomato in control animals showed that axons project to the medial striatum and the cingulate cortex, in contrast with control mice, where these regions are normally not highly innervated by deeper layer neurons. An increase in the amount of axons reaching the medial portion of the dunnart striatum can be detected when the mouse-specific SATB2-SKI overexpression constructs were transfected (Figure 6.16A-C, F). No difference in the amount of axons reaching the cingulate cortex was found when SATB2-SKI overexpression constructs were electroporated, probably due to the fact that, in wild type fat-tailed dunnart, the cingulate cortex is already hyperconnected (Figure 6.16A-C, G).

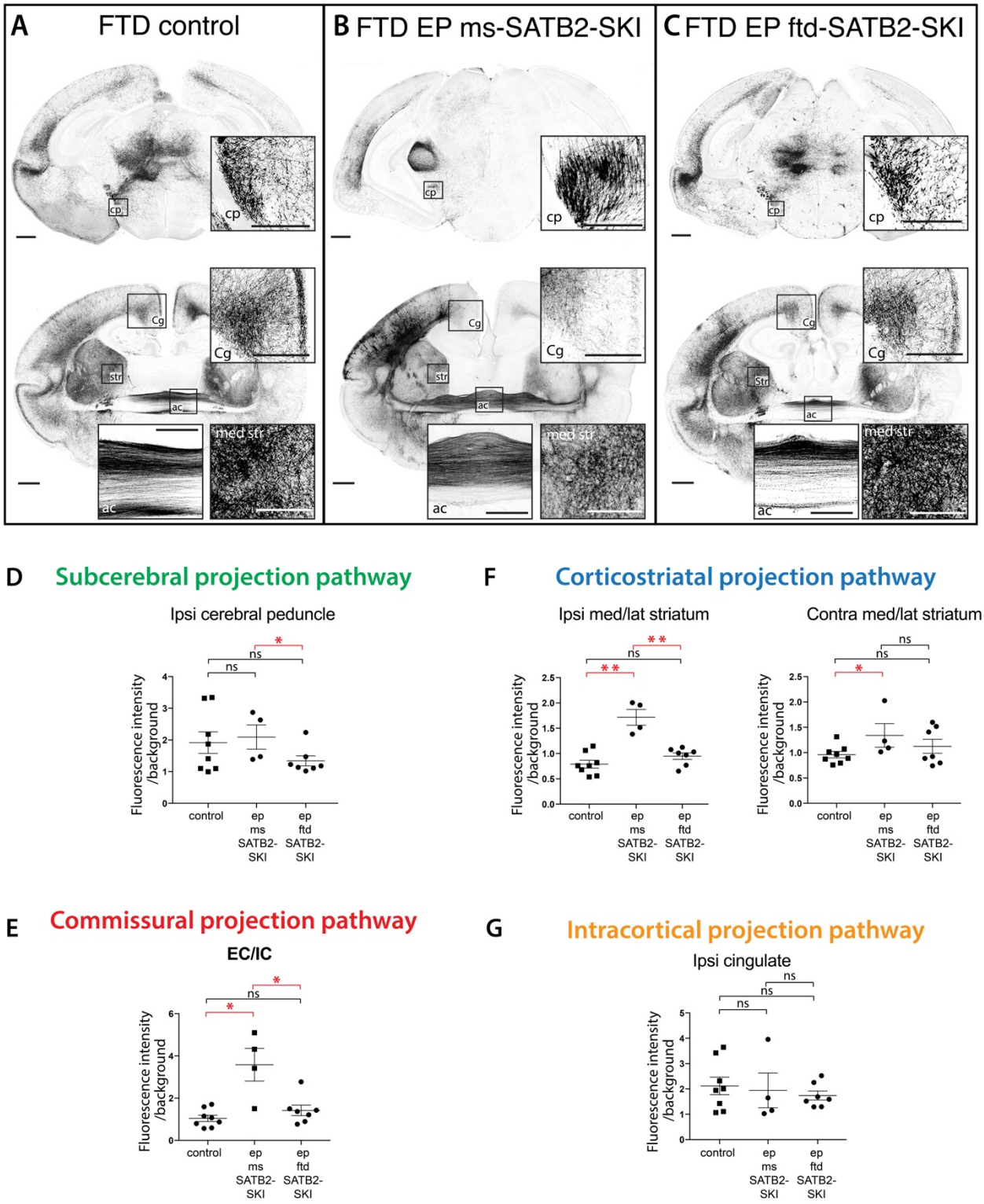

Figure 6.16: Ectopic expression of either mouse- or dunnart-specific SATB2-SKI in the deeper layers of the dunnart neocortex can alter the pattern of axonal projection.

Coronal brain sections of dunnart electroporated with tdTomato alone (**A**) or with SATB2-SKI mouse-specific (**B**) or dunnart-specific (**C**) overexpression construct. **D**: Analysis of the intensity of fluorescence, normalised for the intensity of the background, showed that there was no statistically

significant difference in the amount of projections to the cerebral peduncle from cells electroporated with the SATB2-SKI mouse-specific or dunnart-specific overexpression construct, compared to control animals. **E**: Analysis of the intensity of fluorescence in the external capsule, normalised for the intensity of fluorescence in the internal capsule, suggests that, in experimental animals, more axons undertake a commissural fate, instead of projecting to subcortical targets via the internal capsule, especially when the mouse-specific constructs were electroporated. **F**: More axons projected to the medial-ipsilateral and medial-contralateral portions of the striatum, when the mouse-specific constructs were electroporated. **E**: No difference was detected in the analysis of intensity of fluorescence in the cingulate of experimental animals compared to controls. Ac = anterior commissure, contra = contralateral, cp = cerebral peduncle, Cg = cingulate cortex, EC = external capsule, EP = electroporated, FTD = fat-tailed dunnart, IC = internal capsule, ipsi = ipsilateral, Ms = mouse, ns = non-significant, str = striatum. Scale bars: 500 μm in panels with whole brain sections, 250 μm in panels with insets of ac, ipsi and contra str; 50 μm in panel with insets of cp ($n \geq 4$ animals per treatment, see also Table 6.1). Data are presented as mean ± SEM, *$P < 0.05$, ** $P < 0.01$, *** $P < 0.001$, Mann-Whitney U tests.

ms-CTIP2 overexpression			ftd-CTIP2 overexpression		
HOST SPECIES	MS	FTD	HOST SPECIES	MS	FTD
Effect on TF expression	↑ CTIP2**** = SATB2 = TBR1	↑ CTIP2** = SATB2 ↑ TBR1**	**Effect on TF expression**	↑ CTIP2**** = SATB2 ↓ TBR1***	↑ CTIP2**** ↓ SATB2* ↑ TBR1*
Effect on projections	↑ cp ipsi **** ↑ cp contra** ↑ Cth proj ipsi**** ↑ Cth proj contra** ↑ Th ipsi**** ↑ Th contra* ↓ cc (ns, trend)	↑ cp ipsi ** = cp contra ↑ Cth proj ipsi** = Cth proj contra = Th ipsi = Th contra ↓ ec/ic**	**Effect on projections**	↑ cp ipsi **** ↑ cp contra** ↑ Cth proj ipsi** ↑ Cth proj contra (ns, trend) ↑ Th ipsi**** ↑ Th contra** ↓ cc**	↑ cp ipsi ** = cp contra ↑ Cth proj ipsi*** = Cth proj contra = Th ipsi = Th contra ↓ ec/ic (ns, trend)

ms-SATB2 overexpression			ftd-SATB2 overexpression		
HOST SPECIES	MS	FTD	HOST SPECIES	MS	FTD
Effect on TF expression	↑ SATB2** = CTIP2	↑ SATB2* = CTIP2	**Effect on TF expression**	↑ SATB2*** = CTIP2	↑ SATB2*** = CTIP2
Effect on projections	= cp ipsi ↑ ac** ↑ med striatum ipsi* ↑ med striatum contra (ns, trend) = cg ipsi migration defect: yes abnormal aggregation: yes	= cp ipsi ↑ ec/ic* ↑ med striatum ipsi** ↑ med striatum contra* = cg ipsi migration defect: no abnormal aggregation: yes	**Effect on projections**	= cp ipsi ↑ ac* ↑ med striatum ipsi*** ↑ med striatum contra* ↑ cg ipsi* migration defect: yes abnormal aggregation: no	= cp ipsi ↑ ec/ic (ns, trend) = med striatum ipsi = med striatum contra = cg ipsi migration defect: no abnormal aggregation: no

Figure 6.17: Summary of the results from CTIP2 and SATB2 manipulations.

Effect of the overexpression of mouse- and dunnart-specific CTIP2 (above) and SATB2 (below) on the expression of transcription factors and projections of manipulated neurons. Ac = anterior commissure, cc = corpus callosum, contra = contralateral, cg = cingulate cortex, cp = cerebral peduncle, CTh = corticothalamic projection, ec = external capsule, FTD = fat-tailed dunnart, ic = internal capsule, ipsi = ipsilateral, med = medial Ms = mouse, ns = non-significant, Th = thalamus. * $P < 0.05$, ** $P < 0.01$, *** $P < 0.001$, **** $P < 0.0001$, Mann-Whitney U tests.

6.3. Discussion

Despite being commonly regarded as a callosal-specifying gene, the data presented in this chapter surprisingly show that the transcription factor SATB2, as well as CTIP2, which is under SATB2 regulation, are expressed in the neocortex of fat-tailed dunnarts, despite not having a corpus callosum (Figure 6.3-6.4) (Alcamo *et al.* 2008, Arlotta *et al.* 2008, Britanova *et al.* 2008, Srinivasan *et al.* 2012, Srivatsa *et al.* 2014). In addition to this, the timing of generation and the overall layering distribution of the cells expressing SATB2 and CTIP2, are broadly conserved across therian mammals (Arlotta *et al.* 2005, Alcamo *et al.* 2008, Britanova *et al.* 2008, Chen *et al.* 2008, Srinivasan *et al.* 2012, Srivatsa *et al.* 2014) (Figure 6.3-6.6).

Nevertheless, there are subtle differences in SATB2 and CTIP2 expression, which could either be incidental or crucially underlie the different patterns of connectivity in marsupials and eutherian mammals. For example, the overall percentage of CTIP2-positive cells was higher in mouse than in dunnart in all the layers of the neocortex (Figure 6.3). It has been previously shown that CTIP2 is not only expressed in subcerebral projection neurons, but also in interneurons (Nikouei *et al.* 2016). Therefore it is unclear which subpopulations of CTIP2 expressing cells are solely or primarily responsible for this difference in expression. Additional experiments investigating these subpopulations using GABAergic interneuron markers, would be required to address this question.

For SATB2 expression, the percentage of SATB2-positive cells was surprisingly higher in L2/3 of the adult dunnart neocortex, and lower in L6, compared to mouse (Figure 6.3). In L6 of the mouse neocortex, a clear band of SATB2-positive cells, which is not present in the dunnart neocortex, is evident from early stages of development (Figure 6.4). It is unclear what the function of this group of cells might be, but it may explain the reason for the early generation of SATB2-positive cells in mice compared to dunnarts, as detected with EdU analysis of neurogenesis (Figure 6.5C, E). Despite this precocious generation of SATB2-positive cells in mice, SATB2 protein is detected earlier in this marsupial species than in mice, beginning at stage 20 (Figure 6.4). A possible explanation could be that SATB2-positive cells are generated early in mouse, but differentiation into mature neurons occurs over a wider developmental window than in marsupials, with SATB2 expression likely not activated immediately after mitotic cell cycle exit, as previously suggested (Britanova *et al.* 2008). This explanation is in line with the previous suggestion that there might be a difference in the timing of neuronal maturation in marsupials compared to eutherian mammals (Harman *et al.* 1995, Marotte and Sheng 2000, Reep 2000), whereby marsupial deeper

layers neurons mature relatively faster than in eutherians, and then migrate to form rapidly expanding layers of loosely packed cells (Reynolds 1985, Marotte *et al.* 1997, Molnár *et al.* 1998).

In addition to the comparable pattern of expression of both SATB2 and CTIP2 in mice and dunnarts, the results from this chapter also show that, despite the different commissural strategy in these two mammalian species, the final projection targets of SATB2- and CTIP2-positive neurons are surprisingly broadly conserved. Indeed, commissural neurons in S1 of the dunnart neocortex, which project their axons laterally at the intermediate zone (Figure 5.3), almost exclusively express SATB2, but not CTIP2 (Figure 6.6C-D and pie chart, n = 3), resembling the expression of transcription factors in callosal neurons in mice (Alcamo *et al.* 2008, Srivatsa *et al.* 2014, Harb *et al.* 2016). This suggests that the expression of SATB2, without CTIP2, is a marker for commissural neurons across mammals, rather than being only callosal. Nevertheless, there is a major difference between mouse and dunnarts in SATB2 and CTIP2 coexpression in commissural neurons, as it has been previously shown that, in postnatal mice, a subgroup of callosal neurons are both SATB2- and CTIP2-positive (about 30% of retrogradely labelled cells after CTB injection in S1) (Harb *et al.* 2016). This SATB2 and CTIP2 coexpression in postnatal mice has been attributed to the expression of the transcriptional adaptor LMO4, which modifies the structure of the DNA preventing SATB2 from downregulating CTIP2 (Harb *et al.* 2016). Considering the absence of SATB2 and CTIP2 coexpression in neocortical commissural neurons of dunnarts, it would be interesting to investigate LMO4 expression in this marsupial species to see if it has a different pattern of expression. In addition to this, cell count analysis performed on brain sections of adult dunnarts and mice, which were stained for SATB2 and CTIP2, revealed that the upper layers of the dunnart neocortex have intrinsically fewer neurons coexpressing SATB2 and CTIP2, which might also explain the absence of commissural neurons expressing CTIP2 (Figure 6.3).

In contrast to the differences between mouse and dunnart in the coexpression of SATB2 and CTIP2 in commissural neurons, more conservation was found between these two mammalian species in deeper layer subcortical projection neurons, where these two transcription factors are highly coexpressed (Figure 6.7) (Britanova *et al.* 2008, Lickiss *et al.* 2012, Srinivasan *et al.* 2012, Harb *et al.* 2016). This evidence shows that deeper layer coexpression is conserved and suggests that SATB2 and CTIP2 cooperation may be crucial for the correct development of subcortical projections across mammals (Leone *et al.* 2014), but also that these two transcription factors might play different roles depending on the stage of development, the neuronal populations that express them and the combination of other transcription factors expressed in the same cells.

Furthermore, our data demonstrate conserved function of SATB2 and CTIP2 proteins, such that they regulate the same neuronal phenotypes in both therian species (see Figure 6.17 for a summary of the results from this section of this chapter). Specifically, overexpression of the mouse- or dunnart-specific CTIP2 proteins in both mice and dunnarts upper layer neurons led to an increase of subcortical projections, specifically projecting towards the thalamus and through the cerebral peduncle. Immunohistochemistry against TBR1, which has long been regarded as a marker for corticothalamic projection neurons (Hevner *et al.* 2001, Bedogni *et al.* 2010, McKenna *et al.* 2011), showed an increase in TBR1 expression in manipulated cells in dunnarts, while the opposite effect was found in mouse, with a decrease of TBR1 expression in neurons that were transfected with CTIP2 overexpression construct. This result in mice is in line with previous studies that have hypothesised a possible reciprocal negative interaction between CTIP2 and TBR1, based on analysis of expression of these genes in *Ctip2*- and *Tbr1*-knockout experiments (McKenna *et al.* 2011, Srinivasan *et al.* 2012) (Figure 1.3). Our data suggest that the increase of corticothalamic projections in mouse is not due to an increase of TBR1 expression in manipulated neurons, but more importantly that there might be a difference, between mice and dunnarts, in the molecular network involving CTIP2 and TBR1. In mice, ectopic subcerebral projections were also detected in the hemisphere contralateral to the electroporated patch, suggesting that some axons extending from manipulated upper layer neurons might project to subcerebral ectopic targets after having crossed the midline via the corpus callosum. In dunnarts, this is not clearly evident and a possible reason could be that the axons from electroporated neurons might require more time to grow in this species compared to mouse, and this could also explain why, in dunnarts, there are many axons extending through the ipsilateral corticothalamic projection, but not many actually reaching the ipsilateral thalamus. Future experiments examining these same experimental manipulations in an older stage of dunnarts would help to elucidate this possibility.

Altogether, our results indicate that the mouse- and dunnart-cDNA sequence of CTIP2 elicited similar outcomes in both dunnarts and mice, suggesting a conservation of the protein function in both species, specifically in regulating corticofugal projection neuron identity throughout the mammalian lineage. This evidence further strengthens the hypothesis that ancient building blocks have been conserved during evolution. Future experiments are required to explore whether the small differences found between species may underlie differing projection fates, or are incidental by-products of evolution.

The results from the overexpression of the mouse- or dunnart-specific SATB2 and its cofactor SKI (Baranek *et al.* 2012) in deeper layer neurons of the mouse neocortex at stage 20 (E12) show that, in both cases, there is an increase in the amount of axons crossing the midline via

the anterior commissure, resembling the marsupial phenotype. This result is particularly surprising, as SATB2 has been previously shown to be crucial for the formation of the corpus callosum, likely by regulating the medial projection of axons extending from migrating neurons in the mouse intermediate zone (Alcamo *et al.* 2008, Britanova *et al.* 2008, Lickiss *et al.* 2012, Hatanaka *et al.* 2016). The reasons for this specific projection pattern are unclear, however it could be speculated that the relative timing of the overexpression may account for wiring diversity, as usually SATB2 is not detectable in the mouse somatosensory neocortex on the day in which the overexpression experiment was performed, (stage 20; E12), while in the dunnart neocortex it is already expressed by stage 20 (P8-11) (Figure 6.4). Future experiments could explore this hypothesis by overexpressing SATB2 at an age in which this transcription factor is firstly detected in the neocortex in mouse to establish whether the phenotype remains the same. In line with the hypothesis that mice might acquire a more "marsupial phenotype" when SATB2 is overexpressed at early stages of development, analysis of the intensity of fluorescence in the striatum of experimental animals shows that there was an increase in the amount of axons reaching the medial striatum, which is a normal target for neocortical neurons in dunnarts but not in mice (Figures 6.14 and 6.16). In addition to the projection phenotype, in mice that received either the mouse-specific or the dunnart-specific constructs there was a clear migration defect, with electroporated neurons remaining at the germinative zone/white matter area, which was not seen in dunnarts.

The electroporation of SATB2 and SKI mouse-specific overexpression constructs in deeper layer pyramidal neurons of dunnarts resulted in more axons projecting through the external capsule, relative to the internal capsule (significant for the mouse constructs and marginal for the dunnart ones, Figure 6.16), thus undertaking a commissural projection fate. Apart from this, no major differences were found between both groups of experimental animals and controls. A possible explanation for this is that, in dunnarts, SATB2 protein is already detected during stage 20, which is when the electroporation of the overexpression constructs was performed in order to match the age of the experiments performed in mice, and therefore its overexpression made less of an impact to phenotype as compared to mouse.

Interestingly, in both mice and dunnarts that were electroporated with the mouse-specific SATB2 and SKI over-expression constructs, there was an abnormal aggregation of electroporated cells, particularly evident in dunnarts, as well as tumour-like formations below the cortical plate of manipulated mice, which is in line with the already described role of SATB2 in tumorigenesis in other systems (Naik *et al.* 2018).

Altogether, the results from the manipulatory experiments, summarised in Figure 6.17, suggest that marsupial and eutherian mammals share some aspects of the molecular regulation of neuronal projection fate, with the overexpression of CTIP2 causing more axons to undertake a subcortical projection fate and SATB2 ectopic expression leading more axons to reach the contralateral hemisphere. Some of the differences in terms of the effect of these manipulations on other transcription factors can be further investigated with additional experiments, such as chromatin-immunoprecipitation sequencing analyses , which would be crucial to identify the binding sites for SATB2 and CTIP2 proteins in an unbiased way and thus evaluate the extent to which their transcriptional roles are conserved across therian mammals.

Chapter 7. General discussion

7.1. Broadly conserved mechanisms of neocortical development in mammalian species with different commissural strategies

The *ex utero* and protracted development of the telencephalon in marsupials, as well as the different commissural strategy in these species without corpus callosum, suggests that different temporal sequences of events and/or molecular networks might control the development of the neocortex and its connections in mammals. On the other hand, experiments investigating the birthdate of long-range projection neurons in fat-tailed dunnarts and mice showed that the main patterns and milestones of neurogenesis, such as the generation of deeper and upper neocortical layers, are conserved across therian mammals (chapter 3). In addition to this, chapter 4 of this thesis revealed a conservation of the organisational principles characterising the mature interhemispheric cortical connectome, which predates the evolution of the corpus callosum (Suárez *et al.* 2018). Interestingly, the topographic arrangement of neocortical interhemispheric projections within the corpus callosum and the anterior commissure, as well as the homotopic, heterotopic and hyperconnected circuits, are similar in eutherian and non-eutherian mammals, despite the different initial axonal elongation of neocortical commissural neurons in these species (chapter 5). In fact, in eutherian mammals, neocortical commissural neurons project their axons medially (Lickiss *et al.* 2012, Hatanaka *et al.* 2016), while in marsupials they project laterally (Figure 5.3). Nevertheless, investigation of the expression and the function of transcription factors known to regulate the directionality of initial axonal elongation in eutherians (i.e., SATB2 and CTIP2) revealed a conservation of important aspects of the molecular network regulating projection fate determination across mammals (chapter 6). Collectively, this thesis has thus shown that key aspects of neocortical development, previously thought to be novel traits of eutherians related to the evolution of the corpus callosum, are remarkably conserved between mammalian lineages with different commissural strategies. Future experiments would be required to investigate whether and how the steps of cortical and commissure development described in this thesis are related to each other. For example, whether the conservation of the interhemispheric connectome in mature animals is a result of the conservation of a transcriptional network involved in regulating long-range projection neurons, or instead whether these processes are independent of one another will require further examination.

7.2. Possible mechanisms involved in the different cortical wiring strategies in mammals

Despite the surprisingly high number of similarities uncovered by this thesis in the characteristics of marsupial and eutherian neocortical connections, important questions remain open about the precise mechanisms that explain the different routes taken by commissural axons in both lineages. Future studies will be required to determine if any of the subtle differences between species identified in this thesis could be mechanistically linked to such important phenotypic difference.

The most striking and the earliest detectable difference in terms of commissure development in marsupials and eutherians is in the initial axonal elongation of neocortical commissural neurons, as they migrate towards their appropriate layer in the cortical plate, whereby these neurons project their axons medially in eutherians and laterally in marsupials (Figure 5.3). The evidence presented in chapter 5 suggests that this difference is established during early stages of development, instead of resulting from a process of medial and lateral branching followed by selective pruning. However, it is still unclear what mechanisms might determine this major difference in projections within the intermediate zone. Previous studies have suggested that transcription factors, such as SATB2 and NGN2, might be involved in the regulation of the initial medial axonal elongation in mice (Hand and Polleux 2011, Lickiss *et al.* 2012, Hatanaka *et al.* 2016). Based on the evidence from *Satb2*-knockout mice, which resemble the marsupial phenotype with neocortical commissural neurons projecting laterally at the intermediate zone and crossing the midline via the anterior commissure (Alcamo *et al.* 2008, Britanova *et al.* 2008), it could have been hypothesised that the different axonal projection in marsupials might be due to an absence of SATB2 expression in the neocortex of non-eutherian mammals. Surprisingly, the pattern of expression and function of SATB2 in fat-tailed dunnarts (chapter 6) suggests that the lateral initial axonal elongation of neocortical commissural neurons in marsupials is not due to an absence of SATB2 expression in the neocortex and that maybe other transcription factors might be involved in this different initial step of commissural development. Another possible scenario is that the same transcription factors might be expressed in marsupials and eutherian mammals, but the difference might lie in the timing of expression, in the relative proportions of cells expressing a specific transcription factor, or even in the relative amounts of transcription factors expressed by each cell type, rather than just the presence or absence of any of those proteins alone. For example, SATB2 protein has been detected at earlier stages in the neocortex of fat-tailed dunnarts compared to mice, and the overexpression of this transcription factor at early stages of development in mouse leads to an increase in the number

of axons projecting through the anterior commissure, just as in the marsupial wildtype (Figure 6.14). Similarly, it has been previously suggested that small differences in the relative timing or speed of developmental features in distinct species (heterochrony) can result in substantial changes in the phenotype (De Beer 1940, Gould 1977). However, further experiments, such as a systematic analysis of temporal dynamics of gene expression in marsupials and eutherians coupled with precisely-timed genetic manipulations involving selective knock-down or knock-out of these genes (e.g., using CRISPR/Cas9), as well as analyses of DNA-binding motifs, would be required to investigate whether and how the different timing in transcription factors expression between these two lineages could account for the different commissural phenotypes.

In addition to the initial axonal elongation, the correct formation of the corpus callosum in eutherian mammals also requires that the tissue around the interhemispheric fissure is remodelled by differentiated midline zipper glia to create fused substrate for callosal axons to cross the midline (Gobius *et al.* 2016). This event does not occur in non-eutherian mammals (marsupials and monotremes), leaving both halves of the septum unfused and impeding axons from crossing the midline (Gobius *et al.* 2016, Gobius *et al.* 2017). Failure to remodel the interhemispheric fissure is likely to be the major underlying cause of complete agenesis of the corpus callosum in humans (Gobius *et al.* 2016) and it has been previously suggested that, when this occurs, some commissural axons might reroute via the anterior commissure, in both humans and rodents (Barr and Corballis 2002, Barr and Corballis 2003, Tovar-Moll *et al.* 2014). Given this, it is possible to speculate that, in marsupials, commissural neurons might send two branches during cortical development, one medial and one lateral, and then prune the medial branch because it cannot cross the midline through non-permissive unfused septum, while the lateral projection is maintained and cross the midline via the anterior commissure. The results from chapter 5 do not support this scenario, since commissural neurons in fat-tailed dunnarts extend their axons exclusively laterally within the intermediate zone from the beginning of axonal elongation, without any branches. It is still unclear whether medially projecting axons arriving to the midline at a specific timepoint of cortical development might facilitate the differentiation of midline zipper glia and the remodelling of the interhemispheric fissure in eutherian mammals, or whether the remodelling of the interhemispheric fissure directs initial axonal elongation medially by initiating a signalling cascade, or whether these processes occur independently from one another. Interestingly, however, our data showing the existence of medially projecting neurons that target the ipsilateral cingulate cortex at later stages of cortical development of fat-tailed dunnarts indicate that the medial turning phenotype is present, yet these axons cannot cross the midline perhaps due to the absence of a permissive tissue. Other aspects of commissure development that would require further investigation are the spatial and

temporal patterns of expression of axon guidance cues during commissure formation in both marsupials and eutherians, which might also account for the different commissural strategies in these two mammalian lineages.

Another significant difference between marsupials and eutherians identified in this thesis is in the network of transcription factors regulating projection fate in long-range projection neurons. For example, overexpression of CTIP2 in mice leads to a decrease in TBR1 expression, in line with what has been previously described in the literature (Figure 6.12) (Srinivasan *et al.* 2012), whereas TBR1 expression increases when CTIP2 is overexpressed in fat-tailed dunnarts. Further experiments, including co-immunoprecipitation (CO-Ip) and chromatin immunoprecipitation and sequencing (ChIP-seq) in both mice and fat-tailed dunnarts, using specific antibodies binding to transcription factors (i.e. CTIP2 and SATB2), would be crucial to identify any differences in binding partners and cofactors, as well as in the binding sites of these proteins and explore their downstream effectors, thus further elucidating their mechanisms of action in regulating projection fate.

7.3. Future applications for the fat-tailed dunnart as an animal model

The majority of our knowledge about mammalian brain development and evolution comes from *in vitro* or *ex vivo* experiments, due to the *in utero* development of the neocortex and its connections in eutherian mammals, such as mice, which cannot survive outside the uterus. On the other hand, the *ex utero* development of the cortex in marsupials has enabled the establishment of new experimental paradigms to study cortical development *in vivo*, with approaches that would be more challenging, or even unfeasible, in eutherian mammals. As a result, the fat-tailed dunnart can be exploited in many different ways to address several questions about brain development and evolution, from the molecular regulation of neocortical formation to neuronal activity during brain wiring, using, for example, live multi-photon calcium imaging. This is particularly relevant as multiple studies in postnatal mice and *in vitro* have shown that spontaneous activity can affect the formation of cortical circuits during early stages of brain formation (Hanson *et al.* 2004, Mizuno *et al.* 2007, Ackman *et al.* 2014, Suárez *et al.* 2014a). In addition to this, altered brain activity in foetuses whose mothers were prescribed anti-depressant drugs during pregnancy has been correlated with neurodevelopmental disorders, such as autism (Coghlan *et al.* 2012, Christensen *et al.* 2013). In this regard, the fat-tailed dunnart as an animal model offers the unprecedent opportunity to study the effect of spontaneous activity, as well as environmental influences, on early stages of cortical formation, equivalent to embryonic stages in mouse and humans.

7.4. The importance of evolutionary studies to understand human brain development and pathology

Understanding how the mammalian brain evolved has long been a focus of major interest for neuroscientists, as it can provide insight into the mechanisms involved in brain development and function. Adopting a comparative approach and studying how specific anatomical structures develop in phylogenetically distinct extant species is a powerful strategy to shed light on conserved and divergent brain features across evolution (de Sousa and Wood 2007). These include the divergence into the nuclear arrangement of the dorsal telencephalon of bird and reptiles and the six-layered neocortex and the increase in intra- and interhemispheric connectivity in mammals from an unknown common ancestor (Cheung *et al.* 2010, Molnár 2011, Suárez *et al.* 2014b). This knowledge can ultimately aid the understanding of the origin, expansion and development of the mammalian neocortex, as well as its connectivity and activity (Guillemot *et al.* 2006, Rakic 2009), thus providing insights into the phylogenetic origin of specific anatomical structures, such as the corpus callosum in eutherian mammals.

The corpus callosum is the largest interhemispheric tract in the brain of eutherian mammals (Funnell *et al.* 2000) and its incorrect development is associated with numerous neurological disorders (Swayze *et al.* 1990, Funnell *et al.* 2000, Mihrshahi 2006, Paul *et al.* 2007, Gilliam *et al.* 2011, Hinkley *et al.* 2012, Lungu and Stip 2012, Fenlon and Richards 2015), including attention deficit hyperactivity disorder (Gilliam *et al.* 2011, Cocchi *et al.* 2012), schizophrenia (Swayze *et al.* 1990, Lungu and Stip 2012), autism (Wass 2011, Paul *et al.* 2014), bipolar disorders (Trehout *et al.* 2017), intellectual disabilities (Paul *et al.* 2014, Margari *et al.* 2016) and behavioural problems (Sarkar *et al.* 2013, Zhang *et al.* 2014, Labadi and Beke 2017, Menks *et al.* 2017, Menks *et al.* 2017). Interestingly, it has been previously shown that some people with agenesis of the corpus callosum with broadly preserved functions of interhemispheric integration display an enlarged anterior commissure that connects both neocortical hemispheres (Barr and Corballis 2002, Sarnat 2007, Tovar-Moll *et al.* 2014, van Meer *et al.* 2016). A thicker anterior commissure has also been reported in some cases of agenesis of the corpus callosum in mouse (Alcamo *et al.* 2008, Britanova *et al.* 2008). This evidence suggests that there might be a rerouting through evolutionary older commissures in cases of corpus callosum agenesis, such that neocortical commissural neurons might exploit developmental plasticity of ancient developmental mechanisms which lead to functional interhemispheric connectomes. As a result, investigating the development of the anterior commissure in marsupials can help us to understand the evolution of new anatomical features, the

causes of brain wiring disorders and the mechanisms of brain plasticity in humans under healthy and pathological conditions.

Altogether, this thesis introduces the fat-tailed dunnart as an innovative and advantageous animal model to study brain evolution and development. In addition, this project provides mechanistic insights into the main principles guiding mammalian brain formation and evolution. Using a comparative approach that investigates developmental processes in both marsupial and eutherian species, this thesis concludes that key aspects of neocortical neurogenesis, neuronal projection fate determination, and targeting, many of which were previously assumed to be novel traits of eutherians related to the evolution of the corpus callosum, are remarkably conserved between mammalian lineages, despite the different commissural routes. This conservation indicates that such mechanisms may be critical for the formation of functional cortical circuits in therian mammals, regardless of commissural route.

Bibliography

Ackman, J. B., H. Zeng and M. C. Crair (2014). "Structured dynamics of neural activity across developing neocortex." bioRxiv.

Alboitiz, F. and J. Montiel (2003). "One hundred million years of interhemispheric communication: the history of the corpus callosum." Braz J Med Biol Res **36**: 409-420.

Alcamo, E. A., L. Chirivella, M. Dautzenberg, G. Dobreva, I. Farinas, R. Grosschedl and S. K. McConnell (2008). "Satb2 regulates callosal projection neuron identity in the developing cerebral cortex." Neuron **57**(3): 364-377.

Alitto, H. J. and W. M. Usrey (2003). "Corticothalamic feedback and sensory processing." Curr Opin Neurobiol **13**: 440-445.

Allendoerfer, K. L. and C. J. Shatz (1994). "The subplate, a transient neocortical structure: its role in the development of connections between thalamus and cortex." Annu Rev Neurosci **17**: 185-218.

Anderson, S. A., D. D. Eisenstat, L. Shi and J. L. R. Rubenstein (1997). "Interneuron migration from basal forebrain to neocortex: dependence on Dlx genes." Science **278**: 474-477.

Andrews, W., A. Liapi, C. Plachez, L. Camurri, J. Zhang, S. Mori, . . . L. J. Richards (2006). "Robo1 regulates the development of major axon tracts and interneuron migration in the forebrain." Development **133**(11): 2243-2252.

Angevine, J. B. and R. L. Sidman (1961). "Autoradiographic study of cell migration during histogenesis of cerebral cortex in mouse." Nature **1962**: 766-768.

Arendt, D., A. S. Denes, G. Jékely and K. Tessmar-Raible (2008). "The evolution of nervous system centralization." Philos Trans R Soc Lond B Biol Sci **363**: 1523-1528.

Arlotta, P., B. J. Molyneaux, J. Chen, J. Inoue, R. Kominami and J. D. Macklis (2005). "Neuronal subtype-specific genes that control corticospinal motor neuron development in vivo." Neuron **45**(2): 207-221.

Arlotta, P., B. J. Molyneaux, D. Jabaudon, Y. Yoshida and J. D. Macklis (2008). "Ctip2 controls the differentiation of medium spiny neurons and the establishment of the cellular architecture of the striatum." J Neurosci **28**(3): 622-632.

Armand, J. (1982). "The origin, course and terminations of corticospinal fibers in various mammals." Prog Brain Res **57**: 329-360.

Ashwell, K. W. (2010). The neurobiology of Australian marsupials: brain evolution in the other mammalian radiation. New York, Cambridge University Press.

Ashwell, K. W. (2016). "Anterior commissure versus corpus callosum: a quantitative comparison across mammals." Zoology (Jena) **119**: 126-136.

Ashwell, K. W., L. R. Marotte, L. Li and P. M. E. Waite (1996). "Anterior commissure of the wallaby (macropus eugenii): adult morphology and development." J Comp Neurol **336**: 478-494.

Ashwell, K. W., P. M. E. Waite and L. R. Marotte (1996). "Ontogeny of the projection tracts and commissural fibres in the forebrain of the tammar wallaby." Brain Behav Evol **47**: 8-22.

Ashwell, K. W. S., B. M. McAllan and J. K. Mai (2010). Atlas of the brain of the stripe-faced dunnart (Sminthopsis macroura). The Neurobiology of Marsupials. New York, Cambridge University Press.

Asprer, J. S., B. Lee, C. S. Wu, T. Vadakkan, M. E. Dickinson, H. C. Lu and S. K. Lee (2011). "LMO4 functions as a co-activator of neurogenin 2 in the developing cortex." Development **138**(13): 2823-2832.

Atoji, Y., J. M. Wild, Y. Yamamoto and Y. Suzuki (2002). "Intratelencephalic connections of the hippocampus in pigeons (Columba livia)." J Comp Neurol **447**: 177-199.

Bagnard, D., M. Lohrum, D. Uziel, A. W. Püschel and J. Bolz (1998). "Semaphorins act as attractive and repulsive guidance signals during the development of cortical projections " Development **125**: 5043-5053.

Baranek, C., M. Dittrich, S. Parthasarathy, C. G. Bonnon, O. Britanova, D. Lanshakov, . . . S. Atanasoski (2012). "Protooncogene Ski cooperates with the chromatinremodeling factor Satb2 in specifying callosal neurons." Proc Natl Acad Sci U S A **109**: 3546-3551.

Barr, M. S. and M. C. Corballis (2002). "The role of the anterior commissure in callosal agenesis." Neuropsychology **16**(4): 459-471.

Barr, M. S. and M. C. Corballis (2003). "Redundancy gain in the acallosal brain." Neuropsychology **17**(2): 213-220.

Baumgart, J. and N. Grebe (2015). "C57BL/6-specific conditions for efficient in utero electroporation of the central nervous system." J Neurosci Methods **240**: 116-124.

Bayer, S. A. (1986). "Neurogenesis in the rat primary olfactory cortex." Int J Dev Neurosci **4**: 251-271.

Bedogni, F., R. D. Hodge, G. E. Elsen, B. R. Nelson, R. A. M. Daza, R. P. Beyer, . . . R. F. Hevner (2010). "Tbr1 regulates regional and laminar identity of postmitotic neurons in developing neocortex " Proc Natl Acad Sci U S A **107**: 13129-13134.

Benadiba, C., D. Magnani, M. Niquille, L. Morle, D. Valloton, H. Nawabi, . . . B. Durand (2012). "The ciliogenic transcription factor RFX3 regulates early midline distribution of guidepost neurons required for corpus callosum development." PLoS Genet **8**(3): e1002606.

Berman, J. I., M. R. Lanza, L. Blaskey, J. C. Edgar, T. P. L. Robert (2013). "High Angular Resolution Diffusion Imaging (HARDI) probabilistic tractography of the auditory radiation." AJNR Am J Neuroradiol **34**(8) 1573-1578.

Bielle, F., A. Griveau, N. Narboux-Neme, S. Vigneau, M. Sigrist, S. Arber, . . . A. Pierani (2005). "Multiple origins of Cajal-Retzius cells at the borders of the developing pallium." Nat Neurosci **8**(8): 1002-1012.

Blue, M. E. and J. G. Parnavelas (1983). "The formation and maturation of synapses in the visual cortex of the rat. II. Quantitative analysis." J Neurocytol **12**: 697-712.

Boyd, E. H., D. N. Pandya and K. E. Bignall (1971). "Homotopic and nonhomotopic interhemispheric cortical projections in the squirrel monkey." Exp Neurol **32**: 256-274.

Bravo, H., J. Olavarria and S. Martinich (1990). "Patterns of interhemispheric and striate-peristriate connections in visual cortex of the South American marsupial Marmosa elegans (mouse opossum)." Anat Embryol (Berl) **182**(6): 583-589.

Briscoe, S. D. and C. W. Ragsdale (2018). "Homology, neocortex and the evolution of developmental mechanisms." Science **362**: 190-193.

Britanova, O., C. de Juan Romero, A. Cheung, K. Y. Kwan, M. Schwark, A. Gyorgy, . . . V. Tarabykin (2008). "Satb2 is a postmitotic determinant for upper-layer neuron specification in the neocortex." Neuron **57**(3): 378-392.

Cabana, T. and G. F. Martin (1985). "The development of commissural connections of somatic motor-sensory areas of neocortex in the North American opossum." Anat Embryol **171**: 121-128.

Calloni, S. F., J. S. Cohen, A. Meoded, J. Juusola, F. M. Triulzi, T. A. G. M. Huisman, . . . A. Fatemi (2017). "Compound heterozygous variants in ROBO1 cause a neurodevelopmental disorder with absence of transverse pontine fibers and thinning of the anterior commissure and corpus callosum." Pediatr Neurol **70**: 70-74.

Campbell, K. and M. Götz (2002). "Radial glia: multi-purpose cells for vertebrate brain development." Trend Neurosci **25**: 235-238.

Cappaert, N. L. M., N. M. Van Strien and M. P. Witter (2015). Hippocampal formation. The rat nervous system. G. Paxinos. San Diego, Academic Press. **4th**.

Cargnin, F., J. S. Kwon, S. Katzman, B. Chen, J. W. Lee and S. K. Lee (2018). "FOXG1 orchestrates neocortical organization and cortico-cortical connections." Neuron **100**: 1083-1096.

Cepko, C. (2014). "Intrinsically different retinal progenitor cells produce specific types of progeny." Nat Rev Neurosci **15**(9): 615-627.

Chen, B., L. R. Schaevitz and S. K. McConnell (2005). "Fezl regulates the differentiation and axon targeting of layer 5 subcortical projection neurons in cerebral cortex." Proc Natl Acad Sci U S A **102**(47): 17184-17189.

Chen, B., S. S. Wang, A. M. Hattox, H. Rayburn, S. B. Nelson and S. K. McConnell (2008). "The Fezf2-Ctip2 genetic pathway regulates the fate choice of subcortical projection neurons in the developing cerebral cortex." Proc Natl Acad Sci U S A **105**(32): 11382-11387.

Chen, K. S., L. Harris, J. W. C. Lim, T. J. Harvey, M. Piper, R. M. Gronostajski, . . . J. Bunt (2017). "Differential neuronal and glial expression of nuclear factor I proteins in the cerebral cortex of adult mice." J Comp Neurol **525**(11): 2465-2483.

Cheung, A. F., S. Kondo, O. Abdel-Mannan, R. A. Chodroff, T. M. Sirey, L. E. Bluy, . . . Z. Molnár (2010). "The subventricular zone is the developmental milestone of a 6-layered neocortex: comparisons in metatherian and eutherian mammals." Cereb Cortex **20**(5): 1071-1081.

Christensen, J., T. Koops Grønborg, M. J. Sørensen, D. Schendel, E. Thorlund Parner, L. Henning Pedersen and M. Vestergaard (2013). "Prenatal valproate exposure and risk of autism spectrum disorders and childhood autism." JAMA **309**: 1696-1703.

Cocchi, L., I. E. Bramati, A. Zalesky, E. Furukawa, L. F. Fontenelle, J. Moll, . . . P. Mattos (2012). "Altered functional brain connectivity in a non-clinical sample of young adults with attention-deficit/hyperactivity disorder." J Neurosci **32**: 17753-17761.

Coghlan, S., J. Horder, B. Inkster, M. A. Mendez, D. G. Murphy and D. J. Nutt (2012). "GABA system dysfunction in autism and related disorders: from synapse to symptoms." Neurosci Biobehav Rev **36**: 2044-2055.

Cooper, J. A. (2008). "A mechanism for inside-out lamination in the neocortex." Trends Neurosci **31**(3): 113-119.

Corbin, J. G., S. Nery and G. Fishell (2001). "Telencephalic cells take a tangent: non-radial migration in the mammalian forebrain." Nat Neurosci **4 Suppl**: 1177-1182.

Csillag, A. and C. M. Montagnese (2005). "Thalamotelencephalic organization in birds." Brain Res Bull **66**: 303-310.

Cubelos, B., C. G. Briz, G. M. Esteban-Ortega and M. Nieto (2014). "Cux1 and Cux2 selectively target basal and apical dendritic compartments of layer II-III cortical neurons." Dev Neurobiol **75**: 163-172.

Cui, Z., C. R. Gerfen and W. S. Young (2013). "Hypothalamic and other connections with dorsal CA2 area of the mouse hippocampus." J Comp Neurol **521**: 1844-1866.

Cummings, D. M., D. Malun and P. C. Brunjes (1996). "Development of the anterior commissure in the opossum: midline extracellular space and glia coincide with early axon decussation." J Neurobiol **32**: 403-414.

D'Arcangelo, G., G. G. Miao, S. C. Chen, H. D. Soares, J. I. Morgan and T. Curran (1995). "A protein related to extracellular matrix protein deleted in the mouse mutant reeler." Nature **374**: 719-723.

Darki, F., S. Massinen, E. Salmela, H. Matsson, M. Peyrard-Janvid, T. Klingberg and J. Kere (2016). "Human ROBO1 regulates white matter structure in corpus callosum." Brain Struct Funct **222**: 707-716.

De Beer, G. R. (1940). Embryos and ancestors. Oxford, Oxford University Press.

De Benedictis, A., L. Petit, M. Descoteaux, C. E. Marras, M. Barbareschi, F. Corsini, . . . S. Sarubbo (2016). "New insights in the homotopic and heterotopic connectivity of the frontal portion of the human corpus callosum revealed by microdissection and diffusion tractography." Human Brain Mapping **37**(12): 4718-4735.

de Frutos, C. A., G. Bouvier, Y. Arai, M. S. Thion, L. Lokmane, M. Keita, . . . S. Garel (2016). "Reallocation of olfactory Cajal-Retzius cells shapes neocortex architecture." Neuron **92**: 435-448.

de Lacoste, M. C., J. B. Kirkpatrick and E. D. Ross (1985). "Topography of the human corpus callosum." J Neuropathol Exp Neurol **44**: 578-591.

de Sousa, A. A. and B. A. Wood (2007). The hominin fossil record and the emergence of the modern human central nervous system. The evolution of primate nervous systems. P. T. M. and K. J. H. Oxford, Academic Press: 291-336.

Deck, M., L. Lokmane, S. Chauvet, C. Mailhes, M. Keita, M. Niquille, . . . S. Garel (2013). "Pathfinding of corticothalamic axons relies on a rendezvous with thalamic projections." Neuron **77**(3): 472-484.

Desai, A. R. and S. K. McConnell (2000). "Progressive restriction in fate potential by neural progenitors during cerebral cortical development." Development **127**: 2863-2872.

Dreher, B. and S. R. Robinson (1988). "Development of the retinofugal pathway in birds and mammals: evidence for a common timetable." Brain Behav Evol **31**: 369-390.

Dugas-Ford, J., J. J. Rowell and C. W. Ragsdale (2012). "Cell-type homologies and the origins of the neocortex." Proc Natl Acad Sci U S A **109**: 16974-16979.

Easton, C. R., K. Weir, A. Scott, S. P. Moen, Z. Barger, A. Folch, . . . W. J. Moody (2014). "Genetic elimination of GABAergic neurotransmission reveals two distinct pacemakers for

spontaneous waves of activity in the developing mouse cortex." J Neurosci **34**(11): 3854-3863.

Economo, M. N., N. G. Clack, L. D. Lavis, C. R. Gerfen, K. Svoboda, E. W. Myers and J. Chandrashekar (2016). "A platform for brain-wide imaging and reconstruction of individual neurons." Elife **5**: e10566.

Eckler, M. J., T. D. Nguyen, W. L. Mckenna, B. L. Fastow, C. Guo, J. L. R. Rubenstein, B. Chen (2015). "Cux2-positive radial glial cells generate diverse subtype of neocortical projection neurons and macroglia." Neuron **86**: 1100-1108.

Englund, C., A. Fink, C. Lau, D. Pham, R. A. Daza, A. Bulfone, . . . R. F. Hevner (2005). "Pax6, Tbr2, and Tbr1 are expressed sequentially by radial glia, intermediate progenitor cells, and postmitotic neurons in developing neocortex." J Neurosci **25**(1): 247-251.

Fame, R. M., J. L. MacDonald, S. L. Dunwoodie, E. Takahashi and J. D. Macklis (2016). "Cited2 regulates neocortical Layer II/III generation and somatosensory callosal projection neuron development and connectivity." J Neurosci **36**(24): 6403-6419.

Fame, R. M., J. L. MacDonald and J. D. Macklis (2011). "Development, specification, and diversity of callosal projection neurons." Trends Neurosci **34**(1): 41-50.

Faunes, M., J. Francisco Botelho, P. Ahumada Galleguillos and J. Mpodozis (2015). "On the hodological criterion for homology." Front Neurosci **9**: 223.

Fenlon, L. R. and L. J. Richards (2015). "Contralateral targeting of the corpus callosum in normal and pathological brain function." Trends Neurosci **38**: 264-272.

Fenlon, L. R., R. Suárez and L. J. Richards (2017). "The anatomy, organisation and development of contralateral callosal projections of the mouse somatosensory cortex." Brain and Neuroscience Advances **1**: 1-9.

Fernandez, A. S., C. Pieau, J. Repérant, E. Boncinelli and M. Wassef (1998). "Expression of the Emx-1 and Dlx-1 homeobox genes define three molecularly distinct domains in the telencephalon of mouse, chick, turtle and frog embryos: implications for the evolution of telencephalic subdivisions in amniotes." Development **125**: 2099-2111.

Flower, W. H. (1865). "On the commissures of the cerebral hemispheres of the Marsupialia and Monotremata as compared with those of the placental mammals." Proc R Soc Lond **14**: 71-74.

Franco, S. J., C. Gil-Sanz, I. Martinez-Garay, A. Espinosa, S. R. Harkins-Perry, C. Ramos and U. Müller (2012). "Fate-restricted neural progenitors in the mammalian cerebral cortex." Science **337**: 746-749.

Frantz, G. D. and S. K. McConnell (1996). "Restriction of late cerebral cortical progenitors to an upper-layer fate." Neuron **17**: 55-61.

Friauf, E., S. K. McConnell and C. J. Shatz (1990). "Functional synaptic circuits in the subplate during fetal and early postnatal development of cat visual cortex." J Neurosci **10**: 2601-2613.

Friauf, E. and C. J. Shatz (1991). "Changing patterns of synaptic input to subplate and cortical plate during development of visual cortex." J Neurophysiol **66**: 2059-2071.

Frotscher, M. (1997). "Dual role of Cajal-Retzius cells and reelin in cortical development." Cell Tissue Res **290**: 315-322.

Funnell, M. G., P. M. Corballis and M. S. Gazzaniga (2000). "Cortical and subcortical interhemispheric interactions following partial and complete callosotomy." Arch Neurol **57**: 185-189.

Galazo, M. J., J. G. Emsley and J. D. Macklis (2016). "Corticothalamic projection neuron development beyond subtype specification: Fog2 and intersectional controls regulate intraclass neuronal diversity." Neuron **91**(1): 90-106.

Gao, P., M. P. Postiglione, T. G. Krieger, L. Hernandez, C. Wang, Z. Han, . . . S. H. Shi (2014). "Deterministic progenitor behavior and unitary production of neurons in the neocortex." Cell **159**(4): 775-788.

Garcez, P. P., N. P. Henrique, D. A. Furtado, J. Bolz, R. Lent and D. Uziel (2007). "Axons of callosal neurons bifurcate transiently at the white matter before consolidating an interhemispheric projection." Eur J Neurosci **25**(5): 1384-1394.

García-Moreno, F. and Z. Molnár (2015). "Subset of early radial glial progenitors that contribute to the development of callosal neurons is absent from avian brain." Proc Natl Acad Sci U S A **112**: e5058-5067.

Gazzaniga, M. S. (2000). "Cerebral specialization and interhemispheric communication: Does the corpus callosum enable the human condition?" Brain **123**: 1293–1326.

Gazzaniga, M. S., J. E. Bogen and R. W. Sperry (1962). "Some functional effects of sectioning the cerebral commissures in man." Proc Natl Acad Sci U S A **48**: 1765–1769.

Ghosh, A., A. Antonini, S. K. McConnell and C. J. Shatz (1990). "Requirement for subplate neurons in the formation of thalamocortical connections." Nature **347**: 179-181.

Ghosh, A. and C. J. Shatz (1993). "A role for subplate neurons in the patterning of connections from thalamus to neocortex." Development **117**: 1031-1047.

Gil-Sanz, C., S. J. Franco, I. Martinez-Garay, A. Espinosa, S. Harkins-Perry and U. Muller (2013). "Cajal-Retzius cells instruct neuronal migration by coincidence signaling between secreted and contact-dependent guidance cues." Neuron **79**(3): 461-477.

Gil-Sanz, A. Espinosa, S. P. Fregoso, K. K. Bluske, C. L. Cunningham, I. Martinez-Garay, H. Zeng, S. J. Franco, U. Müller (2015). "Lineage tracing using Cux2-Cre and Cux2-CreERT2 mice." Neuron **86**:1091-1099.

Gilliam, M., M. Stockman, M. Malek, W. Sharp, D. Greenstein, F. Lalonde, . . . P. Shaw (2011). "Developmental trajectories of the corpus callosum in attention-deficit/hyperactivity disorder." Biol Psychiatry **69**: 839-846.

Gillies, K. and D. J. Price (1993). "The fates of cells in the developing cerebral cortex of normal and methylazoxymethanol acetate-lesioned mice." Eur J Neurosci **5**: 73-84.

Gilmore, E. C. and K. Herrup (1997). "Cortical development: layers of complexity." Curr Biol **7**(4): 231-234.

Glass, H. C., G. M. Shaw, C. Ma and E. H. Sherr (2008). "Agenesis of the corpus callosum in California 1983-2003: a population-based study." Am J Med Genet A **146A**(19): 2495-2500.

Gobius, I., L. Morcom, R. Suárez, J. Bunt, P. Bukshpun, W. Reardon, . . . L. J. Richards (2016). "Astroglial-mediated remodeling of the interhemispheric midline is required for the formation of the corpus callosum." Cell Rep **17**(3): 735-747.

Gobius, I., R. Suárez, L. Morcom, A. Paolino, T. J. Edwards, P. Kozulin and L. J. Richards (2017). "Astroglial-mediated remodeling of the interhemispheric midline during telencephalic development is exclusive to eutherian mammals." Neural Dev **12**(1): 9.

Goffinet, A. M., C. Daumerie, B. Langerwerf and C. Pieau (1986). "Neurogenesis in reptilian cortical structures: 3h-thymidine autoradiographic analysis." J Comp Neurol **243**: 106-116.

Götz, M., A. Stoykova and P. Gruss (1998). "Pax6 controls radial glia differentiation in the cerebral cortex." Neuron **21**: 1031-1044.

Gould, S. J. (1977). Ontogeny and Phylogeny. Cambridge, MA, Belknap Press.

Grant, E., A. Hoerder-Suabedissen and Z. Molnár (2012). "Development of the corticothalamic projections." Front Neurosci **6**: 53.

Greig, L. C., M. B. Woodworth, C. Greppi and J. D. Macklis (2016). "Ctip1 controls acquisition of sensory area identity and establishment of sensory input fields in the developing neocortex." Neuron **90**(2): 261-277.

Guillemot, F. (2007). "Spatial and temporal specification of neural fates by transcription factor codes." Development **134**(21): 3771-3780.

Guillemot, F., Z. Molnár, V. Tarabykin and A. Stoykova (2006). "Molecular mechanisms of cortical differentiation." Eur J Neurosci **23**(4): 857-868.

Guo, C., M. J. Eckler, W. L. McKenna, G. L. McKinsey, J. L. Rubenstein and B. Chen (2013). "Fezf2 expression identifies a multipotent progenitor for neocortical projection neurons, astrocytes, and oligodendrocytes." Neuron **80**(5): 1167-1174.

Hallman, L. E., B. R. Schofield and C. S. Lin (1988). "Dendritic morphology and axon collaterals of corticotectal, corticopontine, and callosal neurons in layer V of primary visual cortex of the hooded rat." J Comp Neurol **272**: 149-160.

Han, W., K. Y. Kwan, S. Shim, M. M. S. Lam, Y. Shin, X. Xu, . . . N. Šestan (2011). "TBR1 directly represses Fezf2 to control the laminar origin and development of the corticospinal tract." Proc Natl Acad Sci U S A **108**: 3041-3046.

Hand, R. and F. Polleux (2011). "Neurogenin2 regulates the initial axon guidance of cortical pyramidal neurons projecting medially to the corpus callosum." Neural Dev **6**: 30.

Hand, R. A., S. Khalid, E. Tam and A. L. Kolodkin (2015). "Axon dynamics during neocortical laminar innervation." Cell Rep **12**(2): 172-182.

Hanson, M. G. and L. T. Landmesser (2004). "Normal patterns of spontaneous activity are required for correct motor axon guidance and the expression of specific guidance molecules." Neuron **43**(5): 687-701.

Harb, K., E. Magrinelli, C. S. Nicolas, N. Lukianets, L. Frangeul, M. Pietri, . . . C. Alfano (2016). "Area-specific development of distinct projection neuron subclasses is regulated by postnatal epigenetic modifications." Elife **5**: e09531.

Harman, A. M., N. J. Eastough and L. D. Beazley (1995). "Development of the visual cortex in a wallaby - phylogenetic implications." Brain Behav Evol **45**: 138-152.

Hatanaka, Y., T. Namikawa, K. Yamauchi, Y. Kawaguchi (2015). "Cortical divergent projections in mice originate from two sequentially generated, distinct populations of excitatory cortical neurons with different initial axonal outgrowth characteristics." Cereb Cortex **26**(5): 2257-2270.

Heath, C. J. and E. G. Jones (1971). "Interhemispheric pathways in the absence of a corpus callosum." J Anat **109**: 253-270.

Hecht, M., Y. Bromberg and B. Rost (2015). "Better prediction of functional effects for sequence variants." BMC Genomics **16**: 1-12.

Hedin-Pereira, C., R. Lent and S. Jhaveri (1999). "Morphogenesis of callosal arbors in the parietal cortex of hamsters." Cereb Cortex **9**: 50-64.

Hevner, R. F., L. Shi, N. Justice, Y. P. Hsueh, M. Sheng, S. Smiga, . . . J. L. R. Rubenstein (2001). "Tbr1 regulates differentiation of the preplate and layer 6." Neuron **29**: 353-366.

Hinkley, L. B., E. J. Marco, A. M. Findlay, S. Honma, R. J. Jeremy, Z. Strominger, . . . E. H. Sherr (2012). "The role of corpus callosum development in functional connectivity and cognitive processing." PLoS One **7**(8): e39804.

Hisaoka, T., Y. Nakamura, E. Senba and Y. Morikawa (2010). "The forkhead transcription factors, Foxp1 and Foxp2, identify different subpopulations of projection neurons in the mouse cerebral cortex." Neuroscience **166**(2): 551-563.

Hoerder-Suabedissen, A. and Z. Molnár (2015). "Development, evolution and pathology of neocortical subplate neurons." Nat Rev Neurosci **16**(3): 133-146.

Hofer, S. and J. Frahm (2006). "Topography of the human corpus callosum revisited: comprehensive fiber tractography using diffusion tensor magnetic resonance imaging." Neuroimage **32**(3): 989-994.

Houzel, J. C., M. L. Carvalho and R. Lent (2002). "Interhemispheric connections between primary visual areas: beyond the midline rule." Braz J Med Biol Res **35**: 1441–1453.

Innocenti, G. (1990). The development of cortical projections. Systems approaches to developmental neurobiology. P. A. R. e. al. New York, Plenum Press.

Jarvis, E. D. (2009). Evolution of the pallium in birds and reptiles. Encyclopedia of Neuroscience. M. D. Binder, N. Hirokawa and U. Windhorst, Springer Berlin Heidelberg**:** 1390-1400.

Jarvis, E. D., O. Güntürkün, L. Bruce, A. Csillag, H. Karten, W. Kuenzel, . . . A. B. Butler (2005). "Avian brains and a new understanding of vertebrate brain evolution." Nat Rev Neurosci **6**: 151-159.

Jones, E. G. (1985). The thalamus. New York, Plenum.

Jones, E. G. (2002). "Thalamic circuitry and thalamocortical synchrony." Philos Trans R Soc Lond B Biol Sci **357**: 1659-1673.

Joshi, P. S., B. J. Molyneaux, L. Feng, X. Xie, J. D. Macklis and L. Gan (2008). "Bhlhb5 regulates the postmitotic acquisition of area identities in layers II-V of the developing neocortex." Neuron **60**(2): 258-272.

Kanold, P. O. and H. J. Luhmann (2010). "The subplate and early cortical circuits." Annu Rev Neurosci **33**: 23-48.

Kanold, P. O. K., P.; Reid, R. C.; Shatz, C. J. (2003). "Role of subplate neurons in functional maturation of visual cortical columns." Science **301**: 521-526.

Kaplan, E. S., K. A. Ramos-Laguna, A. B. Mihalas, R. A. M. Daza and R. F. Hevner (2017). "Neocortical Sox9+ radial glia generate glutamatergic neurons for all layers, but lack discernible evidence of early laminar fate restriction." Neural Dev **12**(1): 14.

Karten, H. J. (1991). "Homology and evolutionary origin of the neocortex." Brain Behav Evol **38**: 264-272.

Karten, H. J. (1997). "Evolutionary developmental biology meets the brain: the origins of mammalian cortex." Proc Natl Acad Sci U S A **94**: 2800-2804.

Kepecs, A. and G. Fishell (2014). "Interneuron cell types are fit to function." Nature **505**(7483): 318-326.

Kim, J., C. J. Matney, A. Blankenship, S. Hestrin and S. P. Brown (2014). "Layer 6 corticothalamic neurons activate a cortical output layer, layer 5a." J Neurosci **34**(29): 9656-9664.

Kim, M. Y., H. Y. Kim, J. Hong, D. Kim, H. Lee, E. Cheong, . . . K. Y. Choi (2016). "CXXC5 plays a role as a transcription activator for myelin genes on oligodendrocyte differentiation." Glia **64**(3): 350-362.

Koester, S. E. and D. D. M. O'Leary (1994). "Axons of early generated neurons in cingulate cortex pioneer the corpus callosum." J Neurosci **14**: 6608-6620.

König, N. and R. Marty (1981). "Early neurogenesis and synaptogenesis in cerebral cortex." Bibl Anat **19**: 152-160.

Kostovic, I. and P. Rakic (1980). "Cytology and time of origin of interstitial neurons in the white matter in infant and adult human and monkey telencephalon." J Neurocyt **9**: 219-242.

Kostovic, I. and P. Rakic (1990). "Developmental history of the transient subplate zone in the visual and somatosensory cortex of the macaque monkey and human brain." J Comp Neurol **297**: 441-470.

Kozulin, P., G. Almarza, I. Gobius and L. J. Richards (2016). Investigating early formation of the cerebral cortex by in utero electroporation: Methods and Protocols. Prenatal and postnatal determinants of development. D. W. Walker. New York, United States, Humana Press. **109:** 3-20.

Kretz, R. and G. Rager (1990). "Reciprocal heterotopic callosal connections between the two striate areas in Tupaia." Exp Brain Res **82**: 271-278.

Kriegstein, A., S. Noctor and V. Martínez-Cedeño (2006). "Patterns of neural stem and progenitor cell division may underlie evolutionary cortical expansion." Nat Rev Neurosci **7**: 883-890.

Krubitzer, L., J. C. Clarey, R. Tweedale and M. B. Calford (1998). "Interhemispheric connections of somatosensory cortex in the flying fox." J Comp Neurol **402**: 538-559.

Labadi, B. and A. M. Beke (2017). "Mental state understanding in children with agenesis of the corpus callosum." Front Psychol **8**.

Lai, T., D. Jabaudon, B. J. Molyneaux, E. Azim, P. Arlotta, J. R. Menezes and J. D. Macklis (2008). "SOX5 controls the sequential generation of distinct corticofugal neuron subtypes." Neuron **57**(2): 232-247.

Lavado, A., M. Ware, J. Pare and X. Cao (2014). "The tumor suppressor Nf2 regulates corpus callosum development by inhibiting the transcriptional coactivator Yap." Development **141**(21): 4182-4193.

Lavdas, A. A. G., M.; Pachnis, V.; Parnavelas, J. G. (1999). "The medial ganglionic eminence gives rise to a population of early neurons in the developing cerebral cortex." J Neurosci **99**: 7881-7888.

Leamey, C. A., K. A. Glendining, G. Kreiman, N. D. Kang, K. H. Wang, R. Fassler, . . . M. Sur (2008). "Differential gene expression between sensory neocortical areas: potential roles for Ten_m3 and Bcl6 in patterning visual and somatosensory pathways." Cereb Cortex **18**(1): 53-66.

Lent, R., D. Uziel, M. Baudrimont and C. Fallet (2005). "Cellular and molecular tunnels surrounding the forebrain commissures of human fetuses." J Comp Neurol **483**(4): 375-382.

Leone, D. P., W. E. Heavner, E. A. Ferenczi, G. Dobreva, J. R. Huguenard, R. Grosschedl and S. K. McConnell (2014). "Satb2 regulates the differentiation of both callosal and subcerebral projection neurons in the developing cerebral cortex." Cereb Cortex **25**: 3406-3419.

Leone, D. P., K. Srinivasan, B. Chen, E. Alcamo and S. K. McConnell (2008). "The determination of projection neuron identity in the developing cerebral cortex." Curr Opin Neurobiol **18**(1): 28-35.

Letzner, S., A. Simon and O. Güntürkün (2016). "Connectivity and neurochemistry of the commissura anterior of the pigeon (Columba livia)." J Comp Neurol **524**: 343-361.

Leventer, R. J., R. Guerrini and W. B. Dobyns (2008). "Malformations of cortical development and epilepsy." Dialogues Clin Neurosci **10**: 47-62.

Li, H., S. A. Shuster, J. Li and L. Luo (2018). "Linking neuronal lineage and wiring specificity." Neural Dev **13**(1): 1-19.

Lickiss, T., A. F. Cheung, C. E. Hutchinson, J. S. Taylor and Z. Molnár (2012). "Examining the relationship between early axon growth and transcription factor expression in the developing cerebral cortex." J Anat **220**(3): 201-211.

Lindwall, C., T. Fothergill and L. J. Richards (2007). "Commissure formation in the mammalian forebrain." Curr Opin Neurobiol **17**(1): 3-14.

Lodato, S. and P. Arlotta (2015). "Generating neuronal diversity in the mammalian cerebral cortex." Annu Rev Cell Dev Biol **31**: 699-720.

Lodato, S., B. J. Molyneaux, E. Zuccaro, L. A. Goff, H. H. Chen, W. Yuan, . . . P. Arlotta (2014). "Gene co-regulation by Fezf2 selects neurotransmitter identity and connectivity of corticospinal neurons." Nat Neurosci **17**: 1046-1054.

López-Bendito, G. and Z. Molnár (2003). "Thalamocortical development: how are we going to get there?" Nat Rev Neurosci **4**(4): 276-289.

Lungu, O. and E. Stip (2012). "Agenesis of corpus callosum and emotional information processing in schizophrenia." Front Psychiatry **3**: 1-8.

Luskin, M. B. (1993). "Restricted proliferation and migration of postnatally generated neurons derived from the forebrain subventricular zone." Neuron **11**: 173-189.

Mallamaci, A., S. Mercurio, L. Muzio, C. Cecchi, C. L. Pardini, P. Gruss and E. Boncinelli (2000). "The lack of Emx2 causes impairment of reelin signaling and defects of neuronal migration in the developing cerebral cortex." J Neurosci **20**: 1109-1118.

Margari, L., R. Palumbi, M. G. Campa, F. F. Operto, M. Buttiglione, F. Craig, . . . A. Verrotti (2016). "Clinical manifestations in children and adolescents with corpus callosum abnormalities." J Neurol **263**(10): 1939-1945.

Marín-Padilla, M. (1998). "Cajal–Retzius cells and the development of the neocortex " Trend Neurosci **21**: 64-71.

Marotte, L. R., C. A. Leamey and P. M. E. Waite (1997). "Timecourse of development of the wallaby trigeminal pathway: iii. thalamocortical and corticothalamic projections." J Comp Neurol **387**: 194-214.

Marotte, L. R. and X. M. Sheng (2000). "Neurogenesis and identification of developing layers in the visual cortex of the wallaby (macropus eugenii)." J Comp Neurol **416**: 131-142.

Marsh, A. P., D. Heron, T. J. Edwards, A. Quartier, C. Galea, C. Nava, . . . C. Depienne (2017). "Mutations in DCC cause isolated agenesis of the corpus callosum with incomplete penetrance." Nat Genet **49**: 511-514.

Martin, G. F., D. Megirian and A. Roebuck (1970). "The corticospinal tract of the marsupial phalanger (Trichosurus vulpecula)." J Comp Neurol: 245-258.

Martínez-Cerdeño, V., S. C. Noctor and A. R. Kriegstein (2006). "The role of intermediate progenitor cells in the evolutionary expansion of the cerebral cortex." Cereb Cortex **16 Suppl 1**: i152-161.

Martinich, S., M. N. Pontes and C. E. Rocha-Miranda (2000). "Patterns of corticocortical, corticotectal, and commissural connections in the opossum visual cortex." J Comp Neurol **416**(2): 224-244.

Matsuda, T. and C. L. Cepko (2004). "Electroporation and RNA interference in the rodent retina in vivo and in vitro." Proc Natl Acad Sci U S A **101**: 16-22.

Matsui, A., A. C. Yoshida, M. Kubota, M. Ogawa and T. Shimogori (2011). "Mouse in utero electroporation: controlled spatiotemporal gene transfection." J Vis Exp(54).

McConnell, S. K. (1988). "Development and decision-making in the mammalian cerebral cortex." Brain Res Rew **13**: 1-23.

McConnell, S. K. (1995). "Constructing the cerebral cortex: neurogenesis and fate determination." Neuron **15**: 761-768.

McConnell, S. K., A. Ghosh and C. J. Shatz (1994). "Subplate pioneers and the formation of descending connections from cerebral cortex." J Neurosci **14**: 1892-1907.

McKenna, W. L., J. Betancourt, K. A. Larkin, B. Abrams, C. Guo, J. L. Rubenstein and B. Chen (2011). "Tbr1 and Fezf2 regulate alternate corticofugal neuronal identities during neocortical development." J Neurosci **31**(2): 549-564.

McKenna, W. L., C. F. Ortiz-Londono, T. K. Mathew, K. Hoang, S. Katzman and B. Chen (2015). "Mutual regulation between Satb2 and Fezf2 promotes subcerebral projection neuron identity in the developing cerebral cortex." Proc Natl Acad Sci U S A **112**(37): 11702-11707.

Medina, L. and A. Reiner (2000). "Do birds possess homologues of mammalian visual, somatosensory, and motor cortices?" Trend Neurosci **23**: 1-12.

Menks, W. M., R. Furger, C. Lenz, L. V. Fehlbaum, C. Stadler and N. M. Raschle (2017). "Microstructural white matter alterations in the corpus callosum of girls with conduct disorder." J Am Acad Child Adolesc Psychiatry **56**: 258-265.

Menks, W. M., C. Stadler and N. M. Raschle (2017). "What can be learned from white matter alterations in antisocial girls." J Neurol Neuromed **2**: 16-20.

Métin, C., J. P. Baudoin, S. Rakic and J. G. Parnavelas (2006). "Cell and molecular mechanisms involved in the migration of cortical interneurons." Eur J Neurosci **23**(4): 894-900.

Meyer, G. (2010). "Building a human cortex: the evolutionary differentiation of Cajal-Retzius cells and the cortical hem." J Anat **217**(4): 334-343.

Mi, D., Z. Li, L. Lim, M. Li, M. Moissidis, Y. Yang, . . . O. Marín (2018). "Early emergence of cortical interneuron diversity in the mouse embryo." Science **360**: 81-85.

Mihrshahi, R. (2006). "The corpus callosum as an evolutionary innovation." J Exp Zool B Mol Dev Evol **306**(1): 8-17.

Mione, M. C., C. Danevic, P. Boardman, B. Harris and J. G. Parnavelas (1994). "Lineage analysis reveals neurotransmitter (GABA or glutamate) but not calcium-binding protein homogeneity in clonally related cortical neurons." J Neurosci **14**: 107-123.

Mizuno, H., T. Hirano and Y. Tagawa (2007). "Evidence for activity-dependent cortical wiring: formation of interhemispheric connections in neonatal mouse visual cortex requires projection neuron activity." J Neurosci **27**(25): 6760-6770.

Mizuno, H., W. Luo, E. Tarusawa, Y. M. Saito, T. Sato, Y. Yoshimura, . . . T. Iwasato (2014). "NMDAR-regulated dynamics of layer 4 neuronal dendrites during thalamocortical reorganization in neonates." Neuron **82**(2): 365-379.

Moffat, J. J., M. Ka, E. M. Jung and W. Y. Kim (2015). "Genes and brain malformations associated with abnormal neuron positioning." Mol Brain **8**(1): 72.

Molliver, M. E. K., I.; Van der Loos, H. (1973). "The development of synapses in cerebral cortex of the human fetus " Brain Res **50**: 403-407.

Molnár, Z. (2011). "Evolution of cerebral cortical development." Brain Behav Evol **78**(1): 94-107.

Molnár, Z. and C. Blakemore (1995). "How do thalamic axons find their way to the cortex?" Trends Neurosci **18**: 289-297.

Molnár, Z., S. Higashi and G. López-Bendito (2003). "Choreography of early thalamocortical development " Cereb Cortex **13**: 661-669.

Molnár, Z. and A. Hoerder-Suabedissen (2016). "Regional scattering of primate subplate." Proc Natl Acad Sci U S A **113**(35): 9676-9678.

Molnár, Z., J. H. Kaas, J. A. de Carlos, R. F. Hevner, E. Lein and P. Nemec (2014). "Evolution and development of the mammalian cerebral cortex." Brain Behav Evol **83**(2): 126-139.

Molnár, Z., G. W. Knott, C. Blakemore and N. R. Saunders (1998). "Development of thalamocortical projections in the South American gray short-tailed opossum (Monodelphis domestica)." J Comp Neurol **398**: 491-514.

Molnár, Z., C. Métin, A. Stoykova, V. Tarabykin, D. J. Price, F. Francis, . . . H. Kennedy (2006). "Comparative aspects of cerebral cortical development." Eur J Neurosci **23**(4): 921-934.

Molyneaux, B. J., P. Arlotta, R. M. Fame, J. L. MacDonald, K. L. MacQuarrie and J. D. Macklis (2009). "Novel subtype-specific genes identify distinct subpopulations of callosal projection neurons." J Neurosci **29**(39): 12343-12354.

Molyneaux, B. J., L. A. Goff, G. L. Rinn and P. Arlotta (2015). "DeCoN:Genome-wide analysis of in vivo transcriptional dynamics during pyramidal neuron fate selection in neocortex." Neuron **85**: 1-14.

Montiel, J. F. and F. Aboitiz (2018). "Homology in amniote brain evolution: the rise of molecular evidence." Brain Behav Evol **91**: 59-64.

Mori, S., J. D. Tournier (2014). "Moving Beyond DTI: High Angular Resolution Diffusion Imaging (HARDI) - Introduction to Diffusion Tensor Imaging" Academic Press.

Morton, S. R. (1978). "An ecological study of Sminthopsis crassicaudata (Marsupialia: Dasyuridae) III. Reproduction and life history." Aust Wildl Res **5**: 183-211.

Muralidharan, B., Z. Khatri, U. Maheshwari, R. Gupta, B. Roy, S. J. Pradhan, . . . S. Tole (2017). "Lhx2 interacts with the NuRD complex and regulates cortical neuron subtype determinants Fezf2 and Sox11." J Neurosci **37**: 194-203.

Naik, R. and S. Galande (2018). "SATB family chromatin organizers as master regulators of tumor progression." Oncogene.

Namiki, S., H. Norimoto, C. Kobayashi, K. Nakatani, N. Matsuki and Y. Ikegaya (2013). "Layer III neurons control synchronized waves in the immature cerebral cortex." J Neurosci **33**(3): 987-1001.

Nery, S., G. Fishell and J. G. Corbin (2002). "The caudal ganglionic eminence is a source of distinct cortical and subcortical cell populations." Nat Neurosci **5**(12): 1279-1287.

Nikouei, K., A. B. Muñoz-Manchado and J. Hjerling-Leffler (2016). "BCL11B_CTIP2 is highly expressed in GABAergic interneurons of the mouse somatosensory cortex." J Chem Neuroanat **71**: 1-5.

Niwa, H., K. Yamamura and J. Miyazaki (1991). "Efficient selection for high-expression transfectants with a novel eukaryotic vector." Gene **108**: 193-200.

Noctor, S. C., V. Martínez-Cerdeño, L. Ivic and A. R. Kriegstein (2004). "Cortical neurons arise in symmetric and asymmetric division zones and migrate through specific phases." Nat Neurosci **7**(2): 136-144.

Nomura, T., M. Takahashi, Y. Hara and N. Osumi (2008). "Patterns of neurogenesis and amplitude of Reelin expression are essential for making a mammalian-type cortex." PLoS One **3**(1): e1454.

Nomura, T., W. Yamashita, H. Gotoh and K. Ono (2018). "Species-specific mechanisms of neuron subtype specification reveal evolutionary plasticity of amniote brain development." Cell Rep **22**(12): 3142-3151.

Norris, C. R. and K. Kalil (1991). "Guidance of callosal axons by radial glia in the developing cerebral cortex." J Neurosci **11**: 3481-3492.

O'Leary, D. D. M. and T. Terashima (1988). "Cortical axons branch to multiple subcortical targets by interstitial axon budding: implications for target recognition and 'waiting periods'." Neuron **1**: 901-910.

Ogawa, M., T. Miyata, K. Nakajima, K. Yagyu, M. Seike, K. Ikenaka, . . . K. Mikoshiba (1995). "The reeler gene-associated antigen on Cajai-Retzius neurons is a crucial molecule for laminar organization of cortical neurons." Neuron **14**: 899-912.

Ohtaka-Maruyama, C., M. Okamoto, K. Endo, M. Oshima, N. Kaneko, H. Okado, T. Miyata, N. Maeda (2018). "Synaptic transmission from subplate neurons controls radial migration of neocortical neurons." Science **360**: 313-317.

Oishi, K., M. Aramaki and K. Nakajima (2016). "Mutually repressive interaction between Brn1/2 and Rorb contributes to the establishment of neocortical layer 2/3 and layer 4." Proc Natl Acad Sci U S A **113**(12): 3371-3376.

Okamoto, M., T. Miyata, D. Konno, H. R. Ueda, T. Kasukawa, M. Hashimoto, . . . A. Kawaguchi (2016). "Cell-cycle-independent transitions in temporal identity of mammalian neural progenitor cells." Nat Commun **7**.

Olavarria, J. and R. C. Van Sluyters (1985). "Organization and postnatal development of callosal connections in the visual cortex of the rat." J Comp Neurol **239**: 1-26.

Owen, R. (1837). "On the structure of the brain in marsupial animals." Phil Trans R Soc Lond **127**: 87-96.

Paolino, A., L. R. Fenlon, P. Kozulin, L. J. Richards and R. Suárez (2018). "Multiple events of gene manipulation via in pouch electroporation in a marsupial model of mammalian forebrain development." J Neurosci Methods **293**: 45-52.

Paolino, A., L. R. Fenlon, R. Suárez and L. J. Richards (2018). "Transcriptional control of long-range cortical projections." Curr Opin Neurobiol **53**: 57-65.

Parnavelas, J. G. B., J. A.; Franke, E.; Luskin, M. B. (1991). "Separate progenitor cells give rise to pyramidal and nonpyramidal neurons in the rat telencephalon." Cereb Cortex **1**: 463-468.

Paterson, A. K. and S. W. Bottjer (2017). "Cortical inter-hemispheric circuits for multimodal vocal learning in songbirds." J Comp Neurol **525**(15): 3312-3340.

Paul, L. K., W. S. Brown, R. Adolphs, J. M. Tyszka, L. J. Richards, P. Mukherjee and E. H. Sherr (2007). "Agenesis of the corpus callosum: genetic, developmental and functional aspects of connectivity." Nat Rev Neurosci **8**(4): 287-299.

Paul, L. K., C. Corsello, D. P. Kennedy and R. Adolphs (2014). "Agenesis of the corpus callosum and autism: a comprehensive comparison." Brain **137**: 1813-1829.

Pearce, A. R. and L. R. Marotte (2003). "The first thalamocortical synapses are made in the cortical plate in the developing visual cortex of the wallaby (Macropus eugenii)." J Comp Neurol **461**(2): 205-216.

Pearson, B. J. and C. Q. Doe (2004). "Specification of temporal identity in the developing nervous system." Annu Rev Cell Dev Biol **20**: 619-647.

Pires-Neto, M. A., S. Braga de Souza and R. Lent (1998). "Molecular tunnels and boundaries for growing axons in the anterior commissure of hamster embryos " J Comp Neurol **339**: 176-188.

Pires-Neto, M. A. and R. Lent (1993). "The prenatal development of the anterior commissure in hamsters: pioneer fibers lead the way." Brain Res Dev Brain Res **72**: 59-66.

Poiley, S. (1960). "A systematic method of breeder rotation for non-inbred laboratory animal colonies." Proc Anim Care Panel **10**: 159-166.

Price, J. L. (1973). "An autoradiographic study of complementary laminar patterns of termination of afferent fibers to the olfactory cortex." J Comp Neurol **150**: 87-108.

Puelles, L., E. Kuwana, E. Puelles, A. Bulfone, K. Shimamura, J. Keleher, . . . J. L. R. Rubenstein (2000). "Pallial and subpallial derivatives in the embryonic chick and mouse telencephalon, traced by the expression of the genes Dlx2, Emx1, Nkx2.1, Pax6, and Tbr1." J Comp Neurol **424**: 409-438.

Putnam, S. J., D. Megirian and J. W. Manning (1968). "Marsupial interhemispheric relation." J Comp Neurol **132**: 227-234.

Puzzolo, E. and A. Mallamaci (2010). "Cortico-cerebral histogenesis in the opossum Monodelphis domestica: generation of a hexalaminar neocortex in the absence of a basal proliferative compartment." Neural Dev **5**: 8.

Rakic, P. (1977). "Prenatal development of the visual system in rhesus monkey." Phil Trans R Soc Lond **278**: 245-260.

Rakic, P. (1995). "A small step for the cell, a giant leap for mankind- a hypothesis of neocortical expansion during evolution." Trend Neurosci **18**: 383-388.

Rakic, P. (2009). "Evolution of the neocortex: a perspective from developmental biology." Nat Rev Neurosci **10**(10): 724-735.

Ramos, R. L., M. T. Danny and J. C. Brumberg (2008). "Physiology and morphology of callosal projection neurons in mouse." Neuroscience **153**: 654-663.

Rash, B. G. and L. J. Richards (2001). "A role for cingulate pioneering axons in the development of the corpus callosum." J Comp Neurol **434**: 147-157.

Reep, R. L. (2000). "Cortical layer VII and persistent subplate cells in mammalian brains." Brain Behav Evol **56**: 212-234.

Reillo, I., C. de Juan Romero, A. Cárdenas, F. Clascá, M. A. Martínez-Martinez and V. Borrell (2017). "A complex code of extrinsic influences on cortical progenitor cells of higher mammals." Cereb Cortex **27**(9): 4586-4606.

Reynolds, M. L. (1985). "Postnatal development of the telenecephalon of the tammar wallaby (Macropus eugenii)." Anat Embryol **173**: 81-94.

Richards, L. J., S. E. Koester, R. Tuttle and D. D. M. O'Leary (1997). "Directed growth of early cortical axons is influenced by a chemoattractant released from an intermediate target." J Neurosci **17**: 2445-2458.

Robinson, S. R. (1982). "Interocular transfer in a marsupial: the brushed-tailed possum (Trichosurus vulpecula)." Brain Behav **21**: 114-124.

Rodríguez-Tornos, F. M., C. G. Briz, L. A. Weiss, A. Sebastián-Serrano, S. Ares, M. Navarrete, . . . M. Nieto (2016). "Cux1 enables Interhemispheric connections of layer II/III neurons by regulating Kv1-dependent firing." Neuron **89**(3): 494-506.

Rossi, A. M., V. M. Fernandes and C. Desplan (2016). "Timing temporal transitions during brain development." Curr Opin Neurobiol **42**: 84-92.

Rudy, B., G. Fishell, S. Lee and J. Hjerling-Leffler (2011). "Three groups of interneurons account for nearly 100% of neocortical GABAergic neurons." Dev Neurobiol **71**(1): 45-61.

Santacana, M., M. Heredia and F. Valverde (1992). "Transient pattern of exuberant projections of olfactory axons during development in the rat." Dev Brain Res **70**: 213-222.

Sarkar, S., M. C. Craig, M. Catani, F. Dell'Acqua, T. Fahy, Q. Deeley and D. G. M. Murphy (2013). "Frontotemporal white-matter microstructural abnormalities in adolescents with conduct disorder: a diffusion tensor imaging study." Psychol Med **43**(2): 401-411.

Sarnat, H. B. (2007). Embryology and malformations of the forebrain commissures. Handbook of Clinical Neurology. Elsevier. **87**: 67-87.

Sauerland, C., B. R. Menzies, M. Glatzle, J. Seeger, M. B. Renfree and S. A. Fietz (2016). "The basal radial glia occurs in marsupials and underlies the evolution of an expanded neocortex in therian mammals." Cereb Cortex **28**: 145-157.

Schindelin, J., I. Arganda-Carreras, E. Frise, V. Kaynig, M. Longair, T. Pietzsch, . . . A. Cardona (2012). "Fiji: an open-source platform for biological-image analysis." Nat Methods **9**(7): 676-682.

Schneider, N. Y. (2011). "The development of the olfactory organs in newly hatched monotremes and neonate marsupials." J Anat **219**(2): 229-242.

Schneider, N. Y., T. P. Fletcher, G. Shaw and M. B. Renfree (2009). "The olfactory system of the tammar wallaby is developed at birth and directs the neonate to its mother's pouch odours." Reproduction **138**(5): 849-857.

Schwartz, M. L., P. Rakic and P. S. Goldman-Rakic (1991). "Early phenotype expression of cortical neurons: evidence that a subclass of migrating neurons have callosal axons." Proc Natl Acad Sci U S A **88**: 1354-1358.

Seelke, A. M., J. C. Dooley and L. A. Krubitzer (2013). "Differential changes in the cellular composition of the developing marsupial brain." J Comp Neurol **521**(11): 2602-2620.

Seelke, A. M., J. C. Dooley and L. A. Krubitzer (2014). "The cellular composition of the marsupial neocortex." J Comp Neurol **522**(10): 2286-2298.

Semmler, H., M. Chiodin, X. Bailly, P. Martinez and A. Wanninger (2010). "Steps towards a centralized nervous system in basal bilaterians: insights from neurogenesis of the acoel Symsagittifera roscoffensis." Dev Growth Differ **52**: 701-713.

Sessa, A., C. A. Mao, A. K. Hadjantonakis, W. H. Klein and V. Broccoli (2008). "Tbr2 directs conversion of radial glia into basal precursors and guides neuronal amplification by indirect neurogenesis in the developing neocortex." Neuron **60**(1): 56-69.

Shang, E., K. W. S. Ashwell, L. R. Marotte and P. M. E. Waite (1997). "Development of commissural neurons in the wallaby (Macropus eugenii)." J Comp Neurol **387**: 507-523.

Sheng, X. M., L. R. Marotte and R. F. Mark (1990). "Development of connections to and from the visual cortex in the wallaby (Macropus eugenii)." J Comp Neurol **300**(2): 196-210.

Shinohara, Y., A. Hosoya, K. Yahagi, A. S. Ferecskó, K. Yaguchi, A. Sík, . . . H. Hirase (2012). "Hippocampal CA3 and CA2 have distinct bilateral innervation patterns to CA1 in rodents." Eur J Neurosci **35**: 702-710.

Shoukimas, G. M. and J. W. Hinds (1978). "The development of the cerebral cortex in the embryonic mouse: an electron microscopic serial section analysis " J Comp Neurol **179**: 795-830.

Shu, T. (2003). "The glial sling is a migratory population of developing neurons." Development **130**(13): 2929-2937.

Shu, T., A. C. Puche and L. J. Richards (2003). "Development of midline glial populations at the corticoseptal boundary." J Neurobiol **57**(1): 81-94.

Shu, T. and L. J. Richards (2001). "Cortical axon guidance by the glial wedge during the development of the corpus callosum." J Neurosci **21**: 2749-2758.

Silver, J. (1993). "Glia-neuron interactions at the midline of the developing mammalian brain and spinal cord." Perspect Dev Neurobiol **1**: 227-236.

Silver, J., S. E. Lorenz, D. Wahlsten and J. Coughlin (1982). "Axonal guidance during development of the great cerebral commissures: descriptive and experimental studies, in vivo, on the role of preformed glial pathways." J Comp Neurol **210**: 10-29.

Sloniewski, P., K. G. Usunoff and C. Pilgrim (1986). "Retrograde transport of fluorescent tracers reveals extensive ipsi- and contralateral claustrocortical connections in the rat." J Comp Neurol **246**: 467-477.

Smart, I. H. M. and M. Smart (1982). "Growth patterns in the lateral wall of the mouse telencephalon: I. Autoradiographic studies of the histogenesis of the isocortex and adjacent areas." J Anat **134**: 273-298.

Smith, G. E. (1902). "On a peculiarity of the cerebral commissures in certain Marsupialia, not hitherto recognised as a distinctive feature of the Diprotodontia." Proc R Soc Lond **70**: 226-231.

Smith, J. B. and K. D. Alloway (2014). "Interhemispheric claustral circuits coordinate sensory and motor cortical areas that regulate exploratory behaviors." Front Syst Neurosci **8**: 93.

Smith, K. K. (2001). "Early development of the neural plate, neural crest and facial region of marsupials." J Anat **199**: 121-131.

Smith, K. M., Y. Ohkubo, M. E. Maragnoli, M. R. Rasin, M. L. Schwartz, N. Sestan and F. M. Vaccarino (2006). "Midline radial glia translocation and corpus callosum formation require FGF signaling." Nat Neurosci **9**(6): 787-797.

Son, A. I., K. Hashimoto-Torii, P. Rakic, P. Levitt and M. Torii (2016). "Epha4 has distinct functionality from Epha7 in the corticothalamic system during mouse brain development." J Comp Neurol **524**: 2080-2092.

Srinivasan, K., D. P. Leone, R. K. Bateson, G. Dobreva, Y. Kohwi, T. Kohwi-Shigematsu, . . . S. K. McConnell (2012). "A network of genetic repression and derepression specifies projection fates in the developing neocortex." Proc Natl Acad Sci U S A **109**: 19071-19078.

Srivatsa, S., S. Parthasarathy, O. Britanova, I. Bormuth, A. L. Donahoo, S. L. Ackerman, . . . V. Tarabykin (2014). "Unc5C and DCC act downstream of Ctip2 and Satb2 and contribute to corpus callosum formation." Nat Commun **5**: 1-15.

Striedter, G. F. (1997). "The telencephalon of tetrapods in evolution." Brain Behav Evol **49**: 179-213.

Striedter, G. F. and S. Beydler (1997). "Distribution of radial glia in the developing telencephalon of chicks." J Comp Neurol **387**: 399-420.

Striedter, G. F. and B. P. Keefer (2000). "Cell migration and aggregation in the developing telencephalon: pulse-labeling chick embryos with bromodeoxyuridine." J Neurosci **20**: 8021-8030.

Suárez, R. (2017). Evolution of telencephalic commissures: conservation and change of developmental systems in the origin of brain wiring novelties. Evolution of Nervous Systems. United Kingdom Academic Press: 205-223.

Suárez, R., L. R. Fenlon, R. Marek, L. Avitan, P. Sah, G. J. Goodhill and L. J. Richards (2014). "Balanced interhemispheric cortical activity is required for correct targeting of the corpus callosum." Neuron **82**(6): 1289-1298.

Suárez, R., I. Gobius and L. J. Richards (2014). "Evolution and development of interhemispheric connections in the vertebrate forebrain." Front Human Neurosci **8**: 1-14.

Suárez, R., A. Paolino, L. R. Fenlon, L. R. Morcom, P. Kozulin, N. D. Kurniawan and L. J. Richards (2018). "A pan-mammalian map of interhemispheric brain connections predates the evolution of the corpus callosum." Proc Natl Acad Sci U S A **115**(38): 9622-9627.

Suárez, R., A. Paolino, P. Kozulin, L. R. Fenlon, L. R. Morcom, R. Englebright, . . . L. J. Richards (2017). "Development of body, head and brain features in the Australian fat-tailed dunnart (Sminthopsis crassicaudata; Marsupialia: Dasyuridae); A postnatal model of forebrain formation." PLoS One **12**(9): e0184450.

Sugitani, Y., S. Nakai, O. Minowa, M. Nishi, K. Jishage, H. Kawano, . . . T. Noda (2002). "Brn-1 and Brn-2 share crucial roles in the production and positioning of mouse neocortical neurons." Genes & Development **16**(1): 1760-1765.

Swanson, L. W., J. D. Hahn and O. Sporns (2017). "Organizing principles for the cerebral cortex network of commissural and association connections." Proc Natl Acad Sci U S A **114**(45): E9692-E9701.

Swayze, V. W., N. C. Andreasen, J. C. Ehrhardt, W. T. C. Yuh, R. J. Alliger and G. A. Cohen (1990). "Developmental abnormalities of the corpus callosum in schizophrenia." Arch Neurol **47**: 805-808.

Tabata, H. and K. Nakajima (2008). "Labeling embryonic mouse central nervous system cells by in utero electroporation." Dev Growth Differ **50**(6): 507-511.

Takahashi, T., T. Goto, S. Miyama, R. S. Nowakowski and V. S. Caviness Jr (1999). "Sequence of neuron origin and neocortical laminar fate- relation to cell cycle of origin in the developing murine cerebral wall." J Neurosci **19**: 10357-10371.

Takiguchi-Hayashi, K., M. Sekiguchi, S. Ashigaki, M. Takamatsu, H. Hasegawa, R. Suzuki-Migishima, . . . Y. Tanabe (2004). "Generation of reelin-positive marginal zone cells from the caudomedial wall of telencephalic vesicles." J Neurosci **24**(9): 2286-2295.

Taniguchi, Y., T. Young-Pearse, A. Sawa and A. Kamiya (2012). "In utero electroporation as a tool for genetic manipulation in vivo to study psychiatric disorders: from genes to circuits and behaviors." Neuroscientist **18**(2): 169-179.

Ten Donkelaar, H. J. (1982). "Organization of descending pathways to the spinal cord in amphibians and reptiles." Progress in brain research. Elsevier **57**: 25-67.

Ten Donkelaar, H. J. (1988). "Evolution of the red nucleus and rubrospinal tract." Behav Brain Res **28**: 9-20.

Thieler, K. (1989). The house mouse: atlas of embryonic development. New York, Springer-Verlag.

Thomson, A. M. (2010). "Neocortical layer 6, a review." Front Neuroanat **4**: 13.

Tole, S., G. Gutin, L. Bhatnagar, R. Remedios and J. M. Hébert (2005). "Development of midline cell types and commissural axon tracts requires Fgfr1 in the cerebrum." Dev Biol **289**: 141-151.

Torii, M., P. Rakic and P. Levitt (2013). "Role of EphA/ephrin--a signaling in the development of topographic maps in mouse corticothalamic projections." J Comp Neurol **521**(3): 626-637.

Tosches, M. A., T. M. Yamawaki, R. K. Naumann, A. A. Jacobi, G. Tushev and G. Laurent (2018). "Evolution of pallium, hippocampus, and cortical cell types revealed by single-cell transcriptomics in reptiles." Science **360**: 881-888.

Tovar-Moll, F., J. Moll, R. de Oliveira-Souza, I. Bramati, P. A. Andreiuolo and R. Lent (2007). "Neuroplasticity in human callosal dysgenesis: a diffusion tensor imaging study." Cereb Cortex **17**(3): 531-541.

Tovar-Moll, F., M. Monteiro, J. Andrade, I. E. Bramati, R. Vianna-Barbosa, T. Marins, . . . R. Lent (2014). "Structural and functional brain rewiring clarifies preserved interhemispheric transfer in humans born without the corpus callosum." Proc Natl Acad Sci U S A **111**(21): 7843-7848.

Trehout, M., E. Leroux, N. Delcroix and S. Dollfus (2017). "Relationships between corpus callosum and language lateralization in patients with schizophrenia and bipolar disorders." Bipolar Disord **19**: 496-504.

Tremblay, R., S. Lee and B. Rudy (2016). "GABAergic interneurons in the neocortex: from cellular properties to circuits." Neuron **91**(2): 260-292.

van Meer, N., A. C. Houtman, P. Van Schuerbeek, T. Vanderhasselt, C. Milleret and M. P. Ten Tusscher (2016). "Interhemispheric connections between the primary visual cortical areas via the anterior commissure in human callosal Agenesis." Front Syst Neurosci **10**: 101.

Wada, K., C. C. Chen and E. D. Jarvis (2017). Molecular profiling reveals insight into avian brain organization and functional columnar commonalities with mammals. Brain Evolution by Design, Diversity and Commonality in Animals. S. S. e. a. (eds.). Japan, Springer.

Wang, C. L., L. Zhang, Y. Zhou, J. Zhou, X. J. Yang, S. M. Duan, . . . Y. Q. Ding (2007). "Activity-dependent development of callosal projections in the somatosensory cortex." J Neurosci **27**(42): 11334-11342.

Wang, G. and S. A. Scott (2000). "The “waiting period” of sensory and motor axons in early chick hindlimb: its role in axon pathfinding and neuronal maturation." J Neurosci **20**: 5358-5366.

Wang, Q., L. Ng, J. A. Harris, D. Feng, Y. Li, J. J. Royall, . . . H. Zeng (2016). "Organization of the connections between claustrum and cortex in the mouse." J Comp Neurol **525**: 1317-1346.

Wang, W. Z., F. M. Oeschger, J. F. Montiel, F. García-Moreno, A. Hoerder-Suabedissen, L. Krubitzer, . . . Z. Molnár (2011). "Comparative aspects of subplate zone studied with gene expression in sauropsids and mammals." Cereb Cortex **21**(10): 2187-2203.

Wang, Y., A. Brzozowska-Prechtl and H. J. Karten (2010). "Laminar and columnar auditory cortex in avian brain." Proc Natl Acad Sci U S A **107**: 12676-12681.

Ware, M., V. Dupe and F. R. Schubert (2015). "Evolutionary conservation of the early axon scaffold in the vertebrate brain." Dev Dyn **244**: 1202-1214.

Wass, S. (2011). "Distortions and disconnections: disrupted brain connectivity in autism." Brain Cogn **75**(1): 18-28.

Watson, C. R. R. and B. W. Freeman (1977). "The corticospinal tract in the kangaroo." Brain Behav Evol **14**: 341-351.

Webster, D. M. S., L. H. Rogers, J. D. Pettigrew and J. D. Steeves (1990). "Origins of descending spinal pathways in prehensile birds: do parrots have a homologue to the corticospinal tract of mammals?" Brain Behav Evol **36**: 216-226.

Welniarz, Q., I. Dusart and E. Roze (2016). "The corticospinal tract: Evolution, development, and human disorders." Dev Neurobiol **77**: 810-829.

Wichterle, H. T., D. H.; Nery, S.; Fishell, G.; Alvarez-Buylla, A. (2001). "In utero fate mapping reveals distinct migratory pathways and fates of neurons born in the mammalian basal forebrain." Development **128**: 3759-3771.

Wise, S. P. and E. G. Jones (1978). "Developmental studies of thalamocortical and commissural connection in the rat somatic sensory cortex." J Comp Neurol **178**: 187-208.

Witelson, S. F. (1985). "The brain connection: The corpus callosum is larger in left-handers." Science **229**: 665-668.

Woodworth, M. B., L. C. Greig, K. X. Liu, G. C. Ippolito, H. O. Tucker and J. D. Macklis (2016). "Ctip1 regulates the balance between specification of distinct projection neuron subtypes in deep cortical layers." Cell Rep **15**(5): 999-1012.

Yorke, C. H. and V. S. Caviness (1975). "Interhemispheric neocortical connections of the corpus callosum in the normal mouse: a study based on anterograde and retrograde methods." J Comp Neurol **164**: 233-245.

Yoshida, M., S. Assimacopoulos, K. R. Jones, E. A. Groves (2006). "Massive loss of Cajal-Retzius cells does not disrupt neocortical layer order." Development **133**: 537-545.

Zhang, J., X. Zhu, X. Wang, J. Gao, H. Shi, B. Huang, . . . S. Yao (2014). "Increased structural connectivity in corpus callosum in adolescent males with conduct disorder." J Am Acad Child Adolesc Psychiatry **53**(4): 466-475 e461.

Zhang, L., N. N. Song, J. Y. Chen, Y. Huang, H. Li and Y. Q. Ding (2012). "Satb2 is required for dendritic arborization and soma spacing in mouse cerebral cortex." Cereb Cortex **22**(7): 1510-1519.

Zhou, J., Y. Wen, L. She, Y. N. Sui, L. Liu, L. J. Richards and M. M. Poo (2013). "Axon position within the corpus callosum determines contralateral cortical projection." Proc Natl Acad Sci U S A **110**(29): E2714-2723.

Appendix 1

ANALYSIS of protein Homology for CTIP2

```
ctip2td         MSRRKQGNPQHLSQRETITPEADHVEAAIVDEDEGLEIEEPGGLGLTAGGTDPDLLTCGQ
ctip2du         MSRRKQGNPQHLSQRETITPEADHVEAAIVDEDEGLEIEEPGGLGLTAGGTDPDLLTCGQ
ctip2op         MSRRKQGNPQHLSQRETITPEADHVEAAIVDEDEGLEIEEPGGLGLTTGGTDPDLLTCGQ
ctip2hu         MSRRKQGNPQHLSQRELITPEADHVEAAILEEDEGLEIEEPSGLGLMVGGPDPDLLTCGQ
ctip2do         MSRRKQGNPQHLSQRELITPEADHVEAAILEEDEGLEIEEPSSLGLMVGGPDPDLLTCGQ
ctip2mo         MSRRKQGNPQHLSQRELITPEADHVEATILEEDEGLEIEEPSSLGLMVGGPDPDLLTCGQ
ctip2ra         MSRRKQGNPQHLSQRELITPEADHVEAAILEEDEGLEIEEPSSLGLMVGGPDPDLLTCGQ
                ****************:**********:*::**********..*** .**.*********

ctip2td         CQMNFPLRDILVFIEHKKKQCSGSLGVCYEKSLDKSSPPPSSRSELRKVSEPVEIGIQVT
ctip2du         CQMNFPLRDILVFIEHKKKQCSGSLGVCYEKSLDKSSPPPSSRSELRKVSEPVEIGIQVT
ctip2op         CQMNFPLRDILVFIEHKKKQCSGSLGVCYEKSLDKSSPPPSSRSELRKVSEPVEIGIQVT
ctip2hu         CQMNFPLGDILVFIEHKRKQCGGSLGACYDKALDKDSPPPSSRSELRKVSEPVEIGIQVT
ctip2do         CQMNFPLGDILVFIEHKKKQCGGSLGACYDKGLDKGSPPPSSRSELRKVSEPVEIGIQVT
ctip2mo         CQMNFPLGDILVFIEHKKKQCG-GLGPCYDKVLDKSSPPPSSRSELRRVSEPVEIGIQVT
ctip2ra         CQMNFPLGDILVFIEHKKKQCG-GLGSCYDKVLDKGSPPPSSRSELRRVSEPVEIGIQVT
                ******* *********:***. .** **:* ***.***********:************

ctip2td         PDEEDRLLTPTKGICPKQENIAGPSRPAKLPAAP--LTASSHPHTSVITPPLRTLASLPP
ctip2du         PDEEDRLLTPTKGICPKQENIAGPSRPAKLPAAP--ITASSHPHTSVITPPLRTLASLPP
ctip2op         PDEDDRLLTPTKGICPKQENIAGPSRPAKLPAAP--ITASSHPHTSVITPPLRSLASLPP
ctip2hu         PDEDDHLLSPTKGICPKQENIAGPCRPAQLPAVAPIAASS-HPHSSVITSPLRALGALPP
ctip2do         PDEDDHLLSPTKGICPKQENIAGPCRPAQLPATAPIAASS-HPHSSVITPPLRTLGALPP
ctip2mo         PDEDDHLLSPTKGICPKQENIAGPCRPAQLPSMAPIAASSSHPPTSVITSPLRALGVLPP
ctip2ra         PDEDDHLLSPTKGICPKQENIAGPCRPAQLPSMAPIAASSSHPPTSVITSPLRALGVLPP
                ***:*:**:***************.***:**: .   ::* ** :****.***:*. ***

ctip2td         CFSLPCCAGHSVSVGGTQAESQTETSGTFGCHCQLSGKDEPSSYICTTCKQPFNSAWFLL
ctip2du         CFSLPCCAGHSVSVGGTQAESQTETSGTFGCHCQLSGKDEPSSYICTTCKQPFNSAWFLL
ctip2op         CFSLPCCAGHSVSVGGTQAESQTDTSGTFGCHCQLSGKDEPSSYICTTCKQPFNSAWFLL
ctip2hu         CLPLPCCSARPVSGDGTQGEGQTEAP--FGCQCQLSGKDEPSSYICTTCKQPFNSAWFLL
ctip2do         CFPLPCCSARPVSGDGTQGEGQTEAP--FGCQCQLSGKDEPSSYICTTCKQPFNSAWFLL
ctip2mo         CFPLPCCGARPISGDGTQGEGQMEAP--FGCQCELSGKDEPSSYICTTCKQPFNSAWFLL
ctip2ra         CFPLPCCGARPISGDGTQGEGQMEAP--FGCQCKD----EPSSYICTTCKQPFNSAWFLL
                *:.****..:.:* .***.*.* ::.  ***:*:     ********************

ctip2td         QHAQNTHGFRIYLETSPSNSSLTPRITIPPPLGPEAVAQSPLMNFLGDNNPFSLLRMTGP
ctip2du         QHAQNTHGFRIYLETSPSNSSLTPRITIPPPLGPEAVAQSPLMNFLGDNNPFSLLRMTGP
ctip2op         QHAQNTHGFRIYLETSPSNSSLTPRITIPPPLGPEAVAQSPLMNFLGDNNPFSLLRMTGP
ctip2hu         QHAQNTHGFRIYLEPGPASSSLTPRLTIPPPLGPEAVAQSPLMNFLGDSNPFNLLRMTGP
ctip2do         QHAQNTHGFRIYLEPGPASSSLTPRLTIPPPLGPEAVAQSPLMNFLGDSNPFNLLRMTGP
ctip2mo         QHAQNTHGFRIYLEPGPASTSLTPRLTIPPPLGPETVAQSPLMNFLGDSNPFNLLRMTGP
ctip2ra         QHAQNTHGFRIYLEPGPASTSLTPRLTIPPPLGPEAVAQSPLMNFLGDSNPFNLLRMTGP
```

```
                **************..*:.:*****:*********:************.***.*******

ctip2td         ILRDHPGFGEGRLPNTPPLFSPPPRHHLDPHRLRAEAMGLVAQHPSAFDRVMRLNPMAID
ctip2du         ILRDHPGFGEGRLPNTPPLFSPPPRHHLDPHRLSAEEMGLVAQHPSAFDRVMRLNPMAID
ctip2op         ILRDHPGFGEGRLPNTPPLFSPPPRHHLDPHRLSAEEMGLVAQHPSAFDRVMRLNPMAID
ctip2hu         ILRDHPGFGEGRLPGTPPLFSPPPRHHLDPHRLSAEEMGLVAQHPSAFDRVMRLNPMAID
ctip2do         ILRDHPGFGEGRLPGTPPLFSPPPRHHLDPHRLSAEEMGLVAQHPSAFDRVMRLNPMAID
ctip2mo         ILRDHPGFGEGRLPGTPPLFSPPPRHHLDPHRLSAEEMGLVAQHPSAFDRVMRLNPMAID
ctip2ra         ILRDHPGFGEGRLPGTPPLFSPPPRHHLDPHRLSAEEMGLVAQHPSAFDRVMRLNPMAID
                **************.****************** ** **********************

ctip2td         SPAMDFSRRLRELAGNNSTPPPVSPNRSNPMHRLLNPFQPSPKSPFMSTPPLPPMPPSST
ctip2du         SPAMDFSRRLRELAGNNSTPPPVSPNRSNPMHRLLNPFQPSPKSPFMSTPPLPPMPPSST
ctip2op         SPAMDFSRRLRELAGNNSTPPPVSPNRSNPMHRLLNPFQPSPKSPFLSTPPLPPMPPSST
ctip2hu         SPAMDFSRRLRELAGNSSTPPPVSPGRGNPMHRLLNPFQPSPKSPFLSTPPLPPMPPGGT
ctip2do         SPAMDFSRRLRELAGNSSTPPPVSPGRGNPMHRLLNPFQPSPKSPFLSTPPLPPMPPGGT
ctip2mo         SPAMDFSRRLRELAGNSSTPPPVSPGRGNPMHRLLNPFQPSPKSPFLSTPPLPPMPAG-T
ctip2ra         SPAMDFSRRLRELAGNSSTPPPVSPGRGNPMHRLLNPFQPSPKSPFLSTPPLPPMPTG-T
                ****************.********.*.******************:*********.. *

ctip2td         TPPQPQAKSKSCEFCGKTFKFQSNLIVHRRSHTGEKPYKCQLCDHACSQASKLKRHMKTH
ctip2du         TPPQPQAKSKSCEFCGKTFKFQSNLIVHRRSHTGEKPYKCQLCDHACSQASKLKRHMKTH
ctip2op         TPPQPQAKSKSCEFCGKTFKFQSNLIVHRRSHTGEKPYKCQLCDHACSQASKLKRHMKTH
ctip2hu         PPPQPPAKSKSCEFCGKTFKFQSNLIVHRRSHTGEKPYKCQLCDHACSQASKLKRHMKTH
ctip2do         PPPQPPAKSKSCEFCGKTFKFQSNLIVHRRSHTGEKPYKCQLCDHACSQASKLKRHMKTH
ctip2mo         PPPQPPAKSKSCEFCGKTFKFQSNLIVHRRSHTGEKPYKCQLCDHACSQASKLKRHMKTH
ctip2ra         PPPQPPAKSKSCEFCGKTFKFQSNLIVHRRSHTGEKPYKCQLCDHACSQASKLKRHMKTH
                .**** ***************************************************

ctip2td         MHKAGSMTGRSDDGLSTTSSPEPGTSELTGEGLKSSEADFRNE-SDPSLG---HDNEEEE
ctip2du         MHKAGSMTGRSDDGLSTTSSPEPGTSELTGEGLKSSEADFRNE-SDPSLG---HDNEEEE
ctip2op         MHKAGSMTGRSDDGLSTTSSPEPGTSELTGEGLKSSEADFRNE-SDPSLG---HDNEEEE
ctip2hu         MHKAGSLAGRSDDGLSAASSPEPGTSELAGEGLKAADGDFRHHESDPSLGHEPEEEDEEE
ctip2do         MHKAGSLAGRSDDGLSAASSPEPGTSELAGEGLKAADGDFRHHESDPSLGHEPEEDDEEE
ctip2mo         MHKAGSLAGRSDDGLSAASSPEPGTSELPGD-LKAADGDFRHHESDPSLGPEPED-DEDE
ctip2ra         MHKAGSLAGRSDDGLSAASSPEPGTSELPGD-LKAADGDFRHHESDPSLGPEPED-DEDE
                ******::********::**********.*: **::::.***:. ******   .: :*:*

ctip2td         EEEEEEEELENESRPESSFSMDSELSRNRENG----------------------------
ctip2du         EEEEEEE-LENESRPESSFSMDSELSRNRENG----------------------------
ctip2op         EEEEEEEELENESRPESSFSMDSELSRNRENG----------------------------
ctip2hu         EEEEEELLLENESRPESSFSMDSELSRNRENGGGGVPGVPGAGG----------------
ctip2do         EEEEEELLLENESRPESSFSMDSELSRNRENGGVGGVGVGVGGVGGVGVGVAGGVGVGVG
ctip2mo         EEEEEELLLENESRPESSFSMDSELGRGRENGGGVPPGVAGAG----------------
ctip2ra         EEEEEELLLENESRPESSFSMDSELGRGRENGGGVPPGVAGAG----------------
                ******  *****************.*.****
```

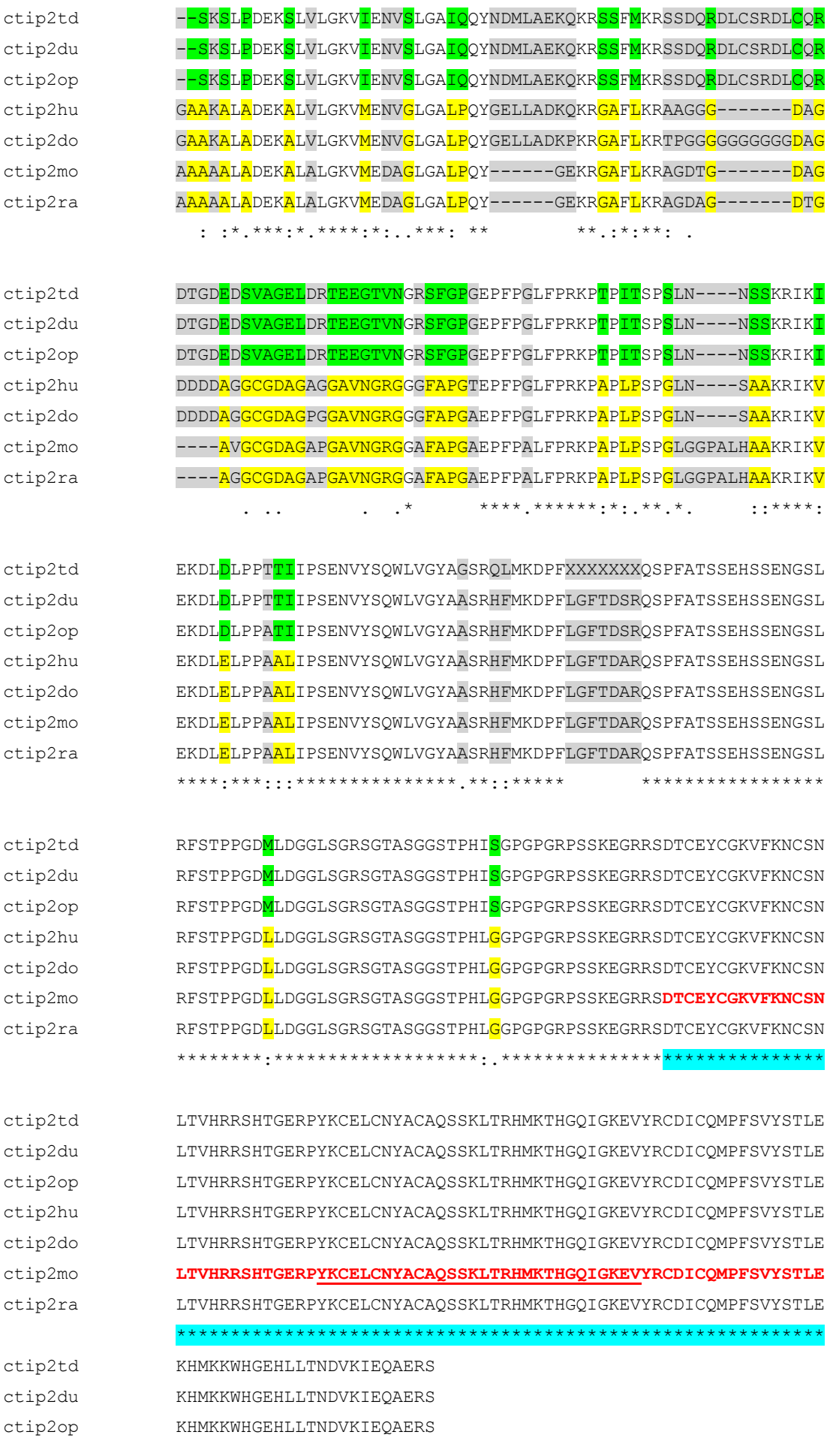
ctip2td --SKSLPDEKSLVLGKVIENVSLGAIQQYNDMLAEKQKRSSFMKRSSDQRDLCSRDLCQR
ctip2du --SKSLPDEKSLVLGKVIENVSLGAIQQYNDMLAEKQKRSSFMKRSSDQRDLCSRDLCQR
ctip2op --SKSLPDEKSLVLGKVIENVSLGAIQQYNDMLAEKQKRSSFMKRSSDQRDLCSRDLCQR
ctip2hu GAAKALADEKALVLGKVMENVGLGALPQYGELLADKQKRGAFLKRAAGGG-------DAG
ctip2do GAAKALADEKALVLGKVMENVGLGALPQYGELLADKPKRGAFLKRTPGGGGGGGGGDAG
ctip2mo AAAAALADEKALALGKVMEDAGLGALPQY------GEKRGAFLKRAGDTG-------DAG
ctip2ra AAAAALADEKALALGKVMEDAGLGALPQY------GEKRGAFLKRAGDAG-------DTG
ctip2td DTGDEDSVAGELDRTEEGTVNGRSFGPGEPFPGLFPRKPTPITSPSLN----NSSKRIKI
ctip2du DTGDEDSVAGELDRTEEGTVNGRSFGPGEPFPGLFPRKPTPITSPSLN----NSSKRIKI
ctip2op DTGDEDSVAGELDRTEEGTVNGRSFGPGEPFPGLFPRKPTPITSPSLN----NSSKRIKI
ctip2hu DDDDAGGCGDAGAGGAVNGRGGGFAPGTEPFPGLFPRKPAPLPSPGLN----SAAKRIKV
ctip2do DDDDAGGCGDAGPGGAVNGRGGGFAPGAEPFPGLFPRKPAPLPSPGLN----SAAKRIKV
ctip2mo ----AVGCGDAGAPGAVNGRGGAFAPGAEPFPALFPRKPAPLPSPGLGGPALHAAKRIKV
ctip2ra ----AGGCGDAGAPGAVNGRGGAFAPGAEPFPALFPRKPAPLPSPGLGGPALHAAKRIKV
ctip2td EKDLDLPPTTIIPSENVYSQWLVGYAGSRQLMKDPFXXXXXXXQSPFATSSEHSSENGSL
ctip2du EKDLDLPPTTIIPSENVYSQWLVGYAASRHFMKDPFLGFTDSRQSPFATSSEHSSENGSL
ctip2op EKDLDLPPATIIPSENVYSQWLVGYAASRHFMKDPFLGFTDSRQSPFATSSEHSSENGSL
ctip2hu EKDLELPPAALIPSENVYSQWLVGYAASRHFMKDPFLGFTDARQSPFATSSEHSSENGSL
ctip2do EKDLELPPAALIPSENVYSQWLVGYAASRHFMKDPFLGFTDARQSPFATSSEHSSENGSL
ctip2mo EKDLELPPAALIPSENVYSQWLVGYAASRHFMKDPFLGFTDARQSPFATSSEHSSENGSL
ctip2ra EKDLELPPAALIPSENVYSQWLVGYAASRHFMKDPFLGFTDARQSPFATSSEHSSENGSL
ctip2td RFSTPPGDMLDGGLSGRSGTASGGSTPHISGPGPGRPSSKEGRRSDTCEYCGKVFKNCSN
ctip2du RFSTPPGDMLDGGLSGRSGTASGGSTPHISGPGPGRPSSKEGRRSDTCEYCGKVFKNCSN
ctip2op RFSTPPGDMLDGGLSGRSGTASGGSTPHISGPGPGRPSSKEGRRSDTCEYCGKVFKNCSN
ctip2hu RFSTPPGDLLDGGLSGRSGTASGGSTPHLGGPGPGRPSSKEGRRSDTCEYCGKVFKNCSN
ctip2do RFSTPPGDLLDGGLSGRSGTASGGSTPHLGGPGPGRPSSKEGRRSDTCEYCGKVFKNCSN
ctip2mo RFSTPPGDLLDGGLSGRSGTASGGSTPHLGGPGPGRPSSKEGRRSDTCEYCGKVFKNCSN
ctip2ra RFSTPPGDLLDGGLSGRSGTASGGSTPHLGGPGPGRPSSKEGRRSDTCEYCGKVFKNCSN
ctip2td LTVHRRSHTGERPYKCELCNYACAQSSKLTRHMKTHGQIGKEVYRCDICQMPFSVYSTLE
ctip2du LTVHRRSHTGERPYKCELCNYACAQSSKLTRHMKTHGQIGKEVYRCDICQMPFSVYSTLE
ctip2op LTVHRRSHTGERPYKCELCNYACAQSSKLTRHMKTHGQIGKEVYRCDICQMPFSVYSTLE
ctip2hu LTVHRRSHTGERPYKCELCNYACAQSSKLTRHMKTHGQIGKEVYRCDICQMPFSVYSTLE
ctip2do LTVHRRSHTGERPYKCELCNYACAQSSKLTRHMKTHGQIGKEVYRCDICQMPFSVYSTLE
ctip2mo LTVHRRSHTGERPYKCELCNYACAQSSKLTRHMKTHGQIGKEVYRCDICQMPFSVYSTLE
ctip2ra LTVHRRSHTGERPYKCELCNYACAQSSKLTRHMKTHGQIGKEVYRCDICQMPFSVYSTLE
ctip2td KHMKKWHGEHLLTNDVKIEQAERS
ctip2du KHMKKWHGEHLLTNDVKIEQAERS
ctip2op KHMKKWHGEHLLTNDVKIEQAERS

```
ctip2hu          KHMKKWHGEHLLTNDVKIEQAERS
ctip2do          KHMKKWHGEHLLTNDVKIEQAERS
ctip2mo          KHMKKWHGEHLLTNDVKIEQAERS
ctip2ra          KHMKKWHGEHLLTNDVKIEQAERS
                 **********************
```

ANALYSIS of protein Homology for SATB2

```
satb2td          MERRSESPCLRDSPDRRSGSPDVKGPPPVKVARLEQNGSPMGARGRPNGSVTKSVGG---
satb2du          MERRSESPCLRDSPDRRSGSPDVKGPPPVKVARLEQNGSPMGARGRPNGSVTKSVGG---
satb2op          ------------------------------------------------------MLQG---
satb2hu          MERRSESPCLRDSPDRRSGSPDVKGPPPVKVARLEQNGSPMGARGRPNGAVAKAVGG---
satb2do          MERRSESPCLRDSPDRRSGSPDVKGPPPVKVARLEQNGSPMGARGRPNGAVAKAVGG---
satb2mo          MERRSESPCLRDSPDRRSGSPDVKGPPPVKVARLEQNGSPMGARGRPNGAVAKAVGG---
satb2ra          MERRSESPCLRDSPDRRSGSPDVKGPPPVKVARLEQNGSPMGARGRPNGAVAKAVGGNSP
                                                                      : *

satb2td          ----LMIPVFCVVEQLDSSLEYDNREEHAEFVLVRKDVLFSQLVETALLALGYSHSSAAQ
satb2du          ----LMIPVFCVVEQLDSSLEYDNREEHAEFVLVRKDVLFSQLVETALLALGYSHSSAAQ
satb2op          ----LMIPVFCVVEQLDSSLEYDNREEHAEFVLVRKDVLFSQLVETALLALGYSHSSAAQ
satb2hu          ----LMIPVFCVVEQLDGSLEYDNREEHAEFVLVRKDVLFSQLVETALLALGYSHSSAAQ
satb2do          ----LMIPVFCVVEQLDGSLEYDNREEHAEFVLVRKDVLFSQLVETALLALGYSHSSAAQ
satb2mo          ----LMIPVFCVVEQLDGSLEYDNREEHAEFVLVRKDVLFSQLVETALLALGYSHSSAAQ
satb2ra          ELGGLMIPVFCVVEQLDGSLEYDNREEHAEFVLVRKDVLFSQLVETALLALGYSHSSAAQ
                     *************.******************************************

satb2td          AQGIIKLGRWNPLPLSYVTDAPDATVADMLQDVYHVVTLKIQLQSCSKLEDLPAEQWNHA
satb2du          AQGIIKLGRWNPLPLSYVTDAPDATVADMLQDVYHVVTLKIQLQSCSKLEDLPAEQWNHA
satb2op          AQGIIKLGRWNPLPLSYVTDAPDATVADMLQDVYHVVTLKIQLQSCSKLEDLPAEQWNHA
satb2hu          AQGIIKLGRWNPLPLSYVTDAPDATVADMLQDVYHVVTLKIQLQSCSKLEDLPAEQWNHA
satb2do          AQGIIKLGRWNPLPLSYVTDAPDATVADMLQDVYHVVTLKIQLQSCSKLEDLPAEQWNHA
satb2mo          AQGIIKLGRWNPLPLSYVTDAPDATVADMLQDVYHVVTLKIQLQSCSKLEDLPAEQWNHA
satb2ra          AQGIIKLGRWNPLPLSYVTDAPDATVADMLQDVYHVVTLKIQLQSCSKLEDLPAEQWNHA
                 ************************************************************

satb2td          TVRNALKELLKEMNQSTLAKECPLSQSMISSIVNSTYYANVSATKCQEFGRWYKKYKKIK
satb2du          TVRNALKELLKEMNQSTLAKECPLSQSMISSIVNSTYYANVSATKCQEFGRWYKKYKKIK
satb2op          TVRNALKELLKEMNQSTLAKECPLSQSMISSIVNSTYYANVSATKCQEFGRWYKKYKKIK
satb2hu          TVRNALKELLKEMNQSTLAKECPLSQSMISSIVNSTYYANVSATKCQEFGRWYKKYKKIK
satb2do          TVRNALKELLKEMNQSTLAKECPLSQSMISSIVNSTYYANVSATKCQEFGRWYKKYKKIK
satb2mo          TVRNALKELLKEMNQSTLAKECPLSQSMISSIVNSTYYANVSATKCQEFGRWYKKYKKIK
satb2ra          TVRNALKELLKEMNQSTLAKECPLSQSMISSIVNSTYYANVSATKCQEFGRWYKKYKKIK
                 ************************************************************

satb2td          VERVERENLTDYCVLGQRPMHLPNMNQLATLGKTNEQSPHSQIHHSTPIRNQVPTLQPIM
satb2du          VERVERENLTDYCVLGQRPMHLPNMNQLANLGKTNEQSPHSQIHHSTPIRNQVPTLQPIM
satb2op          VERVERENLSDYCVLGQRPMHLPNMNQLATLGKTNEQSPHSQIHHSTPIRNQVPTLQPIM
```

```
satb2hu         VERVERENLSDYCVLGQRPMHLPNMNQLASLGKTNEQSPHSQIHHSTPIRNQVPALQPIM
satb2do         VERVERENLSDYCVLGQRPMHLPNMNQLASLGKTNEQSPHSQIHHSTPIRNQVPALQPIM
satb2mo         VERVERENLSDYCVLGQRPMHLPNMNQLASLGKTNEQSPHSQIHHSTPIRNQVPALQPIM
satb2ra         VERVERENLSDYCVLGQRPMHLPNMNQLASLGKTNEQSPHSQIHHSTPIRNQVPALQPIM
                *********:******************.**********************:*****

satb2td         SPGLLSPQLSPQLVRQQIAMAHLINQQIAVSRLLAHQHPQAINQQFLNHPPIPRAVKPEP
satb2du         SPGLLSPQLSPQLVRQQIAMAHLINQQIAVSRLLAHQHPQAINQQFLNHPPIPRAVKPEP
satb2op         SPGLLSPQLSPQLVRQQIAMAHLINQQIAVSRLLAHQHPQAINQQFLNHPPIPRAVKPEP
satb2hu         SPGLLSPQLSPQLVRQQIAMAHLINQQIAVSRLLAHQHPQAINQQFLNHPPIPRAVKPEP
satb2do         SPGLLSPQLSPQLVRQQIAMAHLINQQIAVSRLLAHQHPQAINQQFLNHPPIPRAVKPEP
satb2mo         SPGLLSPQLSPQLVRQQIAMAHLINQQIAVSRLLAHQHPQAINQQFLNHPPIPRAVKPEP
satb2ra         SPGLLSPQLSPQLVRQQIAMAHLINQQIAVSRLLAHQHPQAINQQFLNHPPIPRAVKPEP
                ************************************************************

satb2td         TNSSVEVSPDIYQQVRDELKRASVSQAVFARVAFNRTQGLLSEILRKEEDPRTASQSLLV
satb2du         TNSSVEVSPDIYQQVRDELKRASVSQAVFARVAFNRTQGLLSEILRKEEDPRTASQSLLV
satb2op         TNSSVEVSPDIYQQVRDELKRASVSQAVFARVAFNRTQGLLSEILRKEEDPRTASQSLLV
satb2hu         TNSSVEVSPDIYQQVRDELKRASVSQAVFARVAFNRTQGLLSEILRKEEDPRTASQSLLV
satb2do         TNSSVEVSPDIYQQVRDELKRASVSQAVFARVAFNRTQGLLSEILRKEEDPRTASQSLLV
satb2mo         TNSSVEVSPDIYQQVRDELKRASVSQAVFARVAFNRTQGLLSEILRKEEDPRTASQSLLV
satb2ra         TNSSVEVSPDIYQQVRDELKRASVSQAVFARVAFNRTQGLLSEILRKEEDPRTASQSLLV
                ************************************************************

satb2td         NLRAMQNFLNLPEVERDRIYQDERERSMNPNVSMVSSASSSPSSSRTPQAKTSTPTTDLP
satb2du         NLRAMQNFLNLPEVERDRIYQDERERSMNPNVSMVSSASSSPSSSRTPQAKTSTPTTDLP
satb2op         NLRAMQNFLNLPEVERDRIYQDERERSMNPNVSMVSSASSSPSSSRTPQAKTSTPTTDLP
satb2hu         NLRAMQNFLNLPEVERDRIYQDERERSMNPNVSMVSSASSSPSSSRTPQAKTSTPTTDLP
satb2do         NLRAMQNFLNLPEVERDRIYQDERERSMNPNVSMVSSASSSPSSSRTPQAKTSTPTTDLP
satb2mo         NLRAMQNFLNLPEVERDRIYQDERERSMNPNVSMVSSASSSPSSSRTPQAKTSTPTTDLP
satb2ra         NLRAMQNFLNLPEVERDRIYQDERERSMNPNVSMVSSASSSPSSSRTPQAKTSTPTTDLP
                ************************************************************

satb2td         IKVEGANVNITAAIYDEIQQEMKRAKVSQALFAKVAANKSQGWLCELLRWKENPSPENRT
satb2du         IKVEGANVNITAAIYDEIQQEMKRAKVSQALFAKVAANKSQGWLCELLRWKENPSPENRT
satb2op         IKVEGANVNITAAIYDEIQQEMKRAKVSQALFAKVAANKSQGWLCELLRWKENPSPENRT
satb2hu         IKVDGANINITAAIYDEIQQEMKRAKVSQALFAKVAANKSQGWLCELLRWKENPSPENRT
satb2do         IKVDGANVNITAAIYDEIQQEMKRAKVSQALFAKVAANKSQGWLCELLRWKENPSPENRT
satb2mo         IKVDGANVNITAAIYDEIQQEMKRAKVSQALFAKVAANKSQGWLCELLRWKENPSPENRT
satb2ra         IKVDGANVNITAAIYDEIQQEMKRAKVSQALFAKVAANKSQGWLCELLRWKENPSPENRT
                ***:***:************************************************

satb2td         LWENLCTIRRFLNLPQHERDVIYEEESRHHHSERMQHVVQLTPEPVQVLHRQQSQPAKET
satb2du         LWENLCTIRRFLNLPQHERDVIYEEESRHHHSERMQHVVQLTPEPVQVLHRQQSQPAKES
satb2op         LWENLCTIRRFLNLPQHERDVIYEEESRHHHSERMQHVVQLTPEPVQVLHRQQSQPAKES
satb2hu         LWENLCTIRRFLNLPQHERDVIYEEESRHHHSERMQHVVQLPPEPVQVLHRQQSQPAKES
satb2do         LWENLCTIRRFLNLPQHERDVIYEEESRHHHSERMQHVVQLPPEPVQVLHRQQSQPAKES
```

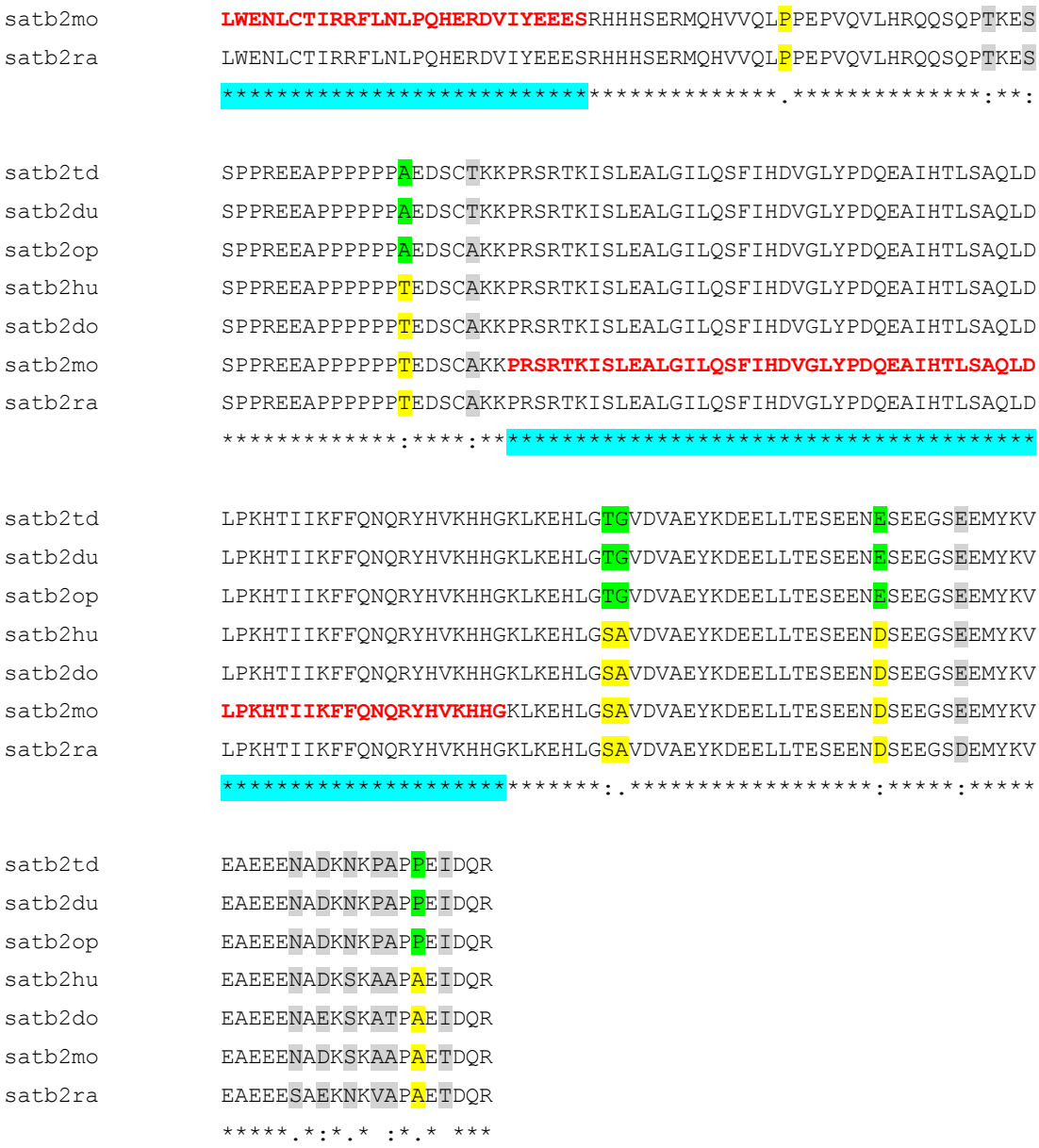

Figure A1: Analysis of homology of SATB2 and CTIP2 proteins between marsupials and eutherian mammals.

The sequences of amino acids of SATB2 and CTIP2 proteins were compared in marsupials (td = Tasmanian devil, du = fat-tailed dunnart, op = opossum) and eutherian mammals (hu = human, do = dog, mo = mouse, ra = rat). The functional domains are in red and bold font. The asterisks below the functional domains are highlighted in light blue and represent perfect homology of the sequence of amino acids among species. The marsupial-specific amino acids are highlighted in green, while the eutherian-specific amino acids are highlighted in yellow. Amino acids that changed inconsistently among species are shown in grey. This analysis shows that the sequence of amino acids of the SATB2 DNA binding domains are broadly conserved, apart from one amino acid in the second DNA binding domain that is different in marsupials (glutamic acid) compared to eutherian

mammals (aspartic acid). For CTIP2, the six zinc finger domains are 100% conserved across therian mammals.

Appendix 2

Table A2: Description of important events of corticogenesis and body development in dunnart and mouse at different stages.

S	FTD (Suárez, Paolino et al. 2017; Paolino et al. 2017)	FTD description (Suárez, Paolino et al. 2017; Paolino et al. 2017)	FTD description (additional observations)	Ms (Theiler)	Ms description (Theiler)	Ms description (additional observations)
18	**P 0-3**	Telencephalic vesicles present. Dorsal pallium at stage of preplate and ventricular zone. Large diencephalon and midbrain. Hairless, translucent and shiny skin. Forelimbs with elbow. Mostly fused digits. Hindlimb paddle, partly fused with the tail. Completely fused digits. Joeys are curled and difficult to stretch. Milk spot visible. Little body movement. Prominent mandibular prognathism. Frontal mouth opening. Eye pigment slightly visible. Lens vesicle just closed. No ear buds. Large nostrils.	Detection of **CTIP2** expression	**E 10.5-11.25**	Closure of lens vesicle. Nasal pits. Cervical somites no longer visible. Absent audit ory hillocks. Anterior footplate.	Detection of **CTIP2** expression
19	**P 4-7**	Piriform cortex and olfactory tubercle better defined. Distinct hands, digits partly fused. Hindlimbs and tail buds distinguishable, still fused. Joeys easier to uncurl. Alternate forelimb movement.		**E 11-12.25**	Lens vesicle completely separated from the surface epithelium. Anterior, but no posterior, footplate. Auditory hillocks first visible. Absent retin	

		Darker eye pigment, no face pigmentation. Developing lens fibres. Short and thin hair, only on top of the head.			al pigmentation and sign of fingers.	
20	**P 8-11**	Dorsal pallium without a defined cortical plate. Prominent lateral olfactory tract, endopiriform and piriform regions. More opaque skin. Small claws in separated forelimb digits. Hindlimb digits mostly fused. Jugular and carotid processes defined. Small ear buds. Slight pigment on top of snout. Lens epithelium and fibres enlarged. Retinal layers slightly visible. Optic stalk.	Beginning of deeper layers neurogenesis. Electroporation performed between P10 and P12 to label deeper layer neurons. Detection of **SATB2** expression	**E 11.5-13**	Earliest sign of fingers. Posterior footplate apparent. Retina pigmentation apparent. Tongue well-defined. Brain vesicles clear. Absent 5 rows of whiskers, indented.	Deeper layers neurogenesis. Electroporation performed at E12 to label deeper layer neurons
21	**P 12-16**	Prominent lateral olfactory tract, endopiriform and piriform regions. Internal, and external capsules clearly defined. Anterior commissure present. Cortical plate appears. Larger subpallium region. Dorsal pallium without a defined cortical plate. Opaque skin. Hindlimbs and tail unfused and well defined. Hindlimb digits partly fused. Joeys can be completely uncurled. Movement of front-temporal head muscles. Underbite less prominent. Mild pigment on top of snout. Short, thick hair only on top of the head.	Deeper layers and layer 4 neurogenesis. At P16, neurons that were EP at P10 extend their axons laterally (no axons projecting medially).	**E 12.5-14**	Anterior footplate indented. Elbow and wrist identifiable. 5 rows of whiskers. Umbilical hernia now clearly apparent. Absent hair follicles. Fingers separate distally.	Initial axonal elongation from deeper layer neurons Detection of **SATB2** expression

		Thicker cornea, lens well developed. Clear retinal layers. Optic nerve.				
22	**P 17-19**	Olfactory tubercle and layer 2 of piriform cortex clearly defined. Large, pigmented forelimb claws. Hindlimb digits separated, with small claws. Large jugular and carotid processes visible. Larger ear buds. Darker hair on top of the head. Darker pigment on top of snout.	Axons extending from deeper layer neurons reaching the midline. Beginning of upper layers neurogenesis.	**E 13.5-15**	Fingers separate distally, only indentations between digits of the posterior footplate. Long bones of limbs present. Hair follicles in pectoral, pelvic and trunk regions. Absent open eyelids. Hair follicles in cephalic region.	
23	**P 20-23**	Expansion of subventricular and intermediate zones. Ventralisation of the piriform cortex. Short, light hair on face and body. Hindlimb digits well defined, with small claws. Underbite less prominent. Larger, darker eye pigment. Larger ear buds.	Peak of upper layer neurogenesis. Electroporation performed between P20 and P22 to label upper layer neurons. At P23, few axons extending from deeper layer neurons (EP at P10) start to project medially. Few commissural	**E 15**	Fingers and toes separate. Hair follicles also in cephalic region but not at periphery of vibrissae. Eyelids open. Absent nail primordia, fingers 2-5 parallel.	Upper layers neurogenesis. Electroporation performed at E15 to label upper layer neurons.

			axons from deeper layer neurons have reached the contralateral white matter.			
24	**P 24-26**	Hippocampal commissure first visible. Indentation of piriform and olfactory tubercle cell layers along the lateral olfactory tract. Superior and inferior colliculi distinguishable. Short, light hair on face and body. Darker skin, jugular and carotid processes less visible. Longer, motile hindlimbs, with clear claws. Overall body movement increased and responsive. Mandibulary and maxillary processes aligned. Long, thick, dark hair on top of head. Ear flap is distinguishable. Small whiskers.	Upper layer neurons electroporated during the previous stage present RG shape, with processes reaching the pial surface, a couple of axons turning laterally (initial axonal elongation from upper layer neurons).	**E 16**	Reposition of umbilical hernia. Eyelids closing. Fingers 2-5 are parallel, nail primordia visible on toes. Absent wrin kled skin. Fingers and toes joined together.	Axons extending from deeper layer neurons reaching the midline. Upper layer neurons electroporated during the previous stage present RG shape.
25	**P 27-30**	Ventral expansion of the developing cortical plate. Indentation of the rhinal fissure. Slightly darker body hair. Legs and tail very well developed. Hindlimb claws slightly pigmented. Less curved and more motile body. Snout progression (slight maxillary overbite). Mouth still fused. Larger and darker eye pigment.		**E 17**	Skin is wrinkled. Eyelids are closed. Umbilical hernia is gone. Absent ear extending over auditory meatus. Long whiskers.	

		Ear lobes better defined.				
26	**P 31-35**	Cortical layers 5 and 6 are present and clearly distinguishable. Reduction of the subventricular zone. Longer, darker hair on face and body, especially on tail and back. Large digits with dark and well developed claws. Jugular and carotid processes less visible. Mouth lining visible but still fused. Eyelid grooves become apparent. Dark, larger skin pigment patch on top of snout. Larger whiskers.	At P32, deeper layer neurons EP at P10 extend axons both laterally (towards the internal and external capsules) and medially (towards the cingulate). Commissural axons from deeper layer neurons have reached the contralateral deeper layers. Upper layer neurons that were EP at P20 project their axons laterally (mainly towards the external capsule) and the axons have crossed the midline.	**E 18**	Long whiskers. Eyes barely visible through closed eyelids. Ear covers auditory meatus.	Medial projections extending from the upper layer neurons.
27	**P 36-40**	Cortical layers 2±4 are defined. Longer, darker hair all over body. Jugular and carotid processes not visible. Testes/pouch clearly visible. Fully dependent on their mother, have never left the pouch. Mouth almost unfused, deep groove.	At P40, deeper layer neurons EP at P10 extend axons both laterally (towards internal and external capsules) and medially (towards the cingulate). Commissural axons from	**P0-P3**		At P0, axons from deeper layer neurons reach the contralateral hemisphere. At P3, axons from deeper layer neurons finalise the innervation in the contralateral hemisphere, reaching the pial surface. At P3, axons from

		Eyelid margin is clearly distinct. Ear canal better defined.	deeper layer neurons are still located in the contralateral deeper layers, they have not advanced much compared to previous stage (waiting period). Upper layer neurons that were EP at P20 project both laterally and medially. Commissural axons from upper layer neurons have reached the contralateral deeper layers.			upper layer neurons reach the midline
28	**P 41-50**	Further indentation of the rhinal fissure. Further ventral progression of the cortex. Diencephalon is fully covered by the dorsal cortex. Back completely covered with dark and thick hair, abdomen hair lighter colour. Pups can leave the pouch temporarily. Narrower snout. Mouth unfused, can be fully opened. Very pigmented and large, but unopen, eyes. Fully formed ears with clearly open canal.	At P50, deeper and upper layer neurons (EP at P10 and P20, respectively) extend a lot of axons both laterally (towards internal and external capsules) and medially (towards the cingulate). Commissural axons from deeper and upper layer neurons have reached the pial surface of the contralateral hemisphere.	**P5-P10**		At P5, axons from upper layer neurons reach the contralateral hemisphere. At P9/P10, axons from upper layer neurons finalise the innervation in the contralateral hemisphere, reaching the pial surface.
29	**P 51-70**	Well defined cortical areas and regions, resembling the adult. Mature-looking fur in head and body. Mature-looking narrow snout. Pups often leave the pouch and try solid				

		food. Mouth fully open. Mature-looking whisker pads. Eyes begin to open.				

S = stage, FTD = fat-tailed dunnart, Ms = mouse